STRUCTURE-FUNCTION RELATIONSHIPS OF VARIEGIN: A NOVEL CLASS OF THROMBIN INHIBITORS

KOH CHO YEOW

[B.SC. (PHARM.) (HONS.) NUS]

A THESIS SUBMITTED FOR THE DEGREE OF DOCTOR OF PHILOSOPHY

DEPARTMENT OF BIOLOGICAL SCIENCE, NATIONAL UNIVERSITY OF SINGAPORE

2009

ACKNOWLEDGEMENTS

I would like to thank my supervisor Professor R Manjunatha Kini for his constant encouragement throughout my studies. He provided me an opportunity to work in his lab as an honors student back in August 2003. Coming from a department where undergraduate students do not get involved in much basic research, it was really an eye-opening experience. Few years on I am on a totally different career path and found something that I really enjoyed doing. Thank you very much for everything for the last few years, Boss!

Next, I would like to thank my co-supervisor Associate Professor Kunchithapadam Swaminathan. He is the main driving force behind the solution of the crystal structure. Without his help and expertise the structure solution would not be possible.

I would like to thank the graduate program run by the National University of Singapore for their financial support for my studies.

One of the people that I am most indebted to is my senior Dr. Kang Tse Siang, who also came from Department of Pharmacy to this laboratory a few years ahead of me. He is the main person that introduces to me what the world of research is like, and of course, provided guidance, advice, encouragement and company all the while (even after he went to Scripps for his post-doctoral training). Thank you so much!

All these works would not have been possible without the support of our able collaborators. I would like to thank Dr Maria Kazimirova (and her colleagues) from Institute of Zoology, Slovakia, for her initial works on variegin and being very helpful throughout the course of the project. Thanks to Dr Patricia Nuttall from NERC, UK, for her constructive comments on our first manuscript and the future directions of the work in general. I would also like to thank Dr Ladislav Roller, also from Institute of Zoology, Slovakia, for the discussion on the variegin precursor proteins. Next I would like to thank Dr Pudur Jagadeeswaran from University of North Texas, along with his post-doctoral fellow Dr Kim Seongcheol, and student Uvaraj, for allowing me to work in their laboratory for the zebrafish larvae thrombosis experiments. Thank you Dr

Kim for driving me from Dallas Airport to Denton, and your help in the experiments. Thank you Uvaraj for performing some initial dosage experiments and all your help.

I would also like to thank the others who have being a great help along the way: Dr. Jun Mizuguchi, Dr. Takayuki Imamura, Dr. Chikateru Nozaki, and Dr. Sadaaki Iwanaga from KAKETSUKEN, Japan, for supplying the thrombin used in this project. Dr Go Mei Lin, Dr Koh Hwee Ling and Dr Seetharama Jois, all from Department of Pharmacy, for their supports and advice; Dr Sundramurthy Kumar, for his expert guidance in solution of the crystal structure; Miss Yong Ann Nee, for designing the cover page for our JBC paper; Miss Tay Bee Ling, for all your support in laboratory maintenance and purchasing of products; and Dr Phillip Kuchel and Dr Allen Torres for hosting me in Sydney.

Not forgetting all my wonderful friends, especially those from the Protein Science Laboratory. This really makes a long list, Dileep, Joanna, Rehana, Vivek, Susanta, Li Min, Reza, Banerjee, Kishore, Xingding, Robin, Raghu, Shi Yang, Shifali, Girish, Amrita, Angelina, Sheena, Rocky, Liu Ying, Jia Chyi, Ming Zhi, Bee Har, Nazir, Sandy and others that I have miss out. Thank you for all your helps and for creating a very enjoyable atmosphere for the laboratory.

I am grateful for my family for their support all my life. Thanks papa and mama for your upbringing and everything, my sisters and my brother-in-law, for taking care of me and my parents since I left Malaysia more than 11 years ago. Thanks, my wife, your love and for being with me, and of course, our dear little one.

Thank you!

Cho Yeow

Jan 2009

TABLE OF CONTENTS

SUMMARY

Tick saliva contains potent anti-hemostatic molecules that help ticks obtain their enormous bloodmeal during prolonged feeding. Following the isolation of thrombin inhibitors present in the salivary gland extract from partially fed female *Amblyomma variegatum*, the tropical bont tick, we characterized the most potent, variegin. It is one of the smallest (32 residues) thrombin inhibitors found in nature. Full-length variegin and two truncated variants were chemically synthesized. Despite its small size and flexible structure, variegin binds thrombin with a strong affinity (K_i ~ 10.4 pM) and high specificity. Results using the truncated variants indicate that the seven residues at the N-terminus affect the binding kinetics; when removed, the binding characteristics change from fast to slow. Further, the thrombin active site binding moiety of variegin is in the region of residues 8 to 14, and the exosite-I binding moiety is within residues 15 to 32.

Upon binding to thrombin, variegin is cleaved at the scissile bond between Lys10 and Met11. The sequence resides in the active site binding segment (^{8}EPKMHKT^{14}) is novel. Residues locate C-terminal to the scissile bond (^{11}MHKT^{14}) is mainly responsible for the ability of variegin cleavage product to non-competitively inhibit thrombin. After cleavage, the variegin C-terminal fragment retains strong binding to thrombin (K_i = 14.1 nM) resulting in prolonged inhibition of the enzyme.

Despite our attempts to obtain the three-dimensional structure of thrombin in complex with full-length s-variegin, only the density of its C-terminal cleavage fragment is observed. s-Variegin (cleavage fragment) fits tightly to thrombin in the

catalytic pocket, prime subsites and exosite-I. s-Variegin cleavage fragment perturbs the charge relay system of thrombin catalytic site and the formation of oxyanion hole through a new and extensive hydrogen bonding network, explaining the non-competitive inhibition of thrombin. The structure also reveals other important information and facilitates subsequent design of variegin variants. These variants that have been designed and characterized cover a diverse spectrum of potency, kinetics and mechanism of inhibition, including peptides with affinities ranging from nanomolar to picomolar values, with fast and slow tight-binding, displaying competitive and non-competitive inhibition.

We have then demonstrated that the *in vivo* antithrombotic effects of variegin variants in zebrafish larvae correlate well with their *in vitro* affinities for thrombin with the exception of the slow binding variants. In addition, the thrombin inhibitory activities of the peptides can be reversed by protamine sulfate. Through works conducted within the scope of this project, we have identified and characterized a novel thrombin inhibitor, variegin. It is dissimilar to any other groups of naturally occurring thrombin inhibitors, thus belongs to a new class of its own. A wide selection of peptides with different potencies, kinetics, mechanisms of inhibition were designed and characterized, laying foundation for subsequent development of these inhibitors as therapeutic agent.

LIST OF FIGURES

Chapter three

Chapter four

Chapter five

LIST OF TABLES

Chapter five

ABBREVIATIONS

ACS	acute coronary syndrome
ADAMTS13	a disintegrin and metalloprotease with a thrombospondin type 1 motif, number 13
APC	activated protein C
APTT	activated partial thromboplastin time
AT-III	antithrombin-III
AvGI	*Amblyomma variegatum* Gene Index
BPTI	bovine pancreatic trypsin inhibitor
BSA	bovine serum albumin
CD	circular dichroism
cDNA	complementary deoxyribonucleic acid
CHCA	α-cyano-4-hydroxycinnamic acid
DIPEA	*N*,*N*-diisopropylethylamine
DMF	*N*,*N*-dimethylformamide
dpf	days-post-fertilization
DVE	deep-vein thrombosis
ESI-MS	electrospray ionization mass spectrometry
FA	formic acid
FII	prothrombin
FIIa	thrombin
FIX, FIXa	factor IX, activated factor IX
Fmoc	9-Fluorenylmethyloxycarbonyl
FV, FVa	factor V, activated factor V
FVII, FVIIa	factor VII, activated factor VII
FVIII, FVIIIa	factor VIII, activated factor VIII
FX, FXa	factor X, activated factor X
FXI, FXIa	factor XI, activated factor XI
FXII, FXIIa	factor XII, activated factor XII
FXIIIa	activated factor XIII

Gla	gamma-carboxyglutamic acid
HATU	*O*-(7-azabenzotriazol-1-yl)-1,1,3,-3-tetramethyluronium hexafluorophosphate
HCII	heparin cofactor II
HEPES	4-(2-Hydroxyethyl)piperazine-1-ethanesulfonic acid
HIT	heparin-induced thrombocytopenia
HMWK	high-molecular weight kallikrein
LMWH	low-molecular-weight heparin
MALDI-TOF	matrix-assisted laser desorption/ionization time-of-flight
MI	myocardial infarction
MS	mass spectrometry
NMR	nuclear magnetic resonance
Par4	protease-activated receptor 4
PCI	percutaneous coronary intervention
PDB	Protein Data Bank
PE	pulmonary embolism
PEG	polyethylene glycol
PK	prekallikrein
PL	phospholipids
*p*NA	*p*-nitroaniline
PT	prothrombin time
RMSD	root-mean-square deviations
RP-HPLC	reverse-phase high performance liquid chromatography
RVV-X activator	Russell's viper venom factor X activator
S.D.	standard deviations
S2222	benzoyl-IIe-Glu(Glu-γ -methoxy)-Gly-Arg-*p*-nitroanilide (*p*NA) hydrochloride (HCl)
S2238	*H*-$_{D}$-Phe-pipecolyl (Pip)-Arg-*p*NA•2HCl
S2251	*H*-$_{D}$-Val-Leu-Lys-*p*NA•2HCl
S2288	*H*-$_{D}$-IIe-Pro-Arg-*p*NA•2HCl

S2302	*H*-$_D$-Pro-Phe-Arg-*p*NA•2HCl
S2366	pyroGlu-Pro-Arg-*p*NA•HCl
S2444	pyroGlu-Gly-Arg-*p*NA•HCl
S2586	methoxysuccinyl-Arg-Pro-Tyr-*p*NA•HCl
S2765	benzyloxycarbonyl-D-Arg-Gly-Arg-*p*NA•2HCl
SDS-PAGE	sodium dodecyl sulfate polyacrylamide gel electrophoresis
SERPIN	serine proteinase inhibitor
SGE	salivary gland extract
Spectrozyme® FIXa	*H*-$_D$-Leu-phenylalanyl-Gly-Arg-*p*NA•2-AcOH
TEG	thromboelastography
TF	tissue factor
TFA	Trifluoroacetic acid
TFPI	tissue factor pathway inhibitor
TIGR	The Institute of Genomic Research
TM	thrombomodulin
tPA	tissue plasminogen activator
TT	thrombin time
TTO	time-to-occlusion
UFH	unfractionated heparin
UV	ultraviolet
VTE	venous thromboembolism
VWF	von Willebrand factor

Chapter One

Introduction

1.1. HEMOSTASIS

The circulation of blood is essential for our survival. Hemostasis – the spontaneous arrest of blood loss from ruptured vessels (Jackson and Nemerson, 1980) – involved the interplay of several processes such as vasoconstriction, platelet activation and aggregation, blood coagulation and fibrinolysis. When vascular injury occurs, subendothelial matrix is exposed to the flowing blood. Two pathways proceed to activate platelets in the blood – collagen pathway and tissue factor (TF) pathway. In the collagen pathway, the exposure of subendothelial collagen recruits platelets to the site of injury. Platelets adhere to the exposed collagen through platelet-glycoprotein VI and platelet glycoprotein Ib-V-IX-von Willebrand factor (VWF) interactions. In tissue factor pathway, the activation of platelet is through thrombin cleavage of platelet protease-activated receptor 4 (Par4). Tissue factor (derived from the vessel wall or present in blood) initiates the classical blood coagulation cascade (see below for details) to produce thrombin. Which of the two pathways predominates depends on the injury, although the result, platelet activation, is the same. Activated platelets accumulate on the endothelium, aggregate and recruit inactivated platelets to form platelet thrombus. Associated with this platelet thrombus is fibrin, cleaved from fibrinogen by thrombin. As coagulation propagates, fibrin clot forms to seal the breach in the vessel wall (Furie and Furie, 2007; Furie and Furie, 2008).

1.1.1. Blood coagulation cascade

The classical view of hemostasis places the formation of platelet thrombus (platelet plug) as the initial response to injury. Platelet plug was thought to temporarily reduce blood loss before the formation of fibrin clot through blood

coagulation pathway to strengthen the platelet plug in a meshwork of fibrin (Davie et al., 1991). Recent findings demonstrated that formation of the platelet plug intertwined with thrombin generation and fibrin clot formation as concurrent events (Furie and Furie, 2007; Furie and Furie, 2008). Either way, blood coagulation pathway is the common mechanism to arrest the bleeding. Thus, blood coagulation remains one of the most important parts of hemostasis. The blood coagulation cascade was established in 1964 (Davie and Ratnoff, 1964; Macfarlane, 1964) and has been reviewed in detail elsewhere (Jackson and Nemerson, 1980; Davie et al., 1991). An interesting historical perspective was also published (Davie, 2003). Nonetheless, latest studies of thrombus formation *in vivo* have added valuable information to our knowledge and will be the main focus in the descriptions here.

1.1.2. Initiation phase

The current view on blood coagulation separates the process into two phases – initiation and amplification (Figure 1.1). In the initiation phase, a minute amount of thrombin is generated through a series of events described in the classical extrinsic (tissue factor) pathway of coagulation. Tissue factor is a membrane protein located in the adventitial and medial layers of the vessel wall. Vascular injury exposes tissue factor to circulatory activated factor VII (FVIIa) in flowing blood to form the extrinsic tenase complex in the present of calcium ions (FVIIa-TF-Ca^{2+}). However, TF is also present in the circulating blood, associated with microparticles. It is postulated that microparticles associated TF exist in a latent form and is activated by a yet to be identified mechanism at the site of injury. In either case, formation of the extrinsic tenase complex is pivotal. This complex activates three zymogens – factor VII (FVII), factor IX (FIX) and factor X (FX). Activated FVII binds to free TF to

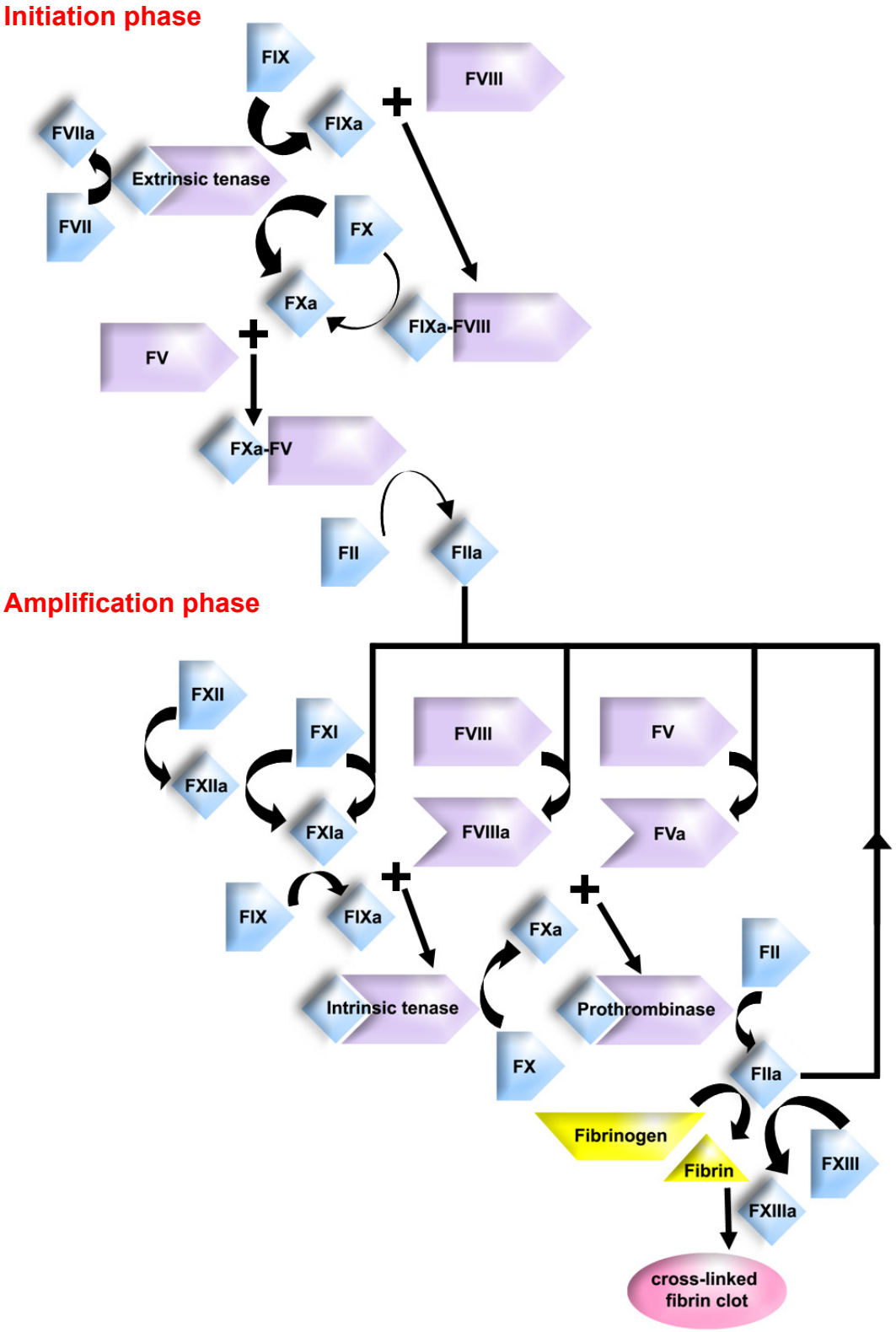

FIGURE 1.1

Blood coagulation cascade – initiation and amplification phase

increase the amount of the extrinsic tenase complex. Activated FIX (FIXa) binds to circulatory factor VIII (FVIII) to generate FXa, albeit inefficiently. Factor X is also directly activated by the extrinsic tenase complex. The overall result is the generation of FXa, which in turn associates with FV as an inefficient complex to generate trace amount of thrombin (FIIa) from prothrombin (FII) (Furie and Furie, 2008).

1.1.3. Amplification phase

With the formation of this low amount of thrombin blood coagulation proceeds to the amplification phase (Figure 1.1), typically described as the intrinsic (contact factor) pathway. Thrombin activates platelets, FVIII, FV and possibly FXI. Platelets contributed phospholipids (PL) surface that is required for the maximum efficiency of coagulation complexes. With the formation of FVIIIa, the fully active intrinsic tenase complex (FIXa-FVIIIa-PL-Ca^{2+}) is assembled which amplified FXa production. Similarly, activated FV (FVa) forms the fully active prothrombinase complex (FXa-FVa-PL-Ca^{2+}). As a result the fully active complexes increase the amount of thrombin produced by at least five orders of magnitude, resulting in a large burst of thrombin (Furie and Furie, 2008). Thrombin cleaves fibrinogen into fibrin which polymerized into the insoluble clot. The fibrin polymers are further strengthened and stabilized through covalent cross-linking driven by thrombin-activated factor XIII (FXIIIa) (Lane et al., 2005).

The activation of factor XI (FXI) by thrombin, although is controversial, also contributes to FXa production. The contact activation – the initiation of contact system pathway *in vitro* – is through factor XII (FXII) and prekallikrein (PK)-high molecular weight kallikrein (HMWK) complex activation on negatively charged

surface in the presence of Zn^{2+}. The activation is reciprocal, amplifying FXIIa and kallikrein formed. The activated factor XII cleaves FXI into FXIa, which in turn activates FIX – the enzyme in the intrinsic tenase complex. Kallikrein also cleaves HK to release bradykinin (Gailani and Renne, 2007). The contact activation was previously thought to be irrelevant *in vivo* in hemostasis. However, recent findings suggested important roles of FXII and FXI in pathological thrombus formation. Thus, by inhibiting FXIIa, it might be possible to prevent thrombosis without perturbing hemostasis (Furie and Furie, 2007; Muller and Renne, 2008).

1.1.4. Fibrinolysis

Once bleeding stops and hemostasis is restored, the clot must be removed. The process of clot dissolution is known as fibrinolysis. The main enzyme responsible for the degradation of fibrin into soluble products is the serine proteinase plasmin. Plasmin circulates as inactive zymogen (plasminogen) in the blood. Two enzymes, tissue plasminogen activator (tPA) (released from vascular endothelial cells following injury) and, to a lesser degree, urokinase (synthesized as a zymogen prourokinase by epithelial cells lining excretory ducts and is activated by proteolytic cleavage) convert plasminogen to plasmin (Zorio et al., 2008).

1.1.5. Physiological inhibitors of blood coagulation

Physiologically, blood coagulation is controlled by: (1) enzymes inactivation through proteinase inhibitors; and (2) cofactors inactivation through enzymes. Among all the proteinase inhibitors, antithrombin-III (AT-III), which belongs to serine proteinase inhibitor (serpin) superfamily, plays an important role. Many blood coagulation enzymes, including thrombin, FIXa, FXa and FXIa are inhibited by AT-

III. The inhibition is mediated through a unique mechanism, which involves the formation of a ternary complex of AT-III, the enzyme and glycosaminoglycans (GAGs; e.g. heparin and heparan sulfate). Like a typical serpin, AT-III irreversibly locks its target proteinases in a covalent acyl-enzyme intermediate for inhibition. The presence of GAGs accelerated the reaction. In contrast to the broad specificity of AT-III, a similar but thrombin-specific serpin, heparin cofactor II (HCII), is also present. A Kunitz-type proteinase inhibitor – tissue factor pathway inhibitor (TFPI) – is responsible for the inhibition of the TF-FVIIa-FXa complex. Proteolytic inactivation of cofactors – FVa and FVIIIa – is achieved through a serine proteinase named activated protein C (APC). Cleavage of FVa and FVIIIa by APC results in a rapid lost of the intrinsic tenase and the prothrombinase complexes and attenuates thrombin production. Interestingly, APC is activated by thrombin associated with membrane bound thrombomodulin (TM). Therefore, by binding to TM, the procoagulant role of thrombin can be switched to an anticoagulant one (Davie et al., 1991).

1.2. THROMBOSIS

As hemostasis is a tightly regulated system, any imbalance could lead to either unclottable blood, resulting in hemorrhagic disorders, or unwanted clot formation, resulting in thrombosis. Thrombosis in particular causes high morbidity and mortality due to vascular occlusion with the consequence of myocardial infarction (MI), stroke, pulmonary embolism (PE), or deep-vein thrombosis (DVT) (Furie and Furie, 2008). Globally, with changing food habits and lifestyles, atherosclerosis and thromboembolic disorders are taking the central stage (Ajjan and Grant, 2006). In the USA alone, it is being estimated that 2 million people develop DVT each year, with 600,000 of them progress to PE, which is fatal in 200,000 patients every year (Gross and Weitz, 2008). Antithrombotic drugs, generally divided into two classes – anticoagulants and antiplatelets, are used to prevent and treat thrombosis. Anticoagulants are effective for initial and long-term management of both the arterial [acute coronary syndrome (ACS) and stroke] and venous [venous thromboembolism (VTE)] thrombosis (Eikelboom and Hirsh, 2007). Antiplatelet drugs are useful for arterial thrombotic events (e.g. in the treatment of ACS and prophylactic management of coronary, cerebral and peripheral artery disease), but is less efficacious than anticoagulants in the prevention of VTE. Such difference is suggested to be due to the underlying mechanisms of diseases in the arterial and venous thrombosis (Wu and Matijevic-Aleksic, 2005). Thus, anticoagulants are crucial for the prevention and treatment of thrombosis.

1.3. CURRENT ANTICOAGULANTS

1.3.1. Heparin

Heparin and vitamin K antagonists (such as warfarin) are the cornerstones of anticoagulation therapy. Unfortunately, both classes of drugs have well-documented limitations such as a narrow therapeutic window and highly variable dose-response. Unfractionated heparin (UFH) is a heterogenous mixture of polysaccharide chains of different molecular sizes (3 to 50 kDa) that binds to AT-III in the blood to facilitate the inhibition of thrombin and FXa by AT-III. Unfractionated heparin also binds to plasma proteins, resulting in highly variable pharmacokinetics. In addition, UFH also induces an immune response called heparin-induced thrombocytopenia (HIT). The recent introduction of low-molecular-weight heparin (LMWH, 3 – 4 kDa) and fondaparinux (1728 Da) that mainly inhibit FXa through AT-III seems to have overcome some of the UFH problems. Plasma proteins binding and incidence of HIT are largely reduced although other difficulties, such as the need for injection and the possibility of HIT, persist (Marder et al., 2004; Wu and Matijevic-Aleksic, 2005; Gross and Weitz, 2008).

1.3.2. Vitamin K antagonists

The coumarin family of Vitamin K antagonists (most commonly warfarin), inhibit vitamin K-dependent γ-carboxylation of FII (prothrombin), FVII, FIX, FX (all are procoagulants), protein C and protein S (both are physiological anticoagulants), impairing their activity. Despite being orally available, warfarin is associated with a long list of disadvantages. It has a slow onset, narrow and highly variable therapeutic dosages and paradoxical hypercoagulability. All these limitations made frequent

coagulation monitoring mandatory, increasing both patient compliance issues and cost of healthcare (Marder et al., 2004; Wu and Matijevic-Aleksic, 2005; Gross and Weitz, 2008).

1.3.3. Direct thrombin inhibitors

Limitations of heparin and warfarin drive the continual and intense efforts to develop new, efficacious and safe anticoagulants, especially those targeting specific coagulation factors (Gross and Weitz, 2008). Some of these leading agents, such as hirudin, bivalirudin, argatroban and dabigatran etexilate, are currently in the market. They are all specific and direct thrombin inhibitors. Hirudin, originally isolated from the medicinal leech *Hirudo medicinalis,* is a 65-residue protein. Recombinant hirudin is approved for the treatment in patients with HIT and thrombosis prophylaxis after major orthopedic surgery. There are a few major drawbacks (includes risk of bleeding, pharmacokinetics that depend on renal function, lack of antidote, immunogenicity and rebound hypercoagulability) associated with the recombinant hirudin. This has rendered the use of the agent largely limited as heparin replacement in patients with HIT (Greinacher and Warkentin, 2008). Bivalirudin is a 20-residue peptide designed based on the hirudin structure and is indicated for invasive cardiology particularly percutaneous coronary intervention (PCI). Unlike hirudin, bivalirudin is eliminated by a combination of proteolytic and renal routes and has negligible immunogenic potential. Compared to hirudin and argatroban, bivalirudin is more widely used. It is gaining more clinical applications for both arterial (e.g. ACS, MI) and venous (HIT) thrombotic events (Warkentin et al., 2008). Argatroban is a small molecule inhibiting the thrombin active site. Clinical usage of argatroban is largely limited to HIT (Yeh and Jang, 2006). Dabigatran etexilate is the latest anticoagulant to reach the market. It

was approved by European Commission in March 2008 for the prevention of venous thromboembolic events in patients who have undergone total hip- or knee-replacement surgery. It is the second orally available direct thrombin inhibitor to gain approval for clinical use, the first being ximelagatran. However, ximelagatran was withdrawn from the market in February 2006 due to concerns in causing liver toxicity. Unlike warfarin, coagulation monitoring is not required for the use of dabigatran etexilate (Eriksson et al., 2008). It is difficult to predict at this point whether dabigatran etexilate will eventually replace warfarin but the complicated nature and clinical settings of thrombosis (e.g. arterial vs. venous thrombosis, acute vs. long term management, thrombosis in pregnant, nursing, renal-impaired or cancer patients) definitely called for more new and safe anticoagulants with different pharmacological and pharmacokinetic properties. Thus, the search for new lead compounds for development of anticoagulants is still very relevant.

1.4. HEMATOPHAGOUS ANIMALS

To search for new lead molecules, extensive research is focused on isolating and characterizing highly specific anticoagulants from blood-feeding (hematophagous) animals. The success of recombinant hirudin, and to a greater extent bivalirudin, demonstrates the utility of these natural products in drug design. Hematophagous animals consist mainly of arthropods in the orders of Ixodida (Ixodidae – hard ticks; Argasidae – soft ticks), Diptera (Culicidae – mosquitoes; Ceratopogonidae – biting midges; Tabanidae – horseflies; Glossinidae – tsetseflies; Simuliidae – blackflies; Phlebotominae – sandflies), Hemiptera (Triatominae – kissing bugs), Phthiraptera (Anoplura – sucking lice) and Siphonaptera (fleas), as well as some annelids in the subclass of Hirudinae (leeches), parasitic nematodes such as hookworms, and even mammals (vampire bats). Physiologically, the duration (e.g. seconds in mosquitoes to months in hookworm), behavior (obligatory or facultative) and mechanisms (e.g. pool-feeding/telmophages in ticks or capillary-feeding/solenophages in mosquitoes) of their blood-feeding habits differ. However, they all face the common physical, mechanical and chemical defenses of their hosts, including the skin and vessel walls, and the hemostatic, inflammatory and immunological responses. In order to obtain the enormous amount of blood required (relative to their body weight), it is essential for hematophagous animals to overcome these barriers with potent pharmacological agents that are capable of attenuating these physiological responses of their hosts (Ribeiro, 1995; Ribeiro and Francischetti, 2003). These agents include vasodilators, anticoagulants, antiplatelets, immunosuppressors and anti-inflammatory compounds (Ribeiro, 1995; Salzet, 2001; Ribeiro and Francischetti, 2003; Champagne, 2004; Hovius et al., 2008).

1.5. EXOGENOUS ANTICOAGULANTS FROM HEMATOPHAGOUS ANIMALS

Over the years, a large number of exogenous anticoagulants from hematophagous animals have been identified, although not many of them have been characterized in detail (Salzet, 2001; Champagne, 2004). These anticoagulants target blood coagulation proteinases to prevent clot formation during their ingestion and digestion of blood meals. Unlike physiological inhibitors of blood coagulation proteinases which mainly comprise two groups (serpin and Kunitz), enormous molecular diversity can be observed in the exogenous anticoagulants from hematophagous animals. Cataloging this vast amount of information is important. Here, an overview on the structure, function and mechanism of exogenous anticoagulants from hematophagous animals is provided to help rationalizing the molecular diversity in this group of proteins. Based on the mechanism of action, these exogenous anticoagulants from hematophagous animals can be broadly classified as: (1) thrombin inhibitors (Table 1.1); (2) FXa inhibitors (Table 2.1); (3) extrinsic tenase complex inhibitors (Table 3.1); (4) intrinsic tenase complex inhibitors (Table 4.1); and (5) contact system proteins inhibitors (Table 5.1). The tables provided a comprehensive list of these anticoagulants as some of the molecules are not discussed in the text due to limitation in writing space.

1.5.1. Thrombin inhibitors (Table 1.1)

1.5.1.1. Hirudin

The most well-known example of thrombin inhibitor, hirudin, was isolated more than 50 years ago from the peripharyngeal glands of the medicinal leech *Hirudo*

TABLE 1.1

Thrombin inhibitors from hematophagous animals

THROMBIN INHIBITORS

	Class	Structure	Mechanism	Example	Species	Reference
1.	Hirudin-like inhibitors	• Single domain of ~ 7 kDa • N-terminal globular core stabilized by 3 disulfide bridges • C-terminal long, extended tail	• Fast, tight-binding, competitive inhibition • N-terminus inhibits active site non-canonically • C-terminus binds to exosite-I	Hirudin Bufrudin Hirullin	*Hirudo medicinalis* *Hirudinaria manillensis* *Hirudinaria manillensis*	(Markwardt, 1994) (Scacheri et al., 1993) (Steiner et al., 1992)
			• Similar to hirudin but C-terminus binds to exosite-II	Haemadin	*Haemadipsa sylvestris*	(Strube et al., 1993) (Richardson et al., 2000)
2.	Kunitz-type proteinase inhibitors	• Single Kunitz domain is ~ 7 kDa • Two tandem Kunitz domains • Soft ticks inhibitors: distorted inhibition loop, lack of basic P1 residue • Hard ticks inhibitors: typical inhibition loop, with basic P1 residue	• Slow, tight-binding, competitive inhibition • N-terminal Kunitz domain inhibits active site non-canonically • C-terminal Kunitz domain binds to exosite-I	Ornithodorin Savignin Monobin	*Ornithodoros moubata* *Ornithodoros savignyi* *Argas monolakensis*	(van de et al., 1996) (Nienaber et al., 1999; Mans et al., 2002) (Mans et al., 2008)
				Amblin Boophilin Hemalin	*Amblyomma hebraeum* *Boophilus microplus* *Haemaphysalis longicornis*	(Lai et al., 2004) (Macedo-Ribeiro et al., 2008) (Liao et al., 2008)
3.	Kazal-type proteinase inhibitors	• Single Kazal domain is ~ 6 kDa • Multiple non-classical Kazal domains in tandem • Typically isolated as two tandem domains proteins but cDNA sequence showed multiple-domains precursors	• Slow, tight-binding, competitive inhibition • N-terminal Kazal domain inhibits active site canonically • C-terminal Kazal domain binds to exosite-I	Rhodniin Dipetalogastin Infestin-1-2	*Rhodnius prolixus* *Dipetalogaster maximus* *Triatoma infestans*	(Friedrich et al., 1993; van de et al., 1995) (Mende et al., 1999) (Campos et al., 2002)

4.	Lipocalin family	• Single domain of ~ 16 kDa • Eight-stranded (A-B-C-D-E-F-G-H) β-barrel and a central ligand-binding pocket • Directional inversion in B and C strands compared to typical lipocalin topology	• Binds to exosite-I only	Triabin	*Triatoma pallidipennis*	(Noeske-Jungblut et al., 1995; Fuentes-Prior et al., 1997)
5.	Anophelin & thrombostasin	• Single domain of ~ 7 to 9 kDa • No cysteines • Acidic segment in the middle of the molecule	• Slow, tight-binding, competitive inhibition • Inhibits active site and exosite-I	Anophelin	*Anopheles albimanus*	(Valenzuela et al., 1999)
			• Lack of kinetic information • Inhibits active site • Exosites binding not determined	Thrombostasin	*Haematobia irritans*	(Zhang et al., 2002)
6.	Madanin & chimadanin	• Single domain of ~ 7 kDa • No cysteines • Containing a 11-residues acidic segment in the middle	• Binds to exosite-I only	Madanin 1 & 2	*Haemaphysalis longicornis*	(Iwanaga et al., 2003)
			• Inhibits active site • Exosites binding not determined	Chimadanin	*Haemaphysalis longicornis*	(Nakajima et al., 2006)
7.	Antistasin-like inhibitor	• Cysteine-rich domain of ~ 7 kDa • Containing a 26-residues segment with conserved cysteines and disulfide linkages • Domain typically repeated in tandem	• Inhibits active site • Exosites binding not determined	Theromin	*Theromyzon tessulatum*	(Salzet et al., 2000)
8.	Granulin-like inhibitor	• Single granulin domain is ~ 6 kDa • 12 conserved cysteines and disulfide linkages	• Inhibits active site • Exosites binding not determined	Leech granulin	*Hirudo nipponia*	(Hong and Kang, 1999)

9.	TTI	• Short peptide of ~ 4 kDa • No cysteines	• Inhibits active site • Exosites binding not determined	TTI	*Glossina morsitans morsitans*	(Cappello et al., 1998)
10.	NTI-1	• Short peptide of ~ 3 kDa	• Non-competitively inhibits active site	NTI-1	*Hyalomma dromedarii*	(Ibrahim et al., 2001a)
11.	Microphilins	• Short peptide of ~ 1.7 kDa	• Binds to exosite-I only	Microphilin (2 isoforms)	*Boophilus microplus*	(Ciprandi et al., 2006)
12.	BmAP	• High molecular weight of 60 kDa	• Inhibits active site • Binds to at least one exosite	BmAP	*Boophilus microplus*	(Horn et al., 2000)
13.	BmGTI	• 26 kDa	• Binds to exosite-I only • Also enhances APC activity	BmGTI	*Boophilus microplus*	(Ricci et al., 2007)
14.	Others	• Lack of detailed structural information	• Slow, tight-binding, competitive inhibitor	Americanin (12 – 16 kDa)	*Amblyomma americanum*	(Zhu et al., 1997a)
			• Lack of functional characterization	Calcaratin (14 kDa)	*Boophilus calcaratus*	(Motoyashiki et al., 2003)
				Unnamed (45 kDa)	*Anopheles stephensi*	(Waidhet-Kouadio et al., 1998)
				Tabanin (7 kDa)	*Tabanus bovinus*	(Arocha-Pinango et al., 1999)
				Simulidin (11 kDa)	*Simulium vittatum*	(Abebe et al., 2008)
				Crude extract	17 species of flies (genus: tabanus)	(Kazimirova et al., 2002)
				Crude extract	3 species of mosquitoes (genus: Anopheles)	(Stark and James, 1996)
				Crude extract	*Simulium argus*	(Abebe et al., 1994)
				Crude extract	*Panstrongylus megistus*	(Pereira et al., 1996)

medicinalis. Hirudin is a 65-residue protein (~ 7 kDa) which specifically inhibits thrombin (Markwardt, 1994). Many hirudin isoforms with minor variations in primary structures were subsequently reported (Scharf et al., 1989; Markwardt, 1994). This family of inhibitors was also isolated from other species of leeches (Steiner et al., 1992; Scacheri et al., 1993) (Table 1.1). Hirudin binds thrombin with a K_i value of 22 fM. The Tyr64 of hirudin is sulfated and desulfated hirudin binds to thrombin 10 times weaker, with a K_i of 207 fM (Stone and Hofsteenge, 1986). Hirudin becomes a slow-binding inhibitor at high ionic strength solutions (0.2 and above) (Stone and Hofsteenge, 1986), highlighting the importance of electrostatic interactions between hirudin and thrombin in the complex formation (Myles et al., 2001).

Three-dimensional (3D) structures of hirudin were determined using nuclear magnetic resonance (NMR) spectroscopy (Clore et al., 1987; Haruyama and Wuthrich, 1989) and its structures complexed with thrombin were determined using X-ray crystallography (Rydel et al., 1990; Grutter et al., 1990; Rydel et al., 1991; Vitali et al., 1992; Liu et al., 2007). Hirudin has an N-terminal domain (residues 1 – 48) folded into a globular unit stabilized by three disulfide bridges, and a long C-terminal domain (residues 49 – 65) in an extended conformation (Figure 1.2 A). The first three residues on hirudin N-terminus bind to a hydrophobic pocket at the active site of thrombin in a non-canonical form (ie. in the opposite direction of natural substrates such as fibrinogen), forming a short parallel β-pleated sheet with thrombin Ser214 – Gly216 [chymotrypsinogen numbering system (Bode et al., 1992)]. In contrast, canonical inhibitor runs in an anti-parallel direction with respect to thrombin Ser214 – Gly216 and possesses a basic P1 residue occupies the acidic S1 site [nomenclature: substrate residues are numbered from the P1-P1′ scissile bond toward the N-terminus

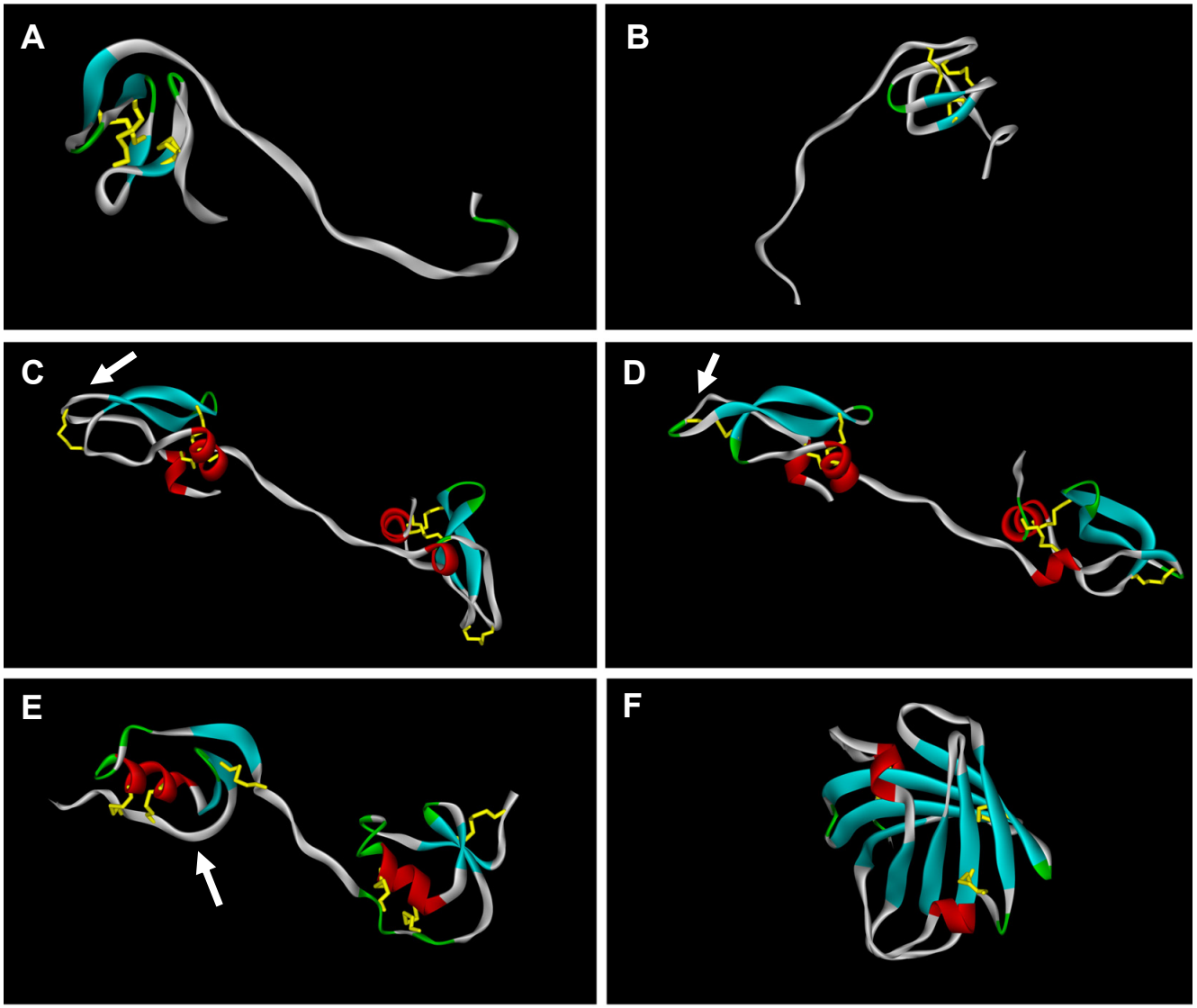

FIGURE 1.2

Thrombin inhibitors from hematophagous animals

(A) Hirudin (PDB: 1HRT): N-terminal core stabilized by three disulfide bridges and a long, extended C-terminal tail

(B) Haemadin (PDB: 1E0F): N-terminal core stabilized by three disulfide bridges and a long, extended C-terminal tail

(C) Boophilin (PDB: 2ODY): two tandem Kunitz domains with normal reactive-site loop (arrow)

(D) Ornithodorin (PDB: 1TOC): two tandem Kunitz domains with distorted reactive-site loop (arrow)

(E) Rhodniin (PDB: 1TBQ): two tandem Kazal domains with typical reactive-site loop (arrow)

(F) Triabin (PDB: 1AVG): eight stranded β-barrel fold

and C-terminus respectively. Corresponding substrate binding pockets on the proteinases are number accordingly with, 'S' replacing 'P' (Schechter and Berger, 1967)]. This primary specificity pocket (S1) on hirudin-bound thrombin is not occupied, differing from those of canonical inhibitors. The N-terminal amino group interacts with thrombin catalytic residues through hydrogen bonds. The C-terminal domain of hirudin is disordered in NMR structures (Clore et al., 1987; Haruyama and Wuthrich, 1989) but binds in ordered, extended conformation to the thrombin exosite-I in crystal structures. The thrombin exosite-I is flanked by two loops (Phe34 – Leu41 and Lys70 – Glu80) that are rich in basic residues (Rydel et al., 1991). The hirudin C-terminus, rich in acidic residues, is inserted into exosite-I through specific electrostatic interactions. In addition, hydrophobic contacts also make significant contributions to the interaction (Rydel et al., 1990; Grutter et al., 1990; Rydel et al., 1991). The specific, tight-binding nature of hirudin is thus a result of the extensive contacts in both the active site and exosite-I of thrombin (Figure 1.3 A).

1.5.1.2. Haemadin

Haemadin was isolated from Indian leech *Haemadipsa sylvestris* (Strube et al., 1993). Although haemadin and hirudin share low sequence similarity, they exhibit a common three dimensional fold (Richardson et al., 2000). Haemadin is slightly smaller than hirudin with 57 residues. Haemadin is a slow and tight-binding inhibitor of thrombin, with K_i = 210 fM (Strube et al., 1993). Similar to hirudin, haemadin has a globular N-terminal core stabilized by three disulfide bridges with an extended, acidic C-terminal tail (Figure 1.2 B). The first three N-terminal residues bind to the active site of thrombin non-canonically, again similar to the C-terminus of hirudin. Interestingly, the haemadin acidic C-terminus binds to the thrombin exosite-II instead

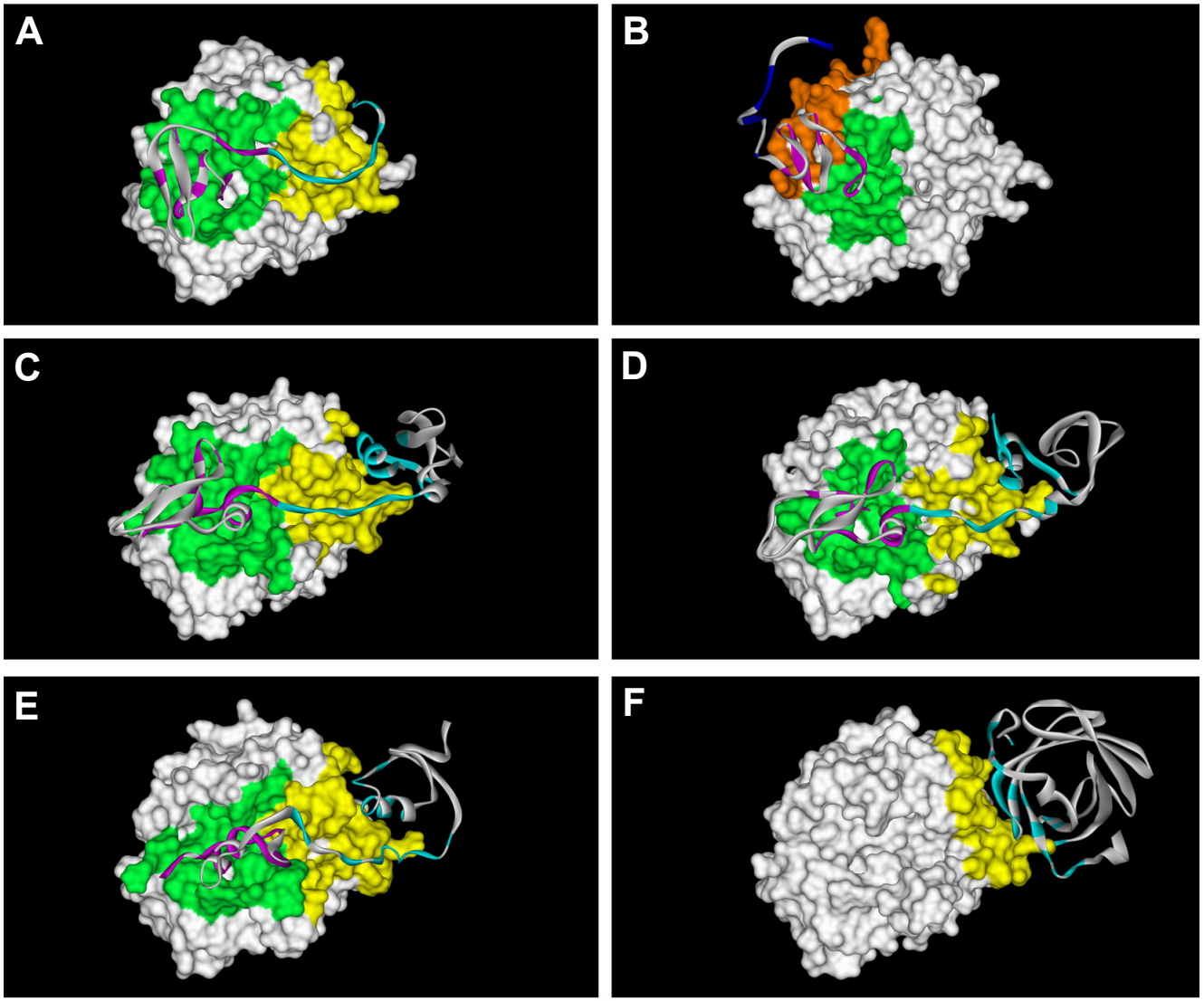

FIGURE 1.3

Thrombin-inhibitors interaction sites

Interface residues between thrombin and its inhibitors are mapped. On thrombin, active site surfaces are colored green, exosite-I surfaces are colored yellow and exosite-II surfaces are colored orange. On inhibitors, active site targeting residues are colored magenta, exosite-I targeting residues are colored cyan and exosite-II targeting residues are colored blue.

(A) Hirudin-thrombin complex (PDB: 1HRT)

(B) Haemadin-thrombin complex (PDB: 1E0F)

(D) Boophilin-thrombin complex (PDB: 2ODY)

(C) Ornithodorin-thrombin complex (PDB: 1TOC)

(E) Rhodniin-thrombin complex (PDB: 1TBQ)

(F) Triabin-thrombin complex (PDB: 1AVG)

of exosite-I (Figure 1.3 B) (Richardson et al., 2000). Thrombin exosite-II is a highly basic surface (more so than exosite-I), situated on the opposite side of exosite-I. Exosite-II is also the heparin-binding site of thrombin (Huntington, 2005). The distinct surfaces targeted by haemadin (exosite-II) and hirudin (exosite-I) despite overall similarity in their 3D structures makes an interesting comparison of the molecular diversity observed in the anticoagulants from hematophagous animals: both are peptide inhibitors of thrombin from leeches, but each targets distinct sites.

1.5.1.3. Kunitz-type proteinase inhibitors

The Kunitz-type serine proteinase inhibitors, also commonly known as bovine pancreatic trypsin inhibitor (BPTI), are one of the most extensively studied families of serine proteinase inhibitors (Laskowski, Jr. and Kato, 1980). A typical Kunitz-type domain has a reactive-site loop which binds and runs antiparallel to the enzyme active site residues Ser214 – Gly216. The basic P1 residue of the inhibitor binds to the S1 specificity pocket of the enzyme, similar to the natural substrates (canonical inhibition) (Bode and Huber, 1992). This structural fold is commonly found in anticoagulants from ticks. Kunitz-type inhibitors identified from two separate families of ticks (Ixodidae – hard ticks and Argasidae – soft ticks) appear to belong to two different protein subclasses, based on their sequences. This provides evidence for the independent evolution of anticoagulant adaptations of blood-feeding behaviors in the hard and soft ticks (Mans et al., 2002b).

Comparing sequence only, Kunitz-type thrombin inhibitors from hard ticks have a reactive-site loop with normal topology (Figure 1.2 C). Molecules in this group include amblin from *Amblyomma hebraeum* (Lai et al., 2004), boophilin from

Boophilus microplus (Macedo-Ribeiro et al., 2008) and hemalin from *Haemaphysalis longicornis* (Liao et al., 2008). These molecules have two tandem Kunitz domains. They typically have a lower affinity for thrombin [amblin K_i = 20 nM (Lai et al., 2004), boophilin K_i = 1.8 nM (Macedo-Ribeiro et al., 2008)] compared to the soft ticks Kunitz-type inhibitors. These molecules were initially thought to bind to the active site of thrombin with their first Kunitz domain in a canonical fashion. However, the recently reported crystal structure of boophilin-thrombin complex revealed that boophilin first Kunitz domain binds to the active site of thrombin non-canonically despite the presence of a reactive-site loop with normal topology (Figure 1.3 C) (Macedo-Ribeiro et al., 2008).

Kunitz-type thrombin inhibitors from soft ticks include ornithodorin from *Ornithodoros moubata* (van de et al., 1996), savignin from *Ornithodoros savignyi* (Nienaber et al., 1999; Mans et al., 2002a) and monobin from *Argas monolakensis* (Mans et al., 2008). Kinetically, savignin (K_i = 4.89 pM) (Nienaber et al., 1999) and monobin (K_i = 7 pM) (Mans et al., 2008) are slow, tight-binding, competitive inhibitors of thrombin. They are atypical Kunitz-type inhibitors as they have two highly distorted tandem Kunitz domains (Figure 1.2 D). This distortion is due to the displacement of a disulfide bridge, and the two domains are connected by an extended linker peptide. In addition to the distorted reactive-site loop, there is also a lack of basic P1 residue. As a result, this group of molecules non-canonically inhibit thrombin, as shown by the crystal structure of the thrombin-ornithodorin (van de et al., 1996). The first of the two Kunitz domains of ornithodorin binds to the thrombin active site. The linker peptide and the second Kunitz domain bind to the thrombin exosite-I (Figure 1.3 D). The distorted reactive-site loop is not in contact with

thrombin. Instead, the first three residues of the N-terminal Kunitz domain run parallel to thrombin Ser214 – Gly219, making several hydrophobic contacts with the thrombin active site, similar to hirudin. The other residues in the first domain of ornithodorin also make contacts with the thrombin 60-loop (Leu59 – Asn62) and autolysis loop (Leu144 – Gly150) near the active site. Interactions between the exosite-I of thrombin and the second Kunitz domain of ornithodorin are mainly mediated through ionic pairings and are strengthened by hydrophobic interactions (van de et al., 1996).

1.5.1.4. Kazal-type proteinase inhibitors

One other commonly encountered serine proteinase inhibitor – the Kazal-type inhibitor (Laskowski, Jr. and Kato, 1980) – is also utilized as the structural scaffold for exogenous anticoagulants. Kazal-type thrombin inhibitors include rhodniin from *Rhodnius prolixus* (Friedrich et al., 1993; van de et al., 1995), dipetalogastin from *Dipetalogaster maximus* (Mende et al., 1999) and infestin from *Triatoma infestans* (Campos et al., 2002). Typically, these molecules consist of multiple non-classical Kazal domains and bind to thrombin in a slow, tight-binding, competitive mode. The first and second cysteines of non-classical Kazal domains are spaced by one or two residues. In contrast, seven or eight spacer residues are found in classical Kazal domains. The K_i for rhodniin, dipetalogastin (domain 3-4) and infestin (domain 1-2) are 0.2 pM (Friedrich et al., 1993), 0.05 pM (Mende et al., 1999) and 25 pM (Campos et al., 2002), respectively. Interestingly, these molecules are typically isolated as proteins with two tandem domains (Figure 1.2 E), although cDNA cloned are usually translated into additional domains [rhodniin – three domains (Friedrich et al., 1993); dipetalogastin – six domains (Mende et al., 1999); infestin – seven domains (Lovato

et al., 2006)]. The crystal structure of the rhodniin–thrombin complex showed a different binding mechanism than the Kunitz-type inhibitors. In Kazal-type inhibitors, the first domain binds to the active site of thrombin canonically. The second Kazal domain (along with inter-domains linker) binds to the exosite-I of thrombin. The reactive-site loop of rhodniin has a P1 His. In contrast to the non-canonical inhibition of Kunitz inhibitors, the imidazole side chain of the P1 His is inserted into the S1 pocket of thrombin. The thrombin 60- and autolysis loops also make contacts with the first Kazal domain. Although the second Kazal domain binds to the exosite-I of thrombin, the interaction appears to exclude the reactive-site loop (Figure 1.3 E). Only two pairs of residues directly form salt bridges, but the second Kazal domain and the linker peptide have an overall positive charge which might help to target the molecule to the negatively charged surface on exosite-I (van de et al., 1995).

The roles of the additional domains revealed by cDNA of Kazal inhibitors were investigated in infestin. Combinations of different domains showed differential specificities towards blood coagulation proteinases (Figure 1.4). Domain 1-2 (Campos et al., 2002) is most specific for thrombin, while the presence of domain 4 (in infestin domains 1-4, 3-4 and 4) (Campos et al., 2002; Campos et al., 2004) switches the specificity towards FXIIa. It should also be noted that the post-translational processing mechanisms of these molecules are yet to be fully elucidated. However, the infestin domains are postulated to be processed between Ala-Glu, releasing single or tandem domains (Lovato et al., 2006). For example, proteins representing domains 1R, 1-2 and 3-4 have the Ala-Glu dipeptide at their boundaries and were all isolated from the anterior midgut homogenate of *Triatoma infestans*.

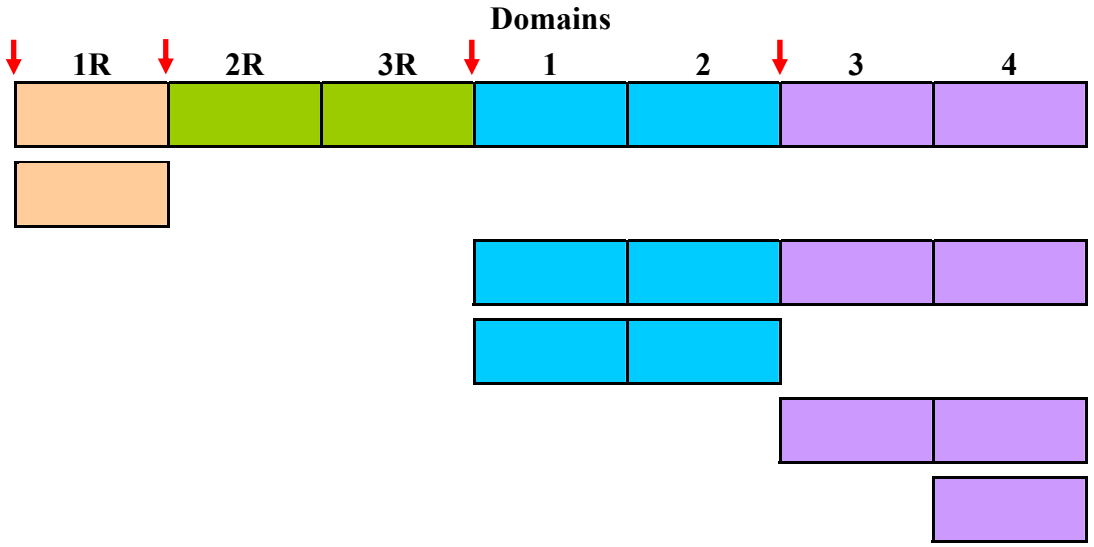

	K_i (nM)				
Trypsin	Thrombin	FXa	FXIIa	Plasmin
		ND		
		NI		
5.2	0.8	59.2	*0.078*	1.1
3.1	*0.025*	NI	NI	NI
3.3	NI	18.2	*0.067*	0.4
11	NI	53	*0.128*	2.1

FIGURE 1.4

Differential specificities showed by different combinations of infestin domains

Kazal-type thrombin inhibitor infestin cDNA is translated into seven tandem domains. Putative site of post-translational cleavage is between Ala-Glu that are present in between domain 1R and signal peptide, domain 1R and 2R, domain 3R and 1, domain 2 and 3 (indicated by red arrow). Matured proteins representing domains 1R, 1-2 and 3-4 were isolated. Combinations of different domains showed differential specificities towards serine proteinases (italic K_i indicates that the binding to that enzyme is the strongest). Domain 1R is not an anticoagulant; instead it inhibits neutrophil elatase, subtilisin A and chymotrypsin. The presence of domain 4 appeared to be responsible for FXIIa specificity. Domain 1-2 is specific for thrombin.

ND: not determined

NI: non inhibitory

1.5.1.5. Lipocalin family

The kissing bug *Triatoma pallidipennis* utilizes the lipocalin fold as a scaffold for anticoagulants. Although the lipocalin family of proteins has low sequence similarity, they all share a characteristic fold of an eight-stranded (A-B-C-D-E-F-G-H), anti-parallel β-barrel and a central ligand-binding pocket. This family of proteins display a wide variety of functions (Flower, 1996). Triabin, isolated from *Triatoma pallidipennis* (Noeske-Jungblut et al., 1995) is the only thrombin inhibitor belonging to this family. Triabin binds to the thrombin exosite-I (but not to the active site) in an equimolar ratio, with a K_i of 3 pM (Noeske-Jungblut et al., 1995). Structurally, triabin deviates slightly from the typical lipocalin topology due to a directional inversion of the B and C strands, creating an up-up-down-down topology in the first four strands of the β-barrel (Figure 1.2 F). In contrast to the hirudin C-terminus, which is inserted into a deep cleft formed by the surface loops in exosite-I of thrombin, the β-barrel structure interacts with a relatively flat surface near the end of the cleft. The contacts are mainly mediated through hydrophobic interactions, covering a larger area of exosite-I (Figure 1.3 F) (Fuentes-Prior et al., 1997).

1.5.1.6. Anophelin

Isolated and cloned from the salivary glands of the mosquito *Anopheles albimanus*, anophelin, a 6.5-kDa protein, belongs to a unique class of thrombin inhibitors (Valenzuela et al., 1999). Anophelin is a slow, tight-binding, competitive inhibitor of thrombin with a K_i of 5.87 pM. Like many other exogenous thrombin inhibitors, anophelin binds to both the active site and exosite-I of thrombin (Francischetti et al., 1999). However, anophelin has a unique amino acid sequence which does not show significant homology to other known proteins (except

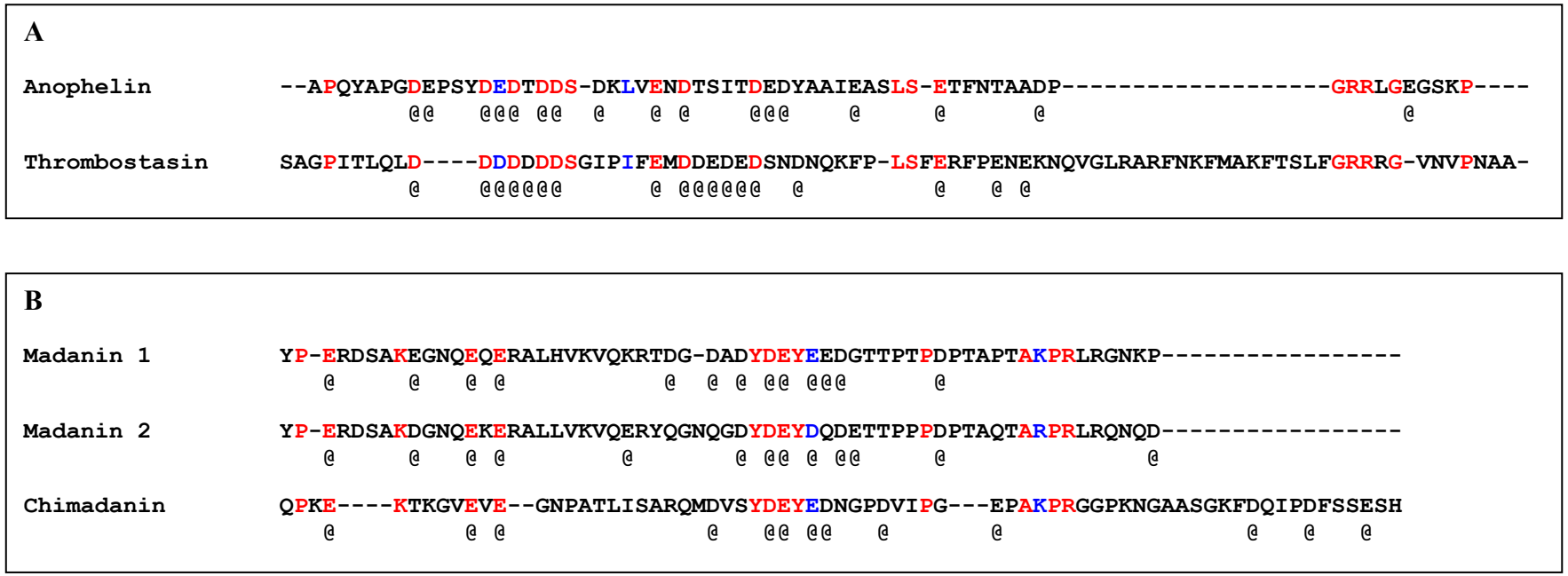

FIGURE 1.5

Sequences of anophelin, thrombostasin, madanins and chimadanin

(A) Sequence alignment of anophelin and thrombostasin showed limited identities. Identical residues are colored red, similar residues are colored blue. Both proteins are rich in acidic residues, marked by the symbol '@'. Identities between the two proteins concentrated in the acidic segment in the middle of the molecules and a short basic segment in the C-terminus.

(B) Sequence alignment of madanins and chimadanin also showed limited identities among each other. Identical residues are colored red, similar residues are colored blue. Similar to anophelin and thrombostasin, the proteins are rich in acidic residues, marked by the symbol '@'. The proteins also bear the similar arrangement of residues (a cluster of acidic residues in the middle along with a short segment of basic residues near C-terminus). Chimadanin has an extension on C-terminus compared to madanins.

thrombostasin, which will be discussed below). Significantly, anophelin contains no cysteines but is rich in acidic residues in the middle segment (Figure 1.5 A) (Valenzuela et al., 1999). The acidic site could target the thrombin exosite-I, similar to the action of hirudin C-terminus. However, the disulfides-stabilized hirudin/Kunitz/Kazal-type domains are not present in anophelin (due to the lack of cysteines), suggesting that a distinct structural feature is used to inhibit the thrombin active site.

1.5.1.7. Thrombostasin

Thrombostasin was isolated from the horn fly *Haematobia irritans*. It is an 81-residue protein that inhibits the thrombin active site. The primary sequence of thrombostasin contains no cysteines and shows very limited homology to anophelin. Interestingly, like anophelin, there appears to be a clustering effect of acidic residues in the middle of the molecule (all 18 acidic residues fall within positions 10 to 48) and a short segment of basic residues near the C-terminus (Figure 1.5 A) (Zhang et al., 2002).

1.5.1.8. Madanins and chimadanin

Madanins (isoforms 1 and 2) (Iwanaga et al., 2003) and chimadanin (Nakajima et al., 2006) are two groups of 7-kDa proteins identified in the salivary glands cDNA libraries of the hard tick *Haemaphysalis longicornis*. Recombinant madanins bind only to the thrombin exosite-I while not affecting thrombin amidolytic activity (commonly used to probe the function of thrombin active site) (Iwanaga et al., 2003). In contrast, recombinant chimadanin inhibits the function of thrombin active site: however, the binding to either exosites was not investigated (Nakajima et al.,

2006). The translated amino acid sequence of madanins and chimadanin are without cysteines and show low similarity with each other, except for an acidic segment in the middle of the molecule and a basic segment near the C-terminus (Figure 1.5 B). Neither proteins show significant homology to other proteins. However, a similar arrangement of residues (a cluster of acidic residues in the middle and a short segment of basic residues near the C-terminus) is seen in both proteins and is also observed in anophelin and thrombostasin. The C-terminus of chimadanin is extended, compared to madanins.

1.5.1.9. Antistasin-like inhibitor

In addition to the hirudin-like fold, leeches also utilize the antistasin-like scaffold to derive thrombin inhibitors [antistasin is a FXa inhibitor (Tuszynski et al., 1987; Nutt et al., 1988), see below for details]. Theromin, an antistasin-like thrombin inhibitor isolated from *Theromyzon tessulatum* inhibits the thrombin active site with a K_i of 12 fM (Salzet et al., 2000). Overall sequence homology between theromin and antistasin is low, but crucially, a 26-residue segment with conserved (six) cysteines and disulfide pattern is present in both. Antistasin is a single chain, 119-residue protein with two tandem repeats (Tuszynski et al., 1987; Nutt et al., 1988), while theromin is a disulfide-linked homodimer of 67-residue chains (proteolytically processed tandem repeats).

1.5.1.10. Tsetse thrombin inhibitor (TTI)

A potent, specific and short thrombin inhibiting peptide was isolated from salivary gland extract (SGE) of the tsetse fly *Glossina morsitans morsitans* and named tsetse thrombin inhibitor (TTI). TTI has 32 residues and contains no cysteines based

on the translated sequence of cloned cDNA. Native TTI potently inhibits thrombin amidolytic activity with a K_i of 584 fM. However, chemically and recombinantly synthesized TTI are substantially less active, with K_i of 166 nM and 150 nM, respectively. The differences in K_i values might be due to post-translational modifications in the native protein (Cappello et al., 1998).

1.5.1.11. Nymphal thrombin inhibitor-1 (NTI-1)

Nymphal thrombin inhibitor-1, isolated from the nymphs of the camel tick *Hyalomma dromedarii* is a unique thrombin inhibitor. The size of the molecule is small (3.2 kDa), similar to TTI but mechanistically it is unique. The peptide non-competitively inhibits thrombin active site with a K_i of 11.7 μM but it also inhibits FXa (5-fold less potent compared to thrombin inhibition). Although the affinity to thrombin is relatively weak compared to other thrombin inhibitors, the non-competitive mode of inhibition for the active site could be an interesting subject for studies (Ibrahim et al., 2001a).

1.5.2. FXa inhibitors (Table 1.2)

1.5.2.1. Kunitz-type proteinase inhibitors

One of the main classes of FXa inhibitors is the atypical, non-canonical Kunitz-type inhibitors from the soft ticks including tick anticoagulant peptide (TAP) from *Ornithodoros moubata* (Waxman et al., 1990) and FXa-inhibitor (FXaI) from *Ornithodoros savignyi* (Gaspar et al., 1996). In contrast to the tandem Kunitz domains arrangement observed in Kunitz-type thrombin inhibitors, TAP and FXaI contain a single domain (Figure 1.6 A). Kinetically, both are slow, tight-binding, competitive inhibitors of FXa. Native and recombinant TAP have K_i values of 0.588 nM

TABLE 1.2

FXa inhibitors from hematophagous animals

FXa INHIBITORS

	Class	Structure	Mechanism	Example	Species	Reference
1.	Kunitz-type proteinase inhibitors	• Single Kunitz domain of ~ 6 to 7 kDa • Distorted inhibition loop, lack of basic P1 residue	• Slow, tight-binding, competitive inhibition • N-terminal Kunitz domain inhibits active site non-canonically • C-terminal Kunitz domain binds to exosite-I	TAP FXaI	*Ornithodoros moubata* *Ornithodoros savignyi*	(Waxman et al., 1990; Wei et al., 1998) (Gaspar et al., 1996)
2.	Ascaris-type proteinase inhibitors	• Single domain of ~ 9 to 11 kDa • 10 conserved cysteine residues and disulfide linkages • Has proteinase inhibition loop with basic P1 residue	• Competitive inhibition • Inhibits active site canonically	NAP5 (AcAP5) NAP6 (AcAP6)	*Ancyclostoma canium* *Ancyclostoma canium*	(Cappello et al., 1995; Stassens et al., 1996; Mieszczanek et al., 2004) (Cappello et al., 1995; Stassens et al., 1996; Mieszczanek et al., 2004)
			• Two-site partial non-competitive inhibition • Inhibits active site • Needs an exosite for full active site inhibition • Also inhibits extrinsic tenase complex	AceAP1	*Ancyclostoma ceylanicum*	(Harrison et al., 2002)
3.	Antistasin-like inhibitors	• Cysteine-rich domain of ~ 7 kDa • Containing a 26-residues segment with conserved cysteines and disulfide linkages • Domain typically repeated in	• Inhibits active site canonically • Interactions with exosites not reported	Antistasin Ghilanten Therostasin	*Haementeria officinalis* *Haementeria ghilianii* *Theromyzon tessulatum*	(Tuszynski et al., 1987; Nutt et al., 1988) (Brankamp et al., 1990) (Chopin et al., 2000)

		tandem (except therostasin)				
4.	Atypical serpins	• Single domain of ~ 45 – 55 kDa • Three β-sheets and eight or nine α-helices • Typically glycosylated • Shorter reactive center loop and different hinge residues compared to typically serpins	• Mechanistically different from typical serpins • Only example so far showed reversible, non-competitive inhibition • Post-translational modification important for activity	AFXa	*Aedes aegypti*	(Stark and James, 1995; Otlewski et al., 2005)
5.	Salp family	• ~ 9 to 14 kDa	• Recombinant salp14 inhibits FXa active site • Recombinant salp9pac is not active	Salp14 Salp9pac	*Ixodes scapularis* *Ixodes scapularis*	(Narasimhan et al., 2002) (Narasimhan et al., 2002)
6.	Hemerythrin family	• Single domain of ~ 15 kDa • Has a topology consist of four helix bundle	• Inhibits active site • Maximal inhibitory activity at low concentration (<1 mM) of $CaCl_2$	Lefaxin	*Haementeria depressa*	(Faria et al., 1999)
7.	Draculin	• Glycoprotein of ~ 90 kDa	• Slow, non-competitive, tight binding inhibitor of active site	Draculin	*Desmodus rotundus*	(Fernandez et al., 1999)
8.	Uncompetitive inhibitors from Hyalomma	• ~ 15 to 17 kDa	• Uncompetitive inhibitors of active site	Unnamed Unnamed	*Hyalomma truncatum* *Hyalomma dromedarii*	(Joubert et al., 1995) (Ibrahim et al., 2001b)
9.	Others	• Lack of detailed structural information	• Lack of functional characterization	Unnamed (16 kDa) Unnamed (28 kDa) Unnamed (18 kDa) Unnamed	*Amblyomma americanum* *Culicoides variipennis sonorensis* *Simulium vittatum* *Haementeria ghilianii*	(Zhu et al., 1997b) (Perez de Leon et al., 1998) (Jacobs et al., 1990) (Condra et al., 1989)

	Crude extract	3 species of mosquitoes	(Stark and James, 1996)
	Crude extract	3 species of black flies	(Abebe et al., 1994)
• Inhibiting prothrombinase complex by attenuating FV activity	Unnamed	*Simulium vittatum*	(Abebe et al., 1996)
	Crude extract	*Dermacentor andersoni*	(Gordon and Allen, 1991)
	Crude extract	*Triatoma infestans*	(Pereira et al., 1996)
• Inhibiting prothrombinase complex by unknown mechanism	Unnamed (65 kDa)	*Rhipicephalus appendiculatus*	(Limo et al., 1991)

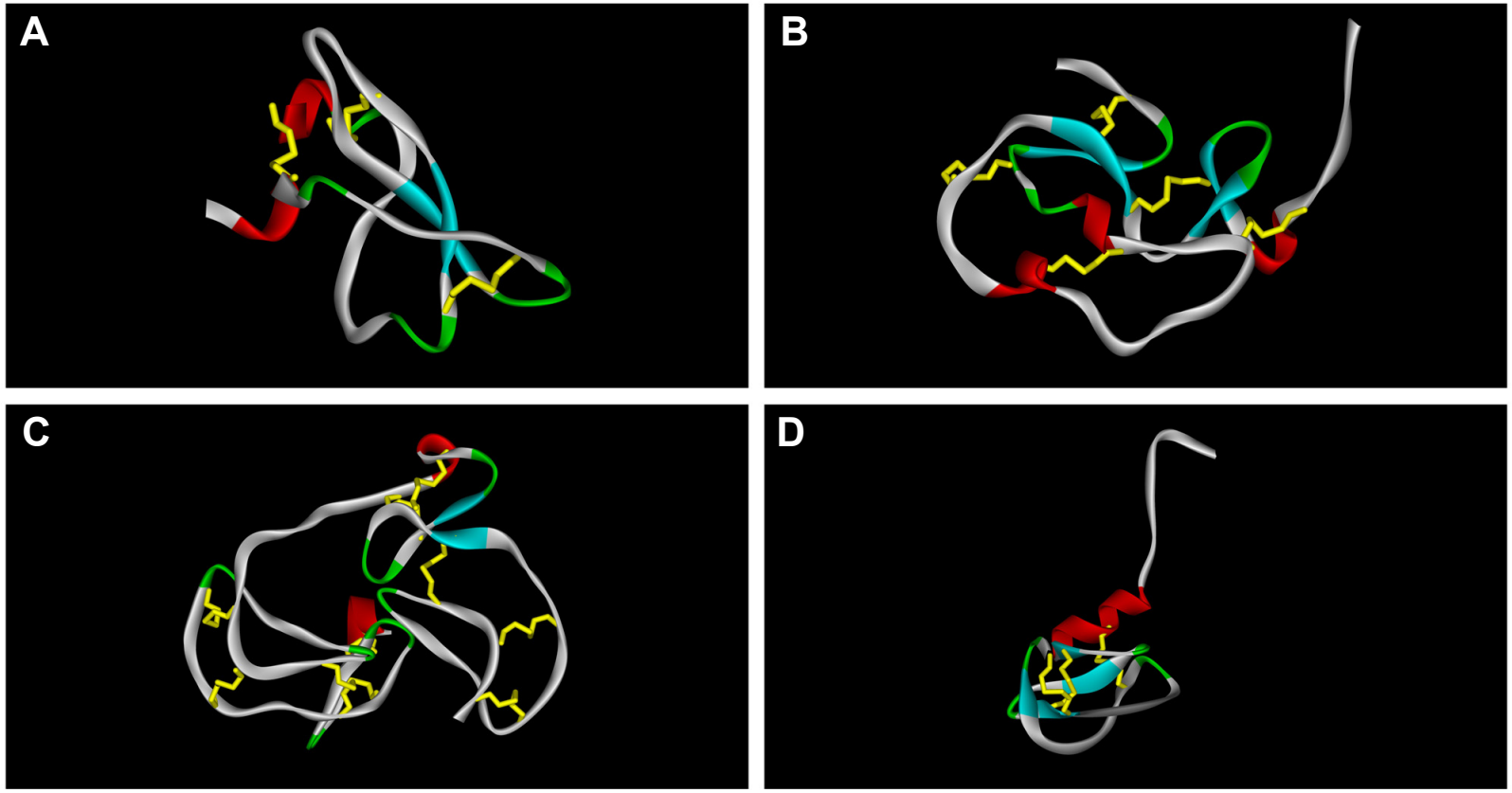

FIGURE 1.6

FXa and extrinsic tenase complex inhibitors from hematophagous animals

(A) FXa inhibitor TAP (PDB: 1KIG): single Kunitz-type domain with distorted reactive-site loop

(B) FXa inhibitor NAP5 (PDB: 2P3F): single Ascaris-type domain

(C) FXa inhibitor antistasin (PDB: 1SKZ): two tandem antistasin-like domains in antistasin

(D) extrinsic tenase complex inhibitor NAPc2 (PDB: 2H9E): single Ascaris-type domain

(Waxman et al., 1990) and 0.18 nM, respectively (Neeper et al., 1990) while native FXaI has a K_i of 0.83 nM (Gaspar et al., 1996). The crystal structure of TAP in complex with FXa (Wei et al., 1998) shows a similar non-canonical mode of active site inhibition as observed in the thrombin-hirudin (Rydel et al., 1990; Grutter et al., 1990; Rydel et al., 1991) and thrombin-ornithodorin interactions (van de et al., 1996). The first three N-terminal residues make multiple important contacts with the FXa active site and catalytic triad. In addition, TAP interacts with some of the residues on the Na^+-binding (Arg222 & Lys224) and autolysis loops (Arg143, Glu146, Lys147 and Arg149) of FXa (Figure 1.7 A) (Wei et al., 1998).

1.5.2.2. Ascaris-type proteinase inhibitors

The Ascaris family of serine proteinase inhibitors are characterized by 10 cysteine residues forming a unique disulfide pattern in a single domain (Grutter, 1994). A group of Ascaris-type FXa inhibitors (75 – 84 residues) were identified in the hookworms *Ancyclostoma caninum* (NAP5/6 or AcAP5/6 and NAPc2/3/4 or AcAPc2/3/4) (Cappello et al., 1995; Stassens et al., 1996; Mieszczanek et al., 2004b) and *Ancyclostoma ceylanicum* (AceAP1) (Harrison et al., 2002). NAP5/6 (Stassens et al., 1996) and AceAP1 (Harrison et al., 2002) inhibit the FXa active site, whereas NAPc2/3/4 binds to an FXa exosite (Stassens et al., 1996; Mieszczanek et al., 2004b; Murakami et al., 2007). Binding of NAPc2/3/4 to FXa facilitates their inhibition of the FVIIa-TF complex (Stassens et al., 1996; Mieszczanek et al., 2004b), thus are considered as extrinsic tenase complex inhibitors (see below for details). Detailed studies on NAP5 showed that it inhibits the FXa active site function competitively, with a K_i of 43 pM (Stassens et al., 1996). NAP5 (Figure 1.6 A) binds to FXa active site canonically, through the reactive-site loop that possesses a P1 Arg (Figure 1.7 B).

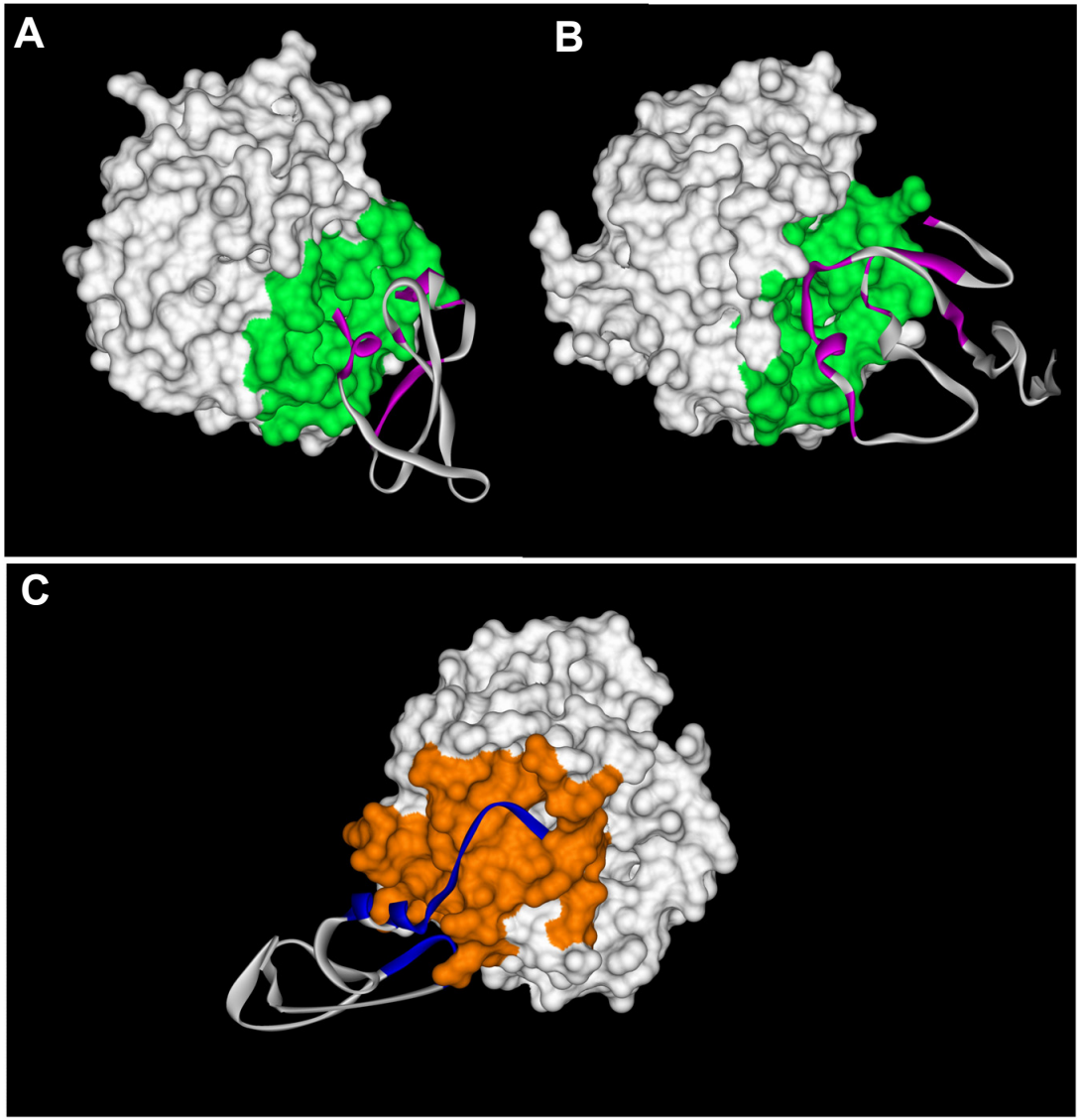

FIGURE 1.7

FXa-inhibitors interaction sites

Interface residues between FXa and its inhibitors are mapped. On FXa, active site surfaces are colored green. The active site includes the active site pocket, Na^{+}-binding loop and autolysis loop. The extended exosite surface including heparin binding exosite is colored orange. On inhibitors, active site targeting residues are colored magenta; exosite targeting residues are colored blue.

(A) FXa-TAP complex (PDB: 1KIG)

(B) FXa-NAP5 complex (PDB: 2P3F)

(C) FXa-NAPc2 complex (PDB: 2H9E): NAPc2 binds to FXa as scaffold to inhibit FVIIa-TF complex, thus is classed as extrinsic tenase complex inhibitor

In addition to the active site, NAP5 interacts with residues on the Na^+-binding (Arg222) and autolysis loops (Arg143, Lys147, Arg150, Gln151), similar to TAP (Rios-Steiner et al., 2007). Interestingly, the C-terminus of NAP5 was observed to interact with a novel FXa exosite (this exosite partially overlaps with the FXa heparin binding exosite) in a symmetry-related FXa molecule (Rios-Steiner et al., 2007). This exosite interaction is similar to that observed in NAPc2-FXa complex (see below for details) (Murakami et al., 2007). Whether this observation is an artefact due to crystal packing or has any physiological consequences remains to be confirmed.

Despite the structural similarity between NAP5 and AceAP1, they have distinct mechanisms of action. Mechanistically, NAP5 is a competitive inhibitor of FXa amidolytic activity while AceAP1 is a two-site, partial non-competitive inhibitor. AceAP1 needs an exosite (yet to be identified) on FXa to which it binds with a lower affinity (700 nM) for full inhibition of the active site (affinity is 2 nM). Moreover, the FXa-AceAP1 complex binds to the FVIIa-TF complex in the same way as the FXa-NAPc2 complex, while NAP5 is devoid of such activity (Harrison et al., 2002; Mieszczanek et al., 2004a).

1.5.2.3. Antistasin-like inhibitors

The antistasin-like domain is utilized widely in leeches as structural scaffold of anticoagulants. FXa inhibitors with antistasin-like domain include antistasin isolated from *Haementeria officinalis* (Tuszynski et al., 1987; Nutt et al., 1988), ghilanten isolated from *Haementeria ghilianii* (Brankamp et al., 1990) and therostasin isolated from *Theromyzon tessulatum* (Chopin et al., 2000). A 119-residue protein, antistasin has two tandem domains containing the 26-residue antistasin-like signature

(PROSITE entry PS51252). Each domain in antistasin has 10 cysteines, forming five intra-domain disulfide bridges (Figure 1.6 C). It is a slow, tight-binding, competitive inhibitor (K_i = 0.3 – 0.6 nM). The inhibition of the FXa active site is through the canonical reactive-site loop residing in the N-terminal domain (Arg as the P1 residue) (Dunwiddie et al., 1989). The crystal structure of antistasin was reported and was modelled in complex with FXa. Other than inhibition of the active site through the canonical reactive-site loop, the complex model suggested possible binding to the Na^+-binding loop (Arg222, Lys223 and Lys224) (Lapatto et al., 1997). Overall sequence similarity between therostasin and antistasin is low, although the domain signature, canonical reactive-site loop and P1 Arg are all conserved. Compared to antistasin, therostasin is more potent (K_i = 34 pM), smaller (82 residues), and has fewer cysteine residues (six residues). However, it does not display the similar tandem domains pattern observed in antistasin (Chopin et al., 2000).

1.5.2.4. Serpin superfamily

Serpins are a superfamily of 45-55 kDa proteins that inhibit their target enzymes by irreversibly locking the proteinases in a covalent acyl-enzyme intermediate (Otlewski et al., 2005). The crude SGE of the mosquitos *Aedes aegypti* was found to inhibit the active site function of FXa through a reversible, non-competitive mechanism (Stark and James, 1995). The only anti-FXa fraction in the extract, named anticoagulant-factor Xa (AFXa, 54 kDa), was isolated and cloned from the salivary glands of *Aedes aegypti*. Its primary sequence shows high similarities with other serpins (e.g. plasminogen activator inhibitor-2). Post-translational modifications of AFXa could be important for activity (four N-linked glycosylation sites are present). However, compared to typical serpins, AFXa has a shorter reactive

center loop and different hinge residues. If the activity of AFXa is the same as that of the SGE (reversible, non-competitive inhibition of FXa), it would be interesting to investigate its differences with the physiological serpin (AT-III), which also inhibits FXa but through a distinct mechanism (irreversible, heparin-dependant, competitive inhibition) (Stark and James, 1998).

1.5.2.5. Draculin

Factor Xa inhibitor is also reported from mammal, the vampire bat. Draculin, an 88.5-kDa glycoprotein, isolated from *Desmodus rotundus* is a non-competitive, tight-binding inhibitor of FXa amidolytic activity, with a K_i of 14.8 nM (Fernandez et al., 1999). The high molecular weight and non-competitive inhibition mechanism of draculin is unique among anticoagulants from hematophagous animals. It showed that hematophagous mammalians, being phylogenetically distant from other invertebrates, are likely to evolve distinct classes of anticoagulants.

1.5.2.6. Uncompetitive FXa inhibitors from Hyalomma

Two uncompetitive inhibitors of FXa amidolytic activity were isolated from *Hyalomma truncatum* (K_i = 0.69 nM) (Joubert et al., 1995) and *Hyalomma dromedarii* (K_i = 134 nM) (Ibrahim et al., 2001b). Both proteins, unnamed, have similar masses (17 kDa and 15 kDa respectively). Example of uncompetitive inhibitor (binding to enzyme-substrate complex but not enzyme) is not commonly found. Thus, detailed characterizations of these molecules could possibly reveal novel FXa exosite(s) that strongly modulate substrate-bound active site function.

1.5.3. Extrinsic tenase complex inhibitors (Table 1.3)

1.5.3.1. Kunitz-type inhibitors

The two main classes of exogenous extrinsic tenase complex inhibitors act through a similar but not identical mechanism as the physiological inhibitor TFPI. Tissue factor pathway inhibitor (TFPI) is a Kunitz-type inhibitor with three tandem domains, binding to both FXa and FVIIa-TF to form a quaternary complex (Crawley and Lane, 2008). The hard tick *Ixodes scapularis* has two different extrinsic tenase complex inhibitors with Kunitz scaffolds. One of them, ixolaris (15.7 kDa), posseses two tandem Kunitz domains and does not bind to the FXa active site, in contrast to TFPI (three domains and binds to the FXa active site). It was hypothesised that the second Kunitz domain first binds to FX/X before binding to the FVIIa-TF complex via its first domain (Francischetti et al., 2002). Ixolaris binding to FX and FXa with affinity between 0.5 – 10 nM (Monteiro et al., 2008). Factor X/Xa residues that are involved in binding to ixolaris are on a surface largely overlaps with their heparin binding proexosite/exosite (Monteiro et al., 2005; Monteiro et al., 2008). In addition, binding of ixolaris to FX (Monteiro et al., 2008) and FXa (Monteiro et al., 2005) impaired their interactions with FVIIIa and prothrombin, respectively. Much less information is available for the inhibition of the FVII-TF complex by the FX/FXa-ixolaris complex. Since ixolaris is a Kunitz-type inhibitor, it is likely that the reactive-site loop on the first Kunitz domain will be utilized to bind to the FVIIa active site. However, the putative P1 residue is Glu, instead of a preferred basic residue (Francischetti et al., 2002). The other extrinsic tenase complex inhibitor, penthalaris, has five tandem Kunitz domains, comparing to only two in ixolaris. Penthalaris uses FX or FXa as scaffold to inhibit the FVIIa-TF complex in the same way as ixolaris.

TABLE 1.3

Extrinsic tenase complex inhibitors from hematophagous animals

EXTRINSIC TENASE COMPLEX INHIBITORS

	Class	Structure	Mechanism	Example	Species	Reference
1.	Kunitz-type proteinase inhibitors	• Single Kunitz domain of ~ 6 to 7 kDa • Multiple Kunitz domains in tandem	• Similar to TFPI • One Kunitz domain binds FX/FXa heparin binding pro-exosite/exosite as scaffold • Another Kunitz domain inhibits to FVIIa-TF complex • Forms inactive extrinsic tenase-inhibitor quaternary complex	Ixolaris Penthalaris	*Ixodes scapularis* *Ixodes scapularis*	(Francischetti et al., 2002; Monteiro et al., 2005; Monteiro et al., 2008) (Francischetti et al., 2004)
2.	Ascaris-type proteinase inhibitors	• Single domain of ~ 9 to 11 kDa • 10 conserved cysteine residues and disulfide linkages • Has a proteinase inhibition loop with basic P1 residue	• Binds FXa exosite as scaffold • Inhibitor-FXa complex binds FVIIa-TF complex • Forms inactive extrinsic tenase-inhibitor quaternary complex	NAPc2/AcAPC2 NAPc3/AcAPC3 NAPc4/AcAPC4	*Ancyclostoma canium* *Ancyclostoma canium* *Ancyclostoma canium*	(Stassens et al., 1996; Mieszczanek et al., 2004) (Stassens et al., 1996; Mieszczanek et al., 2004) (Stassens et al., 1996; Mieszczanek et al., 2004)
			• Forms inactive extrinsic tenase-inhibitor quaternary complex • Binding to FXa is through exosite and active site	AceAP1	*Ancyclostoma ceylanicum*	(Harrison et al., 2002)
3.	Others	• Lack of detailed structural information	• Lack of functional characterization	Crude extract	*Dermacentor andersoni*	(Gordon and Allen, 1991)

The contribution of the three additional Kunitz domains to the interaction/function is not yet clear (Francischetti et al., 2004).

1.5.3.2. Ascaris-type inhibitors

NAPc2/AcAPc2, along with two other isoforms NAPc3/AcAPc3 and NAPc4/AcAPc4 (Stassens et al., 1996; Mieszczanek et al., 2004b), isolated from *Ancyclostoma caninum* have the disulfide pairing signature of the Ascaris family inhibitors. NAPc2/3/4 binds to FX or FXa as a scaffold for the subsequent inhibition of the FVIIa-TF complex. This mechanism of action is similar to ixolaris and penthalaris (Kunitz-type inhibitors). NAPc2 is most potent molecule among these Ascaris inhibitors, binding FX and (inactivated)FXa with a K_d of 1 nM (Buddai et al., 2002). The (inactivated)FXa-NAPc2 complex then inhibits the FVIIa-TF complex with a K_i of 8.4 pM (Stassens et al., 1996). NAPc2 moderately inhibits the FXa amidolytic activity. However, its binding is not directed at FXa active site but at an exosite that includes the FXa C-terminus (Buddai et al., 2002). NMR structures of NAPc2 showed extensive flexibility in solution, especially in the central acidic loop and C-terminus (Duggan et al., 1999). The crystal structure of NAPc2, in complex with active site-inhibited FXa, showed that the extended NAPc2 C-terminus became ordered upon binding to FXa (Figure 1.6 D) (Murakami et al., 2007). Binding of NAPc2 to FXa is mediated through a novel exosite adjacent to, and partially overlapping with, the heparin binding exosite of FXa (Figure 1.7 C) (Rezaie, 2000). This surface, which was also found to be the target for ixolaris, could be the extension of the heparin binding exosite (Monteiro et al., 2005). FXa residues that form this novel exosite includes those residing in the Gln61 – Lys65 loop, the Glu86 – Arg93 β-strand and the Lys236 – Lys243 C-terminal helix (Murakami et al., 2007). NAPc2

is postulated to inhibit canonically the FVIIa active site through its reactive-site loop that contains a P1 Arg residue (Murakami et al., 2007). This reactive-site loop is rich in acidic residues and is disordered in both NMR (Duggan et al., 1999) and the FXa-bound crystal structure (Murakami et al., 2007), indicating possible conformational changes or stabilizations upon binding to FVIIa. NAPc2 completed Phase II clinical trials with promising results (Ledizet et al., 2005; Giugliano et al., 2007) although its development was suspended recently (http://www.nuvelo.com/products/rNAPc2/index.html).

1.5.4. Intrinsic tenase complex inhibitor (Table 1.4)

1.5.4.1. Lipocalin family

Nitrophorin-2 (or Prolixin-s, ~ 20 kDa), isolated from kissing bug *Rhodnius prolixus* (Ribeiro et al., 1995), is an intrinsic tenase complex inhibitor belongs to the lipocalin family (Zhang et al., 1998; Isawa et al., 2000). Four nitric oxide/histamine transporting molecules with high sequence similarities (nitrophorin 1 to 4) were characterized from the kissing bug and all possess vasodilatory (through nitric oxide release) and antihistaminic (through histamine binding) activities. Interestingly, only nitrophorin-2 has a strong anticoagulant activity mediated through specific protein-protein interactions. Nitrophorin-2 binds specifically to FIX/FIXa with a K_d of 13 nM, most likely by targeting the Gla-domain of FIX/FIXa. This binding interferes with FIX activation (by both the FVIIa-TF complex and FXIa) and with FIXa activity in the intrinsic tenase complex (Isawa et al., 2000). Through comparison of the anticoagulant with nitrophorin-1 and 4 (non-anticoagulants), surfaces on nitrophorin-2 involve in FIX/FIXa binding have been suggested (Andersen and Montfort, 2000).

TABLE 1.4

Intrinsic tenase complex inhibitors from hematophagous animals

INTRINSIC TENASE COMPLEX INHIBITORS

	Class	Structure	Mechanism	Example	Species	Reference
1.	Lipocalin family	• Single domain of ~ 16 kDa • Eight-stranded (A-B-C-D-E-F-G-H) antiparallel β-barrel and a central ligand-binding pocket	• Also functions as vasodilator and antihistamine • Binds to FIX/FIXa Gla-domain • Inhibits both FIX activation and FIXa activity in intrinsic tenase complex	Nitrophorin-2 (prolixin-s)	*Rhodnius prolixus*	(Ribeiro et al., 1995; Zhang et al., 1998; Isawa et al., 2000; Andersen and Montfort, 2000)
2.	Others	• Lack of detailed structural information	• Inhibits intrinsic tenase complex activity by attenuating FVIII activity	Crude extract	*Triatoma infestans*	(Pereira et al., 1996)

1.5.5. Contact system proteins inhibitors (Table 1.5)

1.5.5.1. Kunitz-type inhibitors

Haemaphysalin (16 kDa, two tandem Kunitz domains), from the hard tick *Haemaphysalis longicornis* (Kato et al., 2005) binds directly to both FXII and HMWK in the presence of Zn^{2+} and interferes with their associations with activating surfaces. Amidolytic activity of FXIIa and kallikrein are not affected by the inhibitor. As a result of haemaphysalin binding, reciprocal activations of FXII and prekallikrein are disrupted and initiation of the classical intrinsic pathway of coagulation is inhibited (Kato et al., 2005). Similar to haemaphysalin, hamadarin from the mosquito *Anopheles stephensi* has an identical mechanism of inhibition on contact system proteins. Hamadarin also has a mass of 16 kDa, although no sequence information is available to ascertain the identity of hamadarin as a Kunitz-type inhibitor (Isawa et al., 2002).

A group of Kunitz-type inhibitors isolated from *Boophilus microplus* were reported to inhibit the amidolytic activity of plasma kallikrein. Two of them, BmTI-A (15 kDa) (Tanaka et al., 1999) and BmTI-2 (17 kDa) (Sasaki et al., 2004) have two tandem domains while one, BmTI-D (8 kDa) has a single Kunitz domain (Sasaki et al., 2004). They inhibited plasma kallikrein with K_i values of 120 nM, 48 nM and 12 nM, respectively. However, they also inhibited other serine proteinase such as trypsin, chymotrypsin and neutrophil elastase (Tanaka et al., 1999; Sasaki et al., 2004). Similarly, a few inhibitors from *Rhipicephalus sanguineus,* such as RsTIQ2 (12 kDa, two Kunitz domains) and RsTIQ7 (8 kDa, single Kunitz domain), inhibited the amidolytic activity of plasma kallikrein in addition to trypsin, neutrophil elastase and plasmin (Sant'Anna et al., 2003).

TABLE 1.5

Contact system proteins inhibitors from hematophagous animals

CONTACT SYSTEM PROTEINS INHIBITORS

	Class	Structure	Mechanism	Examples	Species	Reference
1.	Kunitz-type proteinase inhibitors	• Single Kunitz domain is ~ 7 kDa • Some of the inhibitors have two tandem Kunitz domains (~ 16 kDa)	• Binds directly to both FXIIa and high molecular weight kininogen (HK) • Inhibits associations of FXIIa and HK with activating membranes	Haemaphysalin	*Haemaphysalis longicornis*	(Kato et al., 2005)
			• Identical with haemaphysalin	Hamadarin	*Anopheles stephensi*	(Isawa et al., 2002)
			• Inhibits plasma kallikrein amidolytic activity • Shows cross specificity for other proteinases such as trypsin, neutrophil elastase and plasmin	BmTI-A/D/2 RsTI-Q2/Q7	*Boophilus microplus* *Rhipicephalus sanguineus*	(Tanaka et al., 1999; Sasaki et al., 2004) (Sant'Anna et al., 2003)
2.	Kazal-type proteinase inhibitors	• Single Kazal domain is ~ 6 kDa • Multiple non-classical Kazal domains • cDNA sequence showed multiple-domains precursors	• Inhibits FXIIa amidolytic activity • Specificity towards different proteinase changes with different tandem repeats	Infestin 1-4 Infestin 3-4 Infestin 4	*Triatoma infestans* *Triatoma infestans* *Triatoma infestans*	(Campos et al., 2002; Campos et al., 2004) (Campos et al., 2002; Campos et al., 2004) (Campos et al., 2002; Campos et al., 2004)
3.	Antistasin-like inhibitors	• Cysteine-rich domain of ~ 5 kDa • Containing a 26-residues segment with conserved cysteines and disulfide linkages	• Inhibits amidolytic activity of plasma kallikrein • Also inhibits tissue kallikrein and trypsin	Piguamerin	*Hirudo nipponia*	(Kim and Kang, 1998)

1.6. MOLECULAR DIVERSITY IN EXOGENOUS ANTICOAGULANTS

Blood-feeding is crucial for the survival of hematophagous organisms and hence they have a large number of anticoagulant proteins in their saliva that specifically target blood coagulation proteinases. Thus, hundreds of millions years of evolution have provided the driving force for the molecular diversity observed in these exogenous anticoagulants. One can observe (1) the functional diversity among closely-related proteins; and (2) the functional convergence among structurally unrelated proteins.

1.6.1. Molecular scaffold

In the first case, a set of molecular scaffolds are being used to target various stages of the blood coagulation cascade. In this scenario, the molecular surface is altered through evolution and tailored to recognize distinct serine proteinases. Generally, the same sets of scaffolds are found in closely-related species, whereas different sets of scaffolds are found in phylogenetically distant species. For example, exogenous anticoagulants from ticks have the Kunitz-type inhibitor scaffold, while those from hookworms and leeches have the Ascaris-type or hirudin-like inhibitor scaffolds, respectively. This is most likely due to the presence of common ancestral molecules. Even in this case, structurally similar inhibitors isolated from different species might be of particular interest, due to their adaptations to difference hosts. Take hirudin and other members of its class as example: molecules similar to hirudin were isolated from other leeches; they are bufrudin (Scacheri et al., 1993) and hirullin (Steiner et al., 1992) from *Hirudinaria manillensis*. *Hirudinaria manillensis* is primarily a mammalian parasite (cf. *Hirudo medicinalis* is an amphibian parasite),

which brings the suggestion that bufrudin and hirullin may be tailored to inhibit mammalian coagulation protein more efficiently. The C-terminal sulfotyrosine of hirudin is not conserved in bufrudin (Scacheri et al., 1993) and hirullin was found to be glycosylated at Thr45 (isoform P6) or Thr50 (isoform P18) (Steiner et al., 1992). Characterizations of these molecules are important for the understanding of structure-function relationships of hirudin. Therefore, further investigations into this family of inhibitors may reveal how post-translational modifications could be used as a strategy to modulate activity of anticoagulants.

At times, the same domains are duplicated and the proteins containing tandem repeats exhibit distinct/altered specificities, as demonstrated by the Kazal-type inhibitors infestins. Derived from the same precursor, specificities of infestins relied on the post-translational processing when a broad specificity inhibitor (infestin 1-4) can be processed into one specific for thrombin (infestin 1-2) and one specific for FXIIa (infestin 3-4) (Campos et al., 2002; Campos et al., 2004) (Figure 1.4). Investigations into the processing mechanisms could answer interesting questions on the regulation of blood-feeding behavior of hematophagous animals.

There is another important mechanism that was responsible for molecular diversity in these exogenous anticoagulants – gene duplications coupled with mutations. When the gene of a domain is repeated in tandem, new functions can be gained through mutations. For instance, soft ticks FXa inhibitors [TAP (Waxman et al., 1990; Wei et al., 1998) and FXaI (Gaspar et al., 1995; Gaspar et al., 1996)] have a single Kunitz domain inhibiting the FXa active site while thrombin inhibitors [ornithodorin (van de et al., 1996), savagnin (Nienaber et al., 1999) and monobin

(Mans et al., 2008)] have two Kunitz domains targeting both the thrombin active site and exosite-I.

In some animals, more than one scaffold is utilized to generate distinct anticoagulants during evolution. For example, anticoagulants from kissing bugs have both the Kazal-type inhibitors (thrombin inhibitors) and the lipocalin family (thrombin and intrinsic tenase complex inhibitors) scaffolds. Similarly, the hirudin-like (thrombin inhibitors) and antistasin-like (FXa inhibitors) scaffolds are widely present in anticoagulants from leeches. Thus, potentially new sets of scaffolds were utilized each time an independent adaptation of blood-feeding behavior occurs, generating a large variety of molecules.

1.6.2. Functional convergence

As distinct from the functional variations of structurally similar protein, the functional convergence of structurally diverse molecules is just as evident. For example, thrombin inhibitors from hematophagous animals belong to at least 13 different classes (Table 1.1), while FXa inhibitors belong to eight or more different classes (Table 1.2). Despite such diversity in structures, they recognize a limited number of molecular surfaces. For example, the thrombin exosite-I and active sites are targeted by the hirudin-like (Electricwala et al., 1991; Scacheri et al., 1993; Markwardt, 1994), Kunitz-type (van de et al., 1996; Macedo-Ribeiro et al., 2008), Kazal-type (Friedrich et al., 1993; van de et al., 1995; Mende et al., 1999; Campos et al., 2002) and anophelin (Valenzuela et al., 1999) thrombin inhibitors. Similarly, both the Kunitz-type [TAP (Waxman et al., 1990; Wei et al., 1998)] and Ascaris-type [NAP5 (Rios-Steiner et al., 2007)] inhibitors targeted the active site, Na^+-binding loop

and autolysis loop of FXa. The presence of multiple classes of molecules for similar function can even be observed in a single species. At least four different classes of thrombin inhibitors can be found in *Boophilus microplus*: (1) boophilin (Macedo-Ribeiro et al., 2008); (2) microphilin (Ciprandi et al., 2006); (3) BmAP (Horn et al., 2000); and (4) BmGTI (Ricci et al., 2007) (Table 1.1). Structure-function relationships of such functionally convergent anticoagulants will help us to delineate their functional sites as well as to design of novel anticoagulants *de novo*.

1.7 AIM AND SCOPE OF THE THESIS

Motivated by the molecular diversity observed in exogenous anticoagulants, as well as the success of hirudin, bivalirudin and NAPc2 in their clinical developments, we aimed to study novel anticoagulants from hematophagous animals. In order to do so, we established a scientific collaboration with Dr Maria Kazimirova from Institute of Zoology, Slovak Academy of Sciences, Slovakia. The presence of thrombin inhibitors in the crude and fractions of SGE of partially engorged (9 days post attachment) females *Amblyomma variegatum* were reported by Dr Kazimirova and colleagues in 2002 (Kazimirova et al., 2002). *Amblyomma variegatum,* the tropical bont tick, is a three-host hard tick that feeds on a number of domesticated animals including cattle, sheep, goats, horses and dogs as well as humans (http://www.cfsph.iastate.edu/FactSheets/pdfs/amblyomma_variegatum.pdf). At the time, she had successfully isolated three fractions of salivary protein with indications of thrombin inhibitory activity and named the most potent peptide as variegin. The only information available was their sequences, although all three fractions showed some degree of heterogeneity. We are interested in understanding the structure-function relationships of variegin. Specifically, the aims of this thesis were:

1. To understand the kinetics, mechanism and specificity of thrombin inhibition by variegin
2. To elucidate the structure-function relationships of variegin
3. To delineate the molecular details involved in thrombin-variegin interaction
4. To design new variants which allow better understanding of the interaction and provide suitable candidates for future drug development

5. To establish the feasibility of developing variegin as a novel anticoagulant by investigating its *in vivo* antithrombotic effects

On the whole, the scope of this thesis covers the approaches used to fulfill these aims, the results obtained, and the discussion of their implications. Explicitly, we chemically synthesized full-length variegin and established its thrombin inhibitory function. Structure-function relationships of the inhibitor are detailed using truncation variants. A three-dimensional structure of thrombin-variegin complex was solved at 2.4 Å resolution, which in turn allowed the design and characterization of new variegin variants with a wide spectrum of activities. Finally, the *in vivo* antithrombotic effects of variegin and variants were demonstrated in the thrombosis model of zebrafish larvae. Therefore, this thesis sets the foundation for future development of variegin as a novel anticoagulant.

Chapter Two

Variegin, a novel class of thrombin inhibitors

2.1. INTRODUCTION

Ticks are hematophagous arthropods and they are pool feeders. Their attachment to host is achieved with chelicerae and toothed hypostome, creating feeding pool of blood in the dermis of their hosts. Ixodid (hard) ticks may feed for a few days or up to two weeks, with their mouthparts cemented into their host skin throughout (Labuda and Nuttall, 2004). During the insertion of hypostome, tick saliva starts to flow to the tip of the mouthparts. Thus, secretion of saliva into feeding pool occurs even before consumption of any blood (Steen et al., 2006). Blood meals ingested by hard ticks in a matter of few days are usually more than a hundred times their own weight (Jaworski, 2003). The secret of successful feeding lies in their saliva. Tick saliva is a complex mixture of potent anti-haemostatic, anti-inflammatory and immunoregulatory molecules. However, the isolation of these salivary molecules is a daunting task, mainly due to the low amount of saliva sample one can collect from these tiny creatures (Valenzuela, 2004). Therefore, a more commonly used approach is to dissect the salivary glands of the ticks and isolate pharmacologically active components from the extracts (SGE).

Blood-feeding typically induces high expression level of salivary proteins as well as remarkable morphological changes in the salivary glands. Such changes are most profound in female hard ticks, with up to 25-fold increase in the mass and proteins content a few days after attachment (Figure 2.1). Similar changes, albeit to a smaller extent, can also be found in males. Once fully engorged (the completion of blood meals), females will drop to the ground, digest the blood meals, lay eggs and then die. Degeneration of salivary glands through apoptosis occurs within a few days

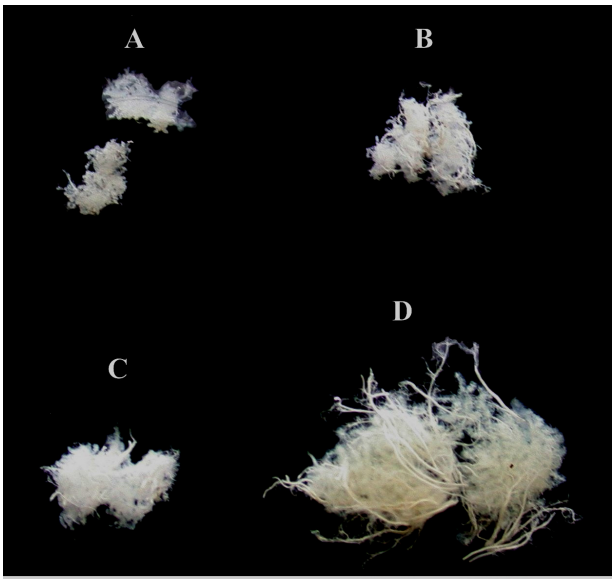

FIGURE 2.1

Dissected salivary glands of *Amblyomma variegatum*, the tropical bont tick (Figure contributed by Dr. Maria Kazimirova, Slovak Academy of Sciences)

Blood meals induced increase in mass and protein content of *Amblyomma variegatum* salivary glands. (A) unfed male (B) unfed female (C) 2-day fed female (D) 9-day fed female.

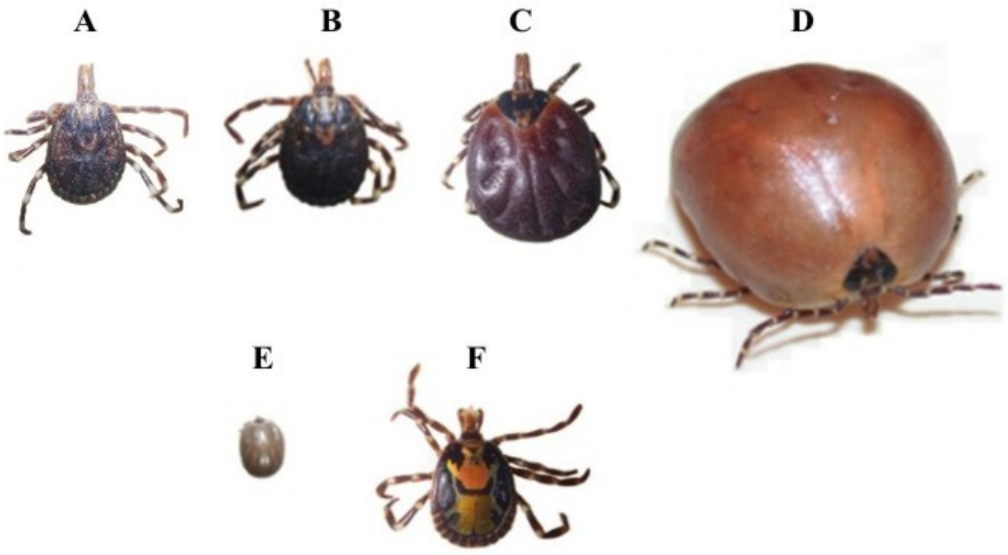

FIGURE 2.2

Pictures of *Amblyomma variegatum* (Figure contributed by Dr. Maria Kazimirova, Slovak Academy of Sciences)

(A) unfed female (B) 2-day fed female (C) 9-day fed female (D) fully engorged, detached female (E) engorged nymph (F) male.

of detachment [see (Bowman and Sauer, 2004) for more detailed descriptions of the physiology and function of salivary glands].

The study on structure-function relationships of variegin started with the chemical synthesis of the full-length peptide by solid-phase peptide synthesis. Other than to obtain a large amount of sample, the use of synthetic peptide also served the purpose of avoiding ambiguity in the protein sequence. Since the protein sequences showed heterogeneity, it is possible that the sequences obtained were misrepresented by the major (but not active) protein in the fractions. Solid-phase peptide synthesis is a robust method to generate large amount of samples, especially when the length of peptide is less than 50 residues. In order to delineate structure-function relationships of the inhibitors, truncation variants were designed based on prior knowledge of thrombin inhibitors. In this case, the inhibitors are short linear peptides, thus any loss of activity in truncation variants is likely to correlate well with the direct loss of functional residues instead of other complications such as alteration of the global fold of the inhibitors. However, the peptides that can be synthesized are largely limited by the availability of building blocks (i.e. the amino acids). In some cases, certain post-translational modifications that occurred in the native peptides cannot be reproduced (which will be discussed later in this chapter). Synthesized crude peptides are purified by reverse-phase high performance liquid chromatography (RP-HPLC), although the presence of chemically and structurally similar side products poses challenges to this process. Parameters such as the choice of column, ion-pairing agent (thus pH of buffers) and the slope of the eluting gradient, need to be optimized for their efficient separation. Activities of native and synthetic peptides are typically assayed by their

abilities to inhibit the thrombin amidolytic and fibrinogenolytic activities. Analysis of data were through mathematical models stated in the Materials and Methods Section.

In summary, this chapter details the purification of a group of thrombin inhibitors from *Amblyomma variegatum* SGE and characterization of the most potent, variegin. The structure-function relationships of variegin, including inhibition mechanism and kinetics, were investigated with the full-length and truncation variants. The functional site of variegin and their target binding sites on thrombin were elucidated which laid the foundation for the subsequent investigations of this new class of thrombin inhibitors.

2.2. MATERIALS AND METHODS

2.2.1. Materials

Human citrated plasma was provided by the Department of Hematology and Transfusiology of the Slovak Institute of Cardiovascular Diseases. Thromboclotin reagent was from Dade AG (Düdingen, Switzerland). Thromboplastin IS reagent and Actin FS Activated PTT reagent were from Dade International Inc. (Miami, Florida, USA). Standard 9-Fluorenylmethyloxycarbonyl (Fmoc)-L-amino acids, Fmoc-PEG-PS (4-hydroxymethylphenoxyacetic acid linker) support resin, *N*,*N*-dimethylformamide (DMF), 20% v/v piperidine in DMF, *O*-(7-azabenzotriazol-1-yl)-1,1,3,-3-tetramethyluronium hexafluorophosphate (HATU) and *N*,*N*-diisopropylethylamine (DIPEA) were from Applied Biosystems (Foster City, California, USA). Trifluoroacetic acid (TFA), formic acid (FA), diethyl ether, acetonitrile, α-cyano-4-hydroxycinnamic acid (CHCA), 1,2-ethanedithiol, thioanisole, bovine chymotrypsin and bovine serum albumin (BSA), were from Sigma Aldrich (St. Louis, Missouri). Human fibrinogen, FXIIa, tPA, urokinase, kallikrein and bovine trypsin were from Merck Chemicals Ltd. (Nottingham, UK). Human FIXa, FXa, FXIa, APC and plasmin were from Hematologic Technologies, Inc. (Essex Junction, Vermont). Human FVIIa and recombinant α-thrombin were gifts from the Chemo-Sero-Therapeutic Research Institute (KAKETSUKEN, Japan) (Soejima et al., 2001; Yonemura et al., 2004). Chromogenic substrates benzoyl-IIe-Glu(Glu-γ-methoxy)-Gly-Arg-*p*-nitroanilide (*p*NA) hydrochloride (HCl) (S2222), *H*-$_D$-Phe-pipecolyl (Pip)-Arg-*p*NA•2HCl (S2238), *H*-$_D$-Val-Leu-Lys-*p*NA•2HCl (S2251), *H*-$_D$-IIe-Pro-Arg-*p*NA•2HCl (S2288), *H*-$_D$-Pro-Phe-Arg-*p*NA•2HCl (S2302), pyroGlu-Pro-Arg-*p*NA•HCl (S2366), pyroGlu-Gly-Arg-*p*NA•HCl (S2444), methoxysuccinyl-Arg-Pro-

Tyr-*p*NA•HCl (S2586) and benzyloxycarbonyl-$_D$-Arg-Gly-Arg-*p*NA•2HCl (S2765) were from Chromogenix (Milano, Italy). Spectrozyme® FIXa (*H*-$_D$-Leu-phenylalanyl-Gly-Arg-*p*NA•2-AcOH) was from American Diagnostica Inc. (Stamford, Connecticut). All other chemicals and reagents used were of analytical grade.

Experiments described in this section were initiated and performed by Dr. Maria Kazimirova, Dr. Peter Takac, Dr. Milan Labuda (Institute of Zoology, Slovak Academy of Sciences), Dr. Adama Trimnell (Seattle Biomedical Research Institute) and Dr. Patricia Nuttall (NERC, Centre for Ecology and Hydrology). Inclusion of these descriptions is for the completeness of the presented data.

2.2.2. Identification of thrombin inhibitors from salivary gland extract of female tropical bont tick, *Amblyomma variegatum*

2.2.2.1. Salivary gland extracts and estimation of protein concentrations

Adult female *Amblyomma variegatum* ticks (Figure 2.2) that had been feeding on laboratory rabbits for 9 days (partially fed) were removed, mounted in Petri dishes dorsal side down, and their salivary glands dissected out into 150 mM NaCl and stored at -70 °C. Prior to use, the frozen salivary glands were incubated at ~ 90 °C for 5 min, homogenized, and centrifuged at 11,000 x g for 15 min. The supernatant fluids were collected and the pellets resuspended in 150 mM NaCl and recentrifuged. Pooled supernatant fluids represented crude SGE. Protein concentration was estimated by the method of Bradford (Bradford, 1976).

2.2.2.2. Purification of variegin isoforms

Variegin was purified by a three-step reverse-phase HPLC procedure with a Beckman Instruments 126/168 DAD HPLC system (Fullerton, California, USA). In the first step (Figure 2.3 A) SGE was loaded onto a Vydac C-4 (5 μm; 250 x 4.6 mm) column (Grace Vydac, Hesperia, California). Pooled fractions that contained the

strongest anticoagulant activity (Figure 2.3 A, fraction AV-III) were subjected to a second step (Figure 2.3 B) using a Beckman Ultrasphere C-18 (5 μm; 250 x 4.6 mm) column. Lastly, individual fractions were further purified using a Vydac C-18 (5 μm; 250 x 4.6 mm) column to obtain three fractions of potent anti-thrombin activity: AV 3/5, AV 5/5 and AV 6/5 (Figure 2.3 C – D). The major component in the AV 6/5 fraction was named n-variegin ('n' denotes the native peptide).

2.2.2.3. Coagulation assays

Thrombin time (TT), prothrombin time (PT) and activated partial thromboplastin time (APTT) assays were used for the initial screens of anticoagulant activities in SGE and fractions. Citrated human plasma (50 μl) was pre-incubated with a maximum of 5 μl of the SGE or the same volume of 150 mM NaCl (control) at 37˚C for 1 min. After adding the corresponding reagents (TT: 50 μl of Thromboclotin reagent; PT: 100 μl of Thromboplastin IS reagent; APTT: 50 μl of Actin FS Activated PTT added for 3 min and reaction started with 50 μl of 20 mM $CaCl_2$), times required for the formation of fibrin clots were determined visually using a stop watch.

The activities of crude SGE and the three fractions (AV 3/5, AV 5/5 and AV 6/5) were verified at the Oxford Hemophilia Centre of Churchill Hospital (Oxford, UK). TT, PT and APTT were performed using an MDA-180 analyser (Organon Teknika Ltd., Cambridge, UK). Ten μl of SGE (1 μg/μl) or diluted fractions containing AV 3/5, AV 5/5 and AV 6/5 (concentrations of undiluted fractions were: 0.07 μg/μl, 0.05 μg/μl, and 0.02 μg/μl, respectively) were added to 290 μl of platelet poor plasma, mixed and incubated for 5 min at 37˚C. The activities were also verified using a Thromboelastograph (TEG) Analyzer (Haemoscope Inc., Skokie, Illinois).

Five µl of samples were added to 335 µl of citrated whole blood, incubated for 5 min and the sample run on the TEG following recalcification.

2.2.2.4. Protein sequence analysis

The molecular weight of proteins present in AV 3/5, AV 5/5 and AV 6/5 was determined by Eurosequence (Groningen, the Netherlands) using a BIFLEX (Bruker-Franzen, Bremen, Germany) matrix-assisted laser desorption/ionization time-of-flight (MALDI-TOF) mass spectrometer equipped with a nitrogen laser (337 nm) and gridless delayed extraction ion source. Partial amino acid sequences were determined by N-terminal Edman-degradation using an automated sequencer (Model 494, Applied Biosystems). The complete sequence for AV 6/5 was determined by MALDI-MS analysis. Swiss-Prot accession number for variegin is P85800.

Experiments described from this section onwards are completed within the scope of this thesis.

2.2.3. Structure-function relationships of variegin

2.2.3.1. Peptide synthesis

All peptides used in the studies were synthesized using solid phase peptide synthesis methods on an Applied Biosystems Pioneer Model 433A Peptide Synthesizer (Foster City, California, USA). The synthesized peptides were assembled on support resins pre-loaded with respective C-terminal amino acids, which cleaves to release peptides with free carboxylic acid at the C-terminus. Fmoc groups of amino acids were removed by 20% v/v piperidine in DMF and coupled using HATU/DIPEA *in situ* neutralization chemistry. Cleavage of synthesized peptides from resins and side chain protection groups were typically carried out using a cocktail of TFA/1,2-ethanedithiol/thioanisole/water (90:4:4:2% v/v) at room temperature for 2 h. Cleaved

peptides were precipitated with cold diethyl ether. Precipitated peptides were dissolved in either water or 0.1% TFA and lyophilized before purification.

2.2.3.2 Purification of synthesized peptides

Synthetic crude peptides were purified to homogeneity by RP-HPLC on ÄKTA™ Purifier System (GE Healthcare, Uppsala, Sweden) with SunFire™ C18 (100 Å, 5 μm; 250 mm x 10 mm) (Waters, Milford, Massachusetts) column. Typically peptides were eluted using an optimized linear elution gradient created by a combination of two solvents (solvent A: 0.1% TFA in water and solvent B: 0.1% TFA and 80% acetonitrile in water). Elutions of peptides were monitored at 215 nm and 280 nm. Chromatograms for purification of peptides can be found in Appendix A.

2.2.3.3. Electrospray ionization mass spectrometry (ESI-MS)

The homogeneity and mass of peptides were assessed using ESI-MS performed on API-300 LC/MS/MS system (Perkin-Elmer Sciex, Selton, Connecticut, USA). The samples were delivered by direct injection. LC-10AD liquid chromatography system (Shimadzu, Kyoto, Japan) was used for solvent delivery (40% acetonitrile in 0.1% FA). Ionspray, orifice and ring voltages were typically set at 4600 V, 50 V and 350 V, respectively. Nitrogen was used as nebulizer and curtain gas. Mass spectra for peptides can be found in Appendix A.

2.2.3.4. Matrix-assisted laser desorption/ionization time-of-flight mass spectrometry (MALDI-TOF MS)

The homogeneity and masses of peptides were also determined using MALDI-TOF MS on a Voyager DE-STR Biospectrometry Workstation (Applied Biosystems,

Foster City, California, USA). Typically, the sample was co-crystallized with an equal volume of the matrix (10 mg/ml of CHCA freshly prepared in 1:1 acetonitrile/water containing 0.3% TFA) on a 100-well stainless steel sample plate. The accelerating voltage was set at 25000V, the grid voltage at 93.0% and the guide wire voltage at 0.3%. Molecular ions were generated using a nitrogen laser (wavelength, 337 nm) at an intensity of 1800–2200. Extraction of ions was delayed by 800 ns. The spectrum obtained was the average of several scans. The spectrum was calibrated using external standards. Mass spectra for peptides can be found in Appendix A.

2.2.3.5. Circular dichroism (CD) spectroscopy

Far-UV CD spectra (260 – 190 nm) of peptides dissolved in 10 mM of sodium phosphate buffer (pH 7.4) were recorded using a Jasco J-810 spectropolarimeter (Easton, Maryland). All measurements were carried out at room temperature using 0.1 cm path length stoppered cuvettes. The instrument optics was flushed with nitrogen gas at 30 L/min. The spectra were recorded using a scan speed of 50 nm/min, a resolution of 0.2 nm and a bandwidth of 2 nm. A total of three scans were recorded and averaged for each spectrum and the baseline (spectrum of buffer) was subtracted.

2.2.3.6. Michaelis-Menten constant (K_m) of S2238 for thrombin

Assays for recombinant α-thrombin amidolytic activity were carried out using small, synthetic chromogenic substrate S2238. Hydrolysis of S2238 release colored product *p*-nitroaniline (*p*NA). Rate of *p*NA formation is proportional to the enzymatic activity and followed at 405 nm. The relation between the initial rate of reaction, V, with concentration of S2238 follow Michaelis-Menten kinetics described by equation **(1)**:

$$V = (V_{max}S) / (S + K_m) \quad \textbf{(1)}$$

where V is the initial rate of reaction, S is the concentration of substrate S2238 and K_m is the Michaelis-Menten constant of substrate for the enzyme (thrombin).

Assays were performed in 96-well microtiter plates in 50 mM Tris buffer (pH 7.4) containing 100 mM NaCl and 1 mg/ml BSA at room temperature. Typically, reactions were started with addition of 100 µl of different concentrations of S2238 (indicated in Results section) into a mixture of 100 µl recombinant α-thrombin and 100 µl buffer. The rates of formation of colored product pNA were followed at 405 nm for 10 min with SPECTRAMax Plus microplate spectrophotometer (Molecular Devices, Sunnyvale, California, USA). Data obtained were fitted to equation **(1)** using Origin software (MicroCal, Northampton, Massachusetts) to calculate K_m and V_{max}.

2.2.3.7. Inhibition of thrombin amidolytic activity

The activities of peptides were determined by the inhibition of recombinant α-thrombin amidolytic activity assayed using the chromogenic substrate S2238. All assays were performed in 96-well microtiter plates in 50 mM Tris buffer (pH 7.4) containing 100 mM NaCl and 1 mg/ml BSA at room temperature. Typically, 100 µl of peptide and 100 µl of recombinant α-thrombin were pre-incubated for different durations before the addition of 100 µl of S2238. Details of each experiment are described along with the graphs representing the results obtained. The rates of formation of colored product *p*NA were followed at 405 nm for 10 min with SPECTRAMax Plus microplate spectrophotometer. Percentage inhibition was calculated by taking the rate of increase in absorbance in the absence of inhibitor as

0%. Dose-response curves were fitted using Origin software to calculate IC_{50} values with the following logistic sigmoidal equation:

$$y = A_2 + (A_1 - A_2) / [1 + (x / x_0)^H] \quad \textbf{(2)}$$

where y is percentage of inhibition, A_2 is right horizontal asymptote, A_1 is left horizontal asymptote, x is log10 of inhibitor concentration, x_0 is point of inflection and H is the slope of the curve. IC_{50} was calculated by substituting '50' into y.

2.2.3.8. Determination of the inhibitory constant K_i

The inhibitory constants, K_i, of all peptides were determined using S2238 as substrate for recombinant α-thrombin. All assays were performed in 96-well microtiter plates using a 50 mM Tris buffer (pH 7.4) containing 100 mM NaCl and 1 mg/ml BSA at room temperature. Typically, 100 µl of recombinant α-thrombin were added to a mixture of 100 µl peptides and 100 µl S2238 to initiate the reactions. Concentrations of peptides and S2238 used vary with experimental setups and will be indicated separately in the 'Results' section. The rates of formation of colored product *p*NA were followed at 405 nm for 10 min with SPECTRAMax Plus microplate spectrophotometer.

When an enzyme is inhibited by an equimolar concentration of inhibitor, the binding of inhibitor to enzyme causes a significant depletion in the concentration of free inhibitors. This tight-binding inhibition is described by equation **(3)** (Stone and Hofsteenge, 1986):

$$V_s = (V_o/2E_t)\ \{[(K_i' + I_t - E_t)^2 + 4K_i'E_t]^{1/2} - (K_i' + I_t - E_t)\} \quad \textbf{(3)}$$

where V_s is steady state velocity in the presence of inhibitor, V_o is velocity observed in the absence of inhibitor, E_t is total enzyme concentration, I_t is total inhibitor concentration and K_i' is apparent inhibitory constant.

For competitive inhibition, K_i is related to K_i' by equation **(4)**:

$$K_i' = K_i\ (1 + S/K_m) \quad \textbf{(4)}$$

where K_i' increases linearly with S, K_i is the inhibitory constant, S is the concentration of substrate and K_m is the Michaelis-Menten constant for S2238.

For non-competitive inhibitors, K_i is related to K_i' by equation **(5)** (Copeland, 2000):

$$K_i' = (S + K_m) / [(K_m/K_i) + (S/\alpha K_i)] \quad \textbf{(5)}$$

where α is the modifying constant of the inhibitor on the affinity of the enzyme for its substrate, and likewise the effect of the substrate on the affinity of the enzyme for the inhibitor. $\alpha < 1$ when binding of one supported the other, $\alpha > 1$ when binding of one impedes the other and when $\alpha = 1$, binding of one has no effect on the other. For mixed-type non-competitive inhibitor, α is either < 1 or > 1. For classical non-competitive inhibitors, $\alpha = 1$, thus,

$$K_i' = K_i \qquad \textbf{(6)}$$

where K_i' remained constant with increasing S, K_i is the inhibitory constant, S is the concentration of substrate S2238 and K_m is the Michaelis-Menten constant for S2238. For peptides that were found to be tight-binding inhibitors their data were fitted to these equations using Origin software.

If the rate of interaction of the inhibitor with the enzyme is slow so that the inhibited steady-state velocity is slowly achieved, the progress curve of product formation of this slow binding inhibition is described by equation **(7)** (Morrison and Walsh, 1988):

$$P = V_f t + (V_i - V_f)\,(1 - e^{-kt}) / k + P_o \qquad \textbf{(7)}$$

where P is the amount of product formed, P_o the is initial amount of product, V_f is final steady state velocity, V_i is initial velocity, t is time, and *k* is apparent first-order rate constant.

There are two possible minimum kinetic mechanisms to describe such slow binding reactions (Morrison and Walsh, 1988; Rezaie, 2004):

$$E + I \underset{K_2}{\overset{K_1}{\rightleftharpoons}} EI^* \qquad \textbf{Scheme (1)}$$

where E is enzyme, I is inhibitor and EI* is stable enzyme-inhibitor complex, K_1 is association rate constant and K_2 is dissociation rate constant. In this scheme, slow

binding is mainly due to the slow K_1. The apparent first-order rate constant *k* will increase linearly with inhibitor concentration. Alternatively:

$$E + I \underset{K_2}{\overset{K_1}{\rightleftharpoons}} EI \underset{K_4}{\overset{K_3}{\rightleftharpoons}} EI^* \qquad \textbf{Scheme (2)}$$

where EI is initial collision complex, K_3 is forward isomerization rate and K_4 is reverse isomerization rate. In this scheme, binding involves rapid formation of an initial collision complex (EI) that subsequently undergoes slow isomerization to the final enzyme-inhibitor complex (EI*). *k* increases hyperbolically with inhibitor concentrations. Dissociation constant of EI (denoted $K_i`$) can be calculated from equation **(8)**:

$$k = K_4 + K_3 I_t / [I_t + K_i`(1 + S / K_m)] \qquad \textbf{(8)}$$

The overall inhibitory constant K_i can be calculated from equation **(9)**:

$$K_i = K_i` [K_4 / (K_3 + K_4)] \qquad \textbf{(9)}$$

For peptides that were found to be a slow binding inhibitor their data were fitted to these equations using Origin software.

2.2.3.9. Serine proteinase specificity

The selectivity profile of one peptide, synthetic variegin (s-variegin) was examined against 13 serine proteinases: fibrinolytic serine proteinases (plasmin, tPA and urokinase), anticoagulant serine proteinase APC, procoagulant serine proteinases

(FXIIa, FXIa, FXa, FIXa, FVIIa, kallikrein and recombinant α-thrombin) and classical serine proteinases (chymotrypsin and trypsin). Effects of s-variegin on these serine proteinases were determined by inhibition of their amidolytic activities assayed using specific chromogenic substrates for respective enzymes. All assays were performed in 96-well microtiter plates using a 50 mM Tris buffer (pH 7.4) containing 100 mM NaCl and 1 mg/ml BSA at room temperature (4 mM of $CaCl_2$ were also present in the buffer for chymotrypsin and activated protein C assays). 100 µl of s-variegin (for assay with recombinant α-thrombin final concentrations are 10 nM, 100 nM and 1000 nM; for assays with other serine proteases final concentrations are 1 µM, 10 µM and 100 µM) were incubated with 100 µl serine proteases for 5 min in room temperature before the addition of 100 µl substrates. The rate reactions were followed at 405 nm for 10 min with SPECTRAMax Plus microplate spectrophotometer. The percentage of inhibition caused by s-variegin was calculated by taking the rate of increase in absorbance in the absence of inhibitor as 0%.

2.2.3.10. Fibrinogen clotting time

The abilities of three peptides (s-variegin, EP25 and AP18) to prolong fibrinogen clotting time were tested using a BBL fibrometer (BD, Franklin Lakes, New Jersey). 200 µl of fibrinogen (final concentration 3 mg/ml) were incubated with 100 µl of peptides (various concentrations) at 37°C. Clotting of fibrinogen was initiated by the addition of 100 µl of recombinant α-thrombin (final concentration 20 nM). All reagents and samples were dissolved in 50 mM Tris buffer (pH 7.4) containing 100 mM NaCl.

2.3. RESULTS

Experiments described in this section were initiated and performed by Dr. Maria Kazimirova, Dr. Peter Takac, Dr. Milan Labuda (Institute of Zoology, Slovak Academy of Sciences), Dr. Adama Trimnell (Seattle Biomedical Research Institute) and Dr. Patricia Nuttall (NERC, Centre for Ecology and Hydrology). Inclusion of these descriptions is for the completeness of the presented data.

2.3.1. Identification of thrombin inhibitors from salivary gland extract of female tropical bont tick, Amblyomma variegatum

2.3.1.1. Purification of variegin isoforms

Crude SGE of *Amblyomma variegatum* exhibited potent anticoagulant activity in all three coagulation assays (PT, APTT and TT) (Table 2.1). Potency was in the order TT >> APTT > PT. Since PT test on the integrity of extrinsic pathway, APTT test on extrinsic pathway and TT test on the conversion of fibrinogen to fibrin by thrombin, the prominent effect of the SGE on TT is an indication of the presence of potent/high amount of antithrombin components. The inhibitions on APTT and PT are likely to be due to the effect of these antithrombin components or/and the presence of weaker/smaller amount of inhibitors acting on other enzymes 'upstream' of thrombin. This observation indicates the SGE is a promising source of potent thrombin inhibitors. To purify these inhibitors, SGE was fractionated by RP-HPLC (Figure 2.3 A). After the first step of purification, the most potent anticoagulant fraction (AV-III) was subjected to a second purification step (Figure 2.3 B). The resulting fractions were screened for antithrombin activity in coagulation and chromogenic substrate assays. Two fractions with the strongest activity (retention time 23.08 and 28.93 min) were further purified in separate runs. The fraction with retention time 23.08 min was separated into two main peaks denoted AV 3/5 and AV 5/5 (Figure 2.3 C). The fraction with retention time 28.93 has one main peak and with a small 'shoulder peak'

TABLE 2.1

Anticoagulation activities of *Amblyomma variegatum* SGE (females fed for 9 days).

Results show the mean of duplicate values. In controls 150 mM NaCl was substituted for SGE.

	PT (s)	APTT (s)	TT (s)
Control	15	28	17
SGE protein (µg)			
0.025			50
0.050			105
0.100			>180
0.250	15	28	
0.500	19	38	
1.000	22	45	
2.500	40	>180	
5.000	>180		

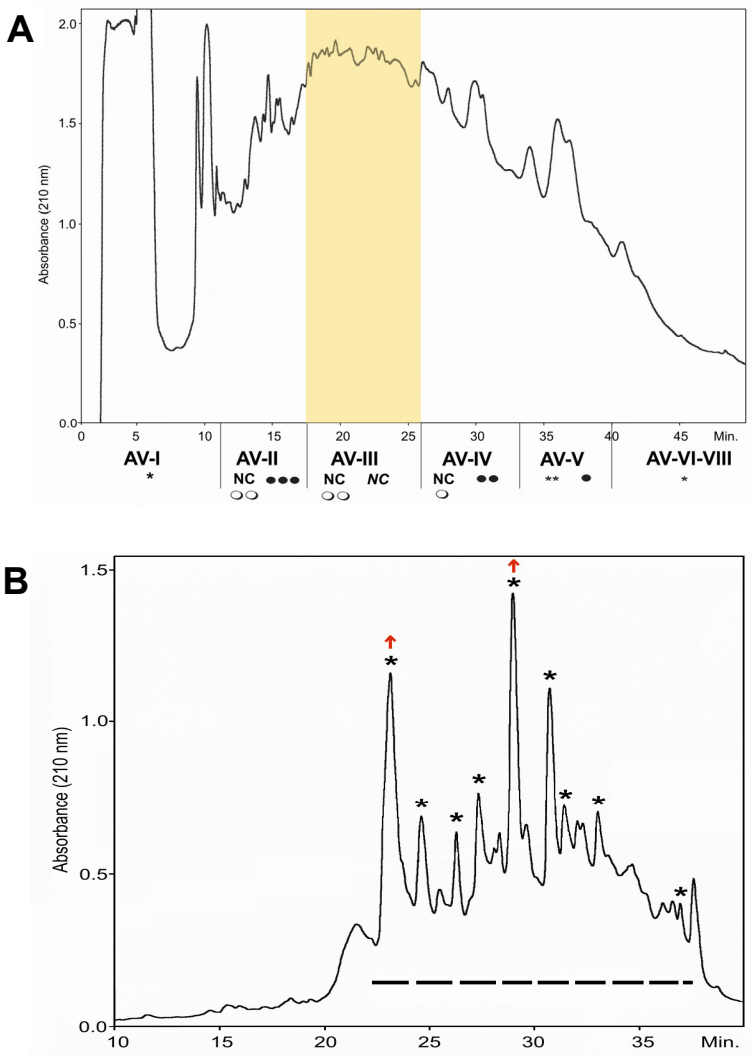

FIGURE 2.3

Purification of variegin isoforms by RP-HPLC

(A) In the first step, SGE was fractionated using a gradient of 10 – 100% ACN over 90 min. Protein concentrations in pooled fractions of AV-I to AV-VIII ranged from 0.08 (AV-I) to 1.39 µg/µl (AV-IV). For TT assays (control clotting time = 19 s): NC – no clot after adding < 0.01 µg protein/50 µl plasma; *** prolonged clotting of > 1 min after adding < 0.01 µg protein/50 µl plasma; ** prolonged clotting of > 40 s (< 1 min) after adding < 0.01 µg protein/50 µl plasma; * any delay (< 40 sec) in clotting in comparison with control. For APTT assays (control clotting time = 40 s): *NC* – no clot after adding < 0.01 µg protein/50 µl plasma; ●●● prolonged clotting of > 1 min after adding < 0.01 µg protein; ●● prolonged clotting of > 1 min after adding < 0.1 µg protein/50 µl plasma; ● any delay (< 1 min) in clotting in comparison with control. For PT assays (control clotting time = 15 s): ○○ prolonged clotting of > 1 min after adding 0.5 µg protein/50 µl plasma; ○ any delay (< 1 min) in clotting compared to control (n = 2).

(B) Fraction AV-III was subjected to a second purification step using a gradient of 10 – 40% ACN over 60 min. Protein concentrations in fractions ranged from 0.05 to 0.17 µg/µl. The range of fractions with anticoagulant activities (dashed line, assayed by PT, APTT and TT) was tested for antithrombin activity with S2238. Fractions indicated with asterisks inhibited thrombin amidolytic activity. Two fractions with the strongest activity (retention time 23.083 and 28.933 min, indicated by red arrows) were subjected to a third step of purification (gradient of 10 – 40% ACN over 60 min) (n = 2).

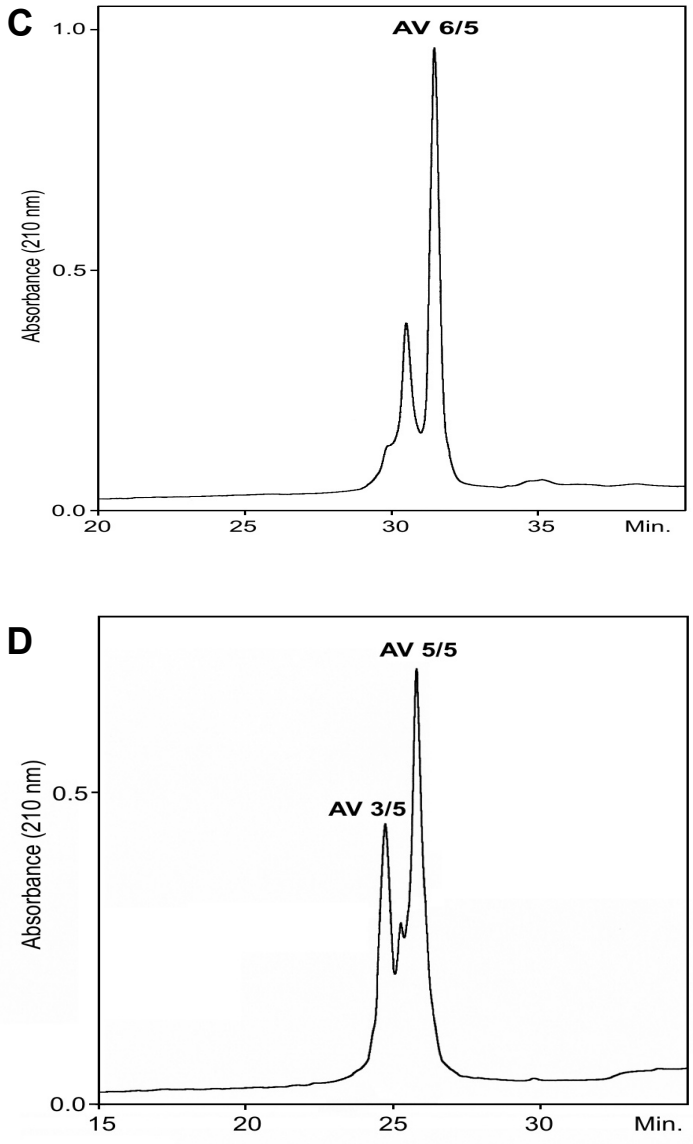

FIGURE 2.3 (continued)

Purification of variegin isoforms by RP-HPLC

(C) The fraction with retention time 23.08 min separated into two main peaks denoted AV 3/5 and AV 5/5.

(D) The fraction with retention time 28.93 has one main peak and a small 'shoulder peak' and was denoted AV 6/5.

and was denoted AV 6/5 (Figure 2.3 D). The anticoagulant activities of these three fractions (AV 3/5, AV 5/5 and AV 6/5) along with crude SGE were verified by PT, APTT, TT and TEG assays. All four assays revealed that AV 6/5 contained the most potent anticoagulant activity, followed by AV 3/5 and AV 5/5 (Table 2.2).

2.3.1.2. Protein sequence analysis

Partial sequences of all three fractions were determined by Edman degradation. For AV 6/5 the sequence and molecular weight were completed by MALDI-TOF. MALDI spectrum of AV 6/5 revealed a major m/z signal of 3769.96 Da (monoisotopic mass = 3768.96 Da) and a minor m/z signal of 3777.79 Da (monoisotopic mass = 3776.79 Da). The main component has the sequence SDQGDVAEPKMHKT(hex)APPFDFEAIPEEYLDDES, where the Thr14 is modified by a hexose moiety. This was named variegin and was further characterized. The minor component (3776.79 Da) is almost identical to variegin, with Glu31 replaced by His. Partial sequences determined by Edman degradation revealed two components in the AV 3/5 fraction (m/z 3953.54 and 3409.57 Da) and three components in AV 5/5 (m/z 3680.23, 3368.94 and 3173.62 Da). All the sequences determined are highly similar to variegin (Figure 2.4), indicates the present of isoforms.

BLAST results indicated that variegin does not show similarity to any known proteins in the database. Interestingly, its C-terminus (DFEAIPEEYL) is almost identical to the C-terminus of hirudin (residues 55 to 64: DFEEIPEEYL). Thus, we hypothesized that variegin C-terminus plays a similar role to hirudin C-terminus in binding to thrombin. However, Tyr63 of hirudin is sulfated (Markwardt, 1994) while

TABLE 2.2

Anticoagulation activities of *A. variegatum* SGE and RP-HPLC fractions.

AV 6/5 showed the most potent activity in all assays. The major component in AV 6/5 was sequenced and named variegin. Since APTT, PT and TT were performed in citrated platelet poor plasma (PPP) - a non-physiological milieu, the activity of the samples were also verified using TEG, which permits coagulation monitoring in whole blood using viscoelastic assessment of clot formation as an endpoint. (PNP: pooled normal plasma; r: r phase, the period of time of latency from the time that blood was placed in the TEG until the initial fibrin formation; k: k phase, a measure of the speed to reach a certain level of clot strength).

Sample (initial concentration)	TEG	PT (s)	APTT (s)	TT (s)
Crude SGE (1 µg/µl)	Complete inhibition	No clot	No clot	No clot
PNP	Normal	13.6	25.6	12.2
AV 6/5 (0.02 µg/µl)	Inhibited	-	-	-
1:200 dilution	-	15.3	59.2	78.9
1:500 dilution	-	14.4	48.3	39.2
AV 3/5 (0.07 µg/µl)	Prolonged r/k	-	-	-
1:200 dilution	-	14.1	46.7	30.8
1:500 dilution	-	14.1	38.8	20.6
AV 5/5 (0.05 µg/µl)	Prolonged r/k	-	-	-
1:200 dilution	-	13.8	38.5	21.4
1:500 dilution	-	13.8	33.7	15.6

```
Variegin (AV6/5)  SDQGDVAEPKMHKTAPPFDFEAIPEEYLDDES
                                                 H
AV3/5             SDQADRAQPKLHRNAPQGDFEAIPDEYL----
                     SG       P
AV5/5             SDQGDVAEPKMHKTAPPGDFEAIPEEYLD---
                     A
```

FIGURE 2.4

Amino acid sequence of variegin and isoforms

Sequences of peptides in fraction AV 6/5 (variegin), AV 3/5 and AV 5/5 are highly similar. Red color are identical residues, blue color similar residues, black color are non-conserved residues, yellow shading indicates hexose modified Thr. The most potent peptide, variegin, was selected for further structure-function relationships studies.

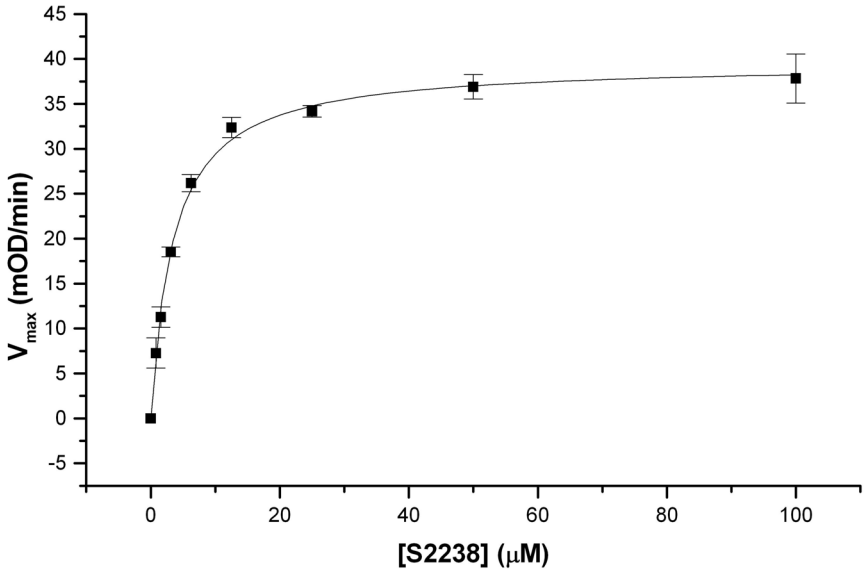

FIGURE 2.5

Michaelis-Menten constant (K_m) of S2238 for thrombin

Plot of reaction velocity (V_{max}) as a function of substrate (S2238) concentration were fitted to the Michaelis-Menten equation (equation 1). K_m calculated with Michaelis-Menten equation is determined to be 3.25 ± 0.56 μM (n = 3, error bars represent S.D.).

the corresponding Tyr27 in variegin is not. In contrast, while Thr14 is modified by a hexose moiety, none of the residues in hirudin is glycosylated.

Experiments described from this section onwards are completed within the scope of this thesis.

2.3.2. Structure-function relationships of variegin

2.3.2.1. Michaelis-Menten constant (K_m) of S2238 for thrombin

In order to facilitate subsequent analysis of data involved in hydrolysis of S2238 by thrombin, K_m of S2238 for recombinant α-thrombin was determined. The initial rate of reaction, V, increased with increasing concentrations of S2238, following Michaelis-Menten kinetics described by equation **(1)** (Figure 2.5). K_m calculated with the equation is 3.25 ± 0.56 μM, similar to other reported values in the literature (Stone and Hofsteenge, 1986; Myles et al., 2001).

2.3.2.2. Inhibition of thrombin amidolytic activity by n-variegin and its K_i

The ability of native variegin (n-variegin) to inhibit thrombin amidolytic activity was assayed with S2238, a small peptidyl substrate that binds only to the active site. N-variegin inhibited the amidolytic activity and progress curves of inhibition showed that steady state equilibrium was achieved upon mixing: a characteristic of fast binding inhibitor (Figure 2.6 A). Significant inhibition (~ 80%) was observed for equimolar concentrations of thrombin and n-variegin (3.33 nM): a characteristic of tight-binding inhibitor. Thus, n-variegin is a fast and tight-binding inhibitor of thrombin. IC_{50} (mean ± S.D.) of the inhibition is 0.99 ± 0.02 nM (Figure 2.6 B). Since the amount of sample available was not enough to perform similar experiments at different concentrations of substrates, competitive nature of the inhibition is assumed based on results obtained with synthetic variegin (s-variegin).

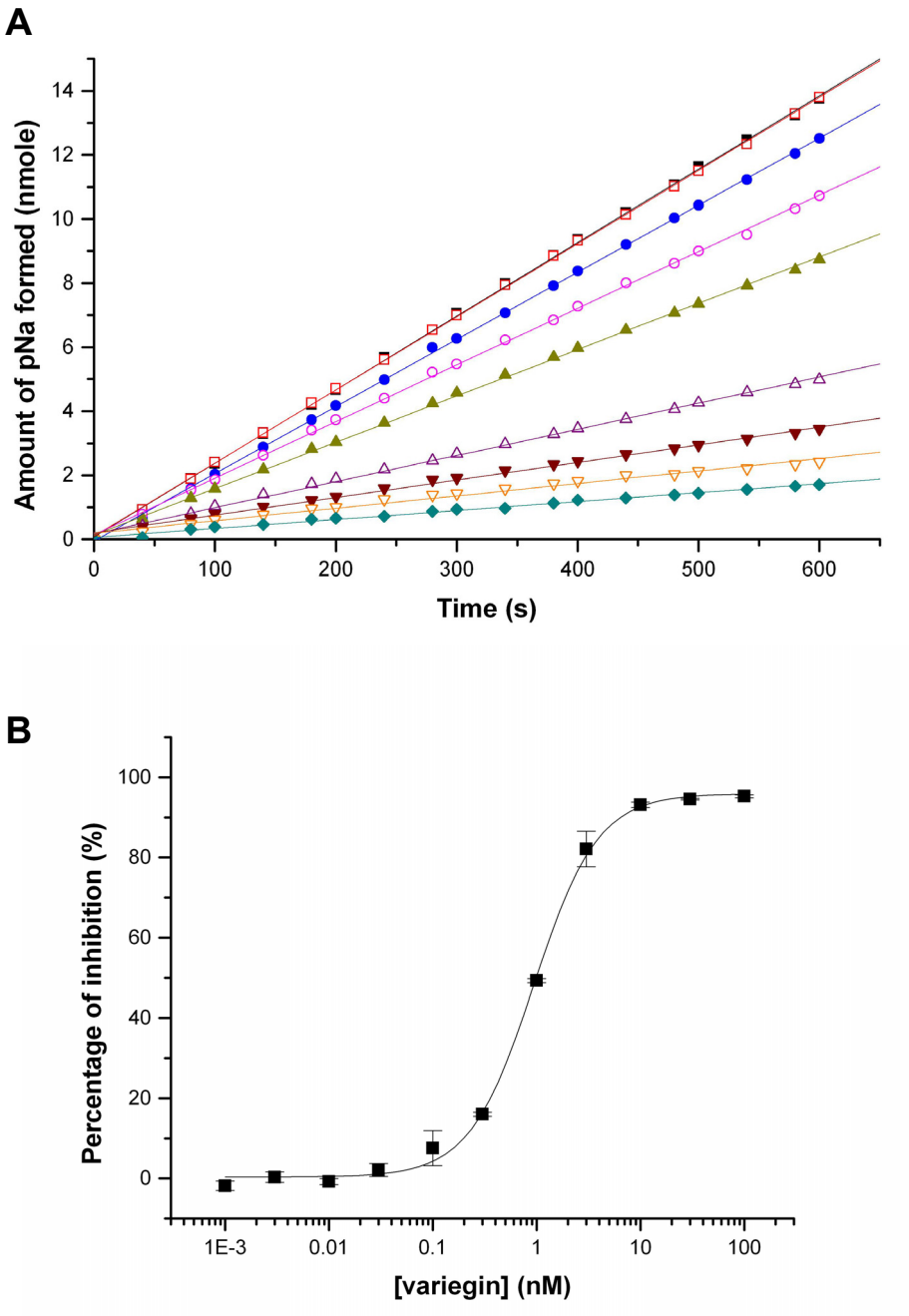

FIGURE 2.6

Thrombin inhibition by n-variegin

(A) Example of linear progression curves of thrombin inhibition by variegin (■: 0.020 nM, □: 0.039 nM, ●: 0.078 nM, ○: 0.156 nM, ▲: 0.313 nM, Δ: 0.625 nM, ▼: 1.25 nM, ▽: 2.5 nM, ♦: 5 nM) using S2238 (100 μM) as substrate, showing steady state equilibrium achieved upon mixing – a characteristic of fast binding inhibitor.

(B) The ability of n-variegin (0.001 nM, 0.003 nM, 0.01 nM, 0.03 nM, 0.1 nM, 0.3 nM, 1 nM, 3 nM, 10 nM, 30 nM and 100 nM) to inhibit thrombin (3.33 nM) amidolytic activity was assayed using active site directed substrate S2238 (100 μM). Dose response curve of thrombin inhibition by variegin (■) showed significant inhibition (~ 80%) for equimolar concentration of thrombin and variegin (3.33 nM). IC_{50} of the inhibition are 0.99 ± 0.02 nM (n = 3, error bars represent S.D.).

Data fitted with equation **(3)**, describing tight-binding inhibitor, showed a K_i of 10.4 ± 1.4 pM [equation **(4)**] (Figure 2.7).

2.3.2.3. Design of deletion variants

For further understanding of structure-function relationships, three peptides were synthesized, purified and characterized. Synthetic variegin (SDQGDVAEPKMHKTAPPFDFEAIPEEYLDDES, s-variegin) has the complete sequence of n-variegin, while EP25 (EPKMHKTAPPFDFEAIPEEYLDDES) and AP18 (APPFDFEAIPEEYLDDES) have seven and 14 residues truncated from the N-terminus, respectively (Table 2.3). The designs of these truncation variants are based on prior knowledge available for thrombin substrates and inhibitors. Full-length variegin were synthesized to confirm the active sequence of variegin. C-terminal sequence of variegin (DFEAIPEEYL), being similar to hirudin, is likely to target thrombin exosite-I. The distance between thrombin active site and exosite-I is approximately 20 Å. Based on observations made earlier in the design of bivalent thrombin inhibitors (Maraganore et al., 1990), this distance can be covered by four to eight Gly residues. In addition, thrombin preferred substrates and canonical inhibitors with a basic P1 residue (most commonly Arg). Since n-variegin inhibits thrombin amidolytic activity, binding to active site is very likely. If variegin inhibits thrombin canonically, within a distant covered by four to eight residues from the putative exosite-I binding segment two basic residues – Lys10 and Lys13 – are the most probable P1 residues. Therefore, truncation variants were designed such that one will contain only exosite-I binding sequence (AP18), while the other will contain both exosite-I and active site binding sequences but devoid of the unique sequence in the N-terminus (EP25). Synthesis of glycosylated Thr was not possible as the building

block (hexose modified Thr) was not available. Thus, unlike native variegin (n-variegin), Thr is not glycosylated in s-variegin and EP25.

2.3.2.4. Synthesis of s-variegin and variants

Full-length synthetic variegin (s-variegin), EP25 and AP18 were synthesized by solid-phase peptide synthesis. Purifications of peptides were carried out with RP-HPLC. Identity and homogeneity of peptides were confirmed with MALDI-TOF MS (Table 2.3). CD spectra of s-variegin, EP25 and AP18 are all similar to that of n-variegin, typical of random coil proteins (Figure 2.8).

2.3.2.5. Selectivity profile of variegin

To determine its selectivity profile, s-variegin was screened against 13 serine proteinases including thrombin. Apart from thrombin, no other serine proteinases was significantly inhibited (≥ 5%) even at 1 μM of s-variegin. Inhibition of > 10% was observed at much higher concentrations of s-variegin. The most susceptible proteinases are plasmin, trypsin and FXIa, which were inhibited ~ 20 to 30% by 100 μM of s-variegin. In contrast, against thrombin, similar ~ 30% inhibition was observed at a concentration at least 4 orders of magnitude lower (~ 3.3 nM) (Figure 2.9). Therefore, s-variegin is a specific and potent thrombin inhibitor. On the other hand, negative values were observed for the inhibition of urokinase and FVIIa, suggesting some degree of activation for these enzymes. While, there seems to be a dose-dependent activation for urokinase, similar activation is less evident and inconclusive in the case of FVIIa. Accurate interpretation of the FVIIa data is difficult due to the lack of a dose-dependent relation as well as the overlapping standard deviations.

TABLE 2.3

Design of variegin truncation variants

In order to investigate structure-function relationships of variegin, synthetic peptides were designed and synthesized based on variegin sequence and prior knowledge of thrombin substrate and inhibitors.

Name	Sequence	Theoretical mass (Da)	Observed mass (Da)	Basis for design
s-variegin	SDQGDVAEPKMHKTAPPFDFEAIPEEYLDDES	3608.9	3609.0	• Full-length sequence of native variegin • To confirm the active sequence of variegin • Thr14 is not glycosylated
EP25	EPKMHKTAPPFDFEAIPEEYLDDES	2936.2	2936.4	• Truncation of 7 residues from N-terminus • To investigate the role of the unique N-terminal while retaining putative P1 residues • Thr14 is not glycosylated
AP18	APPFDFEAIPEEYLDDES	2084.2	2084.4	• Truncation of 14 residues from N-terminus • To test the hypothesis that variegin binding to active site is canonical with either Lys10 or Lys13 as P1 residue • To ascertain the binding of this segment to thrombin exosite-I

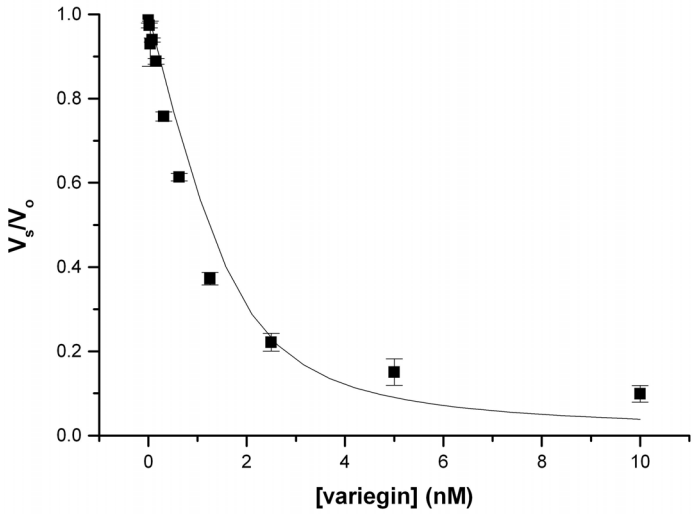

FIGURE 2.7

Inhibitory constant K_i of n-variegin

Since variegin behaved as a tight-binding inhibitor, inhibition of thrombin (1.8 nM) by variegin (■) at similar concentrations (0.020 nM, 0.039 nM, 0.078 nM, 0.156 nM, 0.313 nM, 0.625 nM, 1.25 nM, 2.5 nM, 5 nM, 10 nM) was examined using S2238 (100 µM) as substrate. Data obtained were fitted to equations **(3)** and **(4)** to derive a K_i (mean ± S.D.) of 10.4 ± 1.4 pM (n = 3, error bars represent S.D.).

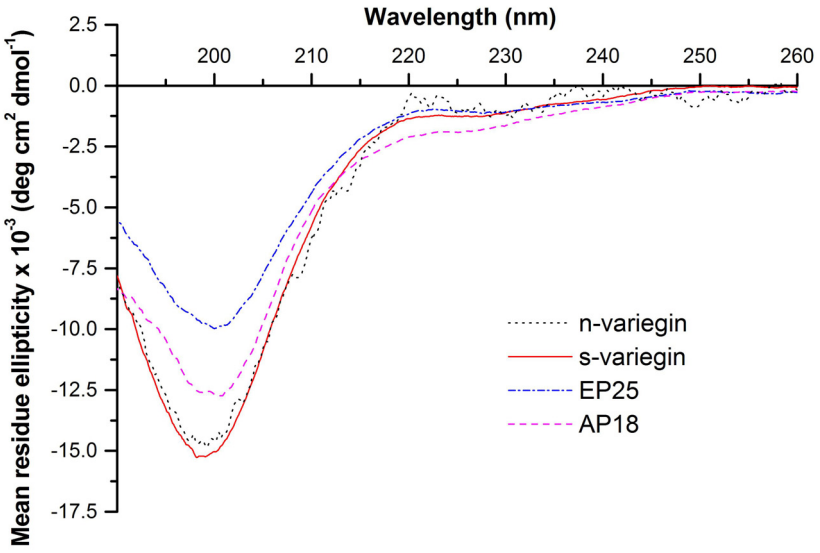

FIGURE 2.8

Variegin and deletion variants lack secondary structures

Far-UV CD spectra (260 – 190 nm) of n-variegin, s-variegin, EP25 and AP18 dissolved in 10 mM of sodium phosphate buffer (pH 7.4). All spectra were typical of random coil protein.

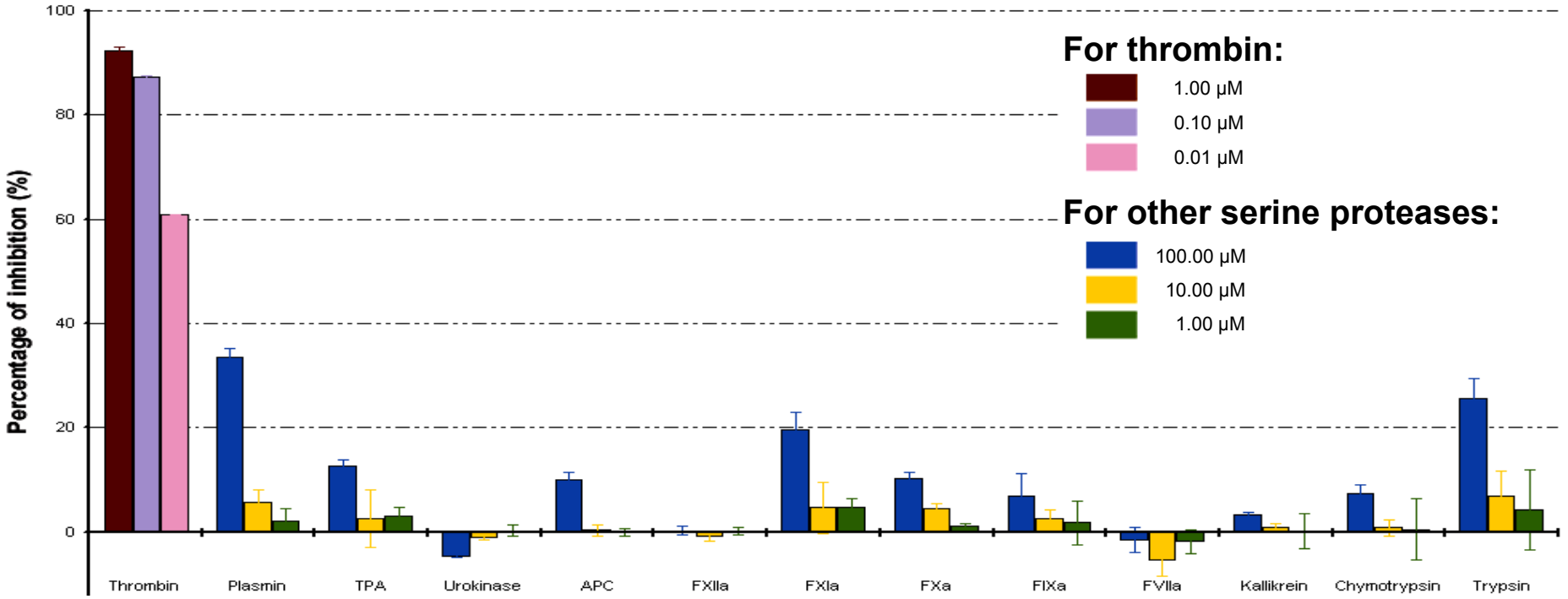

FIGURE 2.9

Selectivity profile of s-variegin

s-Variegin was screened against 13 serine proteases: fibrinolytic serine proteases (plasmin, tPA and urokinase), anticoagulant serine protease APC, procoagulant serine proteases (FXIIa, FXIa, FXa, FIXa, FVIIa, kallikrein and thrombin) and classical serine proteases (chymotrypsin and trypsin). The final concentrations of proteases and substrates are given in parentheses in nM and mM, respectively: plasmin (3.61)/S2251 (1.2), TPA (36.9)/S2288 (1), urokinase (40 U/ml)/S2444 (0.3), APC (2.14)/S2366 (0.67), FXIIa (20)/S2302 (1), FXIa (0.125)/S2366 (1), FXa (0.43)/S2765 (0.65), FIXa (333)/Spectrozyme® FIXa (0.4), FVIIa (460)/S2288 (1), kallikrein (0.93)/S2302 (1.1), α-thrombin (3.33)/S2238 (0.1), chymotrypsin (1.2)/S2586 (0.67) and trypsin (0.87)/S2222 (0.1). Thrombin was tested against three concentrations of s-variegin: (■) represent 0.01 µM, (■) represent 0.1 µM and (■) represent 1 µM. For the other proteases, much higher concentrations of s-variegin were used: (■) represent 1 µM, (■) represent 10 µM and (■) represent 100 µM (n = 3, error bars represent S.D.).

2.3.2.6. Inhibition of thrombin amidolytic activity by s-variegin, EP25 and AP18

s-Variegin is similar to n-variegin in that steady state equilibrium of inhibition was achieved upon mixing. It was 5-fold less active than n-variegin and ~ 30% inhibition was observed at equimolar concentrations of thrombin and s-variegin (3.33 nM). Dose-response curves showed IC_{50} values of around 5.4 nM, independent of pre-incubation time (0 min and 10 min) (Figure 2.10 A). Hence, s-variegin is also a fast and tight binding inhibitor of thrombin. The absence of Thr glycosylation in s-variegin might account for its weaker activity.

EP25 also inhibited the amidolytic activity of thrombin. However, unlike n-variegin and s-variegin, progress curves of inhibition showed two-phase equilibria in the absence of pre-incubation. Steady state equilibrium inhibition was achieved relatively slowly, after 20 min pre-incubation. Dose-response curves of EP25 were dependent on incubation times. Thus the deletion of seven N-terminal residues (SDQGDVA) turned the binding mode from fast to slow. However, potency of EP25 was not affected by the deletion. When the final steady state equilibrium was achieved (20 min pre-incubation) EP25 inhibited thrombin to the same extent as s-variegin. IC_{50} values for EP25 and s-variegin are 5.63 ± 0.45 nM and 5.40 ± 0.95 nM (Figure 2.10 B).

In contrast, AP18 did not inhibit thrombin amidolytic activity even at 300 μM, suggesting that it did not bind to the active site. Instead, AP18 enhanced thrombin amidolytic activity slightly in a dose-dependent manner (Figure 2.10 C). This is consistent with the reported behavior of hirudin C-terminus (Naski et al., 1990). In

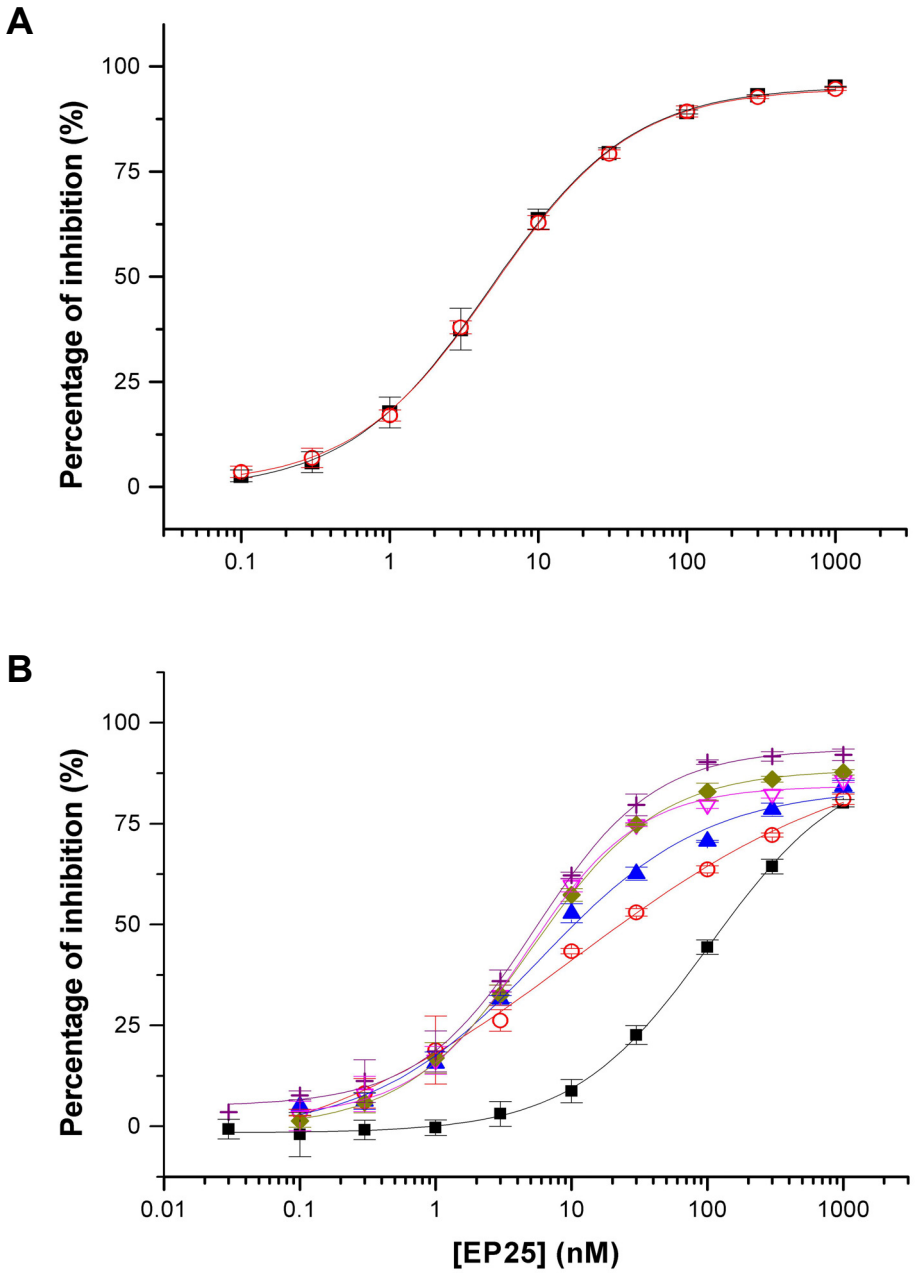

FIGURE 2.10

Inhibition of thrombin by s-variegin, EP25 and AP18

(A) The abilities of s-variegin, EP25 and AP18 to inhibit amidolytic activity of thrombin were assayed using active site directed substrate S2238 (100 µM). Dose response curve of thrombin (3.33 nM) inhibition by s-variegin (0.1 nM, 0.3 nM, 1 nM, 3 nM, 10 nM, 30 nM, 100 nM, 300 nM, 1000 nM) showed significant inhibition (~ 30%) for equimolar concentration of thrombin and variegin (3.33 nM). Dose-response curves of inhibition were independent of pre-incubation time: (■) represents 0 min pre-incubation (IC_{50} = 5.40 ± 0.95 nM and (○) represents 10 min of pre-incubation (IC_{50} = 5.49 ± 0.42 nM (n = 3, error bars represent S.D.).

(B) Dose-response curves of thrombin (3.33 nM) inhibition by EP25 (0.1 nM, 0.3 nM, 1 nM, 3 nM, 10 nM, 30 nM, 100 nM, 300 nM, 1000 nM) showed a pre-incubation time-dependent shift. IC_{50} values are 139.30 ± 7.02 nM without pre-incubation (■), 22.55 ± 2.52 nM with 1 min pre-incubation (○), 10.39 ± 1.53 nM with 2 min pre-incubation (▲), 6.42 ± 0.50 nM with 5 min pre-incubation (▽), 6.80 ± 0.57 nM with 10 min pre-incubation (♦) and 5.63 ± 0.45 nM with 20 min of pre-incubation (+) (n = 3, error bars represent S.D.).

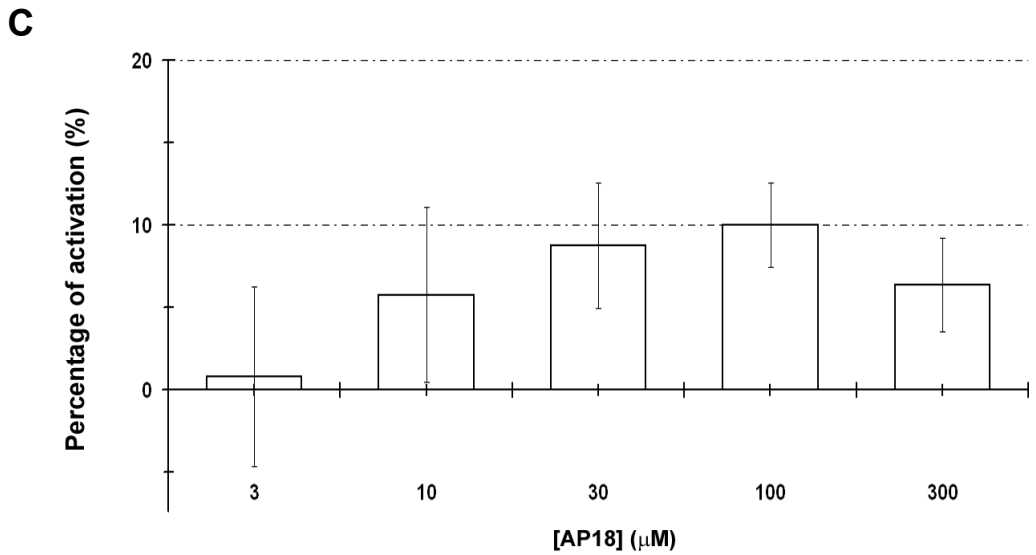

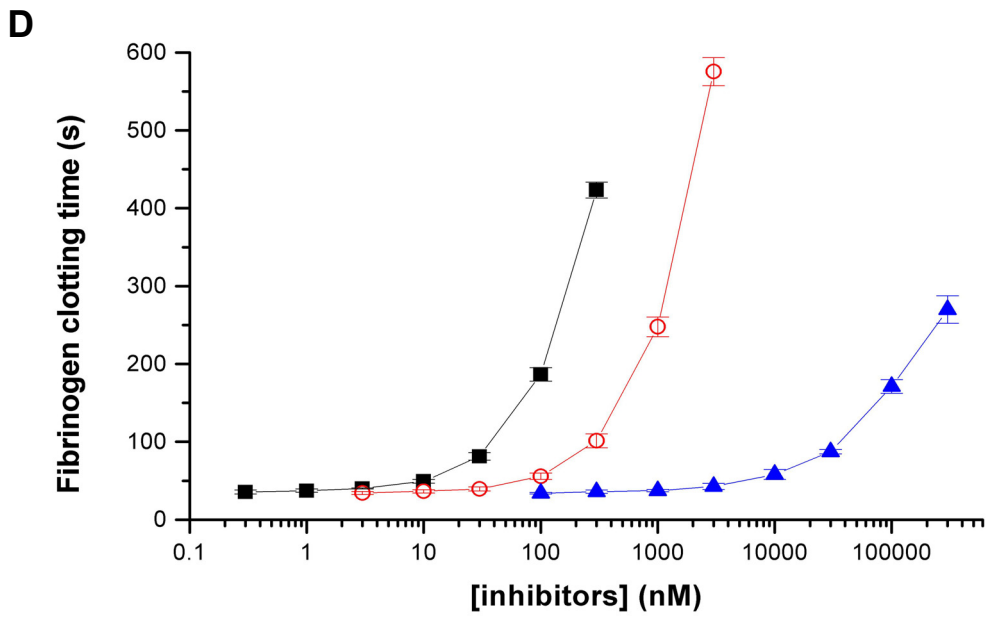

FIGURE 2.10 (continued)

Inhibition of thrombin by s-variegin, EP25 and AP18

(C) AP18 (3 μM, 10 μM, 30 μM, 100 μM, 300 μM) was unable to inhibit thrombin (3.33 nM) amidolytic activity on S2238 (100 μM); instead at high concentrations of AP18, hydrolysis of S2238 were slightly enhanced (n = 3, error bars represent S.D.).

(D) All three peptides, s-variegin (■; 0.3 nM, 1 nM, 3 nM, 10 nM, 30 nM 100 nM, 300 nM), EP25 (○; 3 nM, 10 nM, 30 nM, 100 nM, 300 nM, 1000 nM, 3000 nM) and AP18 (▲; 0.1 μM, 0.3 μM, 1 μM, 3 μM, 10 μM, 30 μM, 100 μM, 300 μM) prolonged fibrinogen clotting times (n = 3, error bars represents S.D.). No pre-incubation of peptides with thrombin was carried out. AP18 inhibited thrombin fibrinogenolytic activity but not amidolytic activity, suggesting binding to exosite-I.

summary, these results suggest that the active site binding moiety on variegin resides within position 8 to 14 (EPKMHKT).

2.3.2.7. Inhibition of thrombin fibrinogenolytic activity

s-Variegin, EP25 and AP18 all prolonged fibrinogen clotting time in a dose-dependent manner (Figure 2.10 D). Fibrinogen binds to both the active site and exosite-I of thrombin (Di Cera, 2003; Huntington, 2005). AP18 inhibited fibrinogenolytic but not amidolytic activity of thrombin, and hence we concluded that the C-terminus of variegin binds to exosite-I. This observation is consistence with that of hirudin C-terminus (Maraganore et al., 1989; Naski et al., 1990). The difference in activity between s-variegin and EP25 is likely to be due to the slow binding mode of EP25.

2.3.2.8. Inhibitory constant K_i of s-variegin and EP25

K_i values of s-variegin and EP25 were determined using S2238 as substrate. S-variegin is a fast and tight binding inhibitor. The apparent inhibitory constants K_i' were determined in the presence of different concentrations of S2238 (Figure 2.11 A). s-Variegin is a competitive inhibitor of thrombin and K_i' increased linearly with increasing concentrations of S2238 [equation **(3)**] (Figure 2.11 B). The true inhibitory constant, K_i was found to be 146.4 ± 13.6 pM, which is 14-fold higher than n-variegin (10.4 ± 1.4 pM). In contrast, EP25 is a slow binding inhibitor of thrombin. Progress curves of inhibition were fitted to equation **(7)** to obtain *k* for each concentration of EP25 (Figure 2.12 A). *k*, the apparent first-order rate constant for the establishment of the equilibrium between initial collision complex (EI) and final stable complex (EI*), increased hyperbolically with EP25 concentration (Figure 2.12 B), as described by

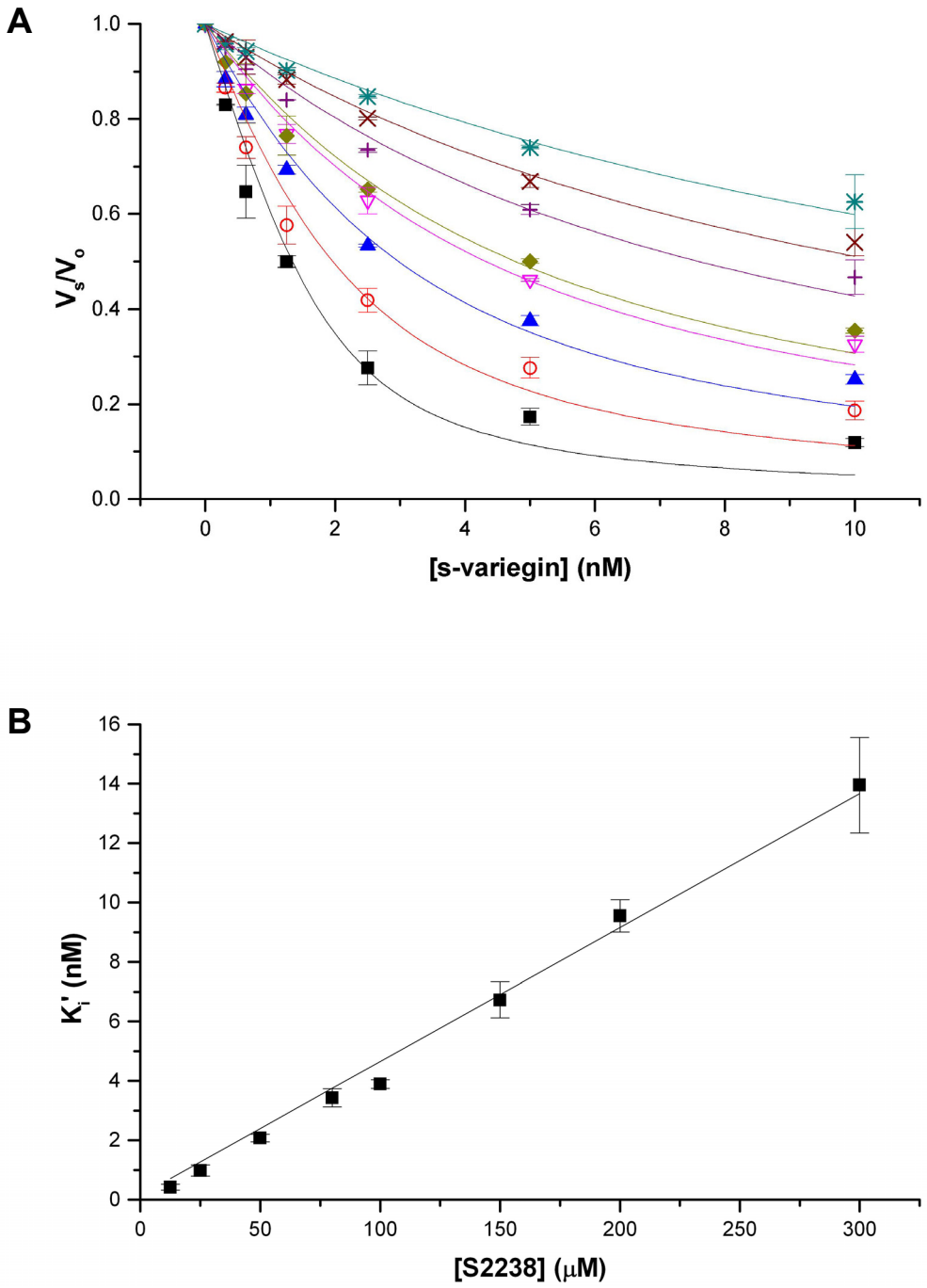

FIGURE 2.11

Inhibitory constant K_i of s-variegin

(A) S-variegin is a fast and tight binding inhibitor of thrombin. S-variegin (0.313 nM, 0.625 nM, 1.25 nM, 2.5 nM, 5 nM, 10 nM) was mixed with different concentrations of S2238: 12.5 μM (■), 25 μM (○), 50 μM (▲), 80 μM (▽), 100 μM (♦), 150 μM (+), 200 μM (×) and 300 μM (✳) to determine K_i'. Reactions were started with the addition of thrombin (1.8 nM). Data were fitted to equation **(3)** (n = 3, error bars represent S.D.).

(B) Plot of K_i' against substrate concentration showed a linear curve, indicating s-variegin competitively inhibited thrombin amidolytic activity on S2238. By fitting the data to equation **(4)**, the inhibitory constant K_i was shown to be 146.4 ± 13.6 pM (error bars represent S.D.).

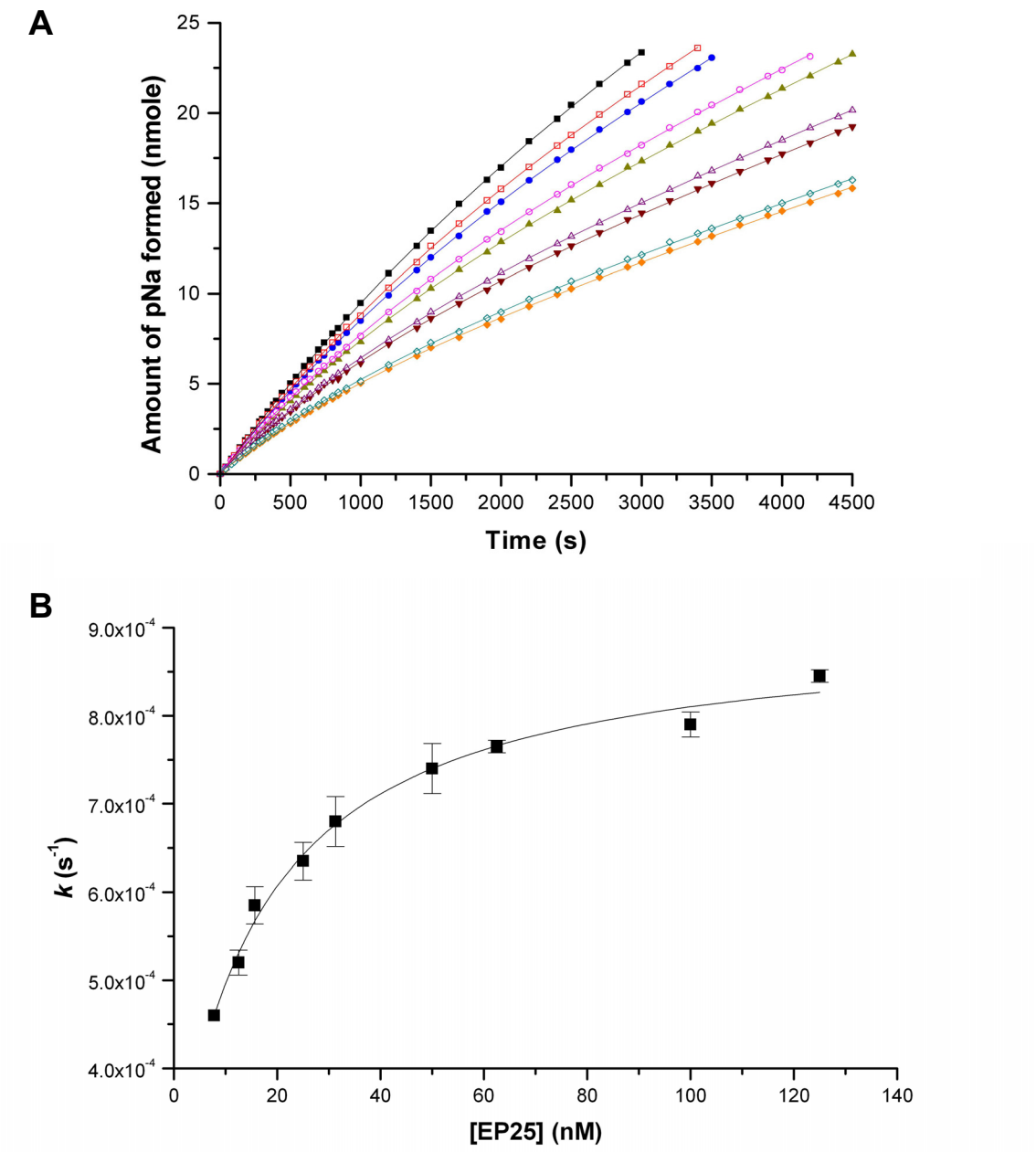

FIGURE 2.12

Inhibitory constant K_i of EP25

(A) Although EP25 also inhibited thrombin at equimolar concentrations if pre-incubated with thrombin, the initial inhibition without pre-incubation was weak. K_i of EP25 was determined without pre-incubation with concentrations at least 8-fold greater than thrombin. Under these assay conditions, binding of EP25 to thrombin does not result in a significant depletion of free EP25 concentration, thus the 'tight-binding' condition was not considered for data fitting. Progression curves of thrombin (0.9 nM) inhibition by different concentrations of EP25: 7.8 nM (■), 12.5 nM (□), 15.6 nM (●), 25 nM (○), 31.3 nM (▲), 50 nM (△), 62.5 nM (▼), 100 nM (◊) and 125 nM (♦), using S2238 (100 µM) as substrate. The progression curves are non-linear, and showed two-phase equilibria typical of slow-binding inhibition. Data were fitted to equation **(7)** to obtain a *k* for each concentration of EP25 used (n = 3, error bars represent S.D.).

(B) Plot of the apparent first-order rate constant k against EP25 concentrations is a hyperbolic curve described by equation **(8)** and hence was fitted to the equation to obtain a K_i` of 529.7 ± 76.7 pM, representing the dissociation constant of initial collision complex EI. The overall inhibitory constant K_i was calculated from equation **(9)** and was found to be 149.8 ± 30.5 pM (error bars represent S.D.).

Scheme **(2)**. Thus, the binding between EP25 and thrombin involves the isomerization of EI to EI*. The dissociation constant of EI (K_i`, mean ± standard deviation, equation **(8)** was 529.7 ± 76.7 pM, while the overall inhibitory constant K_i [equation **(9)**] was 149.8 ± 30.5 pM. Thus K_i of EP25 is essentially the same as K_i of s-variegin (146.4 ± 13.6 pM). These results confirmed that the deletion of seven N-terminal residues did not affect potency but switched the binding mode from fast to slow.

2.4. DISCUSSION

In order to overcome the hemostatic system of their host, it is conceivable that salivary glands of female *Amblyomma variegatum* secrete potent inhibitors targeting thrombin. This is because thrombin plays a central role in maintaining the integrity of hemostasis. Thrombin interacts with most of the zymogens and their cofactors, playing multiple procoagulant and anticoagulant roles in blood coagulation (Di Cera, 2003; Huntington, 2005). As a procoagulant protease, the first traces of thrombin generated in the initiation phase activate FV and FVIII to provide positive feedback leading to the thrombin burst in the amplification phase. Thrombin cleaves fibrinogen to fibrin, forming insoluble clots. Fibrin polymers are further strengthened and stabilized through covalent cross-linking driven by thrombin activated factor XIII. Thrombin also contributes to the generation of a platelet plug, possibly through two mechanisms: (a) it activates platelets by interacting with PARs and glycoprotein V; and (b) it prevents destabilization of the platelet plug, by inactivating ADAMTS13, a disintegrin and metalloprotease with a thrombospondin type 1 motif, number 13, that cleaves VWF. As an anticoagulant protease, thrombin activates protein C in the presence of the cofactor thrombomodulin. APC inactivates FVa and FVIIIa, down-regulating the generation of thrombin (Davie et al., 1991; Di Cera, 2003; Huntington, 2005; Lane et al., 2005).

Variegin is one of the smallest thrombin inhibitors found in nature. Despite its small size and flexible structure, variegin binds to thrombin with strong affinity. Structure-activity studies revealed the interaction of s-variegin with an extended surface area of thrombin. The thrombin active site binding moiety of variegin is in the

region of residues 8 to 14, and the exosite-I binding moiety is within residues 15 to 32. The seven N-terminal residue moiety, while not binding directly to thrombin, affected the binding kinetics; when removed, the binding characteristics of variegin changed from fast to slow.

Over the years, many thrombin inhibitors have been isolated from hematophagous animals and snake venom. However, no similarities were found in the primary structure of variegin and other thrombin inhibitors. The absence of cysteines, consistent with a flexible structure, also differs from prototypic thrombin inhibitors such as hirudin (compact N-terminus, acidic and extended C-terminus) (Rydel et al., 1990; Grutter et al., 1990; Rydel et al., 1991; Schwienhorst, 2006), rhodniin (double domain Kazal-type inhibitor) (Friedrich et al., 1993; van de et al., 1995), ornithodorin (double domain Kunitz-type inhibitor) (van de et al., 1996) and theromin (acidic and antistasin-like N-terminus, compact C-terminus) (Salzet et al., 2000), even though they all bind to the same sites on thrombin (active site and exosite-I) (Figure 2.13 B). Although variegin residues 19 to 28 are almost identical to hirudin C-terminus, their N-termini are completely different (Figure 2.13 A). The first three residues on hirudin N-terminus bind to a hydrophobic pocket at thrombin active site in a non-canonical form, forming a short parallel β-pleated sheet with thrombin Ser214 – Gly217 (Rydel et al., 1990; Grutter et al., 1990; Rydel et al., 1991). It is unlikely that variegin binds to thrombin active site with the same mechanism. The active site binding segment resides in the middle of the molecule. With variegin C-terminus anchoring on thrombin exosite-I, it would be geometrically challenging for the middle segment to approach thrombin active site from the opposite direction as in the case of hirudin. Unlike hirudin, variegin is not sulfated at the Tyr residue and has three extra residues

A

```
N-variegin                                                    SDQGDVAEPKMHKTAPPFDFEAIPEEYLDDES
S-variegin                                                    SDQGDVAEPKMHKTAPPFDFEAIPEEYLDDES
EP25                                                            EPKMHKTAPPFDFEAIPEEYLDDES
AP18                                                              APPFDFEAIPEEYLDDES
Hirulog-1                                                      FPRPGGGGNGDFEEIPEEYL
Hirudin variant 1   VVYTDCTESGQNLCLCEGSNVCGQGNKCILGSDGEKNQCVTGEGTPKPQSHNDGDFEEIPEEYLQ
```

B

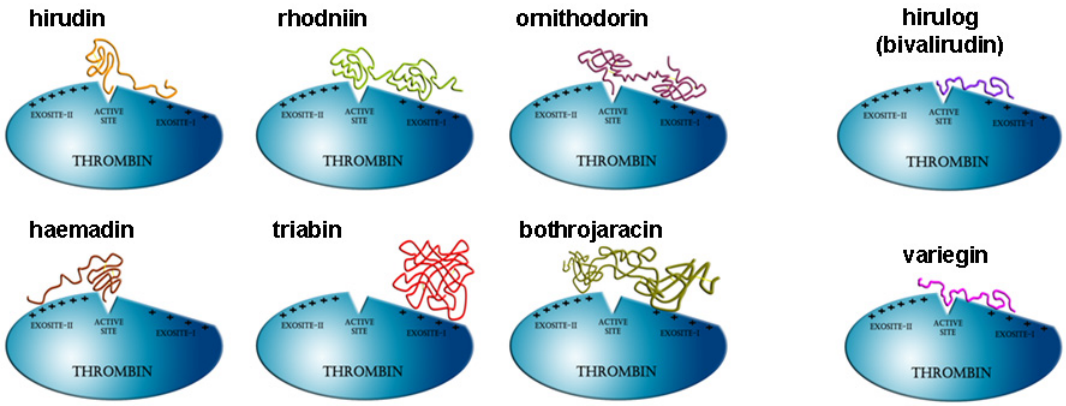

FIGURE 2.13

Comparison of variegin with other thrombin inhibitors

(A) Amino acid sequence alignment of n-variegin, s-variegin, EP25, AP18, hirulog-1 and hirudin show highly similar C-terminal sequences. N-variegin is glycosylated at Thr (T), hirulog-1 contains a $_{D}$-Phe (*F*) and hirudin is sulfated at Tyr (Y). Sequence of TTI is distinctly different from variegin and was not aligned.

(B) Schematic diagram showing different classes of naturally occurring thrombin inhibitors and their structural features. Hirudin: compact N-terminus binds to active site, acidic and extended C-terminus binds to exosite-I; Rhodniin: two Kazal-type domains in head-to-tail arrangement with the N-terminal domain binding to active site and the C-terminal domain binding to exosite-I; Ornithodorin: two Kunitz-type domains in tail-to-tail arrangement with the N-terminal domain binding to active site and the C-terminal domain to exosite-I; Haemadin: compact N-terminal domain binds to active site, acidic and extended C-terminus binds to exosite-II; Triabin: single β-barrel domain binds to exosite-I; Bothrojaracin: two different chains of the C-type lectin domain bind to exosite-I and exosite-II respectively. Other classes of thrombin inhibitors such as theromin and TTI are not represented due to lack of detailed structural information. Structurally variegin is most similar to hirulog (bivalirudin), a synthetic bivalent thrombin inhibitor.

at the C-terminus. Desulfation of hirudin (Stone and Hofsteenge, 1986) or its C-terminal peptide (hirugen) (Maraganore et al., 1989) retained anti-thrombin activity despite a 10-fold reduction in affinity (Stone and Hofsteenge, 1986) and activity (Maraganore et al., 1989). Our results indicated that AP18 binds to exosite-I and slightly enhanced thrombin amidolytic activity, comparable to the reported behavior of hirudin C-terminus (Maraganore et al., 1989; Naski et al., 1990), suggesting similar roles for these two sequences. This appears to be an example of convergent evolution in two phylogenetically distant lineages.

Variegin is also distinct from other thrombin inhibitors such as haemadin (Strube et al., 1993; Richardson et al., 2000), triabin (Noeske-Jungblut et al., 1995; Fuentes-Prior et al., 1997) and bothrojaracin (Zingali et al., 1993). Haemadin has a similar structure to hirudin, binding to the thrombin active site with its N-terminus, but to exosite-II with its extended C-terminus (Strube et al., 1993; Richardson et al., 2000). Triabin only inhibits exosite-I and has a similar structure to lipocalins (Noeske-Jungblut et al., 1995; Fuentes-Prior et al., 1997). Bothrojaracin, a C-type lectin protein, binds to both exosite-I and exosite-II (Zingali et al., 1993) (Figure 2.13 B). Only two other thrombin inhibitors of similar size have been reported to date, but they appear to be unrelated to variegin. Despite also having 32 residues, tsetse thrombin inhibitor (TTI), isolated from tsetse fly *Glossina morsitans morsitans* (Cappello et al., 1996; Cappello et al., 1998), does not share any sequence similarity with variegin (Figure 2.13 A). Another low molecular weight thrombin inhibitor (3.2 kDa) was isolated from the camel tick, *Hyalomma dromedarii* (NTI-1) (Ibrahim et al., 2001a). Unlike variegin, NTI-1 is a weak (K_i = 11.7 μM) and non-competitive

inhibitor of thrombin, binding to only one site on thrombin. Currently, no detailed structural information for NTI-1 is available.

Perhaps variegin is best compared with hirulogs, a group of synthetic bivalent thrombin inhibitors designed by grafting the hirudin C-terminus to the active site binding moiety $_{D}$-Phe-Pro-Arg-Pro through a linker of different number of glycyl residues (e.g. hirulog-1 has four Gly as linker) (Figure 2.13 A) (Maraganore et al., 1990). In particular, the size of EP25 is comparable to hirulog-1, but with a much stronger affinity (K_i of EP25 is ~ 149.8 ± 30.5 pM, while K_i of hirulog-1 is 2.56 nM). However, in contrast to fast binding kinetic of hirulog-1, EP25 is as a slow binding inhibitor. Hirulog-1 was named bivalirudin for its clinical development and eventually entered the market as anticoagulant (Warkentin et al., 2008).

Since the C-termini of variegin and hirulogs, DFEA(E)IPEEYL, are highly similar (Figure 2.13 A), we propose that the improved affinity of variegin is mainly due to residues N-terminal to this sequence. Our results indicate that the active site binding moiety on variegin has the sequence EPKMHKT. Within this sequence lie two basic residues – Lys10 and Lys13 – which could be the P1 site. Either way, this sequence appears to be very different from sequences of most natural substrates of thrombin. For example, Lys at P1, although possible, is very rarely observed. Also, the presence of Glu/Met at P3, Met/glycosylated Thr at P1′ His/Ala at P2′ and glycosylated Thr at P4′ are all uncommon (Bode et al., 1992; Huntington, 2005; Page et al., 2005). Therefore, the identification of this unique active site binding moiety has significant implications for both understanding thrombin substrate preference and the discovery of new leads for developing direct thrombin inhibitors. The determination

of cleavage of variegin by thrombin, the unambiguous identification of the P1 residue, as well as molecular interactions between this unique active site binding moiety with thrombin active site become the next logical steps to proceed. Answers to these questions will be described in details in the next chapter.

Site-directed mutagenesis and intrinsic fluorescence studies suggest the following events during binding of hirudin to thrombin (Jackman et al., 1992; Myles et al., 2001): (1) electrostatic steering due to the complementary electrostatic fields of the hirudin C-terminus and thrombin exosite-I, (2) ionic tethering through direct interactions between specific residues of hirudin C-terminus inducing conformational changes and stabilization of the thrombin-hirudin C-terminal complex, and (3) subsequent binding of hirudin N-terminus to the apolar site near the active site. The conformational changes upon binding of hirudin C-terminus (step 2) detected in intrinsic fluorescence studies were observed to be the rate limiting step (Jackman et al., 1992). Hirudin behaved as a slow binding inhibitor in high ionic strength solution (> 0.2 M) where ionic interactions were impaired (Stone and Hofsteenge, 1986). Interestingly, in variegin, the deletion of seven N-terminal residues led to a switch from a fast binding inhibitor to a slow binding inhibitor without any loss of binding affinity. This slow binding observed for EP25 is presumably due to the loss of N-terminal residues instead of impaired ionic tethering observed for hirudin, suggesting a different rate limiting step. The kinetic studies indicate that the slow binding mode of EP25 probably involves isomerization of the thrombin-EP25 complex. We propose that long-range electrostatic interactions between the C-terminus of EP25 and thrombin exosite-I allow rapid formation of the initial collision complex (EI). This leads to subsequent binding of EPKMHKT to the active site in a slow step to form the

stabilized enzyme-inhibitor complex (EI*) through short range interactions (step 3 is the rate limiting step) (Figure 2.14). By contrast, in the full-length variegin, the N-terminus, possibly through two negatively charged residues in SDQGDVA, provides an additional electrostatic steering (but probably not tethering) effect to pre-orientate the N-terminus close to the active site allowing rapid formation of short-range interactions. The electrostatic steering effect of the N-terminus can be facilitated by the presence of the highly basic exosite-II. Exosite-II is located about 10 Å away from the active site (Page et al., 2005), a distance that can theoretically be covered by the seven N-terminal residues in an extended conformation (Figure 2.14).

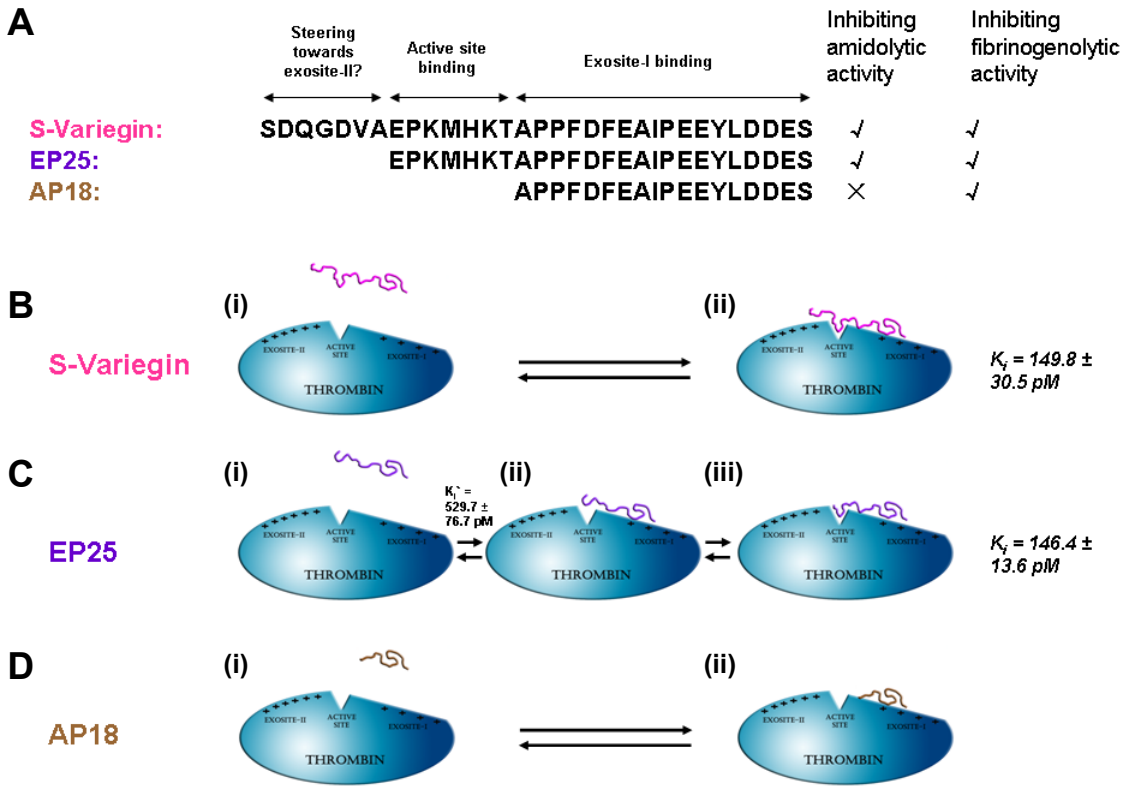

FIGURE 2.14

Proposed binding mechanisms of variegin and deletion variants

(A) The thrombin exosite-I binding moiety of variegin is within residues 15 to 32 and active site binding moiety is in the region of residues 8 to 14. The seven N-terminal residues, while not binding directly to thrombin, affected the binding kinetics; when removed, the binding characteristic of variegin changed from fast to slow, suggesting a possible steering effect to exosite-II.

(B) Proposed binding mechanism of variegin to thrombin: (i) complementary electrostatic charges between variegin N-terminus and thrombin exosite-II as well as between variegin C-terminus and thrombin exosite-I steer variegin to thrombin, (ii) all electrostatic interactions occurred rapidly (tethering) and pre-orient active site binding moiety (EPKMHKT) in correct conformation for fast binding to thrombin active site.

(C) Proposed binding mechanism of EP-25 to thrombin: (i) electrostatic charges on C-terminus steer EP25 to thrombin and subsequently provide specific tethering interaction, (ii) without the steering effect of N-terminal residues (SDQGDVA) the active site binding moiety is not orientated properly to fit the thrombin active site, hence the initial collision complex (EI) has a higher K_i`, and (iii) in a slow step the active site binding moiety (EPKMHKT) adopts the correct conformation for optimum binding and formation of a stabilized complex.

(D) Proposed binding mechanism of AP18 to thrombin: (i) electrostatic charges on C-terminus steer AP18 to thrombin and subsequently provide specific tethering interaction in a fast binding step, (ii) without the active site binding moiety (EPKMHKT) thrombin fibrinogenolytic activity but not amidolytic activity is inhibited. Fibrinogen binding to thrombin requires exosite-I, which is occupied by AP18.

2.5. SUMMARY

Variegin is one of the smallest (32 residues) thrombin inhibitors found in nature. Activity and affinity of n-variegin, s-variegin and two truncation variants (EP25 and AP18) for thrombin were determined. Variegin is a specific, fast and tight-binding, competitive thrombin inhibitor. We have demonstrated that the thrombin active site binding moiety of variegin is in the region of residues 8 to 14, and the exosite-I binding moiety is within residues 15 to 32. The first seven N-terminus residues governed kinetic of binding; without them, the peptide turns into a slow binding inhibitor.

Chapter Three

Thrombin inhibition by a cleavage product of variegin

3.1 INTRODUCTION

As found in the previous chapter, variegin is distinct from all other naturally occurring thrombin inhibitors. Instead, it shared some similarities to a human designed, synthetic thrombin inhibitor hirulog-1/bivalirudin. Between late 1980s and early 1990s, a group of novel thrombin inhibitors called hirulogs were reported (Maraganore et al., 1990; Witting et al., 1992). A peptide containing hirudin C-terminal residues 53 to 64 (NGDFEEIPEEYL) was observed to inhibit the thrombin fibrinogenolytic activity by binding to the exosite-I. The thrombin active site function is not inhibited by the peptide (Maraganore et al., 1989). Based on a model of thrombin structure (Furie et al., 1982), the N-terminal residue of this peptide was estimated to be at least 18 to 20 Å away from side chain hydroxyl group of the thrombin active site residue Ser195. On the other hand, the ability of $_{D}$-FPR, or similar tripeptides to bind to the thrombin active site was long established (Bajusz et al., 1978; Sonder and Fenton, 1984). However, while the hirudin C-terminal peptide lacks active site inhibitory function, $_{D}$-FPR lacks specificity and strong affinity. In order to overcome these problems, a non-sulfated hirudin C-terminal peptide was attached to $_{D}$-FPR through a flexible glycyl linker to cover the distance between the active site and exosite-I. By varying the number of residues in the linker segment, a group of potent bivalent thrombin inhibitors were designed and characterized. One of the molecules, hirulog-1, has four glycine residues in the linker segment. The activities of peptides with higher number of glycine residues do not differ significantly with hirulog-1. A shorter linker segment (two glycines) adversely affected the activity. Therefore, the optimum length of linker spanned four residues,

consistent with the estimation of the distance between the thrombin active site and exosite-I (Maraganore et al., 1990).

Hirulog-1 contains 20 residues and is a fast and tight-binding, competitive inhibitor of thrombin with K_i = 2.56 nM (Witting et al., 1992). Although its affinity to thrombin is about five orders of magnitudes weaker, the size of hirulog-1 is two third smaller than hirudin. Unlike hirudin, hirulog-1 is a canonical inhibitor of thrombin, binding to the active site in a substrate-like manner. Upon binding to thrombin, the substrate-like active site binding moiety of hirulog-1 is cleaved at the peptide bond between Arg3 and Pro4 (Skrzypczak-Jankun et al., 1991; Witting et al., 1992). It was subsequently named bivalirudin for its clinical development and is currently available in the market as Angiomax™ (in USA) or Angiox™ (in EU) (http://www.themedicinescompany.com/products_angiomax.shtml). Bivalirudin has a short plasma half-life (~ 25 min) and is eliminated by a combination of proteolysis and renal clearance (Warkentin et al., 2008). The process of bivalirudin development represented an elegant and successful example of rational drug designs. By taking part of a naturally occurring molecule (hirudin) as template, a molecule with more 'drug-like' properties (e.g. smaller size) was synthesized. It represents a new class of bivalent thrombin inhibitors, which was previously not encountered in nature.

Our data with the variegin truncation variants suggests that variegin inhibits thrombin with a canonical mechanism. Thus, the next few questions that surfaced are whether thrombin hydrolyzes variegin? If it does, how fast does it occur? Where is the cleavage site? What impact does the cleavage have on the activity of variegin? To answer these questions, we analyzed the cleavage process using RP-HPLC. Analysis

by RP-HPLC is a robust method to determine the extent of cleavage. With appropriate selection of column, eluent and elution gradient, cleaved peptides can be separated efficiently based on their hydrophobicity. Cleaved and separated peptides can be easily identified using mass spectrometer. In order to correlate cleavage with activity of peptides, several experiments probing the thrombin amidolytic activity under different conditions were devised. Hirulog-1 (bivalirudin) was synthesized to facilitate comparisons with s-variegin and its variants. In this chapter, careful comparisons between variegin and hirulog-1 are presented. Our results demonstrated nature's ability to produce a molecule that is similar but probably superior to the product of human drug design – hirulog-1/bivalirudin. Thus, variegin represents an interesting insight from nature on drug design.

3.2. MATERIALS AND METHODS

3.2.1 Materials

All materials used were as described in Chapter 2. For details please refer to *'Section 2.2.1. Materials'*.

3.2.2. Synthesis, purification and mass spectrometry analysis of peptides

Synthesis, purification and mass spectrometry analysis of s-variegin, EP25, MH22 and hirulog-1 followed procedures described in Chapter 2. For details please refer to *'Section 2.2.3.1. Peptide synthesis'*.

3.2.3. Thrombin

Two different sources of thrombin, recombinant α-thrombin (based on human α-thrombin sequence) and human plasma derived thrombin, were both generous gifts from the Chemo-Sero-Therapeutic Research Institute (KAKETSUKEN, Japan). Recombinant α-thrombin was desalted with HiTrap™ Desalting Column (GE Healthcare, Uppsala, Sweden) in 20 mM ammonium bicarbonate (NH_4HCO_3) and lyophilized before being used for the RP-HPLC analysis of cleavage. Human plasma derived thrombin was used to test thrombin inhibitory activities of peptides. Peptides generally showed 2-fold stronger inhibition against recombinant α-thrombin than plasma derived thrombin for an as yet to be identified reason. The K_m of S2238 for human plasma derived thrombin was determined to be 3.32 ± 0.35 μM, similar to the value obtained using recombinant α-thrombin (3.25 ± 0.56 μM) and other reported values in the literature (Stone and Hofsteenge, 1986; Myles et al., 2001).

3.2.4. RP-HPLC analysis of the cleavage

Peptides were incubated with recombinant α-thrombin at both 37°C and room temperature in 50 mM Tris buffer (pH 7.4) containing 100 mM NaCl and 1 mg/ml BSA. Reaction mixtures without thrombin were used as control. After various incubation times, the reactions were quenched with 0.1% TFA buffer (pH 1.8) and loaded onto a SunFire^{TM} C18 column attached to an ÄKTA^{TM} Purifier System. New peaks other than those present in the chromatogram of both control reaction mixture and 0 min incubation were identified as cleavage products and subjected to ESI-MS to verify their masses. The peaks were integrated to calculate the area under the peaks and the relative percentage of each peak to determine the extent of cleavage.

3.2.5. Thrombin inhibitory activities of peptides

Activities of s-variegin, EP25, MH22 and hirulog-1 were assayed by their abilities to inhibit the thrombin amidolytic activity on S2238. Assays were typically performed as described in *'Section 2.2.3.7. Inhibition of thrombin amidolytic activity'* of Chapter 2. Effects of pre-incubation times (hence cleavage) on thrombin inhibitory activities of peptides were performed with the same assay, varying pre-incubation times and/or concentrations of BSA. For experiments to ascertain integrity of thrombin exosite-I during extended incubation time, parallel sets of assay were performed with or without addition of freshly prepared inhibitors after 28 h of pre-incubation. All data obtained were fitted using Origin software to equation **(2)** for calculation of IC_{50} values and equations **(3)** to **(9)** for calculation of K_i values depending on the mechanisms of inhibition, as described in *'Section 2.2.3.8. Determination of the inhibitory constant K_i"* of Chapter 2. Details of each experiment are described along with the graphs representing the results obtained.

3.3. RESULTS

3.3.1. Cleavage of peptides by thrombin

Since variegin was hypothesized to canonically bind to the thrombin active site, it may be cleaved by thrombin which is similar to other serine protease inhibitors (Witting et al., 1992; Bode and Huber, 1992). Therefore we examined the cleavage of s-variegin by thrombin and its effects on peptides activities. The RP-HPLC analysis showed that s-variegin was indeed cleaved by thrombin at both 37 °C and room temperature (~ 25 °C). At 0 min of incubation, only peaks corresponding to full-length s-variegin and thrombin were present. Two new peaks representing cleavage products appeared and increased with incubation times (Figure 3.1). These new peaks had masses of 1045 Da (SDQGDVAEPK) and 2582 Da (MHKTAPPFDFEAIPEEYLDDES) respectively, and corresponded to cleavage at the Lys10-Met11 peptide bond. Cleavage proceeded faster at 37 °C (Figure 3.1 A) than at 25 °C (Figure 3.1 B).

In a preliminary experiment to verify the effect of variegin cleavage, s-variegin and EP25 were incubated with thrombin up to 24 h and at various time points assayed for the ability to inhibit the thrombin amidolytic activity. The results showed that both s-variegin and EP25 lost their activities only after prolonged incubation with thrombin (Figure 3.2). Interestingly, at the same temperature (25 °C) and molar ratios (30-fold excess of s-variegin), after 60 min of incubation, ~ 30% of s-variegin was cleaved (Figure 3.1 C), yet no significant loss of inhibitory activity of s-variegin (Figure 3.2 A) and EP25 (Figure 3.2 B) was observed. After 24 h of pre-incubation, only ~ 30% loss of inhibitory activity of s-variegin and EP25 was observed. In the

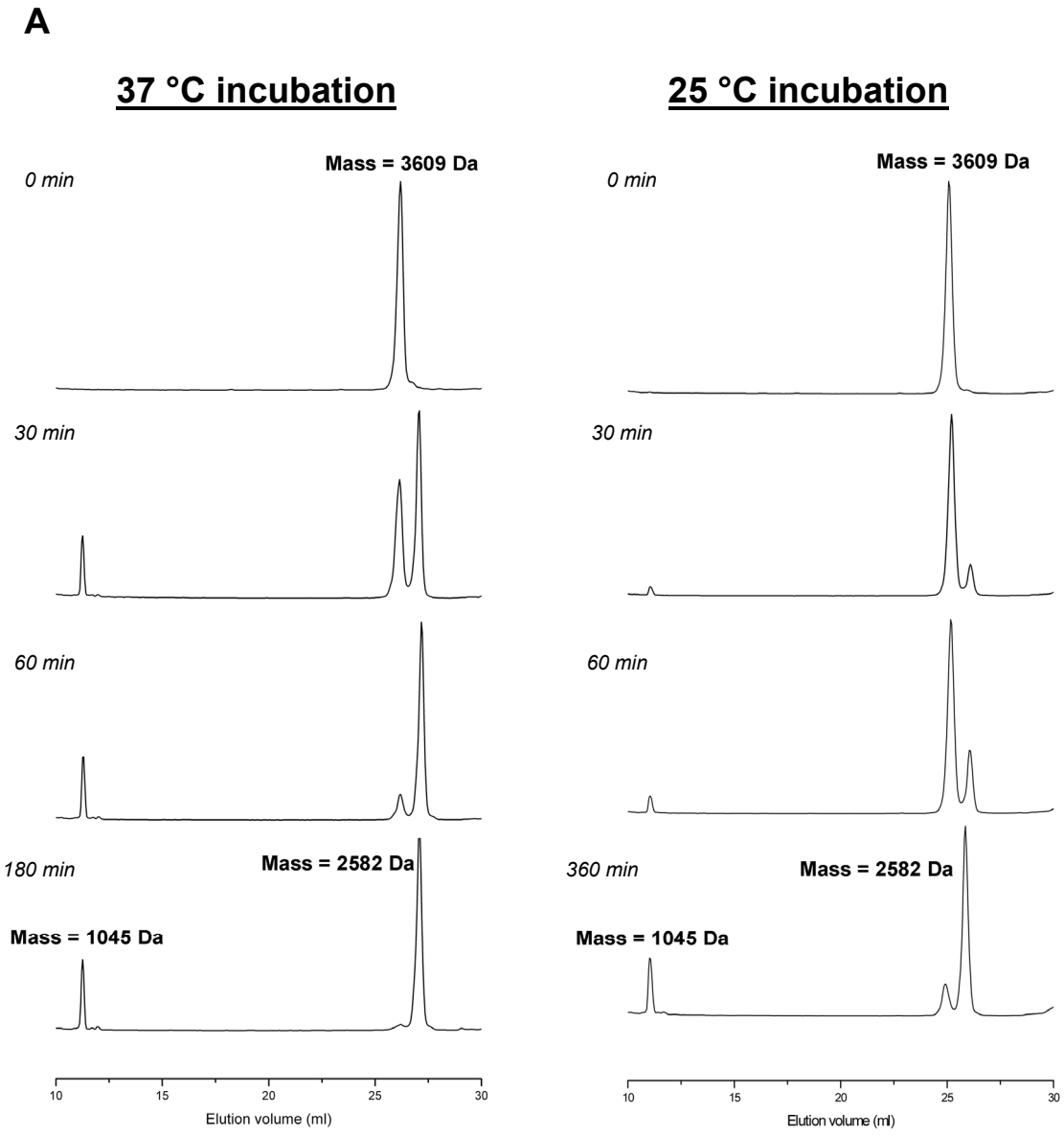

FIGURE 3.1

Cleavage analyses of s-variegin by thrombin at 37 °C and 25 °C

(A) s-variegin (150 μM) was incubated with thrombin (5 μM) for various times at room temperature (n = 2, error bars represent S.D.). S-variegin was present in 30-fold excess of thrombin. Cleavage of s-variegin by thrombin was analyzed with RP-HPLC. Figure showed typical chromatograms of HPLC analysis of the cleavage. At incubation time = 0 min, the single peak corresponds to full-length s-variegin. With incubation, two new peaks appeared corresponding to cleavage products of mass 1045 Da (representing N-terminal fragment SDQGDVAEPK) and 2582 Da (representing C-terminal fragment MHKTAPPFDFEAIPEEYLDDES) while uncleaved s-variegin decreased in quantity. Cleavage proceeded faster at 37 °C than at room temperature (25 °C). Only 180 min was needed for complete cleavage at 37 °C while 360 min was needed for ~ 90% of cleavage at 24 °C.

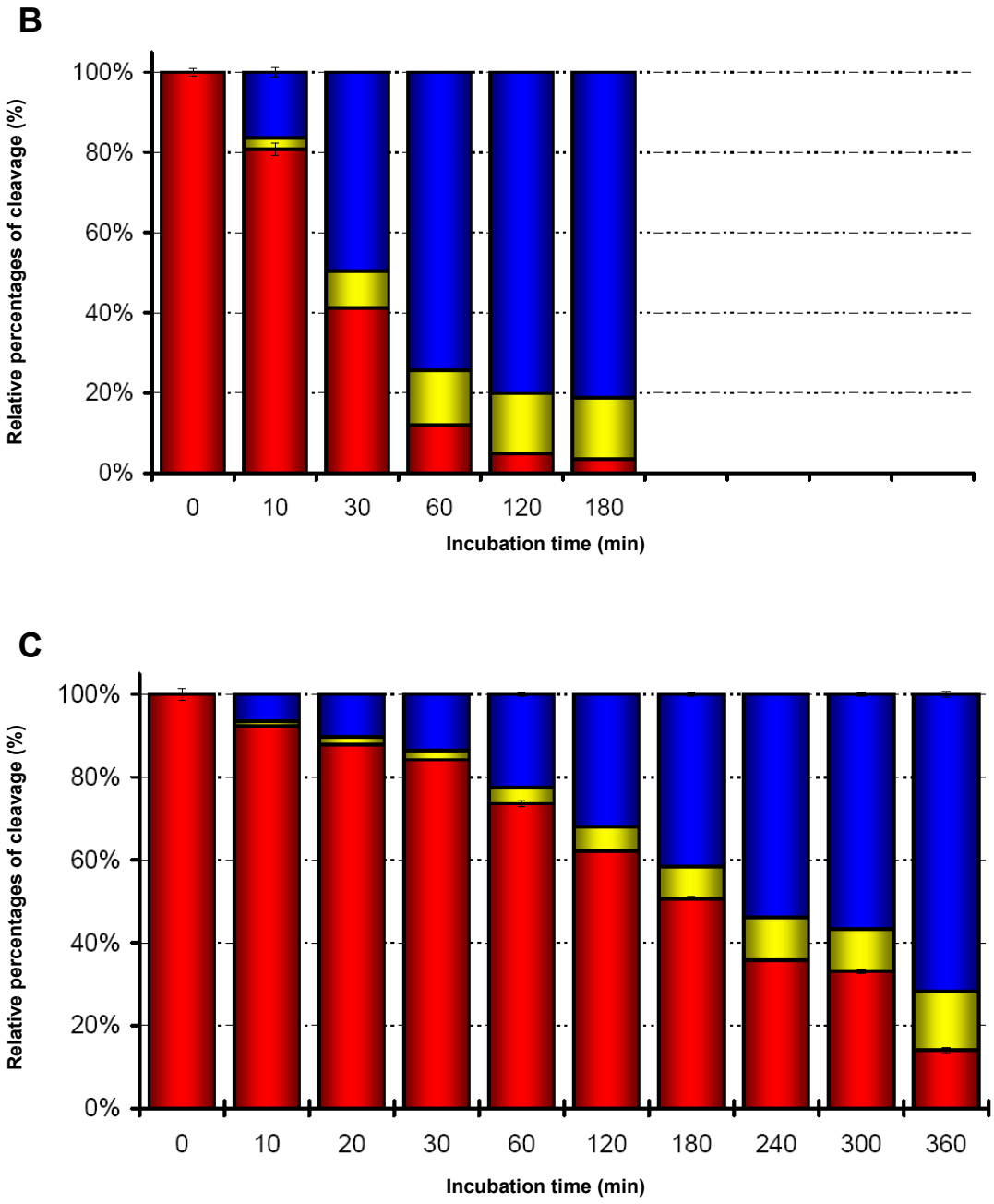

FIGURE 3.1 (continued)

Cleavage analysis of s-variegin by thrombin at 37 °C and 24 °C

Relative percentage of uncleaved s-variegin (■), cleavage product of mass 1045 (representing N-terminal fragment SDQGDVAEPK) (■) and cleavage product of mass 2582 (representing C-terminal fragment MHKTAPPFDFEAIPEEYLDDES) (■) was calculated by integrating area under the peaks in RP-HPLC analysis. Cleavage proceeded faster at 37 °C than at room temperature (24 °C) (n = 2, error bars represent S.D.).

(B) showed results obtained by incubating s-variegin and thrombin at 37 °C. Only 180 min was needed for complete cleavage.

(C) showed results obtained by incubating s-variegin and thrombin at 24 °C. 360 min was needed for ~ 90% of cleavage.

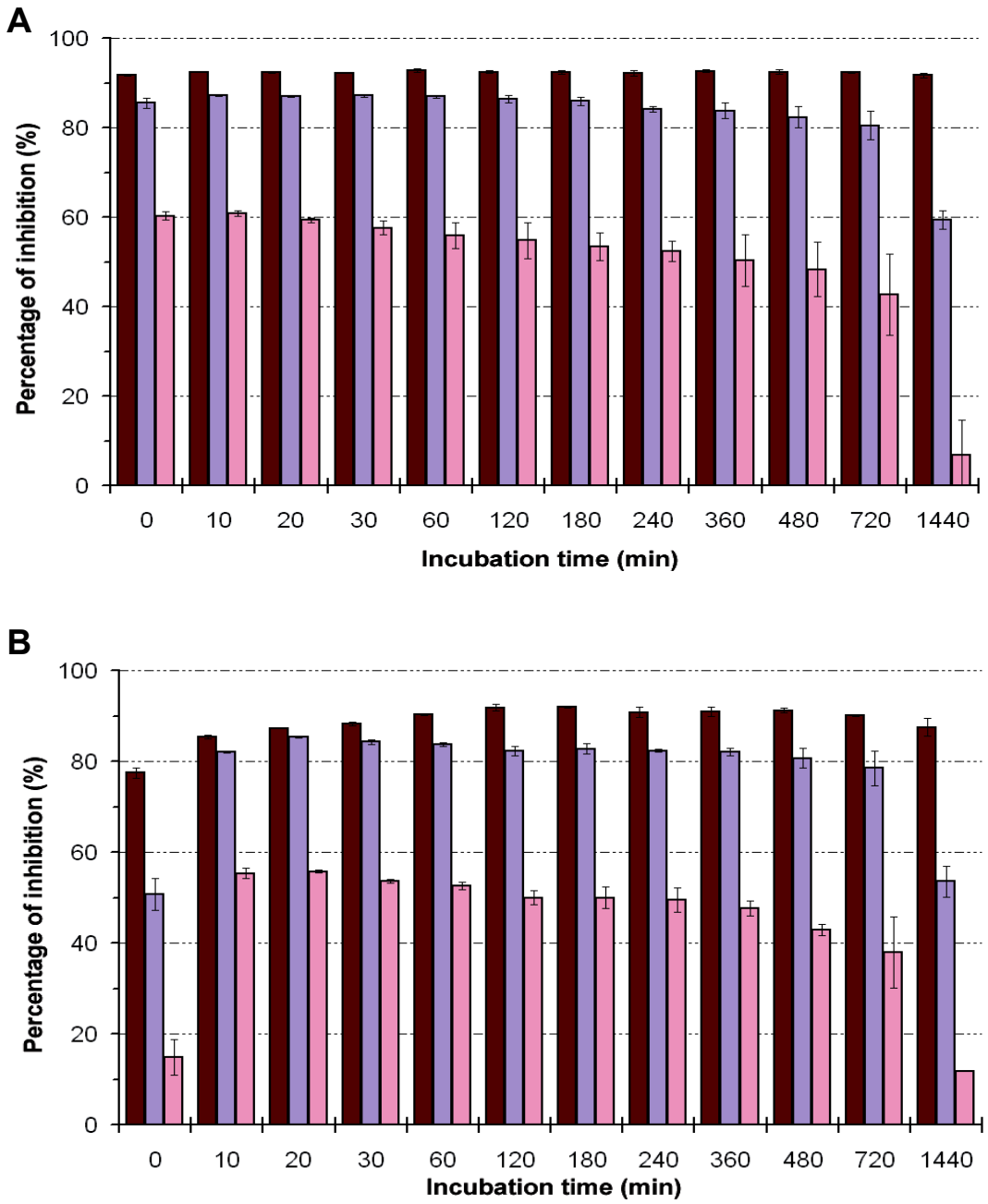

FIGURE 3.2

S-variegin and EP25 retained activities after being cleaved by thrombin

(A) S-variegin was incubated with thrombin (3.33 nM) for up to 24 hr at room temperature and at various time points assayed for the ability to inhibit thrombin amidolytic activity on 100 µM S2238 (n = 3, error bars represent S.D.).

(B) Similar experiments were carried out replacing s-variegin with EP25 (n = 3, error bars represent S.D.).

Concentrations of s-variegin or EP25 are 10 nM (■), 100 nM (■) and 1000 nM (■) (n = 2, error bars represent S.D.). At 100 nM of s-variegin or EP25, the inhibitors were present in 30-fold excess of thrombin identical with the molar ratio used in cleavage experiments, and hence were used primarily for comparison with cleavage data from RP-HPLC analysis (see Figure 3.1).

case of the slow binding inhibition of EP25, percentage inhibition increased with incubation time up to 20 min and then decreased due to cleavage by thrombin (Figure 3.2 B). Thus, it is likely that the cleavage product(s) retains strong binding to the thrombin active site.

3.3.2. Inhibition of thrombin amidolytic activity by cleavage product, MH22

To test if the variegin cleavage product is indeed responsible for its prolonged activity, the C-terminal fragment of cleavage (MHKTAPPFDFEAIPEEYLDDES) was synthesized (Table 3.1). This fragment, MH22, was selected for several reasons. First, the ability of the last 18 residues to bind to thrombin was observed earlier (AP18, see Chapter 2). Second, the first seven N-terminal residues of variegin do not bind to thrombin (see Chapter 2). Thus it is less likely that the other three residues EPK are responsible for the strong and prolonged inhibitory effect of variegin after cleavage (bear in mind that these assays were carried out with S2238 as substrate, which has an optimized structure based on a similar moiety, $_{D}$-FPR). Last, preliminary data from the thrombin-variegin structure obtained by X-ray diffraction suggested that MH22 binds to thrombin after cleavage (see Chapter 4 for details).

MH22 inhibited the thrombin amidolytic activity at equimolar concentration (~ 15%) and progress curves of inhibition showed that steady state equilibrium was achieved upon mixing. Thus, similar to s-variegin, MH22 is a fast and tight-binding inhibitor. Dose-response curve showed a IC_{50} value of 11.46 ± 0.71 nM (Figure 3.3). s-Variegin inhibition of human plasma derived thrombin has a IC_{50} value of 8.25 ± 0.45 nM (Figure 3.3), slightly higher than that of the recombinant α-thrombin (5.40 ± 0.95 nM) (Chapter 2).

TABLE 3.1

Peptide synthesis

Cleavage product of s-variegin (MH22) was synthesized. Hirulog-1 was also synthesized for comparison.

Name	Sequence	Theoretical mass (Da)	Observed mass (Da)	Basis for design
s-variegin	SDQGDVAEPKMHKTAPPFDFEAIPEEYLDDES	3608.9	3609.0	• Full-length sequence of variegin
MH22	MHKTAPPFDFEAIPEEYLDDES	2581.8	2581.8	• Cleavage product of variegin • C-terminal fragment of the scissile bond • Postulated to bind thrombin resulting in prolonged activity of s-variegin after cleavage
Hirulog-1	$_{D}$FPRPGGGGNGDFEEIPEEYL	2180.3	2179.6	• Designed by J. M. Maraganore et. al. (Maraganore et al., 1990; Witting et al., 1992) • Structurally similar to s-variegin • Short, linear peptide that binds thrombin active site and exosite-I • Like s-variegin, binding to thrombin results in cleavage • Synthesized as comparison with s-variegin and MH22

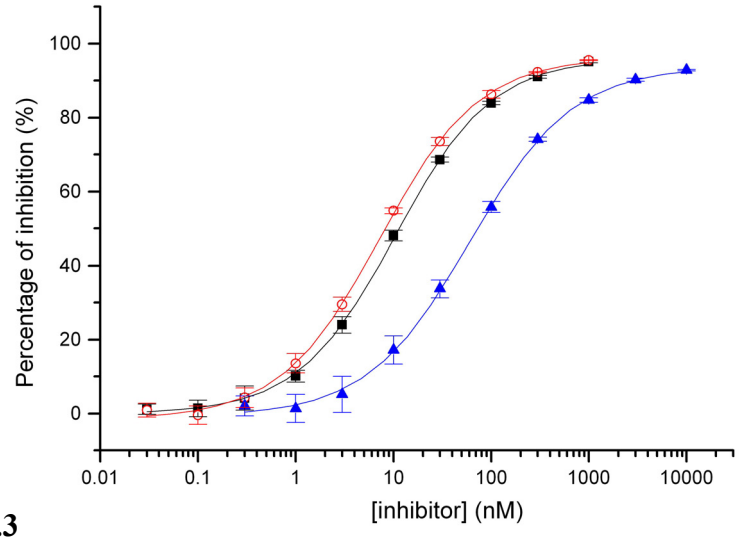

FIGURE 3.3

Inhibition of human plasma thrombin by MH22, s-variegin and hirulog-1

The ability of MH22, s-variegin and hirulog-1 to inhibit amidolytic activity of human plasma derived thrombin were assayed using active site directed substrate S2238 (100 μM). Dose response curves of thrombin (1.65 nM) inhibited by MH22 (■) s-variegin (○) and hirulog-1 (▲) all showed inhibition when they are present in similar molar concentrations with thrombin.

Concentrations used for MH22 (■) and s-variegin are 0.03 nM, 0.1 nM, 0.3 nM, 1 nM, 3 nM, 10 nM, 30 nM, 100 nM, 300 nM and 1000 nM. IC_{50} of inhibition are 11.46 ± 0.71 nM and 8.25 ± 0.45 nM, respectively (n = 3, error bars represent S.D.).

Concentrations used for hirulog-1 (▲) are 0.3 nM, 1 nM, 3 nM, 10 nM, 30 nM, 100 nM, 300 nM, 1000 nM, 3000 nM and 10000 nM. IC_{50} of inhibition is 72.6 ± 3.9 nM (n = 3, error bars represent S.D.)

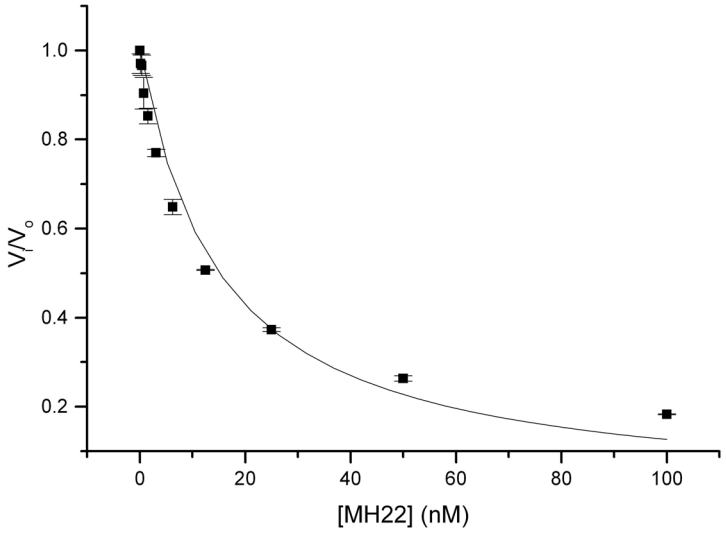

FIGURE 3.4

Apparent inhibitory constant, K_i' of MH22

Since MH22 behaved as a tight-binding inhibitor, inhibition of thrombin (1.65 nM) by MH22 at different concentrations (0.195 nM, 0.391 nM, 0.781 nM, 1.56 nM, 3.12 nM, 6.25 nM, 12.5 nM, 25 nM, 50 nM, 100 nM) were examined using different concentrations of S2238 as substrate. Reactions were started with the addition of thrombin. Shown in the figure are experiments performed with 100 μM S2238. Data obtained were fitted to equations **(3)** to derive an apparent inhibitory constant, K_i' (mean ± S.D.) of 14.31 ± 0.26 nM (n = 3, error bars represent S.D.).

3.3.3. The inhibitory constant K_i of MH22

The inhibitory constant, K_i of MH22 was determined using S2238 as substrate. MH22 is a fast and tight binding inhibitor. The apparent inhibitory constants, K_i' were determined in the presence of different concentrations of S2238 [equation **(3)**, Figure 3.4]. Unlike s-variegin which has K_i' values that increase linearly with increasing concentrations of S2238 [equation **(4)**], MH22 K_i' values remained constant with changes in S2238 concentrations. The behavior of the curve fits the equation that describes non-competitive inhibition where $\alpha = 1$ [equation **(5)**] and hence, $K_i' = K_i$ [equation **(6)**]. Fitting the K_i' values by linear regression derived a value of 14.11 ± 0.29 nM for K_i (Figure 3.5). s-Variegin showed a K_i of 0.318 ± 0.020 nM when assayed with human plasma derived thrombin (the K_i for recombinant α-thrombin was 0.146 ± 0.014 nM). Thus, the full-length peptide s-variegin is a competitive inhibitor, but its cleavage product MH22 is a non-competitive inhibitor of the function of thrombin active site.

3.3.4. Inhibition of thrombin amidolytic activity by hirulog-1 and its K_i

For comparison, hirulog-1 was synthesized based on a sequence reported previously (Maraganore et al., 1990). In our assays, hirulog-1 inhibited (human plasma derived) the thrombin amidolytic activity with IC_{50} = 72.6 ± 3.9 nM (Figure 3.6), which is about 9- and 6-fold weaker than s-variegin and MH22 respectively. The inhibitory constant K_i of hirulog-1 obtained by fitting data to equations describing fast, tight-binding, competitive inhibitors [equations **(3)** and **(4)**] is 2.94 ± 0.12 nM, similar to reported value in the literature [2.56 ± 0.35 nM (Witting et al., 1992)] (Figure 3.6 & 3.7). Thus, the actual affinity of MH22 to thrombin is weaker than hirulog-1 despite the lower IC_{50} value compared to hirulog-1 at saturating concentration of

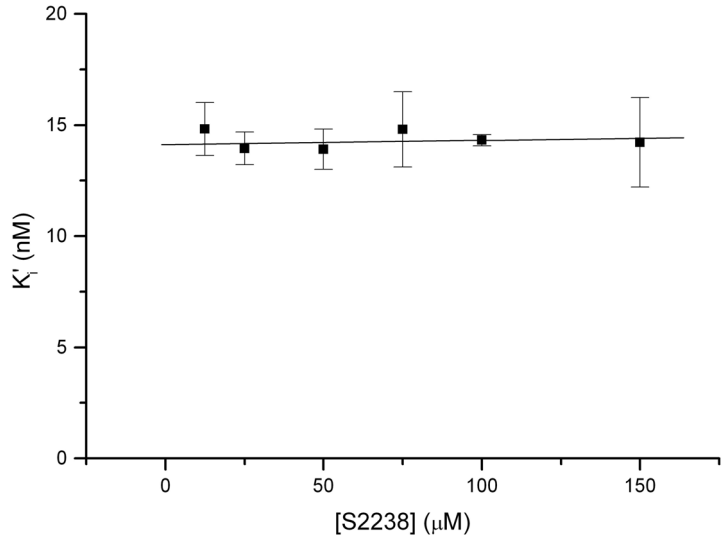

FIGURE 3.5

Inhibitory constant K_i of MH22

Apparent inhibitory constant K_i' of MH22 were determined with six different concentrations of substrate S2238 (12.5 μM, 25 μM, 50 μM, 75 μM, 100 μM and 150 μM). Plot of K_i' against substrate concentrations remained constant throughout, indicating MH22 non-competitively [equations **(5)** & **(6)**] inhibits thrombin amidolytic activity on S2238. Fitting the K_i' values by linear regression derived the inhibitory constant K_i as 14.11 ± 0.29 nM (n = 3 for each S2238 concentration, error bars represent S.D.).

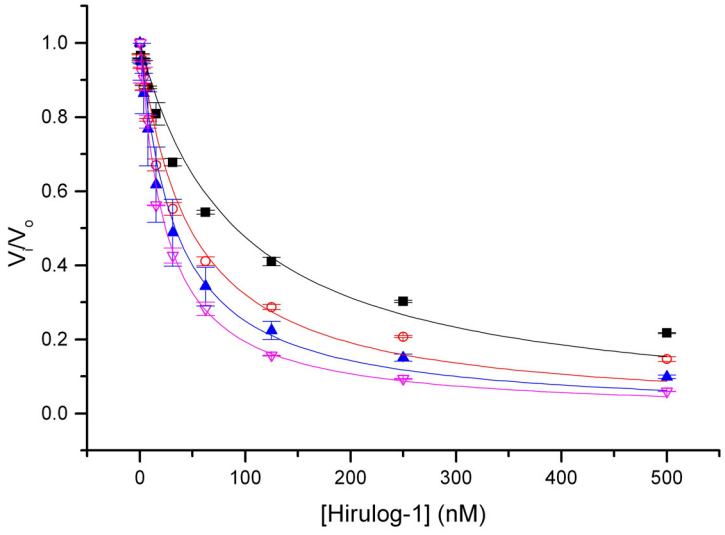

FIGURE 3.6

Apparent inhibitory constant, K_i' of hirulog-1

Inhibitions of thrombin (0.8 nM) by hirulog-1 at various concentrations (0.977 nM, 1.95 nM, 3.91 nM, 7.81 nM, 15.6 nM, 31.3 nM, 62.5 nM, 125 nM, 250 nM and 500 nM) were examined using 12.5 μM (▽), 25 μM (▲), 50 μM (○) and 100 μM (■) of S2238 as substrate. Reactions were started with the addition of thrombin. Data obtained were fitted to equations **(3)** to derive apparent inhibitory constant, K_i' (n = 2, error bars represent S.D.).

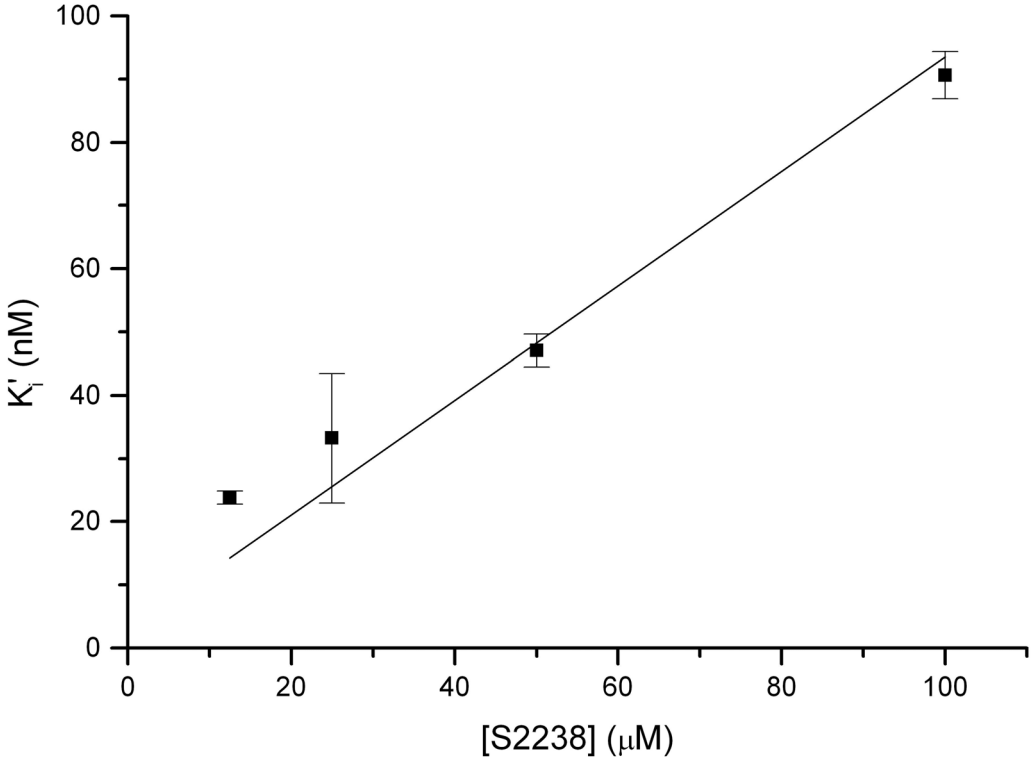

FIGURE 3.7

Inhibitor constant K_i of hirulog-1

Apparent inhibitory constant K_i' of hirulog-1 were determined with four different concentrations of substrate S2238 (12.5 μM, 25 μM, 50 μM and 100 μM). Plot of K_i' against substrate (S2238) concentrations increases linearly with increasing concentrations of substrate, indicates that hirulog-1 competitively inhibited thrombin amidolytic activity on S2238. By fitting the data to equation **(4)**, the inhibitory constant K_i was shown to be 2.94 ± 0.12 nM, similar to reported value in the literature (2.56 ± 0.35 nM) (n =2 for each S2238 concentration, error bars represent S.D.).

substrate (100 μM S2238). Being a competitive inhibitor, hirulog-1 IC_{50} values are significantly increased in higher concentrations of S2238 whereas MH22, a non-competitive inhibitor, has a constant IC_{50} independent of substrate concentrations.

3.3.5. Effect of pre-incubation times on activities of peptides

The RP-HPLC analysis showed cleavage increases with time (Figure 3.1). In order to investigate how cleavage affects the activities, MH22, s-variegin, EP25 and hirulog-1 were pre-incubated with thrombin for different lengths of time before respective residual thrombin amidolytic activities were determined (Table 3.2 and Figure 3.8). Dose-response curves for each peptide at various pre-incubation times were constructed. The IC_{50} of MH22 remained constant for at least 2 h at ~ 13 nM before a slight drop in activity after 18 h (IC_{50} = 28.4 ± 1.8 nM). After 28 h, activity of MH22 dropped sharply (IC_{50} of 479.7 ± 16.0 nM). For s-variegin, IC_{50} changed from 8.25 ± 0.45 nM (without pre-incubation) to 10.37 ± 0.30 nM (after 20 min pre-incubation) and remained constant up to at least 2 h. Similar to MH22, the activity of s-variegin started to decrease slightly after 18 h (IC_{50} = 27.8 ± 5.6 nM) and significantly after 28 h (IC_{50} = 504.2 ± 27.0 nM). Thus, cleavage of s-variegin caused an initial drop in activity. However, the cleavage product MH22 non-competitively inhibited thrombin, explaining the prolonged inhibitory effect of s-variegin. The convergence of IC_{50} values of the two peptides from 20 min onwards supported this assumption. For EP25, which is a slow binding inhibitor, the IC_{50} decreased from 173.1 ± 25.9 nM (without pre-incubation) to 13.12 ± 0.67 nM (after 20 min pre-incubation). Subsequently, a similar trend was observed where the IC_{50} remained constant up to 2 h and increased to 26.8 ± 4.1 nM and 437.9 ± 4.9 nM, respectively, after 18 h and 28 h. Lastly, for hirulog-1, the effect of cleavage was evident after just

TABLE 3.2

Effect of pre-incubation times on peptides activities

MH22, s-variegin, EP25 and hirulog-1 were pre-incubated with thrombin for different lengths of time before respective residual thrombin amidolytic activities were determined. Dose-response curves for each peptide at various pre-incubation times were constructed for calculations of IC_{50} (n = 3).

ND: not determined

Pre-incubation time (min)	IC_{50} (nM) (mean ± S.D.)			
	MH22	s-variegin	EP25	hirulog-1
0	11.46 ± 0.71	8.25 ± 0.45	173.1 ± 26.0	72.6 ± 3.9
10	13.36 ± 0.76	9.62 ± 0.30	14.1 ± 1.1	101.6 ± 13.0
20	12.4 ± 1.9	10.37 ± 0.30	13.12 ± 0.67	ND
30	14.94 ± 0.77	11.5 ± 1.3	13.6 ± 1.3	ND
45	ND	ND	ND	133.9 ± 16.0
120 (2 h)	13.53 ± 0.65	13.2 ± 1.3	12.4 ± 1.8	258.8 ± 26.0
1080 (18 h)	28.4 ± 1.8	27.8 ± 5.6	26.8 ± 4.1	ND
1680 (28 h)	479.7 ± 16.0	504.2 ± 28.0	437.9 ± 4.9	ND

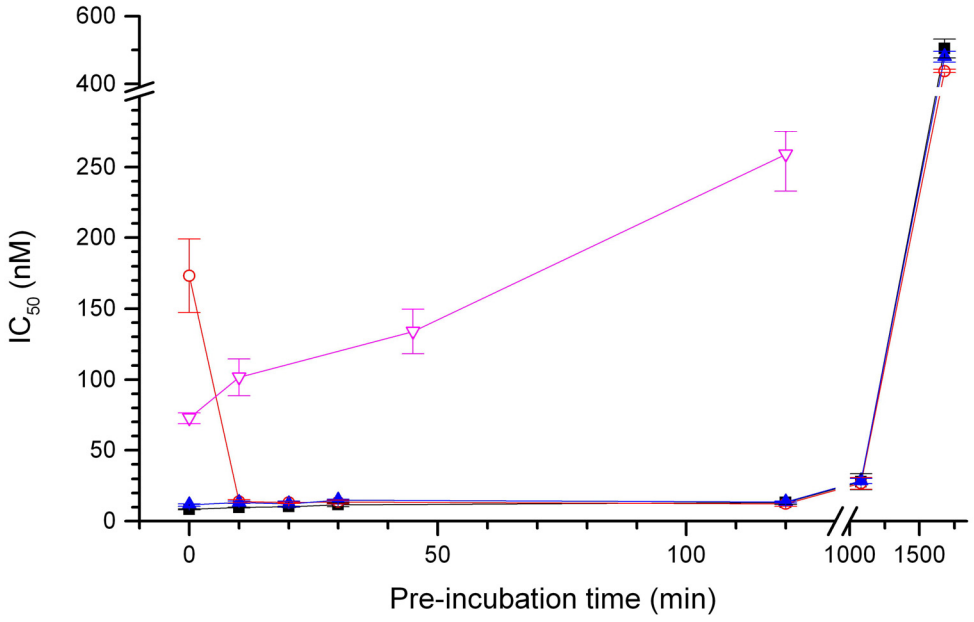

FIGURE 3.8

Effect of pre-incubation times on peptides activities

MH22 (▲), s-variegin (■), EP25 (○) and hirulog-1 (▽) were pre-incubated with thrombin (1.65 nM) for different lengths of time in 1 mg/ml BSA before respective residual thrombin amidolytic activities were determined. Dose-response curves for each peptide at various pre-incubation times were constructed for calculations of IC_{50}. (n = 3, error bars represent S.D.)

Cleavage product of s-variegin and EP25 (which is represented by MH22) inhibited thrombin non-competitively, causing a prolonged potent inhibitory effect of these peptides up to 18 h, before a sudden drop in activity at 28 h. In contrast, IC_{50} of hirulog-1 increase linearly with pre-incubation times, indicates that cleavage directly causes a loss of function.

Concentrations of MH22, s-variegin and EP25 are 0.03 nM, 0.1 nM, 0.3 nM, 1 nM, 3 nM, 10 nM, 30 nM, 100 nM, 300 nM and 1000 nM. Pre-incubation times used are 0 min, 10 min, 20 min, 30 min, 120 min (2 h), 1080 min (18 h) and 1680 min (28 h).

Concentrations of hirulog-1 are 0.1 nM, 0.3 nM, 1 nM, 3 nM, 10 nM, 30 nM, 100 nM, 300 nM, 1000 nM and 3000 nM. Pre-incubation times used are 0 min, 10 min, 45 min and 120 min (2 h).

10 min, where the IC_{50} dropped from 72.6 ± 3.9 nM to 101.6 ± 13.0 nM. The IC_{50} values gradually increased with pre-incubation times. By 2 h, the IC_{50} of hirulog-1 was 258.8 ± 26.0 nM. Therefore, as opposed to s-variegin, the cleavage product of hirulog-1 probably fails to inhibit thrombin, leading to the rapid loss of activity.

3.3.6. Loss of MH22 activity on prolonged pre-incubation

The prolonged inhibitory effects of variegin peptides after cleavage are due to thrombin inhibition by their cleavage product (MH22). Although MH22 inhibited thrombin potently upon mixing, its activity decreased sharply after 28 h pre-incubation (Figure 3.8). Possible explanations for this observation includes: (1) further cleavage by thrombin; (2) α-thrombin was degraded into its beta or gamma forms (due to autolysis) with the loss of exosite-I, thus the target site of MH22 is not available; or (3) non-specific adsorption of MH22 to the reaction wells, reducing the amount of peptides available to inhibit thrombin.

MH22 sequence contains a Lys at position 3 (residue 13 in full-length variegin), which could act as the P1 residue to facilitate a second cleavage. To test this possibility, MH22 was incubated with thrombin up to 28 h at room temperature (25 °C) and the mixture was analyzed for the cleavage products by RP-HPLC. Interestingly, no cleavage in MH22 was observed even after 28 h. On the other hand, ~ 30% of hirulog-1 was cleaved by 2 h and by 18 h, cleavage was complete (Figure 3.9). Therefore, the loss of MH22 activity after 28 h pre-incubation is not due to further cleavage of the peptide.

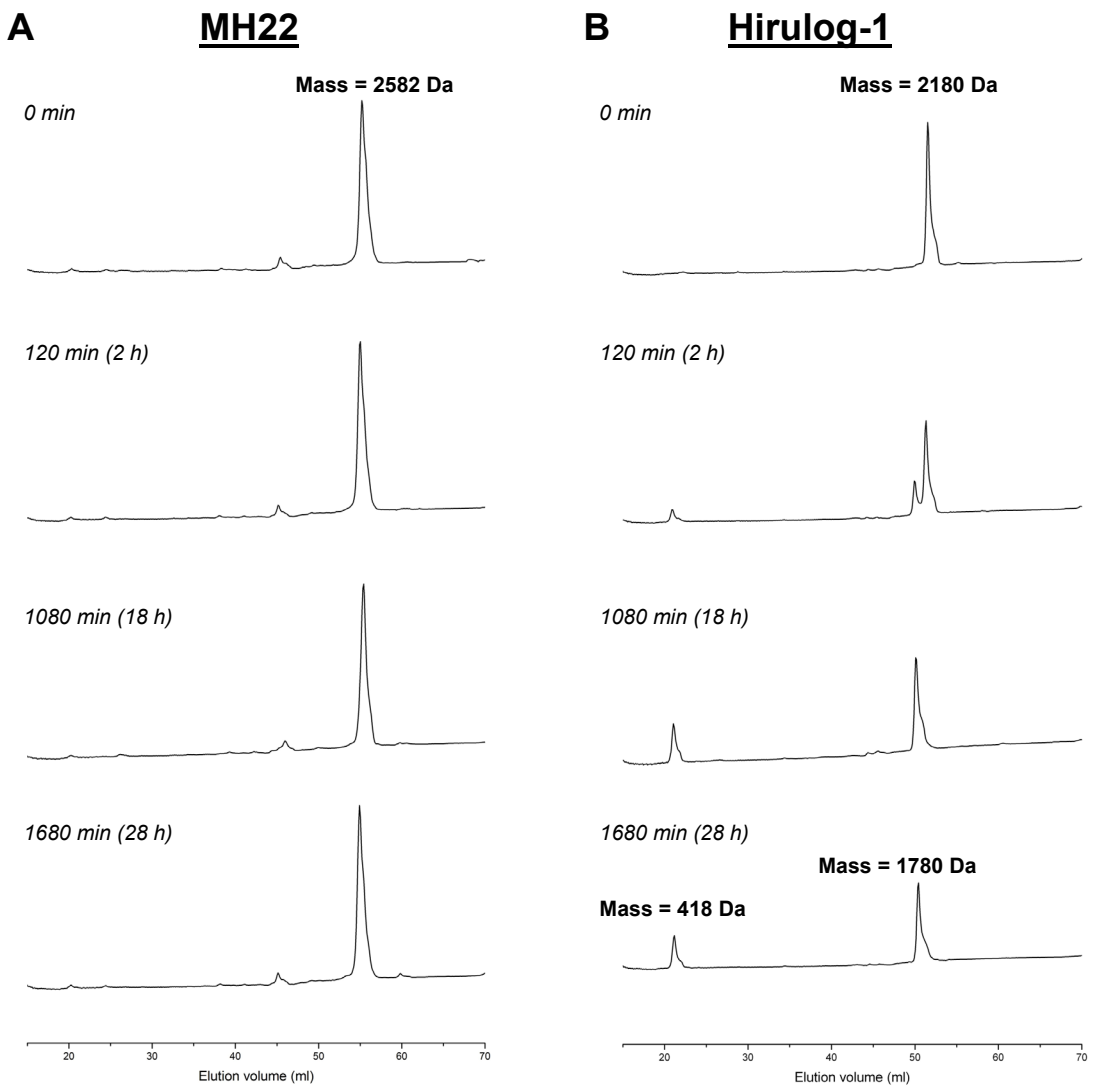

FIGURE 3.9

Cleavage analysis of MH22 and hirulog-1 by thrombin at 25 °C

(A) MH22 (final concentration: 150 μM) was incubated with thrombin (final concentration: 1.5 μM) for various times [0 min, 120 min, 1080 min (18 h), 1680 min (28 h)] at room temperature (n = 3, error bars represent S.D.). Cleavage of the peptides by thrombin was analyzed with RP-HPLC. Figure showed typical chromatograms of HPLC analysis of MH22 cleavage by thrombin. At incubation time = 0 min, the main peak corresponds to intact MH22. No new peak was observed even after 28 h incubation, indicates MH22 did not undergo a second cleavage by thrombin. Therefore, the significant loss of MH22 activity after 28 h is not due to cleavage of the peptide by thrombin.

(B) Same experiment was conducted with hirulog-1 replacing MH22. As incubation time increased, new peaks with 1780 Da (PGGGGNGDFEEIPEEYL) and 418 Da ($_{D}$FPR) appeared. Cleavage of hirulog-1 by thrombin between Arg3-Pro4 causes loss of its thrombin inhibitory activity (Figure 3.8).

Human α-thrombin is known to be susceptible to proteolysis. Trypsin cleaves thrombin at Arg77A-Asn78 bond to produce β_T-thrombin, while thrombin autolysis occurs at an additional Arg67-Ile68 scissile bond resulting in excision of the Ile68 to Arg77A peptide, producing β-thrombin (Boissel et al., 1984; Braun et al., 1988b). Alternatively, cleavage at Arg75-Tyr76 and Arg77A-Asn78 for β-thrombin was also reported (Chang, 1986). When proteolysis occurs only at the Lys149E-Gly150 bond, β′-thrombin is formed (Chang, 1986). A combination of cleavages for β- and β′-thrombin produces γ-thrombin (Rydel et al., 1994). Crucially, these cleavages disrupt the exosite-I of α-thrombin. As a result, clotting activities of β- and γ-thrombin was significantly reduced. Affinities for fibrin, thrombomodulin and hirudin (all target exosite-I) were lost, but amidolytic activities towards small synthetic substrates (e.g. S2238) were not affected (Bode et al., 1992). MH22 contains the exosite-I binding sequence (AP18) characterized in Chapter 2. When thrombin is autolyzed into β and/or γ forms, thrombin exosite-I is lost which might then cause MH22 to lose its inhibitory activity. Therefore, the assays were slightly modified to probe the integrity of the thrombin exosite-I under our experimental conditions. After 28 h pre-incubation (when the IC_{50} of s-variegin and MH22 increased significantly), fixed concentrations of respective peptides (at their IC_{50} without pre-incubation) were added fresh into the reaction mixture before the addition of substrate S2238 (Figure 3.10). It was hypothesized that, if the thrombin exosite-I was disrupted (due to autolysis) after 28 h, freshly added peptides should not inhibit thrombin. On the contrary, if the thrombin exosite-I is intact, freshly added inhibitors should bring about inhibition at least to the same level without pre-incubation (assuming peptides originally present in reaction mixture were all inactive). As shown Figure 3.10, the freshly added peptides were able to inhibit the thrombin amidolytic activity. However,

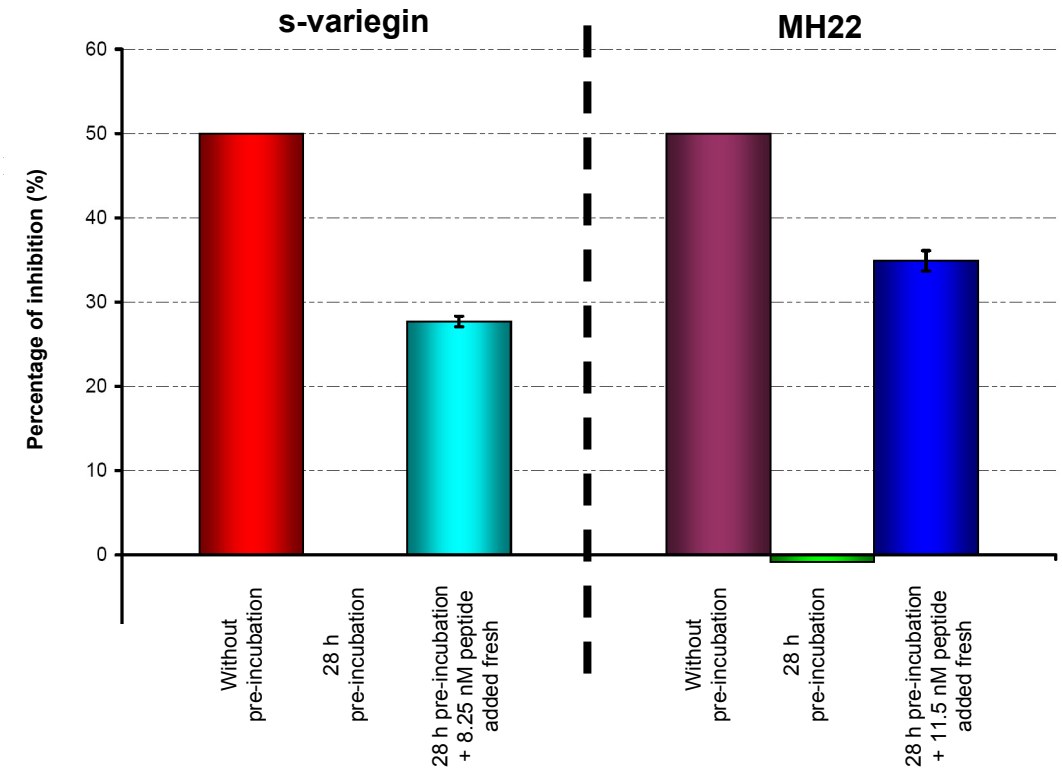

FIGURE 3.10

Determination of α-thrombin stability after 28 h pre-incubation

A modified assay of thrombin amidolytic activity was used to probe for α-thrombin stability after 28 h of pre-incubation. Without pre-incubation, s-variegin inhibited thrombin by ~ 50% at 8.25 nM (red bar), but after 28 h pre-incubation, thrombin inhibitory activity was lost (green bar, not visible). Addition of 8.25 nM of fresh s-variegin after 28 h pre-incubation restored the inhibition partially to 27.70 ± 0.62% (cyan bar) (N = 3, error bars represent S.D.).

Similarly, without pre-incubation, MH22 inhibited thrombin by ~ 50% at 11.5 nM (magenta bar), but after 28 h pre-incubation, thrombin inhibitory activity was lost (green bar). Addition of 11.5 nM of fresh MH22 after 28 h pre-incubation also restored the inhibition partially to 34.9 ± 1.2% (blue bar) (N = 3, error bars represent S.D.).

Overall results suggested that a small degree of activity loss after prolonged incubation can be attributed to thrombin autolysis

the percentages of inhibition were lower than the expected levels. For example, after 8.25 nM of s-variegin were pre-incubated with thrombin for 28 h, no inhibition was observed. Although ~ 50% inhibition was expected if stability of thrombin was not affected by the prolonged incubation, freshly added 8.25 nM s-variegin inhibited thrombin by ~ 28%. Similarly, 11.5 nM of MH22 inhibited thrombin by ~ 50% without pre-incubation, but after 28 h pre-incubation, no inhibition was observed. The freshly added 11.5 nM MH22 inhibited thrombin by ~ 35%, instead of the expected ~ 50%. Thus, there appeared to be a small degree of autolysis occurring with the prolonged pre-incubation. However, since the freshly added peptides were able to partially restore the inhibition, the significant loss of s-variegin and MH22 activities after 28 h cannot be solely attributed to the autolysis of thrombin.

To investigate whether non-specific adsorption of peptides to reaction wells was causing the drops in activities, MH22, s-variegin, EP25 and hirulog-1 were pre-incubated with thrombin for 28 h in a buffer containing various concentrations of BSA (1, 5 and 10 mg/ml). In the case of MH22, s-variegin and EP25, increase in BSA concentrations restored peptides activities almost completely. For MH22, the IC_{50} after 28 h in the presence of 1 mg/ml, 5 mg/ml and 10 mg/ml of BSA are 479.7 ± 16.0 nM, 60.9 ± 3.1 nM and 62.9 ± 10.9 nM, respectively. The IC_{50} s-variegin are 504.2 ± 27.0 nM, 53.4 ± 12.0 nM and 38.99 ± 0.43 nM, in the same order. Similarly, The IC_{50} of EP25 are 437.9 ± 4.9 nM, 39.1 ± 9.4 nM and 38.4 ± 5.4 nM (Figure 3.11). These similar IC_{50} values obtained in 5 mg/ml and 10 mg/ml BSA indicates that restoration of the activities was saturated, although incomplete. Therefore, both the non-specific surface adsorptions of peptides and partial loss of thrombin stability (due to autolysis)

account for the loss of inhibitory activities of variegin (and variants) after the prolonged pre-incubation.

The loss of hirulog-1 activity after 2 h of pre-incubation could not be reversed by increasing concentrations of BSA. The IC_{50} values remained the same (258.8 ± 26 nM, 279.7 ± 4.7 nM, 281.8 ± 6.2 nM for 1 mg/ml, 5 mg/ml and 10 mg/ml of BSA, respectively) (Figure 3.12). Interestingly, between 1 nM to 100 nM, hirulog-1 activated thrombin. The C-terminal segment of hirudin was reported to bind to the exosite-I and enhances thrombin amidolytic activity (Naski et al., 1990). Similar activation was also observed with AP18 [see Chapter 2]. It is likely that the hirulog-1 C-terminus (structurally similar to the hirudin C-terminal segment) remains bound to thrombin after cleavage but, due to its inability to bind to the active site, loses the inhibitory function. Thus, at high concentrations of hirulog-1 (≥ 300 nM in Figure 3.12), the uncleaved hirulog-1 is present in excess, resulting in thrombin inhibition. However, between 1 nM and 100 nM, the amount of uncleaved hirulog-1 is too low to produce observable inhibition. Instead, the effect of cleavage product (which is thrombin activation) predominates and results in the negative values for inhibition.

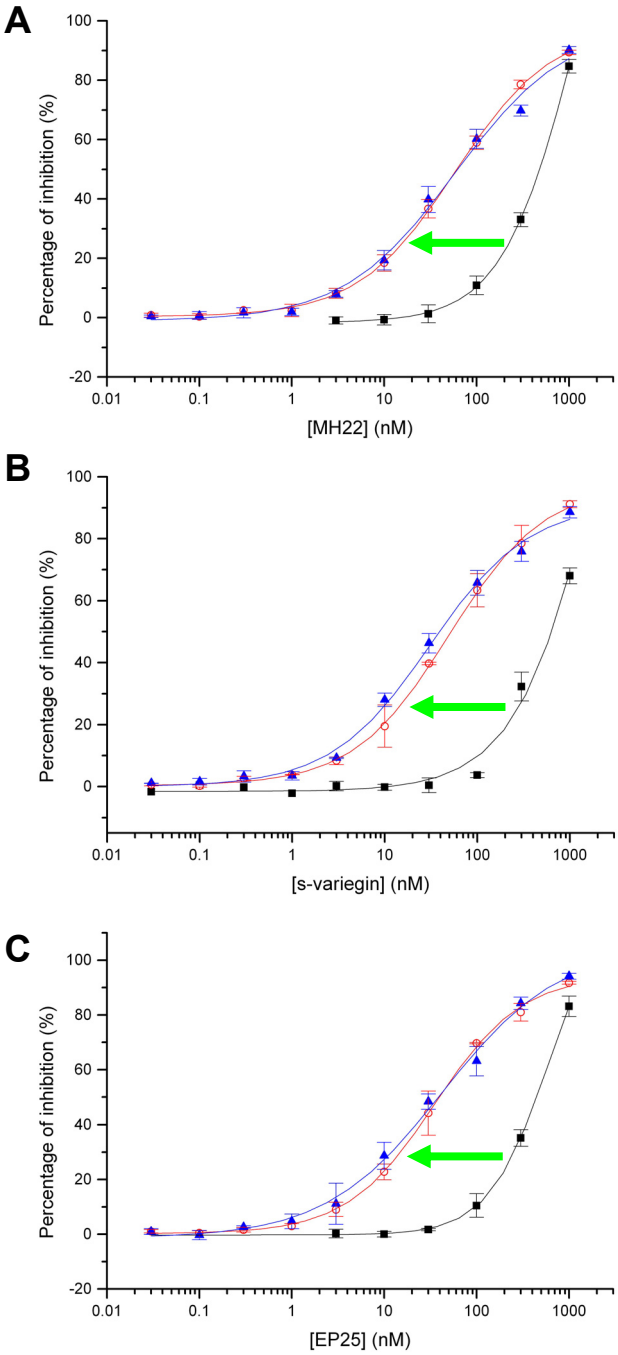

FIGURE 3.11

Non-specific surface adsorption of peptides

Peptides were pre-incubated with thrombin (1.65 nM) for 28 h in 1 mg/ml (■), 5 mg/ml (○) and 10 mg/ml (▲) of BSA before respective residual thrombin amidolytic activities were determined (S2238 = 100 µM). Increasing BSA concentrations almost completely restored peptide activities, indicated by left shift of dose-response curves (green arrows). Concentrations of MH22, s-variegin and EP25 were 0.03 nM, 0.1 nM, 0.3 nM, 1 nM, 3 nM, 10 nM, 30 nM, 100 nM, 300 nM and 1000 nM. (n = 3, error bars represent S.D.)

(A) MH22 IC_{50} are 479.7 ± 16.0 nM (■), 60.9 ± 3.1 nM (○) and 62.9 ± 10.9 nM (▲).

(B) S-variegin IC_{50} are 504.2 ± 27.0 nM (■), 53.4 ± 12.0 nM (○) and 38.99 ± 0.43 nM (▲).

(C) EP25 IC_{50} are 437.9 ± 4.9 nM (■), 39.1 ± 9.4 nM (○) and 38.4 ± 5.4 nM (▲).

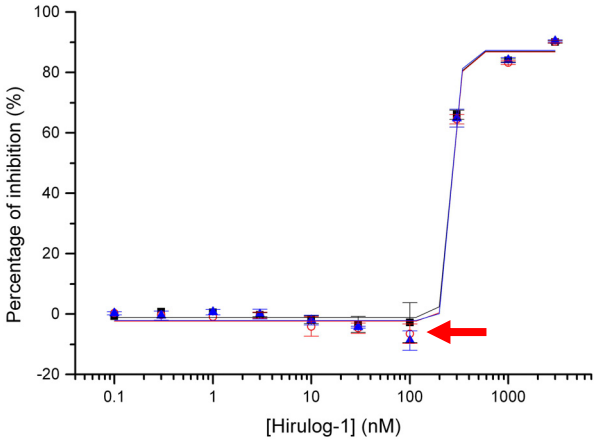

FIGURE 3.12

Non-specific surface adsorption of peptides

Hirulog-1 was pre-incubated with thrombin (1.65 nM) for 28 h in 1 mg/ml (■), 5 mg/ml (○) and 10 mg/ml (▲) of BSA before respective residual thrombin amidolytic activities were determined (S2238 = 100 μM). Concentrations of hirulog-1 are 0.1 nM, 0.3 nM, 1 nM, 3 nM, 10 nM, 30 nM, 100 nM, 300 nM, 1000 nM and 3000 nM. Hirulog-1 IC_{50} are 258.8 ± 26 nM (■), 279.7 ± 4.7 nM (○) and 281.8 ± 6.2 nM (▲). Increasing BSA concentrations did not restore activity of hirulog-1. Between 1 nM to 100 nM thrombin activity was enhanced instead of inhibited. At high concentrations (≥ 300 nM), uncleaved hirulog-1 produced inhibitions. However, between 1 nM to 100 nM, where amount of uncleaved hirulog-1 is too low to produce observable inhibition, effect of cleavage product predominates and presented as negative values for inhibition (red arrow) (n = 3, error bars represent S.D.).

	P3	P2	P1	P1'	P2'	P3'	P4'	Mechanism of inhibition
S-variegin	Glu	Pro	Lys	Met	His	Lys	Thr	Competitive
Hirulog-1	D-Phe	Pro	Arg	Pro	Gly	Gly	Gly	Competitive
MH22				Met	His	Lys	Thr	Classical non-competitive
S2238	D-Phe	Pip	Arg	*p*NA				(substrate)

Cleavage

FIGURE 3.13

s-Variegin and MH22 thrombin active site inhibition

C-terminal sequences of s-variegin and hirulog-1 are almost identical (not shown), hence s-variegin most likely derived its stronger (~ 9-fold) affinity from active site binding residues. Compared to hirulog-1, P1 and P3 residues of s-variegin are sub-optimal for thrombin binding. Arg at P1 and D-Phe at P3 are favorable for thrombin active site binding. The tetrapeptide sequence MHKT is uncommon among thrombin natural substrates/inhibitors.

During amidolysis *p*Na moiety of S2238 occupies S1' subsite of thrombin, thus should theoretically interferes with MH22 (especially Met) binding to the same site (boxed in red). However, MH22 acts as a classical non-competitive inhibitor – binding to both free thrombin and thrombin-substrate complex with the same affinity – indicates that *p*Na and Met binding site are not overlapping.

3.4. DISCUSSION

Based on our data with s-variegin and its truncation variants, we hypothesize that s-variegin binds to the thrombin active site in a canonical manner (*'Section 2.4. Discussion'* in Chapter 2). However, the conformation of s-variegin is in an extended form unlike the commonly found loop structure of canonical inhibitors (Bode and Huber, 1992; Krowarsch et al., 2003). Results presented in this chapter confirmed this hypothesis. Upon incubation with thrombin, s-variegin is cleaved by thrombin at the Lys10-Met11 scissile bond. Despite the cleavage, the variegin inhibitory activity was largely retained. The strong binding of the C-terminal fragment of the cleavage (MH22) to thrombin probably explains the prolonged effect of s-variegin and EP25. Interestingly, MH22 non-competitively inhibits thrombin. However, extended pre-incubation resulted in the eventual loss of peptides activity. This observation is mainly due to thrombin autolysis and non-specific surface adsorption peptides to reaction wells instead of further cleavage by thrombin. In contrast, hirulog-1 rapidly loses its inhibitory function due to the cleavage.

Cleavage analysis of s-variegin showed that the P1 residue is Lys10. The presence of P1 Lys, although possible, is rare (Page et al., 2005). Despite the less preferred P1 residue, variegin inhibition of thrombin is strong and specific, presumably compensated by other interactions. Sequence comparison between s-variegin and hirulog-1 provided some clues to this problem. Under our experimental conditions, compared to hirulog-1, s-variegin binds to thrombin about 9-fold stronger. The difference is unlikely to stem from their interactions with the thrombin exosite-I, since the C-terminal sequences of both peptides are almost identical. s-Variegin active

site binding sequence resides in its middle segment (EPKMHKT), which is also the site where it is most different from hirulog-1. Compared to the corresponding segment in hirulog-1 ($_{D}$FPRPGGG), s-variegin P1 (Lys) and P3 (Glu) residues are both theoretically sub-optimal for thrombin. A number of different P3 residues can be found in natural substrates, but for those that do not require a cofactor for thrombin binding, Gly or Ser (small/small and hydrophilic) usually occupies this position (Huntington, 2005). Moreover, presence of acidic residue in P3 position is known to impair thrombin proteolysis (Le Bonniec and Esmon, 1991). In synthetic substrates, a large, hydrophobic $_{D}$-amino acid is preferred (Vindigni et al., 1997). Thus, the overall stronger binding of s-variegin is most likely derived from its P′ residues, especially the MHKT tetrapeptide sequence (Figure 3.13).

The importance of MHKT sequence was further demonstrated by the ability of variegin cleavage product (MH22) to potently inhibit thrombin. MH22 inhibited the thrombin active site function. In contrast, AP18, without the four residues (MHKT), does not (Chapter 2). Thus, the MHKT sequence is mainly responsible for the active site inhibitory activity of MH22, targeting the S1′ to S4′ subsites on thrombin. This sequence is uncommon among thrombin natural substrates or inhibitors. Generally it was observed that the S1′ subsite of thrombin is limited in size, therefore prefer small and hydrophilic P1′ residues such as Gly and Ser (Bode et al., 1992; Page et al., 2005). However, in variegin, a bulky, hydrophobic residue (Met) is present. The P2′ site of natural thrombin substrates is occupied by Pro, aromatic (Phe/Tyr) or bulky hydrophobic (Val/Ile) residue (Huntington, 2005). Variegin is again different from the norm in that a His is present at the P2′ site. The Arg at P3′ was reported to interact with Glu39 and Glu192 of thrombin (Bode et al., 1992). In variegin, a Lys is present

and could make similar contacts. More importantly, the P4′ of variegin is a glyco-Thr. s-Variegin, which is not glycosylated, recorded 14-fold weaker affinity for thrombin, suggesting strong interaction between the hexose moiety with thrombin.

MH22 non-competitively inhibited thrombin. Typically, a non-competitive inhibitor binds at a site distal from the active site and allosterically inhibits its function. However, the MHKT tetrapeptide are residues immediately after the scissile bond. Intuitively, binding of this segment to thrombin is likely to be within the active site. Substrate used in the experiments, S2238, has a chemical structure of $_{D}$-Phe-Pipecolyl-Arg-*p*NA, with its Arg side chain inserted into the thrombin S1 subsite and cleavage occurs between the Arg-*p*NA bond. With the *p*NA moiety also occupying the S1′ in the immediate proximity of scissile bond during amidolysis, its presence should theoretically interferes with the binding of MH22 to the same site – and the reverse (MH22 obstructing S2238 binding) should also be true (Figure 3.13). In such a case, α should be > 1 [equation **(5)**] and the plot of K_i' against substrate concentrations should increase in a hyperbolic manner with increasing concentrations of substrate (Copeland, 2000). This type of non-competitive inhibition is usually termed 'mixed inhibition'. However, under our experimental conditions, the apparent inhibitory constant, K_i', remained strictly constant with changes in substrate concentrations. Thus, MH22 act as a classical non-competitive inhibitor, binding to both free thrombin and thrombin-substrate complex with the same affinity (Figure 3.14). On the same note, the assumption that *p*NA interferes with MH22 binding does not hold. Therefore, the binding sites of MH22 and *p*NA on thrombin are not overlapping, indicate that the residue immediately after the scissile bond (Met11) may not bind to thrombin or binds at a different site (Figure 3.13).

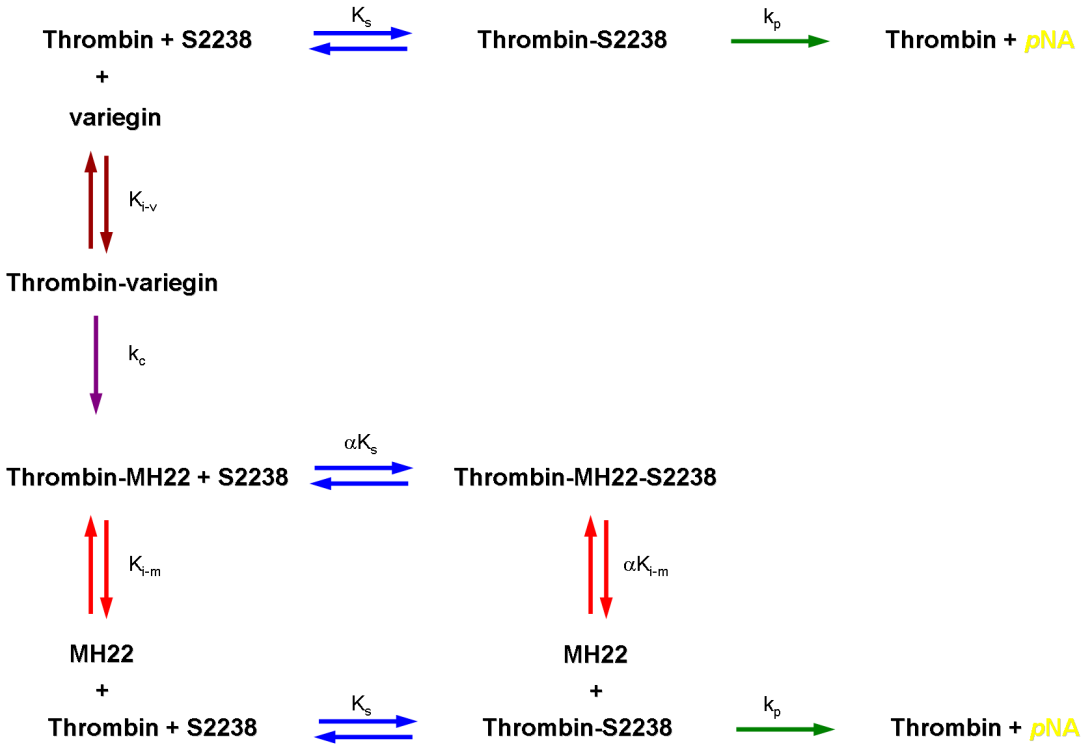

FIGURE 3.14

Equilibrium scheme for variegin inhibition of thrombin

In the absence of variegin, S2238 binds to thrombin (K_s is the equilibrium constant for thrombin-S2238 dissociation, blue arrows) and hydrolyzed by thrombin to release colored product *p*NA (k_p is the forward rate constant for *p*NA formation, green arrow).

In the presence of variegin, thrombin binds to variegin ($K_{i\text{-}v}$ is the inhibitory constant of variegin, brown arrows) thus S2238 hydrolysis is inhibited competitively. Upon binding, thrombin cleaves variegin into MH22 (k_c is the forward rate constant for cleavage, violet arrow).

MH22 remained bound to thrombin, acting as a classical non-competitive inhibitor of thrombin ($K_{i\text{-}m}$ is the inhibitory constant of MH22). MH22 binds to free thrombin or S2238 bound thrombin with the same affinity, $\alpha = 1$, thus $K_{i\text{-}m} = \alpha K_{i\text{-}m}$ (red arrows). Similarly, $K_s = \alpha K_s$, binding of S2238 to thrombin is unaffected by MH22.

In the absence of its N-terminal globular core, a long fragment of hirudin C-terminal (T^{45}PKPQSHNDGDFEEIPEEYLQ^{65}) was reported to either inhibit the thrombin amidolytic activity with hyperbolic uncompetitive ($\alpha = 0.49$) (Schmitz et al., 1991) or hyperbolic competitive mechanisms ($\alpha = 4$) (DiMaio et al., 1990) or non-inhibitory at all (Krstenansky and Mao, 1987). In first two cases, the inhibitory activities are weak, with the K_i of 410 nM (Schmitz et al., 1991) and 110 nM (DiMaio et al., 1990), respectively. In addition, a thrombin inhibitor isolated from the camel tick *Hyalomma dromedarii*, NTI-1, was also reported to be a non-competitive inhibitor of the thrombin active site function. However, its affinity for thrombin is also weak (K_i = 11.7 μM). The molecule also inhibits FXa (5-fold less potent compared to thrombin inhibition) (Ibrahim et al., 2001a). Therefore, to our knowledge, the characterization of MH22 is the first account of a potent and specific classical non-competitive inhibitor of the thrombin active site. Therefore, detailed structure-function relationships studies on MH22 should help in the development of a new group of thrombin inhibitors.

The subsequent loss of peptide activity after more than 28 h of pre-incubation with thrombin was somewhat surprising. Our results show that the autolysis of thrombin partially accounts for this observation. Earlier studies have shown that 50% cleavage time at 25 °C for Lys149E-Gly150 peptide bond and disruption of thrombin exosite-I was 32 h (Chang, 1986). After 28 h of incubations, the freshly added peptides inhibited thrombin, albeit to a lesser extent. The observed lower levels of inhibitions are probably due to the autolysis and loss of binding site (exosite-I) for variegin (and variants). Further, the ability of BSA to restore most of the peptide activity suggested the possibility of non-specific adsorption of peptides to the reaction

wells. Judging from the late elutions of variegin peptides on C18 RP-HPLC columns, these peptides are rather hydrophobic. Thus, adsorption to polystyrene microtiter plates used in experiments is very likely the explaination (Hermanson, 2008). The combined effects of the autolysis of thrombin and nonspecific adsorption of peptides to the reaction wells explain the observed loss of inhibitory activity of variegin peptides. However, these effects are pertinent only to *in vitro* settings (long incubation time, plastic environment etc.) and are irrelevant *in vivo*.

In contrast to s-variegin, the cleavage of hirulog-1 caused an immediate loss of activity. This indicates that hirulog-1 cleavage product is unable to inhibit thrombin, unlike s-variegin products. In fact, a peptide similar to the C-terminal cleavage fragment of hirulog-1 (GGGGGNGDFEEIPEEYL; the first residue in the cleavage fragment of hirulog-1 would be Pro instead of Gly) was unable to inhibit thrombin (Maraganore et al., 1990). It is conceivable that this fragment continues to be bound to thrombin after the cleavage, since the last 12 residues (NGDFEEIPEEYL) binds to the thrombin exosite-I. However, the glycyl linker lacks specific interactions with thrombin (Maraganore et al., 1990; Skrzypczak-Jankun et al., 1991). This peptide, with a sulfated tyrosine (named hirugen), binds to thrombin with the K_i values of 540 to 640 nM (Naski et al., 1990). When desulfated, the affinity typically drops around 10-fold (Maraganore et al., 1989). As hirulog-1 is non-sulfated, the binding of its C-terminal cleavage fragment to thrombin would be at least two orders of magnitude weaker than variegin cleavage product MH22 (K_i = 14.11 ± 0.29 nM). In addition to the weaker binding, the effects of the cleavage products on thrombin are also different. The variegin cleavage product (MH22) continues to potently inhibit thrombin but the hirulog-1 cleavage product paradoxically activated the thrombin active site function.

It is interesting to think that while development of hirulogs represents successful rational drug design, variegin demonstrates the ability of nature to produce similar 'designs' through evolution. Nonetheless, there are also significant differences between them. First, variegin contains only natural amino acids (Koh et al., 2007), while hirulog-1 has a $_{D}$-Phe (Witting et al., 1992). Second, even the synthetic form of variegin (s-variegin), that are without Thr-glycosylation, is a stronger inhibitor of thrombin. For example, the s-variegin K_i (assayed with human plasma derived thrombin) is 0.318 ± 0.020 nM, while the hirulog-1 K_i is 2.94 ± 0.12 nM (similarly assayed with human plasma derived thrombin). The potency of variegin is probably derived from its unique sequence that targets an extended surface on thrombin active site and exosite-I, including the S1′ to S4′ subsites (by using the MHKT sequence). In contrast, the hirulog-1 glycyl linker does not bind to thrombin (Maraganore et al., 1990; Skrzypczak-Jankun et al., 1991). Third, the cleavage of product of variegin MH22 remained tight-bound to thrombin (K_i = 14.11 ± 0.29 nM), while the binding of the hirulog-1 cleavage product to thrombin is about 400-fold weaker (Maraganore et al., 1989; Naski et al., 1990). Last, the variegin cleavage product, MH22, potently and non-competitively inhibits thrombin but the hirulog-1 cleavage product paradoxically activates the function of thrombin active site. Thus, variegin appeared to retain the advantages of hirulog-1 (small size, proteolytic cleavage and hence lower dependency on renal function to eliminate the drug), but with improved potency (lower K_i), probably longer inhibitory effects (cleavage product inhibits thrombin) and better safety profile (no risk of paradoxical activation of thrombin). It is obvious that the differences between the molecule and hirulog-1 are vast and significant which makes it a far more superior candidate for the development of novel anticoagulants.

3.5 SUMMARY

Variegin was shown to bind to thrombin in a substrate-like mechanism. Upon binding, it is cleaved by thrombin between Lys10 and Met11. The variegin C-terminal fragment after cleavage (MH22) remained tightly bound to thrombin and inhibited the enzyme non-competitively with a K_i of 14.11 ± 0.29 nM. The loss of peptide activity after prolonged incubation is not due to a second cleavage by thrombin but due to a combination of the autolysis of thrombin and non-specific adsorption of peptides on the reaction surfaces. In contrast, the cleavage of hirulog-1 by thrombin causes rapid loss of inhibitory action and paradoxically activates the function of thrombin active site.

Chapter Four

The structure of thrombin-s-variegin complex and the design of new variegin variants

4.1. INTRODUCTION

Variegin is a novel, fast and tight-binding competitive inhibitor of thrombin. The peptide is short (32 residues) with a novel sequence. Structurally, it is dissimilar to any other groups of naturally occurring thrombin inhibitors, thus belongs to a class of its own (Koh et al., 2007). Based on biochemical data obtained with variegin truncation variants, the thrombin active site binding moiety of variegin is in the region of residues 8 to 14, and the exosite-I binding moiety is within residues 15 to 32. The seven N-terminal residues govern the binding kinetics; when removed, the binding characteristics of variegin changed from fast to slow (Chapter 2). Binding in a substrate-like mechanism, variegin is cleaved by thrombin at the Lys10-Met11 scissile bond. The C-terminal cleavage fragment of variegin (MH22) remained strongly bound to thrombin, non-competitively inhibiting the enzyme (Chapter 3).

To further understand the molecular details of the thrombin-s-variegin interactions, we solved the 3D structure of this complex by X-ray crystallography. Since the first thrombin crystal structure was solved in 1989 (Bode et al., 1989), X-ray crystallography has been a useful tool for studies of the molecular interactions involving thrombin. The relatively large size of the thrombin-variegin complex (~ 40 kDa) and a reasonable number of successful examples of the thrombin complexes (Bode et al., 1989; Skrzypczak-Jankun et al., 1991; Bode et al., 1992; Qiu et al., 1992) justified the selection of X-ray crystallography as the experimental approach. In order to minimize the amount of sample (especially thrombin) used, the previously reported crystallization conditions for similar thrombin-inhibitors complexes (Skrzypczak-Jankun et al., 1991), instead of using new crystallization screens, were attempted.

After some initial efforts on the optimizations of crystallization and crystal-freezing conditions, the complex structure was solved at 2.4 Å resolution. Based on the structure obtained, 13 new variants of variegin were designed and characterized to further our understanding of the interactions.

Thrombin is a multi-functional molecule. Human α-thrombin is a two-chain (chains A and B) protein. The A-chain is much shorter (36 residues) than the B-chain (259 residues) and the two chains are linked by a disulfide bridge. The B-chain, in particular, carries the catalytic domain, which is mainly responsible for the functions of thrombin (Di Cera, 2003). The active site contains the classical catalytic triad – His57, Asp102 and Ser195. Compared to other blood coagulation serine proteinases, thrombin has a prominent active site cleft which is deep and narrow. This structure is frequently described as a canyon-like cleft. Two insertion loops (60- and autolysis loops) forming the wall of the cleft. The active site of thrombin has an acidic S1 subsite, hence it preferably cleaves substrates with a basic side chain at the P1 position of the scissile bond (Bode et al., 1992; Huntington, 2005). The narrow active site cleft restricts the shape and size of substrates that can be inserted. Of the two insertion loops, the 60-loop (Leu59 – Asn62) is rigid and hydrophobic while the autolysis loop (Leu144 – Gly150) is flexible and hydrophilic. The 60-loop covers the 'top' of the active site and interacts with the hydrophobic residues of the substrate N-terminal to the scissile bond. Conversely, the autolysis loop, which is situated at the 'bottom' of active site cleft, governing interactions with the residues C-terminal to the scissile bond (Huntington, 2005). The surfaces of thrombin active site that interact with the substrate residues N-terminal to the scissile bond are described as 'non-prime subsites' (S subsites) in this thesis. Similarly, the surfaces of active site in contact

with the substrate residues C-terminal to the scissile bond are typically described as 'prime subsites' (S′ subsites) (Page et al., 2005).

Exosite-I is a surface near the prime subsites of thrombin. The bottom of the exosite-I is a deep, canyon-like cleft extending from the prime subsites. The cleft is apolar in nature. The walls of the cleft are formed by two surface loops Phe34 – Leu39 (described as 34-loop in this thesis) and Lys70 – Glu80 (described as 70-loop in this thesis) (Rydel et al., 1991). In contrast to the apolar nature of the canyon-like cleft, the surface of exosite-I is dominated by several positively-charged residues (Skrzypczak-Jankun et al., 1991). The exosite-I interacts with substrates fibrinogen, FV, FVIII, FXI, ADAMTS13 and PAR-1; with cofactors fibrin and thrombomodulin; and with inhibitor heparin cofactor II (Huntington, 2005). Exosite-II is an even more basic surface near the 'non-prime subsites' of the active site, interacting with substrates FV and FVIII; and with cofactors GpIbα, heparin and chondroitin sulphate moiety on thrombomodulin (Huntington, 2005). Occupancy of either exosites can induce allosteric changes to the active site to enhance catalysis. The Na^+ binding loop (Cys220 – Trp225) also provides allosteric control to thrombin function. The Na^+ binding (denoted as 'fast' form) favors the procoagulant functions of thrombin, such as increased binding to fibrinogen and PAR-1 whereas Na^+-free thrombin (denoted as the 'slow' form) favors the anticoagulant functions such as increased protein C activation (Di Cera, 2003; Huntington, 2008). In order to perform precisely its diverse yet sometimes opposing functions, thrombin utilizes these important exosites to ensure its specificity in the recognition and interaction with different substrates/cofactors/inhibitors. By making use of competition for exosites as well as the differences in the local distribution of various substrates and cofactors in the

microenvironment, thrombin is able to function as the central control mechanism to the blood coagulation system (Lane et al., 2005).

This chapter presents first the structure of thrombin-s-variegin complex and then the design and characterization of more variegin variants. Structural observations well complemented activity studies of all variants and instilled great confidence in both sets of data. Important information for both thrombin substrate preference and inhibitor design was elucidated which provided a strong foundation for continuous development of variegin as an anticoagulant.

4.2 MATERIALS AND METHODS

4.2.1. Materials

4-(2-Hydroxyethyl)piperazine-1-ethanesulfonic acid (HEPES), HEPES sodium salt and polyethylene glycol (PEG) 8000 were from Sigma Aldrich (St. Louis, Missouri, USA). Crystallization trays and grease were purchased from Hampton Research (Aliso Viejo, California, USA). All other materials used were as described in Chapter 2. For details please refer to *'Section 2.2.1. Materials'*.

4.2.2. Synthesis, purification and mass spectrometry of peptides

Synthesis, purification and mass spectrometry analysis of s-variegin, EP25, MH22 and hirulog-1 followed the procedures described in Chapter 2. For details please refer to *'Section 2.2.3.1. Peptide synthesis'*. Of special notes are peptides containing sulfotyrosine (DV24Y^{sulf}, DV24K10RY^{sulf} and MH18Y^{sulf}), of which the sulfate groups are acid labile. The cleavage of these peptides was carried out with 90% aqueous TFA on ice for 5 h as previously described (Kitagawa et al., 2001). Purification of the peptides containing sulfotyrosine (DV24Y^{sulf}, DV24K10RY^{sulf} and MH18Y^{sulf}) and phosphotyrosine (DV24Y^{phos} and DV24K10RY^{phos}) were performed with solvent containing 0.1% FA as ion pairing agent instead of TFA. The sulfate moiety on Tyr27 is unstable during ionization in mass spectrometry analysis, thus the non-sulfated masses were observed. Identification of sulfated peptides was on the basis of: (1) non-sulfated masses of the peptides; (2) as opposed to tyrosine residue that absorbs UV at 280 nm, sulfotyrosine residue does not; and (3) sulfated and non-sulfated peptides do not co-elute in RP-HPLC.

4.2.3. Thrombin

Two different sources of thrombin – recombinant α-thrombin (based on human α-thrombin sequence) and human plasma derived thrombin, both were generous gifts from the Chemo-Sero-Therapeutic Research Institute (KAKETSUKEN, Japan). Recombinant α-thrombin was desalted with the HiTrap™ Desalting Column (GE Healthcare, Uppsala, Sweden) in 20 mM ammonium bicarbonate (NH_4HCO_3) and lyophilized before using it for crystallization. Human plasma derived thrombin was used to assay thrombin inhibitory activities of the peptides.

4.2.4. Crystallization of thrombin-s-variegin complex

The reported crystallization conditions that were used to crystallize the thrombin-hirugen and thrombin-hirulog-1 complexes of human α-thrombin (Skrzypczak-Jankun et al., 1991) were modified and optimized. Lyophilized s-variegin was dissolved in 50 mM HEPES buffer (pH 7.4) containing 375 mM NaCl to a concentration of 8.34 μM (3 mg/ml). Desalted, lyophilized recombinant α-thrombin was subsequently dissolved in the s-variegin solution to a final concentration of 5.56 μM (20 mg/ml). The amount of s-variegin in this mixture was 1.5-fold in excess of thrombin. Crystallization of the thrombin-s-variegin complex was achieved using the hanging drop vapor diffusion method. Typically, 1 μl of protein solution was mixed with 1 μl of precipitant buffer (100 mM HEPES buffer pH 7.4, containing 20 to 25% (w/v) PEG 8000 and were equilibrated against 1 ml of precipitant buffer at 4 °C. Crystals appeared after approximately four weeks and were harvested for data collection two weeks later. The entire process for setting up, growing and harvesting of crystals were performed in 4 °C as the crystals are unstable at room temperature.

4.2.5. Data collection

Prior to data collection, the crystals were briefly soaked in a cryoprotectant solution containing the mother liquor, supplemented with 25% (v/v) glycerol, and flash cooled at 100 K in nitrogen (gas) cold stream (Cryostream cooler, Oxford Cryosystem, Oxford, United Kingdom). Synchrotron data were measured at the Beamline X29 (National Synchrotron Light Source, Brookhaven, USA). Data sets were collected (Table 4.1) using the Quantum 4-CCD detector. The diffraction data were processed using the program HKL2000 (Otwinowski and Minor, 1997). The crystal belonged to the monoclinic space group C2 and diffracted up to 2.4 Å resolution with a = 124.66 Å, b = 50.83 Å, c= 61.54 Å and V = 385390.59 $Å^3$ Da^{-1} and corresponded to a solvent content of 59.09%.

4.2.6. Structure solution and refinement

The structure of thrombin-s-variegin complex was solved by the molecular replacement method using the MolRep program (Vagin and Teplyakov, 2000). The coordinates of the thrombin-hirulog-3 structure (PDB code 1ABI) (Qiu et al., 1992) were used as a search model. The rotation search (in resolution shells of 25 to 4 Å) located one thrombin-peptide complex molecule in the asymmetric unit. The rigid body refinement after determining the translation components gave a correlation coefficient of 0.60 and R = 0.48. The resultant electron density map was of good quality. The Fourier and difference Fourier maps clearly showed electron density for s-variegin. Several cycles of map fitting using the program O *version 7.0* (Jones et al., 1991) and refinement using the program CNS *version 1.1* (Brunger et al., 1998) led to convergence of R-values. The crystallographic and refinement statistics are given in Table 4.1. The correctness of stereochemistry of the model was verified using PROCHECK (Laskowsi et al., 1993). Online server PISA (Krissinel and Henrick,

TABLE 4.1

Crystallographic data and refinement statistics*

Data set	Thrombin-s-variegin complex
Crystal	
Space Group	C2
Unit Cell Parameters	a = 124.66 Å b = 50.83 Å c = 61.54 Å α = 90.0° β = 98.7° γ = 90.0°
Data collection	
Resolution range (Å)	50 – 2.4
Wavelength (Å)	0.9795
Observed reflections	261706
Unique reflections	15123
Completeness (%)	98.1
Overall *(I/σI)*	19.4
Redundancy	1.9
R_{sym}[a] (%)	5.4
Refinement and quality	
Resolution range (Å) I>σ(I)	20–2.4
R_{work}[b]	0.2598
R_{free}[c]	0.3301
RMSD bond lengths (Å)	0.007
RMSD bond angles(º)	1.47
Average B-factors (Å^2)	
Protein atoms (2404 atoms)	66.709
Water molecules (203 atoms)	68.160
Ramachandran plot	
Most favored regions (%)	76.2
Additional allowed regions (%)	22.5
Generously allowed regions (%)	1.3
Disallowed regions (%)	0

* Statistics from the current model.

[a] $R_{sym} = \Sigma_{hkl} \Sigma_i [|I_i (hkl) - \langle I(hkl) \rangle|] / \Sigma_{hkl} I(hkl)$

[b] $R_{work} = \Sigma||F_{obs} - F_{calc}|| / \Sigma|F_{obs}|$ where F_{calc} and F_{obs} are the calculated and observed structure factor amplitudes, respectively.

[c] R_{free} = as for R_{work}, but for 8.0% of the total reflections chosen at random and omitted from refinement.

2007) was used to analyze the protein-peptide interface. Swiss-Pdb Viewer was used for the overlaying of structures, calculations of root-mean-square deviations (RMSD) and drawing of figures (Guex and Peitsch, 1997). DS ViewerLite (Accelrys Software, San Diego, California, USA) was also used to draw figures. Superscripted prefix 'T' were added to thrombin residues and superscripted prefix 'V' were added to s-variegin residues for the descriptions of the structure in this chapter.

4.2.7. Thrombin inhibitory activities of peptides

The activities of all peptides were assayed by their abilities to inhibit thrombin amidolytic activity on S2238. Assays were typically performed as described in *'Section 2.2.3.7. Inhibition of thrombin amidolytic activity'* of Chapter 2. In general, activities were assayed without pre-incubation and with 20 min pre-incubation with thrombin in the presence of 1 mg/ml BSA. All data obtained were fitted using Origin software to equation **(2)** for the calculation of IC_{50} values and equations **(3)** to **(9)** for the calculation of K_i values depending on the kinetics and mechanisms of inhibition, as described in *'Section 2.2.3.8. Determination of the inhibitory constant K_i'* of Chapter 2. Details of each experiment are described along with the graphs representing the results obtained.

4.3. RESULTS

4.3.1. Three-dimensional structure of thrombin-variegin complex

The structure was solved by molecular replacement method from synchrotron data and refined to a final R-factor of 0.259 (R_{free} = 0.331) at 2.4 Å resolution (Figure 4.1 A). The Ramachandran plot from an analysis using PROCHECK (Laskowsi et al., 1993) shows that 76.2% of non-glycine residues are in the most favored region and no residues is in the disallowed region. The coordinates file of the structure is attached along with this thesis (see Appendix B). The structure was mainly compared to the thrombin-hirulog-1 (PDB: 2HGT) (Skrzypczak-Jankun et al., 1991) (Figure 4.1 B), thrombin-hirulog-3 (PDB: 1ABI) (Qiu et al., 1992) (Figure 4.1 C) and thrombin-hirugen (PDB: 1HGT) (Skrzypczak-Jankun et al., 1991) (Figure 4.1 D) structures. Among all thrombin inhibitors, variegin is structurally and functionally closest to hirulog-1. Hirulog-3 is a non-hydrolyzable variant of hirulog-1, incorporating a β-homoarginine at position 3. The β-homo-Arg3-Gly4 bond is not a peptide bond, thus is not cleaved by thrombin (Qiu et al., 1992). Otherwise hirulog-3 has an identical sequence to hirulog-1. Hirugen is a short peptide with the following sequence: N-acetyl-NGDFEEIPEEY(SO_3)L. This peptide is derived from hirudin C-terminal residues 53 to 64, with a sulfotyrosine residue. The same sequence, without tyrosine sulfation, is present in the hirulog's C-terminus. Unlike hirulogs, hirugen only binds to the thrombin exosite-I. Comparisons were also made with $_D$-Phe-Pro-Arg chloromethylketone (PPACK)-inhibited thrombin (PDB: 1PPB) (Bode et al., 1989) (Figure 4.1 E) and wild-type, inhibitor- and Na^+-free thrombin (PDB: 2AFQ) (Johnson et al., 2005) (Figure 4.1 F) when necessary. In 1PPB (the first thrombin crystal structure), the thrombin active site is inhibited by PPACK but the exosites are

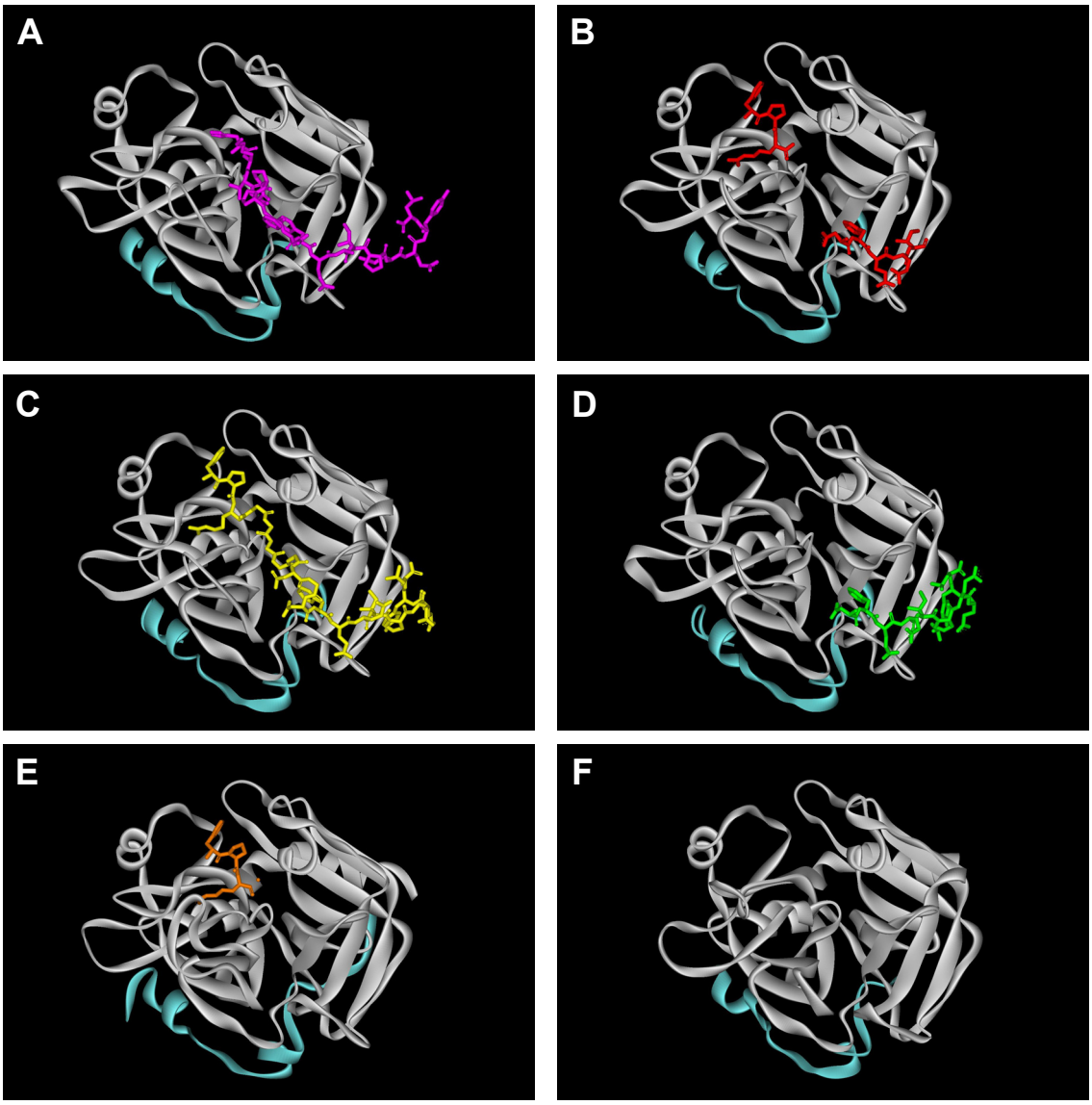

FIGURE 4.1

Structures of thrombin-s-variegin complex compared to other thrombin structures

(A) Thrombin-s-variegin complex structure. Thrombin A-chain backbone is colored as light blue ribbon, B-chain backbone is colored as white ribbon and s-variegin backbone and side chain atoms are showed as pink sticks.

(B) thrombin-hirulog-1 complex structure (PDB: 2HGT). Hirulog-1 colored as red sticks.

(C) thrombin-hirulog-3 complex structure (PDB: 1ABI). Hirulog-3 colored as yellow sticks.

(D) thrombin-hirugen complex structure (PDB: 1HGT). Hirugen colored as green sticks.

(E) thrombin-PPACK complex structure (PDB: 1PPB). PPACK colored as orange sticks.

(F) wild-type, inhibitor- and Na^{+}-free thrombin (PDB: 2AFQ). Structure represents 'slow' form thrombin and is without an inhibitor.

unoccupied. 2AFQ is the first crystal structure of inhibitor-free, wild-type human α-thrombin. However, the structure represents the 'slow' form thrombin, as the crystals were grown in the absence of Na^+ (or other univalent cation). Compared to the 'fast' form thrombin, the Na^+-binding loop is significantly displaced while the active site cleft is constricted and formed a non-catalytic hydrogen bonding network (Johnson et al., 2005).

4.3.2. Thrombin

Electron density for the thrombin-variegin complex structure is well defined except at the termini of the A chain [$^{T}(^{1}$THFGSGE^{1C}) on N-terminus, $^{T}(^{14M}$ DGR^{15}) on C-terminus] and the autolysis loop [$^{T}(^{148}$WTANVGK^{149E})]. The missing residues are all solvent-exposed and often disordered in other reported thrombin structures also (Skrzypczak-Jankun et al., 1991; Qiu et al., 1992; Johnson et al., 2005). The structure of thrombin in the variegin complex superimposes with that in the PPACK (PDB: 1PPB), hirugen (PDB: 1HGT), hirulog-1 (PDB: 2HGT) and hirulog-3 (PDB: 1ABI) complexes. Excluding the disordered regions, the root-mean-square-deviation (RMSD) for the A-chain is less than 0.67 Å (Table 4.2) for all backbone atoms while that for side chain atoms is between 1.59 and 2.27 Å. The RMSD values for the B-chain backbone and side chain atoms are less than 0.73 and 1.33 Å, respectively. This indicates that there is no major conformational change in thrombin whether inhibition is directed at the active site or exosite-I or both. However, the comparison with the inhibitor-free thrombin (PDB: 2AFQ) revealed marked differences in the B-chain backbone and side chain atoms (1.33 Å and 2.30 Å). Since 2AFQ represents the 'slow' form of thrombin, these differences most likely reflect a summation of all the structural changes in the 'slow' and inhibitor-free thrombin.

TABLE 4.2

Root-mean-square deviations (RMSD) between the thrombin-s-variegin complex and other structures

2HGT and 1ABI represent thrombin inhibited at both active site and exosite-I, similar to the thrombin-s-variegin complex. 1HGT represents thrombin inhibited at exosite-I only. 1PPB represents thrombin inhibited at active site only. 2AFQ represents inhibitor and Na^+-free thrombin. Highest differences were found in comparison with 2AFQ mainly due to the extensive changes in surface loops in 'slow' form thrombin. RMSD were calculated from Cα, backbone and side chain atoms for thrombin A-chain and B-chain as well as a C-terminal segment (DFEA(E)IPEEYL) which is common in s-variegin, hirulog-1, hirulog-3 and hirugen. *NP*: relevant atoms are not present.

	2HGT	1ABI	1HGT	1PPB	2AFQ
A-chain			**RMSD (Å)**		
Cα	0.34	0.35	0.35	0.63	0.61
Backbone atoms	0.56	0.60	0.67	0.59	0.75
Side chain atoms	1.68	1.59	2.27	1.75	1.61
B-chain			**RMSD (Å)**		
Cα	0.59	0.55	0.52	0.70	1.35
Backbone atoms	0.65	0.59	0.59	0.73	1.33
Side chain atoms	1.33	1.21	1.19	1.29	2.30
DFEA(E)IPEEYL			**RMSD (Å)**		
Cα	*NP*	3.62	3.87	*NP*	*NP*
Backbone atoms	*NP*	3.40	3.63	*NP*	*NP*
Side chain atoms	*NP*	7.00	7.06	*NP*	*NP*
DFEA(E)I			**RMSD (Å)**		
Cα	1.46	1.22	1.26	*NP*	*NP*
Backbone atoms	1.46	1.24	1.34	*NP*	*NP*
Side chain atoms	3.05	2.96	2.88	*NP*	*NP*
PEEYL			**RMSD (Å)**		
Cα	*NP*	4.98	5.33	*NP*	*NP*
Backbone atoms	*NP*	4.64	4.96	*NP*	*NP*
Side chain atoms	*NP*	9.01	9.11	*NP*	*NP*

Some electron densities were observed near ^{T}Asn60G, which is glycosylated in native thrombin. The recombinant human α-thrombin that was used for crystallization was produced in mouse myeloma cells and hence the N-glycosylation was expected. SDS-PAGE analysis showed that the mass of recombinant α-thrombin is consistent with wild-type and glycosylated α-thrombin. (Yonemura et al., 2004). However, the density was not well-defined for complete modeling of the glycan moiety. Similar observations were made in other thrombin structures also, demonstrating the flexibility of this carbohydrate group (Bode et al., 1992; Qiu et al., 1992).

4.3.3. s-Variegin

Only 17 out of 32 residues (^{V}His12 to ^{V}Leu28) on s-variegin have well-defined densities. The first 11 residues on the s-variegin N-terminus (^{V}Ser1 to ^{V}Met11) and the last four residues on the C-terminus (^{V}Asp29 to ^{V}Ser32) could not be modeled. As discussed previously, the first seven N-terminal residues do not make direct contacts with thrombin (see Chapter 2) and s-variegin is cleaved by thrombin between ^{V}Lys10 and ^{V}Met11. It is likely that the N-terminal cleavage fragment [^{V}(^{1}SDQGDVAEPK^{10})] dissociates from thrombin after cleavage before crystallization occurs. In contrast, biochemical data showed that the C-terminal fragment (Met11 to Ser32, represented by peptide MH22) remains tightly bound to thrombin after the cleavage (see Chapter 3). This was reflected in the structure, where all the observed densities for s-variegin are located within this fragment. Densities for the N-terminal residue of the fragment (^{V}Met11) and last four residues on the C-terminus [^{V}(^{29}DDES^{32})] of the bound fragment are not observed, presumably reflecting flexibility in these terminal positions.

Residues number 11 to 20 in hirulog-1 and hirulog-3 as well as residues 3 to 12 in hirugen have the following sequence DFEEIPEEYL. An almost identical segment of this sequence is present in s-variegin residues 19 to 28 [^{V}(DFEAIPEEYL), the only difference is underlined]. In the hirulog-1 structure, only five of the residues in this segment (DFEEI) were observed (Skrzypczak-Jankun et al., 1991). In the other two structures (hirulog-3 and hirugen), the entire segment is modeled. By aligning thrombin B-chain of respective structures, backbone and side chain (excluding the position where Glu is changed to Ala) atoms RMSD within this region were computed (Table 4.2). Despite having almost identical sequences, there are significant differences between s-variegin and the other three inhibitors, demonstrated by the high RMSD values (1.46 – 3.63 Å for backbone atoms, 3.05 – 7.06 Å for side chain atoms). The most significant difference is observed in the conformation of the last five residues (PEEYL). While these residues in hirulog-3 and hirugen form a 3_{10} helix turn, the corresponding residues in s-variegin remained more or less in an extended confirmation until the last two observed residues ^{V}Tyr27 and ^{V}Leu28. s-Variegin contains four extra residues at the C-terminus which are not observed in the structure. The presence of these four residues might have an influence on the conformation of C-terminal segment ^{V}(^{24}PEEYL^{28}). Interestingly, this segment appeared to exhibit conformational heterogeneity in other structures as well. For example, the hirulog-1 C-terminus is disordered while in one of the recent structures of sulfated hirudin binding to thrombin, this segment forms a one-turn α-helix (Liu et al., 2007) (Figure 4.2).

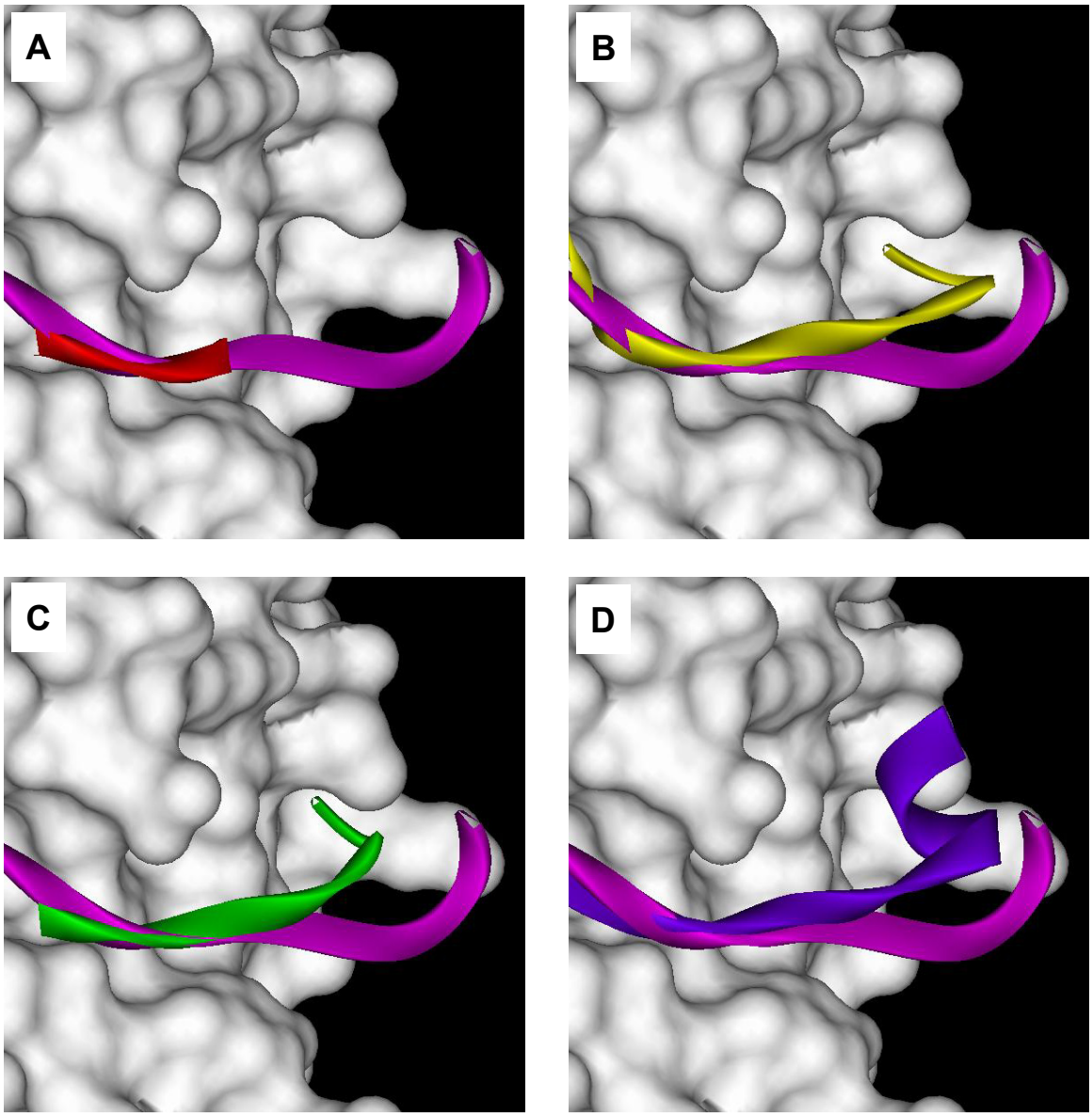

FIGURE 4.2

Differences in C-terminal conformations between s-variegin and hirulog-1, hirulog-3, hirugen and sulfo-hirudin

Despite the presence of analogous residues PEEYL, s-variegin C-terminus (pink ribbon) acquired a vastly different conformation compared to hirulog-1 (red ribbon), hirulog-3 (yellow ribbon), hirugen (green ribbon) and sulfo-hirudin (blue ribbon). C-terminus of s-variegin has four extra residues ($D^{29}DES^{32}$) but their densities were not observed. This segment appeared to exhibit conformational heterogeneity in other structures as well:

(A) Residues PEEYL in hirulog-1 (red ribbon) are disordered and hence missing from structure.

(B) Residues PEEYL in hirulog-3 (yellow ribbon) form a 3_{10} helix turn.

(C) These residues in hirugen (green ribbon), with sulfated tyrosine, also form a 3_{10} helix turn.

(D) Other than Tyr-sulfation, hirudin (blue ribbon) C-terminus has an extra Gln residue, forms a full α-helical turn.

4.3.4. Thrombin-s-variegin interactions

4.3.4.1. Interactions within catalytic pocket

Of the 17 observed s-variegin residues, a selected few N-terminal residues are of special interest. The thrombin-s-variegin structure was compared with the thrombin-hirugen structure (PDB: 1HGT) as they shared one common characteristic, both occupy the exosite-I but not the non-prime subsites of active site (since the N-terminal cleavage fragment of s-variegin is not present). Of the three catalytic residues (^{T}His57, ^{T}Asp102 and ^{T}Ser195), the most striking difference was with the Oγ atom of ^{T}Ser195. In the thrombin-s-variegin structure, the ^{T}Ser195 Oγ is displaced by 1.1 Å. As a result, the hydrogen bond with the Nε of ^{T}His57 (which should be part of the catalytic charge relay system) is absent in the thrombin-s-variegin structure. The distance between the two atoms increased to 3.77 Å (Figure 4.3 A). The corresponding distance in the thrombin-hirugen structure is 2.79 Å (Figure 4.3 A). The displacement of the ^{T}Ser195 Oγ is due to interaction with s-variegin. Particularly, a new and extensive network of hydrogen bonds between ^{V}His12, ^{T}Ser195, ^{T}Gly193 and ^{T}Cys42 as well as a water molecule perturbs the catalytic charge relay network. Crucially, the ^{V}His12 backbone N (donor) is engaged with the Oγ of ^{T}Ser195 (acceptor) through hydrogen bond (2.77 Å) while the ^{V}His12 side chain Nδ (acceptor) could contribute a weak hydrogen bond with the ^{T}Ser195 Oγ (donor) (3.68 Å). In addition, the ^{V}His12 backbone N also hydrogen bonds to the backbone N of ^{T}Gly193 and Sγ of ^{T}Cys42 via a water molecule. Effectively, the electrons on the ^{T}Ser195 Oγ get delocalized into this hydrogen bonding network, rendering it a weak nucleophile and incapable of attacking the backbone C of the substrate efficiently. In addition, involvement of the main chain N of ^{T}Gly193 in this hydrogen network prevents the

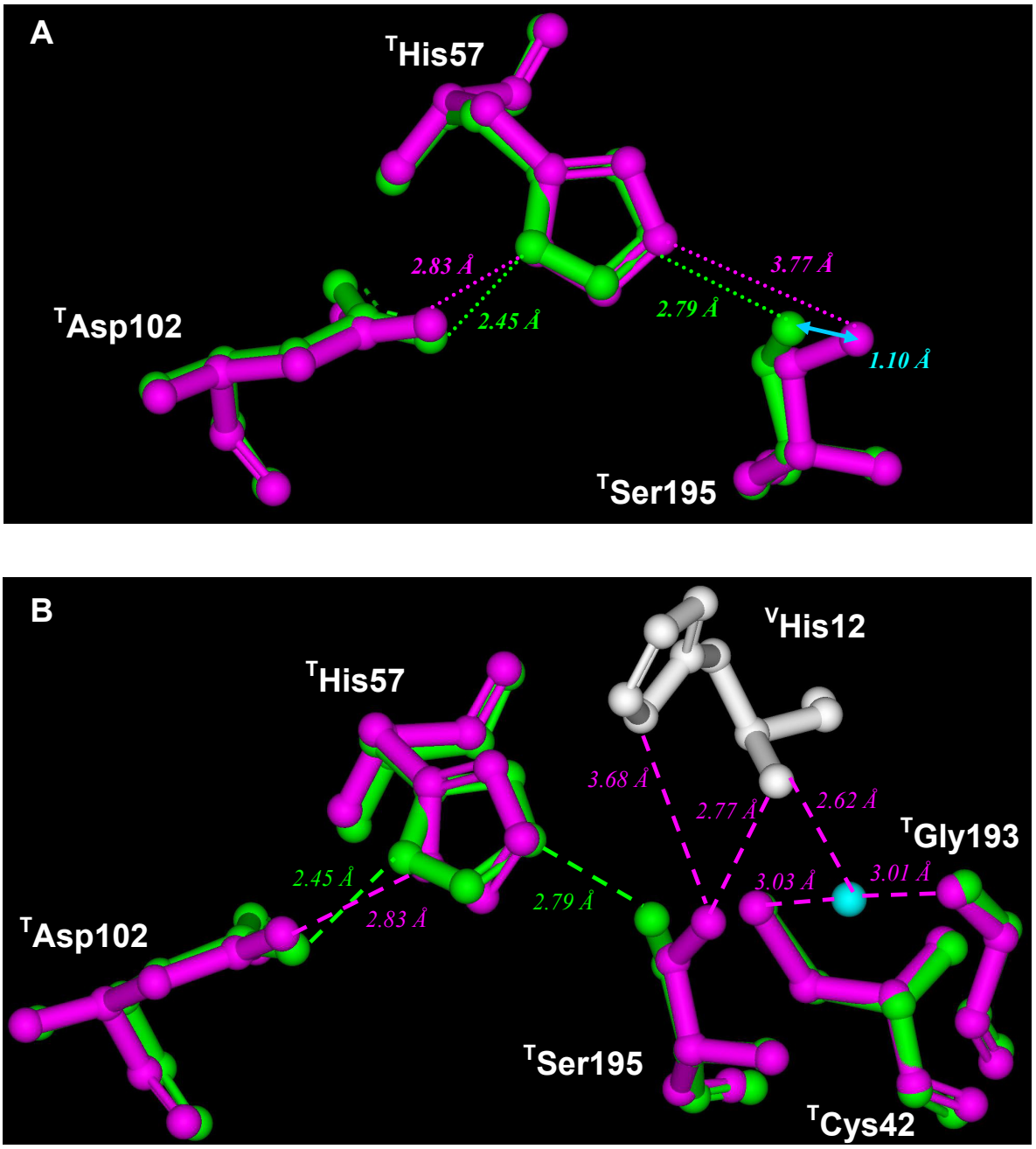

FIGURE 4.3

Thrombin catalytic triads in s-variegin bound and hirugen bound structures

(A) Thrombin catalytic triad ^{T}His57, ^{T}Asp102 and ^{T}Ser195 when unoccupied in thrombin-hirugen structure (green) has the intact charge relay hydrogen bonding system. In thrombin-s-variegin structure (pink), ^{T}Ser195 Oγ is displaced by 1.10 Å (cyan arrow). Distance between ^{T}His57 Nε and ^{T}Ser195 Oγ is 3.77 Å, thus hydrogen bond is not formed and the charge relay system is broken.

(B) The displacement of ^{T}Ser195 Oγ is due to interaction with interactions with s-variegin (gray). ^{V}His12 backbone N (donor) engaged ^{T}Ser195 Oγ (acceptor) through hydrogen bond (2.77 Å) while ^{V}His12 side chain Nδ (acceptor) could contribute a weak hydrogen bond with ^{T}Ser195 Oγ (donor) (3.68 Å). The ^{V}His12 backbone N also forms hydrogen bond with ^{T}Gly193 backbone N and ^{T}Cys42 Sγ via a water molecule (light blue). Thus, ^{T}Ser195 Oγ is rendered a weak neucleophile and incapable of attacking backbone C of substrate. Oxyanion hole formation is also disturbed due to involvement of ^{T}Gly193 backbone N in this hydrogen bond network.

formation of the oxyanion hole, further reducing the catalytic capability of this complex (Figure 4.3 B).

No other major structural changes are observed around the active site cleft, including the non-prime subsites (occupied by substrates residues N-terminal to the scissile bond) and Na^+ binding loop. This indicates that the C-terminal cleavage fragment of s-variegin (MH22) is unlikely to affect binding affinities of small peptidyl substrates, such as S2238. This observation supports the classical non-competitive inhibition observed for MH22. As shown in Figure 3.14 (Chapter 3), the substrate (S2238) binding (K_s) to thrombin was not affected by MH22 (and reverse is also true) but rate of product formation (k_p) of the reaction decreased due to inefficient catalysis. As discussed in Chapter 3 (see Figure 3.13), the condition for the observed classical non-competitive inhibition precludes binding of ^{V}Met11 in the same site occupied by *p*NA moiety of S2238. This assumption is supported by the absence of ^{V}Met11 density in the structure. Thus, ^{V}Met11 might not be in direct contacts with thrombin and was disordered in the complex. The lack of interactions between ^{V}Met11 and thrombin is consistent with the thinking that thrombin S1′ prefer residues with small side chain such as Gly, Ala or Ser (Bode et al., 1992).

4.3.4.2. Interactions within prime subsites of active site

In addition to the extensive network of hydrogen bonds, other interactions between the s-variegin P2′ to P5′ residues (^{V}His12, ^{V}Lys13, ^{V}Thr14 and ^{V}Ala15) with thrombin further anchored this moiety in the prime subsites of thrombin. Extensive interface contacts between the ^{V}His12 to ^{V}Ala15 of s-variegin and thrombin surface formed by residues in the 60-loop, autolysis loop and 34-loop was observed (Figure

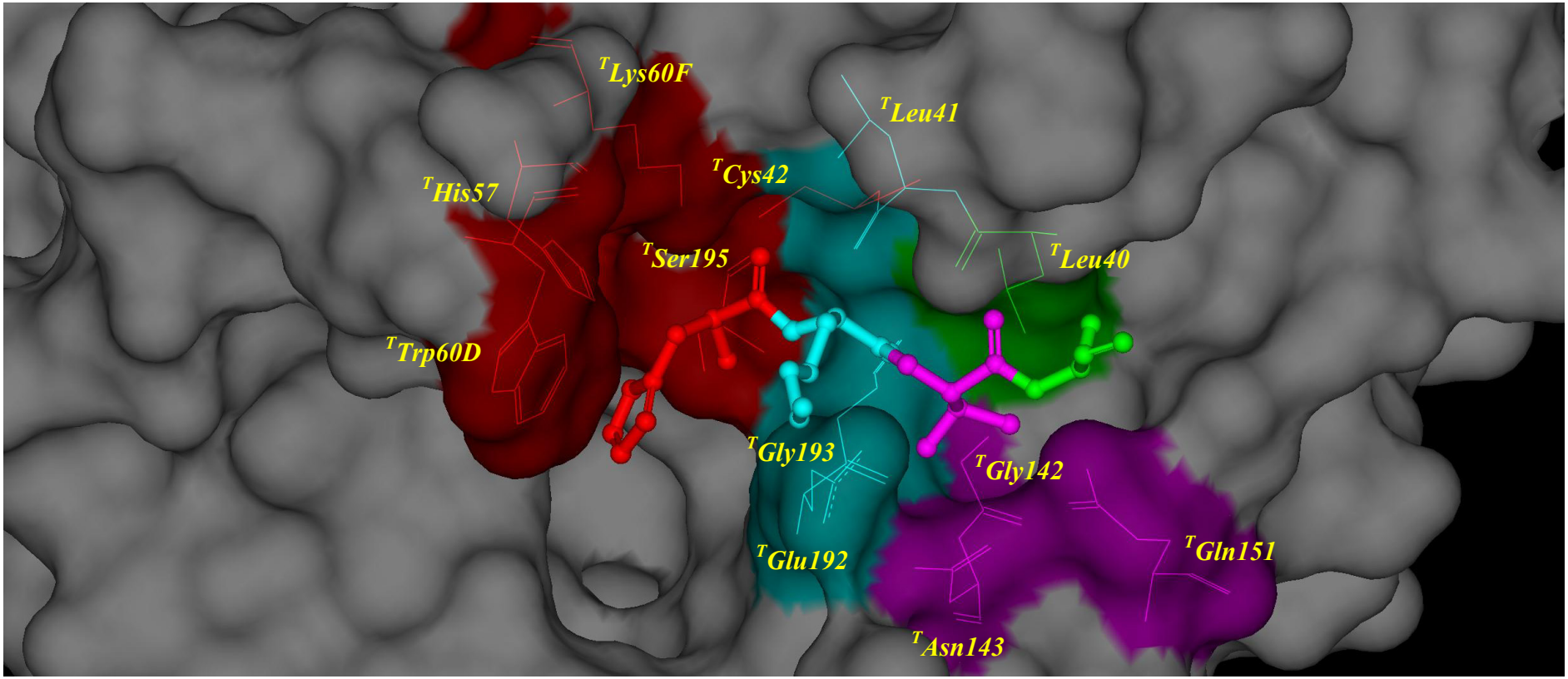

FIGURE 4.4

Prime subsites interactions between thrombin and s-variegin

For s-variegin, only residues P2' to P5' (^{V}His12 to ^{V}Ala15) are shown. Density for s-variegin P1' ^{V}Met11 cannot be traced in the structure. Thrombin S2' subsite (red) (formed by ^{T}Cys42, ^{T}His57, ^{T}Trp60D, ^{T}Lys60F, ^{T}Glu192 and ^{T}Ser195) partially overlaps with the S1' subsite observed in hirulog-3. S-variegin P3' ^{V}Lys13 side chain runs close and parallel with ^{T}Glu192 side chain, and its backbone is in contact with ^{T}Leu41, forming the S3' subsite (cyan). S-variegin P4' ^{V}Thr14 side chain is directed towards the bottom of autolysis loop, occupying a small pocket formed by ^{T}Gly142, ^{T}Asn143, ^{T}Glu192, ^{T}Gly193 and ^{T}Glu151, forming the S4' subsite (pink). Thrombin S5' subsite (green) is lined by ^{T}Leu40 at the bottom, which allows s-variegin P5' ^{V}Ala15 to burry its side chain in the interface.

4.4). Comparing residues to residues, the P2′ of s-variegin (^{V}His12) is displaced by 2.77 Å towards the active site, compared to the P2′ of hirulog-3 (Gly5) (measured by the displacement of Cα atoms). This discrepancy can be partially explained by the use of β-homo-Arg as P1 in hirulog-3, which displaced the backbone atoms of P1′ by about a bond length. It could also be due to the involvement of the ^{V}His12 in the extensive hydrogen bonding network with the thrombin active site, which draws the residues closer towards the ^{T}Ser195 (Figure 4.3 B). Consequently, the ^{V}His12 side chain occupied part of the small S1′ subsite observed in hirulog-3. The ^{V}His12 backbone O is hydrogen bonded to the ^{T}Lys60F Nζ (2.74 Å). The P2′ ^{V}His12 in s-variegin structure is surrounded by and in contact with residues ^{T}Cys42, ^{T}His57, ^{T}Trp60D, ^{T}Lys60F, ^{T}Glu192 and ^{T}Ser195. Partial occupation of the S1′ by ^{V}His12 limits the space available to accommodate the bulky side chain of the P1′ ^{V}Met. Thus, it is possible for the P1′ ^{V}Met to point out into the solvent. The P3′ ^{V}Lys side chain runs close and parallel with the ^{T}Glu192 side chain, allowing hydrophobic interactions between the aliphatic side chains of both residues. However, a strong ionic pairing between ^{V}Lys13 and ^{T}Glu21 is not likely as the distance between the two charges is more than 5.0 Å. The backbone of ^{V}Lys13 is also in contact with the ^{T}Leu41. The P4′ ^{V}Thr side chain appeared to be directed towards the base of the autolysis loop, which made the analysis less certain due to the flexible nature of the loop. Nonetheless, the side chain occupies a small cavity lined by residues ^{T}Gly142, ^{T}Asn143, ^{T}Glu192, ^{T}Gly193 and ^{T}Glu151. Hydrogen bonds are observed between the ^{V}Thr14 Oγ and ^{T}Glu192 backbone O (2.53 Å) and ^{T}Asn143 Oδ (3.29 Å) (Table 4.3). The P5′ Ala side chain was buried deep into the bottom of the canyon-like cleft lined by the Leu40 which provides a hydrophobic contact.

TABLE 4.3

Direct hydrogen bonds between s-variegin and thrombin

Possible direct hydrogen bonds between s-variegin and thrombin are computed with a cutoff of 3.70 Å.

S-variegin		Thrombin		Distance (Å)
Residues	**Atoms**	**Residues**	**Atoms**	
^{V}His12	N	^{T}Ser195	Oγ	2.77
^{V}His12	O	^{T}Lys60F	Nζ	2.74
^{V}His12	Nδ	^{T}Ser195	Oγ	3.68
^{V}Thr14	O	^{T}Leu40	N	3.29
^{V}Thr14	Oγ	^{T}Asn143	Oδ	3.29
^{V}Thr14	Oγ	^{T}Glu192	O	2.53
^{V}Thr14	Oγ	^{T}Glu192	Oε	3.30
^{V}Glu21	N	^{T}Thr74	O	2.76
^{V}Glu21	Oε	^{T}Arg75	Nε	3.02
^{V}Glu21	Oε	^{T}Tyr76	N	3.14

4.3.4.3. Interactions within exosite-I

Thrombin-s-variegin binding in the exosite-I is mainly driven by hydrophobic interactions. On the whole s-variegin fits firmly into the canyon-like cleft extending from the thrombin active site to exosite-I (Figure 4.5 A & B). Many apolar residues in between these loops lined the bottom of the cleft. The walls of the cleft are formed by the 60- and autolysis loop near the thrombin active site as well as the 34- and 70-loops at around the exosite-I (Rydel et al., 1991; Bode et al., 1992; Huntington, 2005). The binding of s-variegin with thrombin is driven mainly by hydrophobic contacts at the apolar bottom and the wall of the cleft. The thrombin residues that are involved in binding are: (i) at the bottom of these surface loops: ^{T}Met32, ^{T}Leu40, ^{T}Leu41, ^{T}Cys42, ^{T}Leu65, ^{T}Arg67, ^{T}Lys81, ^{T}Ile82 and ^{T}Met84; (ii) in the 60-loop: ^{T}Trp60D and ^{T}Lys60F; (iii) in the autolysis loop: ^{T}Gly142, ^{T}Asn143 and ^{T}Gln151; (iv) in the 34-loop: ^{T}Phe34, ^{T}Lys36, ^{T}Pro37, ^{T}Gln38 and ^{T}Glu39; (iv) in the 70-loop: ^{T}Arg73, ^{T}Thr74, ^{T}Arg75, ^{T}Tyr76 and ^{T}Arg77A (Figure 4.5 C). Specific side chains interactions are important, as all but five residues on the entire s-variegin polypeptide chain (^{V}Phe18, ^{V}Asp19, ^{V}Ala22, ^{V}Glu26 and ^{V}Tyr27) have their side chains buried in the interfaces with thrombin (Figure 4.5 D). Also, some of the strongest hydrophobic contacts observed include: (1) ^{V}Phe20 with ^{T}Met32, ^{T}Phe34 (π-π stacking) and ^{T}Leu40; (2) ^{V}Ile23 with ^{T}Phe34, ^{T}Leu65, ^{T}Tyr76 and ^{T}Ile82; (3) ^{V}Pro24 with ^{T}Tyr76.

In contrast to the apolar nature of the bottom of canyon-like cleft, the top surfaces of these loops, especially the 70-loop, are dominated by positively-charged residues. These basic residues include ^{T}Arg35, ^{T}Lys36, ^{T}Arg73, ^{T}Arg75, ^{T}Lys81, ^{T}Arg77A, ^{T}Lys109, ^{T}Lys110 and ^{T}Lys149E, forming a positively-charged entrance over the apolar canyon-like cleft. Despite the presence of multiple acidic residues in s-

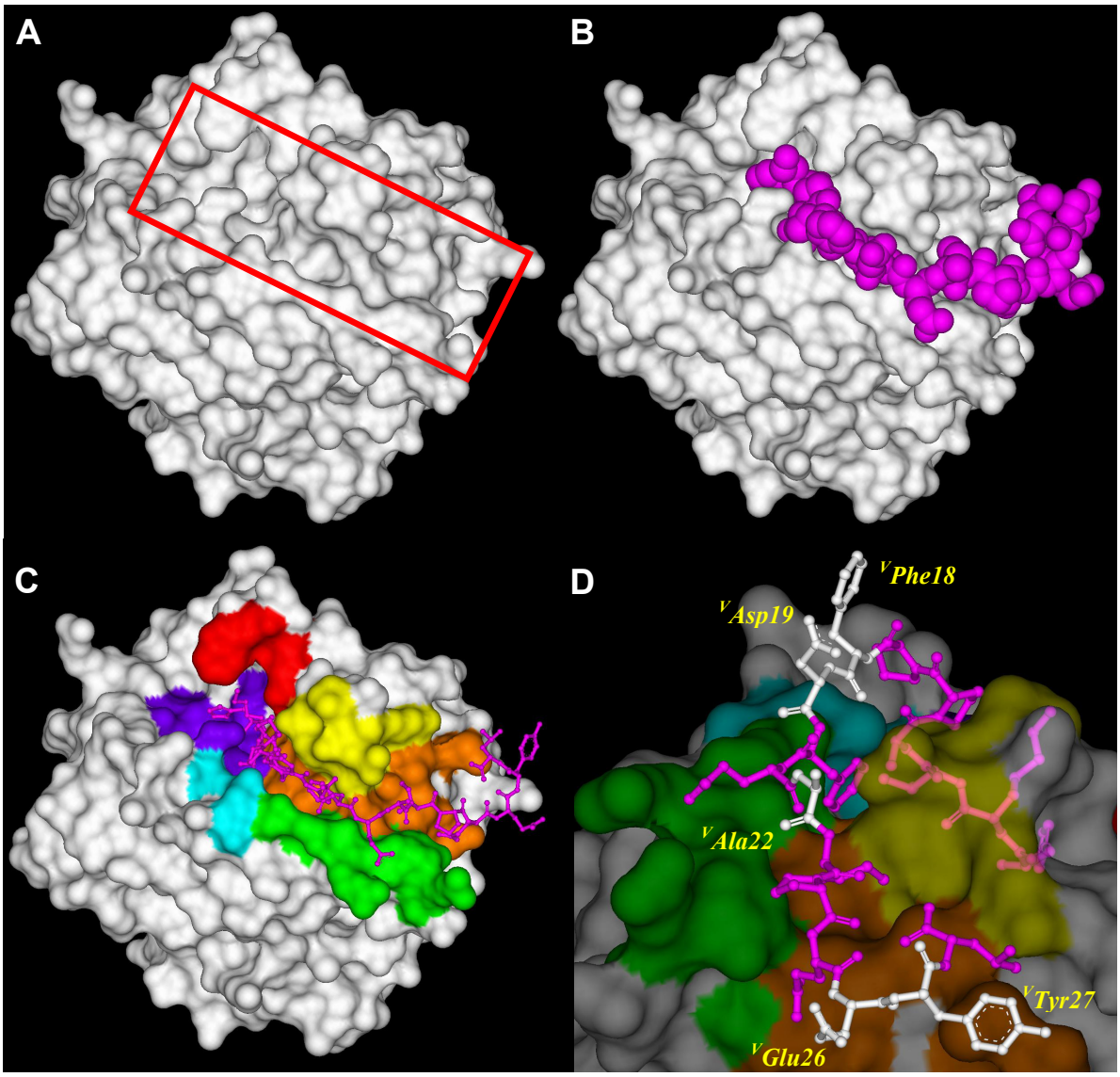

FIGURE 4.5

s-Variegin fitted firmly into the canyon-like cleft

(A) Thrombin has a deep canyon-like cleft (boxed) starting from active site extending to exosite-I

(B) On the whole s-variegin (pink CPK model) fitted firmly at the bottom of the canyon-like cleft in extended conformation, covering catalytic pocket, prime subsites and exosite-I. The bottom of the cleft composed of mainly apolar residues. The walls of the cleft are formed by the 60- and autolysis loop near thrombin active site, along with 34- and 70-loop at exosite-I.

(C) Thrombin residues that interfaced with s-variegin are colored according to their positions: catalytic pocket – blue; 60-loop – red; autolysis loop – cyan; 34-loop – yellow; 70-loop – green; bottom of the cleft – orange. See text for identity of residues that are involved in the interactions. Ball and stick model of s-variegin is shown in pink.

(D) s-Variegin interacts with thrombin through specific side-chain contacts. All but five residues (^{V}Phe18, ^{V}Asp19, ^{V}Ala22, ^{V}Glu26 and ^{V}Tyr27, all colored white) on s-variegin have their side chains buried in the interface with thrombin.

variegin C-terminus (^{V}Asp19, ^{V}Glu21, ^{V}Glu25 and ^{V}Glu26), only one ion pair is formed between ^{V}Glu21 and ^{T}Arg75. Interestingly, in the hirulogs, hirugen and hirudin structures the analogous Glu makes an ion pair with the ^{T}Arg75 of a 2-fold symmetry-related molecule (Rydel et al., 1990; Skrzypczak-Jankun et al., 1991; Qiu et al., 1992). This interaction was suggested to happen within the same thrombin-inhibitor pair in solution although structurally it was not observed (Rydel et al., 1990). In our structure, the ^{T}Arg75 side chain is rotated by 96.8° about Cγ compared to the ^{T}Arg75 of hirulog-3 to facilitate the electrostatic interaction with the ^{V}Glu21, providing structural evidence for the existent of the predicted interaction (Figure 4.6 A). Similarly, in the hirulog-1/3 and hirugen structures, only one ion pair can be observed. However, this interaction is between the ^{T}Arg73 and an Asp corresponds to the ^{V}Asp19. Formation of an equivalent ion pair in the thrombin-s-variegin structure was not possible as the ^{V}Asp19 side chain points in an opposite direction into the solvent. This change in the side chain orientation is most likely due to the kink in s-variegin backbone which is induced by Pro16-Pro17 (see below for further details) (Figure 4.6 B).

At the end of the canyon-like cleft is a relatively flatten surface formed by thrombin residues ^{T}Asp63 – ^{T}Ile68 and ^{T}Lys81 – ^{T}Leu85. Despite being present in close proximity, the s-variegin C-terminal residues ^{V}Pro24 to ^{V}Leu28 stacked loosely on top of this surface with two of the side chains (^{V}Glu26 and ^{V}Tyr27) pointing into the solvent (Figure 4.5 D). This s-variegin segment is in a different conformation when compared to hirulog-3/hirugen despite sharing similar sequences (Figure 4.2). Compared to the constricted canyon-like cleft, the relatively open surface around this region could be responsible for the hirudin/hirulogs/hirugen/s-variegin C-terminal

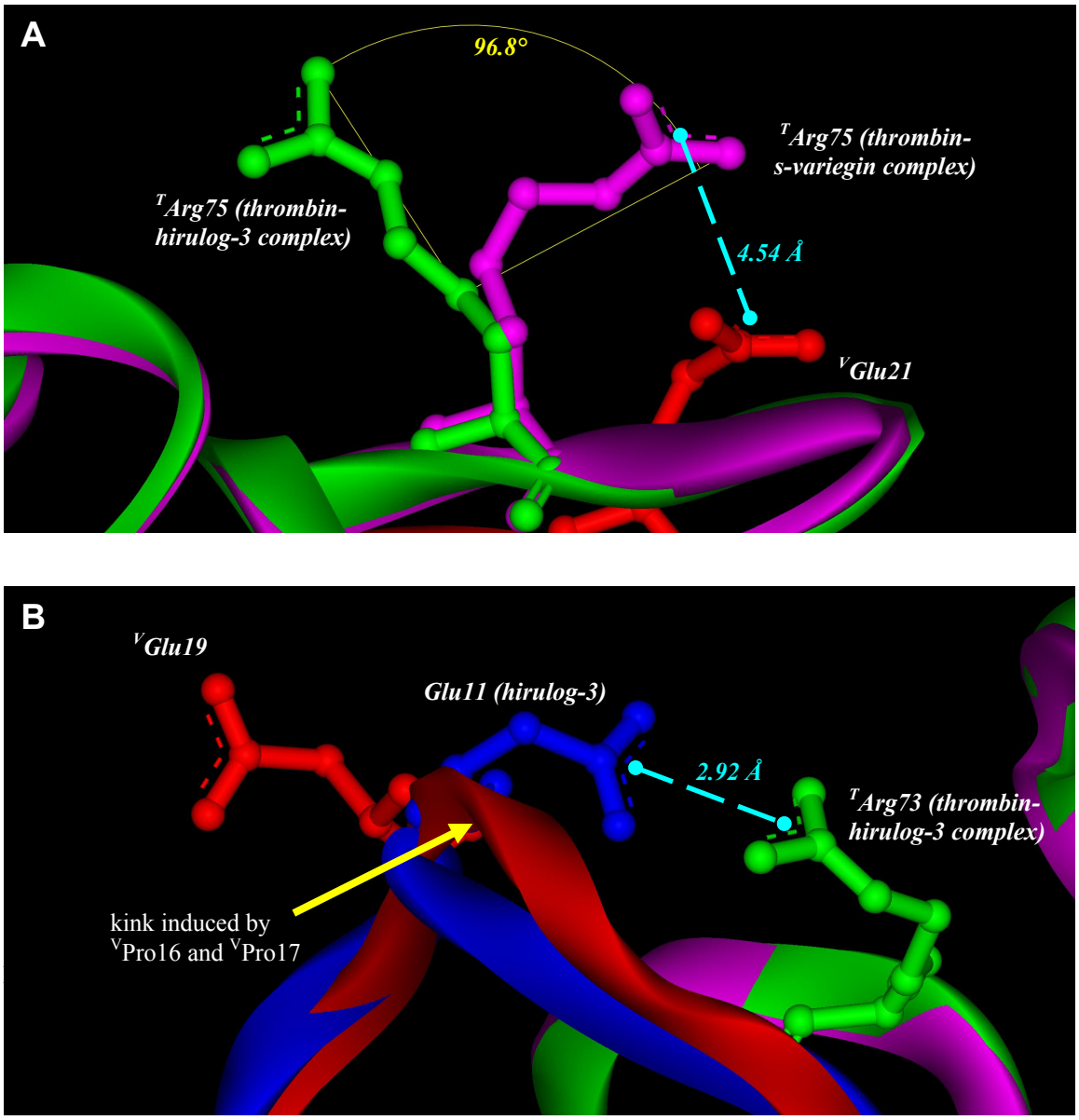

FIGURE 4.6

Ionic pairing in thrombin-s-variegin complex and the differences with thrombin-hirulog-3 structure

(A) The only ion pair (4.54 Å) in thrombin-s-variegin structure is between ^{T}Arg75 and ^{V}Glu21. In hirulog-3/hirugen/hirudin structure, the same pairing occurred between the inhibitor and a 2-fold symmetry-related thrombin. In our structure, ^{T}Arg75 side chain (pink) rotated 96.8° about Cγ compared to ^{T}Arg75 of hirulog-3 (green) to facilitate interaction with ^{V}Glu21 (red).

(B) The strong ion pair (2.92 Å) in thrombin-hirulog-3 structure is absent in thrombin-s-variegin structure since ^{V}Glu19 (red) of s-variegin pointed to an opposite direction compared to the analogous hirulog-3 Glu11 (blue). A kink in s-variegin backbone (red) induced by ^{V}Pro16 and ^{V}Pro17 is likely to be the cause for displacement of ^{V}Glu19 side chain. Pink ribbon represents thrombin in complex with s-variegin.

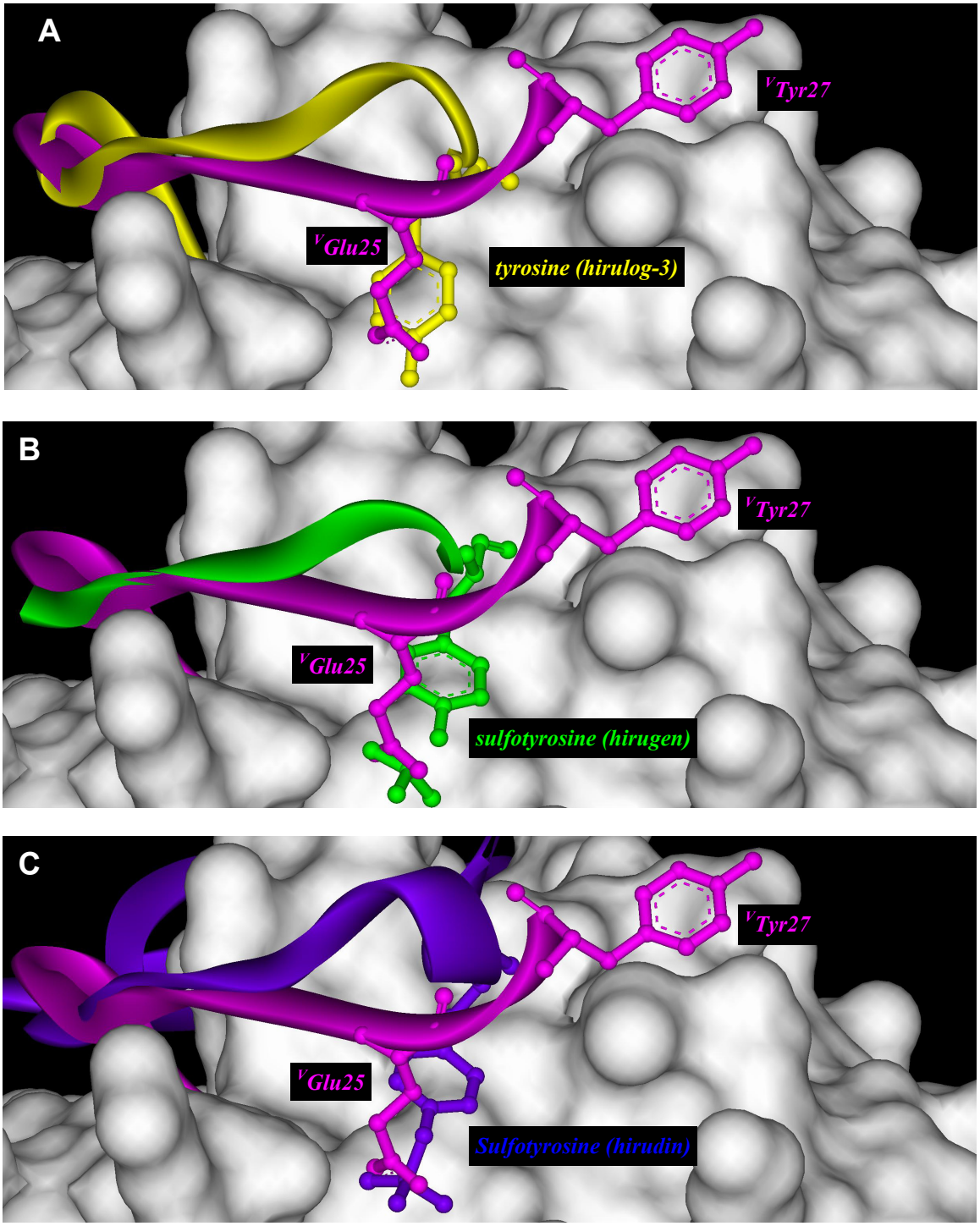

FIGURE 4.7

s-variegin ^{V}Glu25 and ^{V}Tyr27 side chains

(A) Overlaying s-variegin (pink) and hirulog-3 (yellow) based on their thrombin molecule showed ^{V}Glu25 side chain occupies a similar position as hirulog-3 Tyr side chain. The analogous Tyr in s-variegin is occupying a different position and the side chain is pointing into the solvent.

(B) Similar observation is obtained by comparing s-variegin (pink) with hirugen (green). The Tyr in hirugen is sulfated which improved its affinity to thrombin by 10-fold.

(C) Alignment of s-variegin (pink) and sulfo-hirudin (blue) showed similar observations as (A) and (B).

conformational heterogeneity as discussed in the Section 4.3.3. Interestingly, the ^{V}Glu25 side chain occupied a similar position as the side chain of C-terminal Tyr in the hirulog-3/hirugen/hirudin structures (Figure 4.7). Sulfation of this Tyr in hirudin and hirugen caused a 10-fold increase in affinity (Stone and Hofsteenge, 1986; Dodt et al., 1988; Braun et al., 1988a; Maraganore et al., 1989). The sulfate moiety present in the thrombin-hirugen structure (PDB: 1HGT) is involved in a hydrogen bonding network (Skrzypczak-Jankun et al., 1991). For the sulfate moiety in the thrombin-sulfo-hirudin structure (PDB: 2PW8), a salt bridge and a hydrogen bond are formed with ^{T}Lys81 and ^{T}Tyr76 respectively (Liu et al., 2007). Despite occupying a similar position, ^{V}Glu25 does not make similar contacts with thrombin.

4.3.5. Design and characterization of variegin variants

Thirteen new variegin variants were designed based on the thrombin-s-variegin structure as well as background information available on thrombin interactions. The general approach was to first optimize the length of variegin before optimizing several key positions on variegin to obtain maximum interaction with thrombin (Figure 4.8).

4.3.5.1. Optimization of the length of variegin: truncation at the C-terminus

The lack of electron densities for the four s-variegin C-terminal residues [^{V}(^{29}DDES^{32})] in the complex structure indicated that these four residues are unlikely to interact strongly with thrombin. Further, these residues were not present in hirulogs or hirugen. Considering the vast differences between C-terminal conformations of s-variegin and hirulogs/hirugen, it would be interesting to examine the role of these residues. Two truncation variants, EP21 and MH18, corresponded to EP25 and MH22,

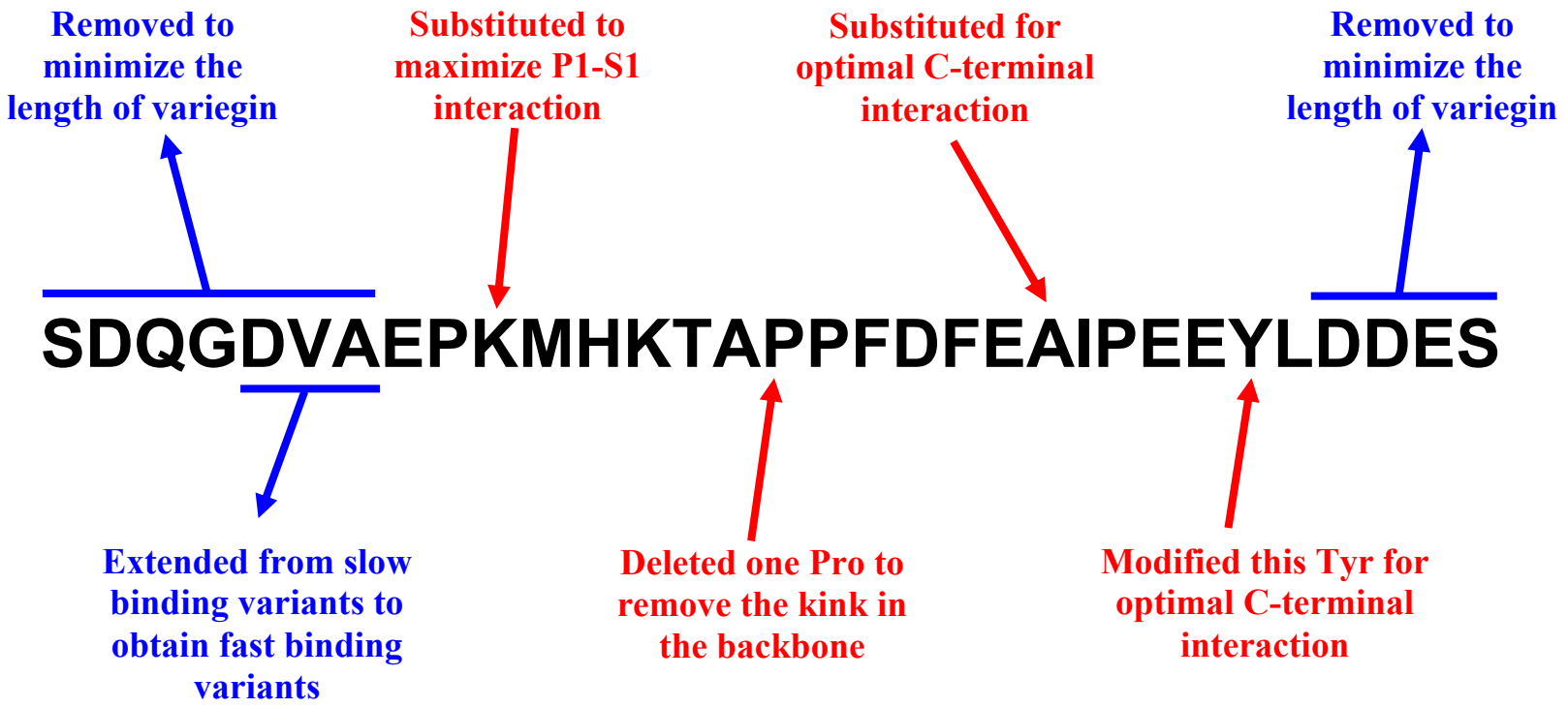

FIGURE 4.8

Design of variegin variants

New variegin variants were designed to improve thrombin-variegin interactions. The approach was to first optimize the length of variegin (blue) before optimizing several key positions on variegin (red).

TABLE 4.4

Optimization of the length of variegin: truncation at the C-terminus

Two new truncation variants EP21 and MH18 were designed and synthesized based on template sequences EP25 and MH22 respectively, for the optimization of the length of variegin.

Name	Sequence	Theoretical mass (Da)	Observed mass (Da)	Basis for design
s-variegin	SDQGDVAEPKMHKTAPPFDFEAIPEEYLDDES	3608.9	3609.0	• Full-length sequence of native variegin • Fast, tight-binding, competitive inhibitor
EP25	EPKMHKTAPPFDFEAIPEEYLDDES	2936.2	2936.4	• Template sequence for EP21 • Slow, tight-binding, competitive inhibitor • Has the same K_i as s-variegin
EP21	EPKMHKTAPPFDFEAIPEEYL	2489.8	2490.2	• Deletion of 4 residues from EP25 C-terminus • To test the hypothesis that the lack of density of these 4 residues in structure is due to the lack of strong interactions with thrombin
MH22	MHKTAPPFDFEAIPEEYLDDES	2581.8	2581.8	• Template sequence for MH18 • C-terminal cleavage fragment of s-variegin and EP25 • Fast, tight-binding, non-competitive inhibitor
MH18	MHKTAPPFDFEAIPEEYL	2135.4	2136.0	• See EP21

respectively, but lacking those four C-terminal residues, were designed and characterized (Table 4.4). Since EP25 and s-variegin binds to thrombin with the same affinity, C-terminal truncation variant of s-variegin was not synthesized.

4.3.5.2. Inhibition of thrombin amidolytic activity by EP21 and MH18

Progress curves of thrombin inhibition by EP21 showed two-phase equilibria in the absence of pre-incubation, typical of a slow binding inhibitor. EP21 activity was dependent on pre-incubation time. The IC_{50} decreased from 176.9 ± 6.8 nM (without pre-incubation) to 16.2 ± 2.9 nM (after 20 min pre-incubation) (Figure 4.9 A). By fitting data to equations **(7)**, **(8)** and **(9)**, the inhibitory constant, K_i, calculated for EP21 inhibition of thrombin is 0.315 ± 0.024 nM (Figure 4.9 B; Table 4.5). All the values are similar to that of EP25 indicates that truncation of four C-terminal residues does not significantly alter the peptide activity.

MH18 inhibited the thrombin amidolytic activity at equimolar concentration (~ 15%) and the steady state equilibrium was achieved upon mixing. Thus, MH18 is a fast, tight-binding inhibitor for thrombin. Dose-response curves showed IC_{50} values of 10.9 ± 1.2 nM (without pre-incubation) and 11.7 ± 1.9 nM (after 20 min pre-incubation) (Figure 4.10 A). These values are essentially identical with the data obtained with MH22 (Table 4.5). The apparent inhibitory constant, K_i' of MH18 were obtained with 100 μM of S2238, fitting the data with equation **(3)** (Figure 4.10 B). Assuming that MH18 is a non-competitive inhibitor like MH22, equation **(5)** and **(6)** was solved to derive the inhibitory constant K_i of 14.9 ± 3.5 nM which is consistent with the K_i of MH22 (Table 4.5). This set of results ascertained the above conclusion that the four C-terminal residues are not involved in binding to thrombin.

TABLE 4.5

Thrombin inhibitory activities of EP21 and MH18

EP21 and MH18 inhibited thrombin with the same mechanisms and potencies as their respective template sequences EP25 and MH22.

Name	Sequence	Pre-incubation tine (min)	IC_{50} (nM)	K_i (nM)	Remarks
s-variegin	SDQGDVAEPKMHKTAPPFDFEAIPEEYLDDES	0	8.25 ± 0.45	0.318 ± 0.020	• Fast, tight-binding, competitive inhibitor
		20	10.37 ± 0.30		
EP25	EPKMHKTAPPFDFEAIPEEYLDDES	0	173.1 ± 26.0	0.37 ± 0.11	• Slow, tight-binding, competitive inhibitor
		20	13.12 ± 0.67		
EP21	EPKMHKTAPPFDFEAIPEEYL	0	176.9 ± 6.8	0.315 ± 0.024	• Slow, tight-binding, competitive inhibitor
		20	16.2 ± 2.9		
MH22	MHKTAPPFDFEAIPEEYLDDES	0	11.46 ± 0.71	14.11 ± 0.29	• Fast, tight-binding, non-competitive inhibitor
		20	12.3 ± 1.9		
MH18	MHKTAPPFDFEAIPEEYL	0	10.9 ± 1.2	14.9 ± 3.5	• Fast, tight-binding, non-competitive inhibitor
		20	11.7 ± 1.9		

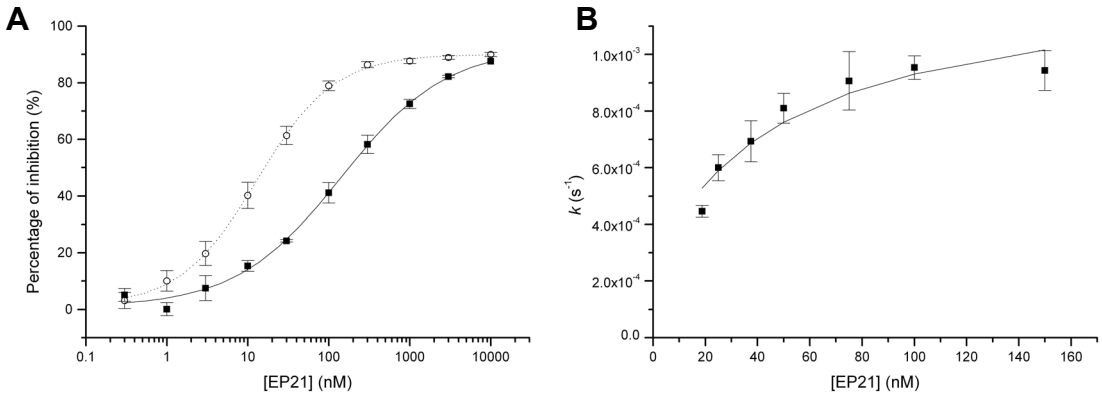

FIGURE 4.9

Variegin variant EP21 (slow, tight-binding, competitive inhibitor)

(A) EP21 (0.3 nM, 1 nM, 3 nM, 10 nM, 30 nM, 100 nM, 300 nM, 1000 nM, 3000 nM and 10000 nM) inhibition of thrombin (1.65 nM) amidolytic activity with S2238 (100 μM) showed a pre-incubation time-dependent shift due to slow binding. IC_{50} are 176.9 ± 6.8 nM without pre-incubation (■ solid line) and 16.2 ± 2.9 nM with 20 min pre-incubation (○ dotted line) (n = 3, error bars represent S.D.).

(B) Progression curves (not shown) of thrombin (1.65 nM) inhibition by different concentrations of EP21 (18.8 nM, 25 nM, 37.5 nM, 50 nM, 75 nM, 100 nM and 150 nM) at 100 μM S2238 were fitted to equation **(7)** describing a slow binding inhibitor to obtain a *k* for each concentrations of EP21 used. Plot of *k* against EP21 concentrations (■ solid line) is a hyperbolic curve described by equation **(8)** and hence was fitted to the equation to obtain a K_i` of 1.66 ± 0.36 nM, representing the dissociation constant of initial collision complex EI. The overall inhibitory constant K_i was calculated from equation **(9)** as 0.315 ± 0.024 nM (n = 3, error bars represent S.D.).

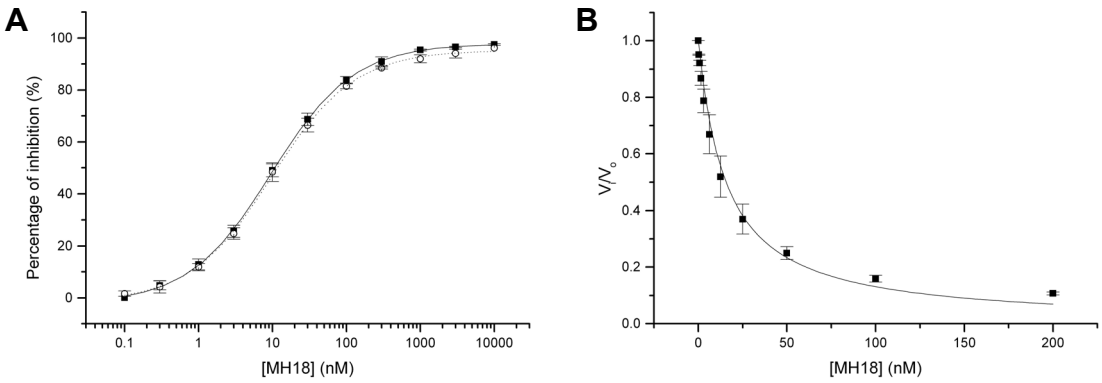

FIGURE 4.10

Variegin variant MH18 (fast, tight-binding, non-competitive inhibitor)

(A) The abilities of MH18 (0.1 nM, 0.3 nM, 1 nM, 3 nM, 10 nM, 30 nM, 100 nM, 300 nM, 1000 nM, 3000 nM and 10000 nM) to inhibit amidolytic activity of thrombin (1.65 nM) were assayed in 100 μM S2238. Dose-response curves are independent of pre-incubation time. IC_{50} are 10.9 ± 1.2 nM without pre-incubation (■ solid line) and 11.7 ± 1.9 nM after 20 min pre-incubation (○ dotted line) (n = 3, error bars represent S.D.).

(B) Since MH18 behaved as a fast and tight-binding inhibitor, thrombin (1.65 nM) inhibition was tested with 0.39 nM, 0.78 nM, 1.56 nM, 3.13 nM, 6.25 nM, 12.5 nM, 25 nM, 50 nM, 100 nM and 200 nM of MH18 at 100 μM of S2238 (■ solid line). Apparent inhibitory constant K_i' obtained by fitting data to equation **(3)** is 14.9 ± 3.5 nM. The inhibitory constant K_i is calculated to be 14.9 ± 3.5 nM based on equations **(5)** and **(6)** (n = 3, error bars represent S.D.).

4.3.5.3. Optimization of the length of variegin: extension at the N-terminus

Our earlier data showed that the seven N-terminal residues of variegin are responsible for its fast binding kinetics; when removed, the binding characteristics changed from fast to slow without loss in affinity (Chapter 2). We then postulated that the highly basic thrombin exosite-II could help to steer variegin N-terminus residues (which contains two negatively charged residues in its sequence ^{1}SDQGDVA^{7}) into an optimal orientation close to the active site, allowing rapid formation of short-range interactions. Since thrombin exosite-II is located about 10 Å away from the active site (Page et al., 2005), this distance could theoretically be covered by at least three N-terminal residues in an extended conformation. In order to produce a peptide that retained the fast-binding property, we designed and characterized a peptide extending EP21 by three residues at the N-terminus. One out of the two acidic N-terminal residues, ^{V}Asp5, is present in this variant, which is named DV24 (Table 4.6).

4.3.5.4. Inhibition of thrombin amidolytic activity by DV24

Instead of the two-phase equilibria usually observed for slow binding inhibitor, DV24 progress curves of thrombin inhibition were similar to s-variegin, reaching steady state equilibrium upon mixing. Thus, DV24 is a fast and tight-binding inhibitor. Activity of DV24 decreased with increasing pre-incubation time due to cleavage by thrombin. Dose-response curves showed IC_{50} values of 7.49 ± 0.28 nM (without pre-incubation) and 10.07 ± 0.60 nM (after 20 min pre-incubation) (Figure 4.11 A, Table 4.7). Assuming competitive inhibition, equations **(3)** and **(4)** were used to derive the inhibitory constant K_i of 0.306 ± 0.029 nM, consistent with K_i of s-variegin (Figure 4.11 B; Table 4.7). Therefore, we managed to design a peptide that is eight residues shorter than s-variegin but retained the fast-binding kinetic with the same K_i.

TABLE 4.6

Optimization of the length of variegin: extension at the N-terminus

One extension variants DV24 was designed and synthesized based on template sequence EP21 for the optimization of the length of variegin.

Name	Sequence	Theoretical mass (Da)	Observed mass (Da)	Basis for design
s-variegin	SDQGDVAEPKMHKTAPPFDFEAIPEEYLDDES	3608.9	3609.0	• Full-length sequence of native variegin • Fast, tight-binding, competitive inhibitor
EP21	EPKMHKTAPPFDFEAIPEEYL	2489.8	2490.2	• Template sequence for DV24 • Slow, tight-binding, competitive inhibitor • Deletion of 4 residues from C-terminus • Has the same K_i as s-variegin and EP25
DV24	DVAEPKMHKTAPPFDFEAIPEEYL	2775.1	2775.3	• Extension of EP21 N-terminus by 3 residues • To test the hypothesis that acidic residue (Asp) in the N-terminus facilitate fast-binding through electrostatic steering effect towards thrombin exosite-II

TABLE 4.7

Thrombin inhibitory activity of DV24

DV24 inhibited thrombin with the same potency as the template sequence EP21. However, unlike EP21 which is a slow binding inhibitor, DV24 is a fast-binding inhibitor, similar to s-variegin.

Name	Sequence	Pre-incubation tine (min)	IC_{50} (nM)	K_i (nM)	Remarks
s-variegin	SDQGDVAEPKMHKTAPPFDFEAIPEEYLDDES	0	8.25 ± 0.45	0.318 ± 0.020	• Fast, tight-binding, competitive inhibitor
		20	10.37 ± 0.30		
EP21	EPKMHKTAPPFDFEAIPEEYL	0	176.9 ± 6.8	0.315 ± 0.024	• Slow, tight-binding, competitive inhibitor
		20	16.2 ± 2.9		
DV24	DVAEPKMHKTAPPFDFEAIPEEYL	0	7.49 ± 0.28	0.306 ± 0.029	• Fast, tight-binding, competitive inhibitor
		20	10.07 ± 0.60		

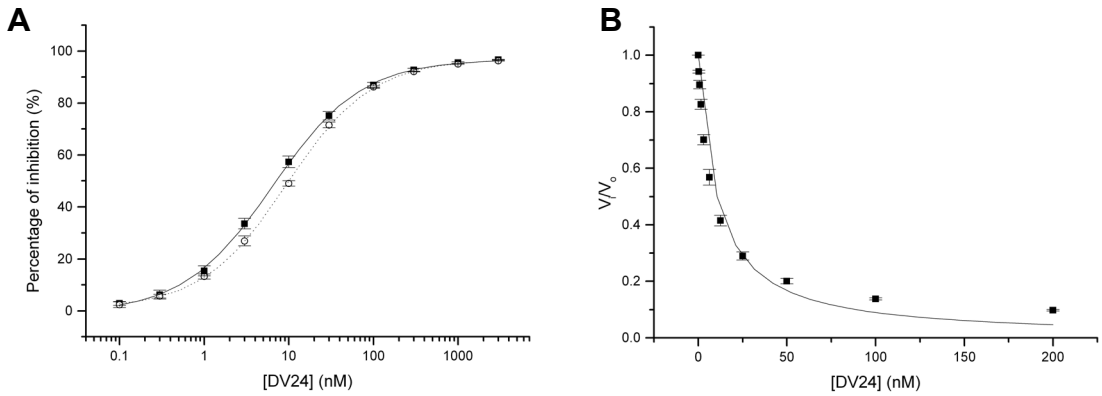

FIGURE 4.11

Variegin variant DV24 (fast, tight-binding, competitive inhibitor)

(A) Dose-response curves of thrombin (1.65 nM) inhibition by DV24 (0.1 nM, 0.3 nM, 1 nM, 3 nM, 10 nM, 30 nM, 100 nM, 300 nM, 1000 nM and 3000 nM) in 100 μM S2238 showed a right shift with increased pre-incubation time due to cleavage. IC_{50} are 7.49 ± 0.28 nM without pre-incubation (■ solid line) and 10.07 ± 0.60 nM with 20 min pre-incubation (○ dotted line) (n = 3, error bars represent S.D.).

(B) Since DV24 behaved as a fast and tight-binding inhibitor, thrombin (1.65 nM) inhibition was tested with 0.39 nM, 0.78 nM, 1.56 nM, 3.13 nM, 6.25 nM, 12.5 nM, 25 nM, 50 nM, 100 nM and 200 nM of DV24 at 100 μM of S2238 (■ solid line). Apparent inhibitory constant K_i' obtained by fitting data to equation **(3)** is 9.74 ± 0.91 nM. The inhibitory constant K_i is calculated to be 0.306 ± 0.029 nM based on equation **(4)** (n = 3, error bars represent S.D.).

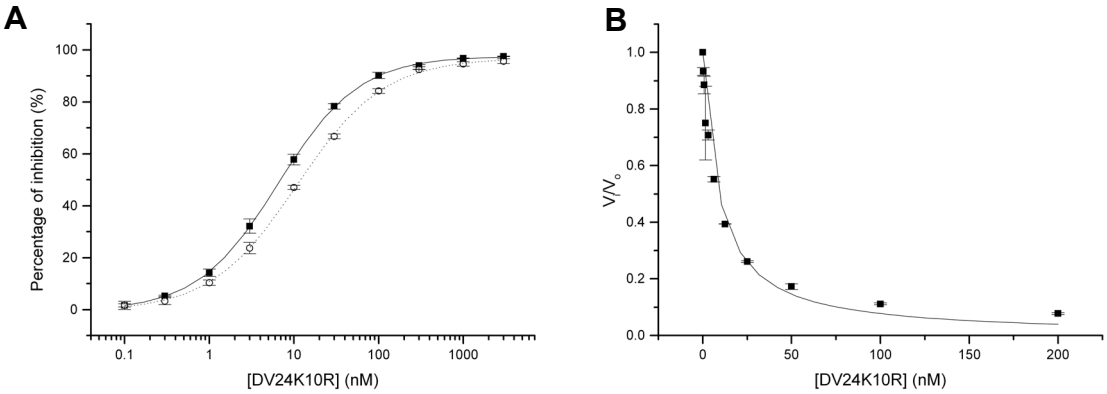

FIGURE 4.12

Variegin variant DV24K10R (fast, tight-binding, competitive inhibitor)

(A) Dose-response curves of thrombin (1.65 nM) inhibition by DV24K10R (0.1 nM, 0.3 nM, 1 nM, 3 nM, 10 nM, 30 nM, 100 nM, 300 nM, 1000 nM and 3000 nM) in 100 μM S2238 showed a right shift with increased pre-incubation time due to cleavage. IC_{50} are 6.98 ± 0.76 nM without pre-incubation (■ solid line) and 12.01 ± 0.41 nM after 20 min pre-incubation (○ dotted line) (n = 3, error bars represent S.D.).

(B) Since DV24K10R behaved as a fast and tight-binding inhibitor, thrombin (1.65 nM) inhibition was tested with 0.39 nM, 0.78 nM, 1.56 nM, 3.13 nM, 6.25 nM, 12.5 nM, 25 nM, 50 nM, 100 nM and 200 nM of DV24K10R at 100 μM of S2238 (■ solid line). Apparent inhibitory constant K_i' obtained by fitting data to equation **(3)** is 8.27 ± 0.85 nM. The inhibitory constant K_i is calculated to be 0.259 ± 0.015 nM based on equation **(4)** (n = 3, error bars represent S.D.).

4.3.5.5. Optimization of thrombin-s-variegin interactions: P1 substitution

One striking difference between variegin and other thrombin substrates/inhibitors is the presence of Lys in the P1 position of the scissile bond. Typically, Arg is found in this position for thrombin substrates. The electrostatic interaction between the side chain guanidinium group of Arg and the side chain carboxylate group of ^{T}Asp189 in the S1 subsite is usually preferred. In contrast, P1 Lys usually interacts with Asp189 through a water molecule (Perona and Craik, 1995), resulting in reduced affinity and specificity (Vindigni et al., 1997). The absence of electron density for residues before the scissile bond [^{V}(^{1}SDQGDVAEPK^{10})] in the thrombin-s-variegin structure probably implies the lack of strong affinity for thrombin within this segment. Therefore, using DV24 as template sequence, the P1 residue Lys10 was replaced by Arg in a new variant named DV24K10R (Table 4.8).

4.3.5.6. Inhibition of thrombin amidolytic activity by DV24K10R

IC_{50} obtained for DV24K10R is 6.98 ± 0.76 nM without pre-incubation, which is similar to IC_{50} of DV24 (7.49 ± 0.28 nM). However, IC_{50} for DV24K10R is 12.01 ± 0.41 nM after 20 min pre-incubation, slightly higher than that of DV24 (10.07 ± 0.60 nM). It is likely that cleavage of the peptide proceeds faster with the presence of P1 Arg (Figure 4.12 A; Table 4.9). Affinity to thrombin has increased slightly, indicated by a small drop in K_i value to 0.259 ± 0.015 nM (compared to 0.306 ± 0.029 nM for DV24) (Figure 4.12 B; Table 4.9). Thus, substitution of Lys10 by Arg only minimally improved thrombin affinity of variegin despite previous observations that P1 Lys generally binds 10-fold weaker than P1 Arg (Page et al., 2005). With this observation in mind, subsequent designs of new variants are typically performed with both Lys and Arg at P1 position.

TABLE 4.8

Optimization of thrombin-s-variegin interactions: P1 substitution

In order to optimize interaction of s-variegin P1 residue with thrombin S1 pocket, DV24K10R was designed and characterized.

Name	Sequence	Theoretical mass (Da)	Observed mass (Da)	Basis for design
s-variegin	SDQGDVAEPKMHKTAPPFDFEAIPEEYLDDES	3608.9	3609.0	• Full-length sequence of native variegin • Fast, tight-binding, competitive inhibitor
DV24	DVAEPKMHKTAPPFDFEAIPEEYL	2775.1	2775.3	• Template sequence for DV24K10R • Fast, tight-binding, competitive inhibitor
DV24K10R	DVAEPRMHKTAPPFDFEAIPEEYL	2803.1	2803.3	• Lys10 replaced by Arg • Arg at this P1 position is the preferred residue for thrombin

TABLE 4.9

Thrombin inhibitory activity of DV24K10R

DV24K10R binds thrombin with minimally improved affinity and with the same mechanism as its template sequence.

Name	Sequence	Pre-incubation tine (min)	IC_{50} (nM)	K_i (nM)	Remarks
s-variegin	SDQGDVAEPKMHKTAPPFDFEAIPEEYLDDES	0	8.25 ± 0.45	0.318 ± 0.020	• Fast, tight-binding, competitive inhibitor
		20	10.37 ± 0.30		
DV24	DVAEPKMHKTAPPFDFEAIPEEYL	0	7.49 ± 0.28	0.306 ± 0.029	• Fast, tight-binding, competitive inhibitor
		20	10.07 ± 0.60		
DV24K10R	DVAEPRMHKTAPPFDFEAIPEEYL	0	6.98 ± 0.76	0.259 ± 0.015	• Fast, tight-binding, competitive inhibitor
		20	12.01 ± 0.41		

4.3.5.7. Optimization of thrombin-s-variegin interactions: removal of backbone kink

The phenyl group of ^{V}Phe20 is inserted into an apolar cavity in thrombin and interacts with ^{T}Phe34 by π-π stacking. This interaction is also present in hirulogs, hirugen and hirudin complex structures and marks the start of the C-terminal segment – DFEA(E)IPEEYL – where s-variegin and hirulogs/hirugen are almost identical. In s-variegin, there are nine residues present in between the P1 Lys residue and the Phe [^{V}(^{11}MHKTAPPFD^{19})]. However, in hirulog-1/3, the same distance is spanned by only eight residues (^{4}PGGGGNGD^{11}). Analysis of the thrombin-s-variegin structure showed that ^{V}Pro16 and ^{V}Pro17 induced a kink in its backbone, causing a slight bend upwards, away from thrombin. This in turn caused a displacement of ^{V}Phe18 and ^{V}Asp19 by about 3.16 Å and 1.70 Å from their corresponding residues in hirulog-3 – Gly10 and Asp11 – as measured by distances between their Cα atoms (Figure 4.13). Crucially, Asp11 of hirulog-3 make an ion pair with ^{T}Arg73 which is absent between the analogous ^{V}Asp19 and ^{T}Arg73 (Figure 4.6 B). In fact ^{V}Asp19 side chain points to the opposite direction into the solvent, creating a 9.22 Å distance between the ^{V}Asp19 Oδ and ^{T}Arg73 NH2 (Figure 4.13). Therefore, Pro16 was deleted from s-variegin sequence to remove the kink in the backbone for the repositioning of ^{V}Asp19 so as to restore the ionic interaction. Using DV24 and DV24K10R as template sequences, variants DV23 and DV23K10R were designed, synthesized and characterized (Table 4.10).

4.3.5.8. Inhibition of thrombin amidolytic activity by DV23 and DV23K10R

Both DV23 and DV23K10R showed decrease in activities compared to their templates. DV23 IC_{50} values are 45.4 ± 1.6 nM (without pre-incubation) and 77.8 ± 6.1 nM (after 20 min pre-incubation) (Figure 4.14 A). DV23 K_i is 2.19 ± 0.23 nM

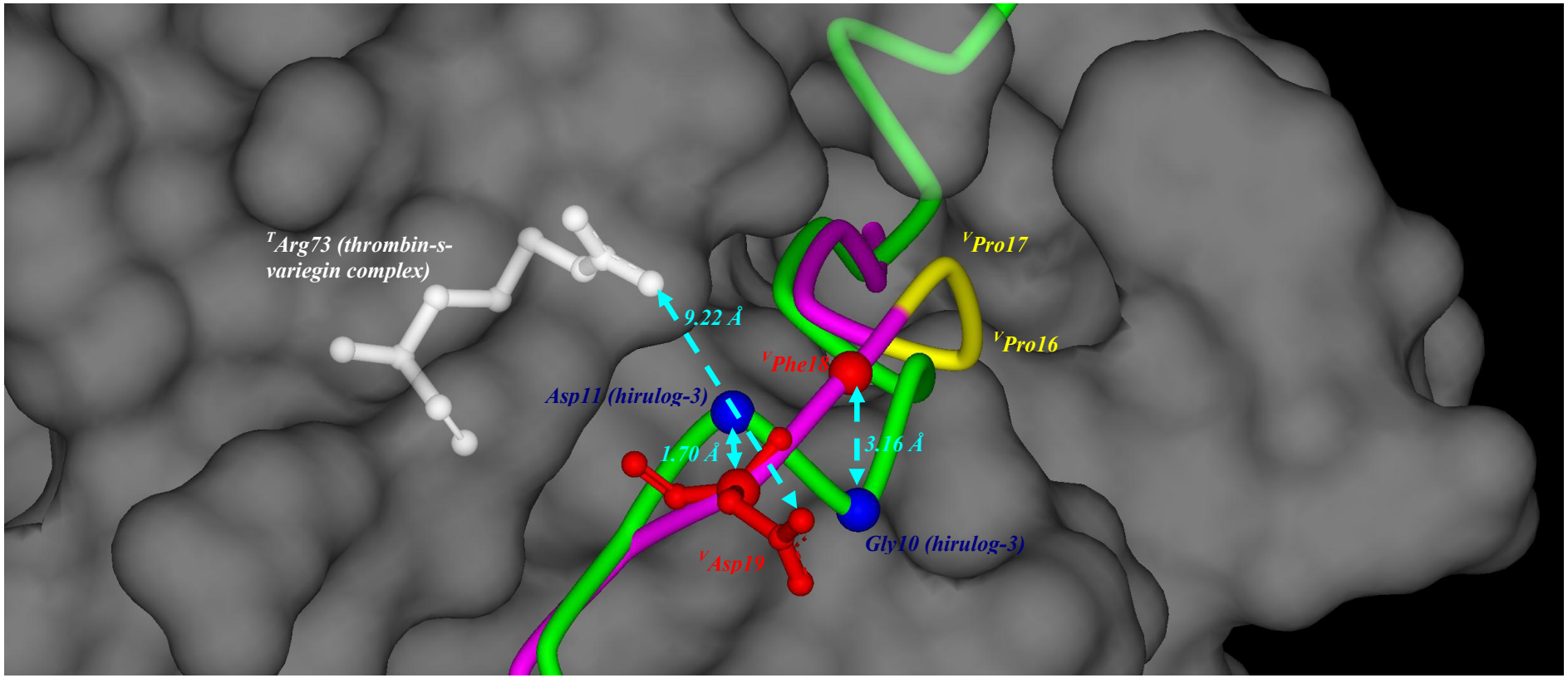

FIGURE 4.13

^{V}Pro16-^{V}Pro17 caused a kink in s-variegin backbone.

The presence of a ^{V}Pro16-^{V}Pro17 (yellow) dipeptide sequence in s-variegin resulted in a kink in its backbone. Overlaying s-variegin (pink, only Cα positions traced) and hirulog-3 (green, only Cα positions traced) based on their thrombin structures revealed displacement of ^{V}Phe18 and ^{V}Asp19 from their corresponding residues Gly10 and Asp11 of hirulog-3 by 3.16 Å and 1.70 Å (measured by Cα positions) (cyan double headed arrow). Consequently, ^{V}Asp19 side chain points to an opposite direction of the analogous Asp11 side chain in hirulog-3. This Asp11 in hirulog-3 makes a strong ion-pair with ^{T}Arg73 (white). Due to the displacement of ^{V}Asp19, the nearest possible distance between ^{T}Arg73 NH2 and ^{V}Asp19 OD1 is 9.22 Å, rendered this interaction in thrombin-s-variegin structure impossible.

TABLE 4.10

Optimization of thrombin-s-variegin interactions: removal of backbone kink

Based on sequences of DV24 and DV24K10R, Pro16 was deleted to produce two variants: DV23 and DV23K10R in an attempt to remove the kink in peptide backbone observed in the thrombin-s-variegin crystal structure.

Name	Sequence	Theoretical mass (Da)	Observed mass (Da)	Basis for design
DV24	DVAEPKMHKTAPPFDFEAIPEEYL	2775.1	2775.3	• Template sequence for DV23 • Fast, tight-binding, competitive inhibitor • Has the same K_i as s-variegin • Lys at P1
DV23	DVAEPKMHKTA PFDFEAIPEEYL	2678.0	2678.2	• Deletion of ^{V}Pro16 • To remove the kink in peptide backbone caused by two proline residues • To test the hypothesis that removal of the kink in the peptide backbone can reposition ^{V}Asp19 for improved activity
DV24K10R	DVAEPRMHKTAPPFDFEAIPEEYL	2803.1	2803.3	• Template sequence for DV23K10R • Fast, tight-binding, competitive inhibitor • Has the same K_i as s-variegin • Arg at P1
DV23K10R	DVAEPRMHKTA PFDFEAIPEEYL	2706.2	2706.2	• See DV23

TABLE 4.11

Thrombin inhibitory activity of DV23 and DV23K10R

Both DV23 and DV23K10R showed decrease in activities compared to their respective templates, DV24 and DV24K10R. The rapid loss of activities after cleavage implies that their cleavage products fail to inhibit thrombin.

Name	Sequence	Pre-incubation tine (min)	IC_{50} (nM)	K_i (nM)	Remarks
DV24	DVAEPKMHKTAPPFDFEAIPEEYL	0	7.49 ± 0.28	0.306 ± 0.029	• Fast, tight-binding, competitive inhibitor
		20	10.07 ± 0.60		
DV23	DVAEPKMHKTA PFDFEAIPEEYL	0	45.4 ± 1.6	2.19 ± 0.23	• Fast, tight-binding, competitive inhibitor
		20	77.8 ± 6.1		
DV24K10R	DVAEPRMHKTAPPFDFEAIPEEYL	0	6.98 ± 0.76	0.259 ± 0.015	• Fast, tight-binding, competitive inhibitor
		20	12.01 ± 0.41		
DV23K10R	DVAEPRMHKTA PFDFEAIPEEYL	0	12.9 ± 1.0	0.600 ± 0.010	• Fast, tight-binding, competitive inhibitor
		20	101.9 ± 1.2		

(Figure 4.14 B). All values showed an average of 7-fold reduction in activity compared to DV24 (Table 4.11). The other variant, DV23K10R is also less active compared to its template, DV24K10R. The peptide IC_{50} are 12.9 ± 1.0 nM (without pre-incubation) and 101.9 ± 1.2 nM (20 min pre-incubation) (Figure 4.15 A). DV23K10R K_i is 0.600 ± 0.010 nM (Figure 4.15 B). Its affinity to thrombin is approximately 2-fold weaker than DV24K10R (Table 4.11). While DV23K10R is more active than DV23 without pre-incubation with thrombin, the trend is reversed after 20 min of pre-incubation. This is in agreement with the observation that peptide with Arg at P1 (DV24K10R) is hydrolyzed by thrombin at a faster rate than peptide with Lys at P1 (DV24) (Section 4.3.5.6.). Moreover, the rapid loss of activity also implies that the cleavage product no longer inhibits thrombin potently. Thus, the deletion of ^{V}Pro16 appears to have an adverse effect on the activities of both the intact peptide and cleavage product. Considering the proximity of variegin P′ residues to ^{V}Pro16, removal of this residue probably compromised the interactions within the prime subsites.

4.3.5.9. Optimization of thrombin-s-variegin interactions: C-terminal Ala22 substitution

Other than the three residues [^{V}(^{30}DES^{32})] extension, C-termini of variegin and hirudin differed in two other ways: (1) a non-conserved substitution of Glu58 in hirudin by ^{V}Ala22 in variegin; and (2) ^{V}Tyr27 is non-sulfated in variegin (and also in hirulogs). We examined the effect these differences in a series of variants. The side chain of ^{V}Ala22 is solvent exposed in crystal structure (Figure 4.5 D) although hirudin Glu58 side chain was observed to make an ion-pair with ^{T}Arg77a of thrombin (Rydel et al., 1990; Rydel et al., 1991). Two new variants, EP25A22E and MH22A22E were

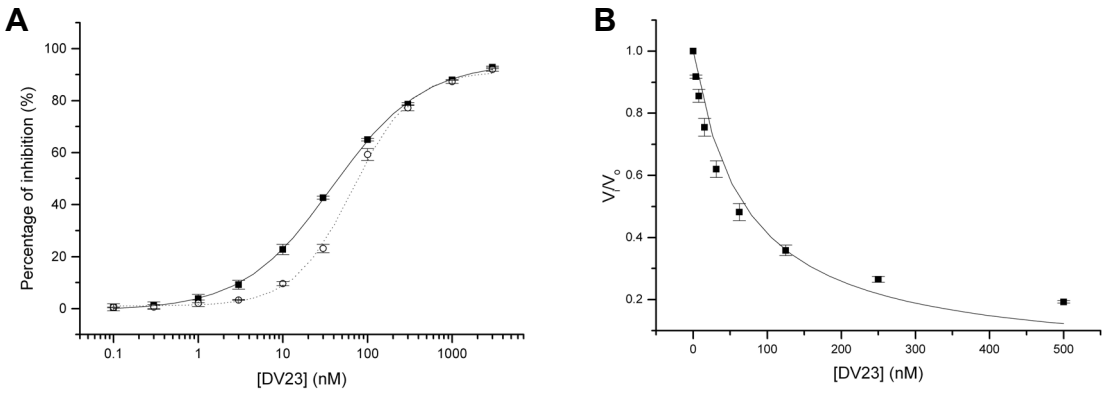

FIGURE 4.14

Variegin variant DV23 (fast, tight-binding, competitive inhibitor)

(A) Dose-response curves of thrombin (1.65 nM) inhibition by DV23 (0.1 nM, 0.3 nM, 1 nM, 3 nM, 10 nM, 30 nM, 100 nM, 300 nM, 1000 nM and 3000 nM) in 100 μM S2238 showed a right shift with increased pre-incubation time due to cleavage. IC_{50} are 45.4 ± 1.6 nM without pre-incubation (■ solid line) and 77.8 ± 6.1 nM after 20 min pre-incubation (○ dotted line) (n = 3, error bars represent S.D.).

(B) Thrombin (1.65 nM) inhibition was tested with 3.91 nM, 7.81 nM, 15.6 nM, 31.3 nM, 62.5 nM, 125 nM, 250 nM and 500 nM of DV23 at 100 μM of S2238 (■). Apparent inhibitory constant K_i' obtained by fitting data to equation **(3)** is 69.6 ± 7.8 nM. The inhibitory constant K_i is calculated to be 2.19 ± 0.23 nM based on equation **(4)** (n = 3, error bars represent S.D.).

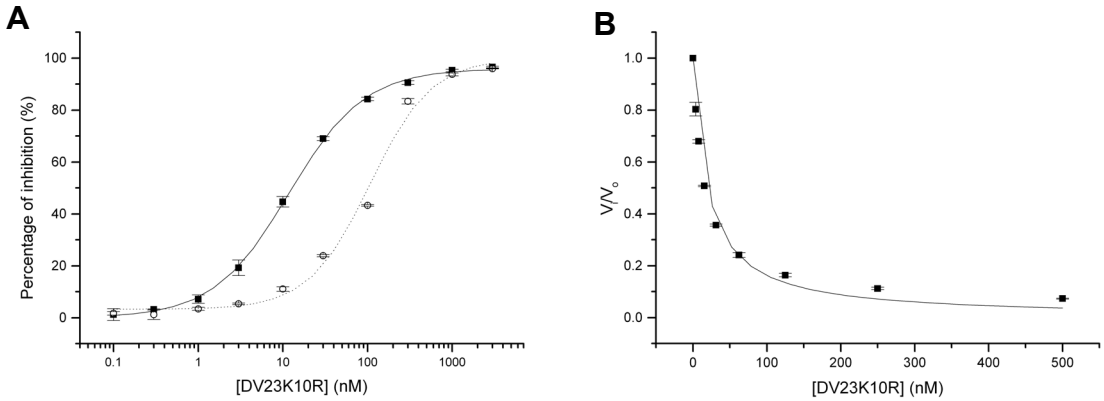

FIGURE 4.15

Variegin variant DV23K10R (fast, tight-binding, competitive inhibitor)

(A) DV23K10R (0.1 nM, 0.3 nM, 1 nM, 3 nM, 10 nM, 30 nM, 100 nM, 300 nM, 1000 nM and 3000 nM) inhibited thrombin (1.65 nM) in the presence of 100 μM S2238. Loss of activities after cleavage is rapid, indicated by the strong right shift of dose-response curve. IC_{50} are 12.9 ± 1.0 nM without pre-incubation (■ solid line) and 101.9 ± 1.2 nM after 20 min pre-incubation (○ dotted line) (n = 3, error bars represent S.D.).

(B) Thrombin (1.65 nM) inhibition was tested with 3.91 nM, 7.81 nM, 15.6 nM, 31.3 nM, 62.5 nM, 125 nM, 250 nM and 500 nM of DV23K10R at 100 μM of S2238 (■ solid line). Apparent inhibitory constant K_i' obtained by fitting data to equation **(3)** is 19.1 ± 1.9 nM. The inhibitory constant K_i is calculated to be 0.600 ± 0.010 nM based on equation **(4)** (n = 3, error bar represents S.D.).

designed. Using EP25 and MH22 as respective template sequence, ^{V}Ala22 in both peptides were replaced by Glu. The four C-terminal residues were retained in both variants to preserve the original local environment of the peptides near the C-terminus (Table 4.12).

4.3.5.10. Inhibition of thrombin amidolytic activity by EP25A22E and MH22A22E

Similar to EP25 and EP21, progress curves of thrombin inhibition by EP25A22E showed two-phase equilibria in the absence of pre-incubation with thrombin. IC_{50} for EP25A22E are 124.3 ± 23.0 nM (without pre-incubation) and decreased to 13.5 ± 2.1 nM (after 20 min pre-incubation) (Figure 4.16 A), similar to of EP25 (Table 4.13). Thus, EP25A22E is a slow and tight-binding inhibitor. The inhibitory constant K_i calculated from equations **(7)** to **(9)** describing slow binding inhibitor, is 0.311 ± 0.070 nM (Figure 4.16 D), again effectively the same as EP25 (Table 4.13). Thus, replacement of ^{V}Ala22 by Glu does not alter activity of variegin variant.

MH22A22E inhibited thrombin amidolytic activity with IC_{50} values of 13.62 ± 0.45 nM (without pre-incubation) and 15.63 ± 0.36 nM (20 min pre-incubation) (Figure 4.17 A). K_i of MH22A22E is 15.1 ± 1.0 nM (Figure 4.17 B). All values match those of MH22 (Table 4.13). This result added confidence to the conclusion that no significant improvement on activity can be achieved by mutating ^{V}Ala22 to Glu.

TABLE 4.12

Optimization of thrombin-s-variegin interactions: C-terminal ^{V}Ala22 substitution

Based on template sequences EP25 and MH22, two variants EP25A22E and MH22A22E were designed to determine the effect ^{V}Ala22 to Glu substitution.

Name	Sequence	Theoretical mass (Da)	Observed mass (Da)	Basis for design
EP25	EPKMHKTAPPFDFEAIPEEYLDDES	2936.2	2936.4	• Template sequence for EP25A22E • Slow, tight-binding, competitive inhibitor • Has the same K_i as s-variegin and EP25
EP25A22E	EPKMHKTAPPFDFEEIPEEYLDDES	2994.2	2994.4	• ^{V}Ala22 replaced by Glu • Glu is present in this position in hirudin forming salt bridge with ^{T}Arg77a of thrombin • Side chain of ^{V}Ala22 in the thrombin-s-variegin structure is solvent exposed • Last four residues were retained to preserve local environment of C-terminus
MH22	MHKTAPPFDFEAIPEEYLDDES	2581.8	2581.8	• Template sequence for MH22A22E • C-terminal cleavage fragment of s-variegin • Fast, tight-binding, non-competitive inhibitor
MH22A22E	MHKTAPPFDFEEIPEEYLDDES	2639.8	2640.1	• See EP25A22E

TABLE 4.13

Thrombin inhibitory activity of EP25A22E and MH22A22E

EP25A22E and MH22A22E inhibited thrombin with the same mechanisms and potencies as their respective template sequences.

Name	Sequence	Pre-incubation tine (min)	IC_{50} (nM)	K_i (nM)	Remarks
EP25	EPKMHKTAPPFDFEAIPEEYLDDES	0	173.1 ± 26.0	0.37 ± 0.11	• Slow, tight-binding, competitive inhibitor
		20	13.12 ± 0.67		
EP25A22E	EPKMHKTAPPFDFEEIPEEYLDDES	0	124.3 ± 23.0	0.311 ± 0.070	• Slow, tight-binding, competitive inhibitor
		20	13.5 ± 2.1		
MH22	MHKTAPPFDFEAIPEEYLDDES	0	11.46 ± 0.71	14.11 ± 0.29	• Fast, tight-binding, non-competitive inhibitor
		20	12.3 ± 1.9		
MH22A22E	MHKTAPPFDFEEIPEEYLDDES	0	13.62 ± 0.45	15.07 ± 1.04	• Fast, tight-binding, non-competitive inhibitor
		20	15.63 ± 0.36		

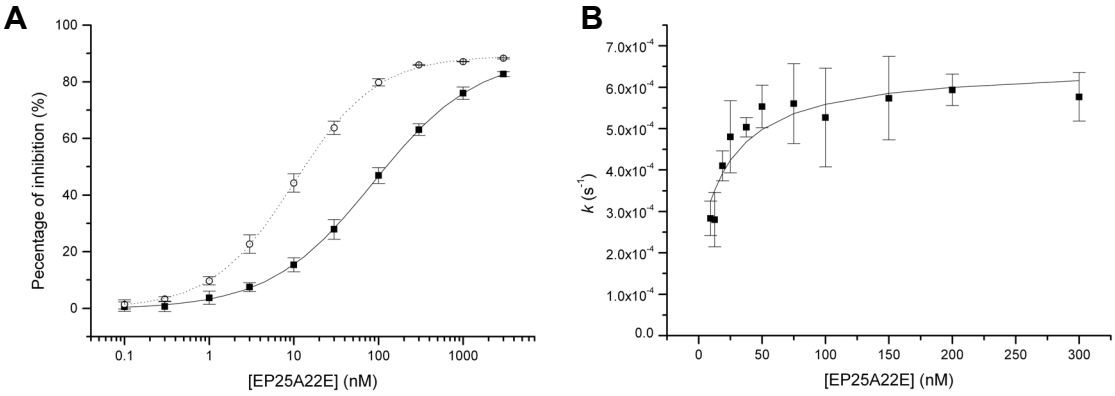

FIGURE 4.16

Variegin variant EP25A22E (slow, tight-binding, competitive inhibitor)

(A) EP25A22E (0.1 nM, 0.3 nM, 1 nM, 3 nM, 10 nM, 30 nM, 100 nM, 300 nM, 1000 nM and 3000 nM) inhibition of thrombin (1.65 nM) amidolytic activity in 100 μM S2238 showed a pre-incubation time-dependent shift due to slow binding. IC_{50} values are 124.3 ± 23.0 nM without pre-incubation (■ solid line) and 13.5 ± 2.1 nM after 20 min pre-incubation (○ dotted line) (n = 3, error bars represent S.D.).

(B) Progression curves (not shown) of thrombin (1.65 nM) inhibition by different concentrations of EP21 (9.38 nM, 12.5 nM, 18.8 nM, 25 nM, 37.5 nM, 50 nM, 75 nM, 100 nM, 150 nM, 200 nM and 300 nM) at 100 μM S2238 were fitted to equation **(7)** describing a slow binding inhibitor to obtain a *k* for each concentrations of EP25A22E used. Plot of *k* against EP25A22E concentrations (■ solid line) is a hyperbolic curve described by equation **(8)** and hence was fitted to the equation to obtain a K_i` of 1.02 ± 0.060 nM, representing the dissociation constant of initial collision complex EI. The overall inhibitory constant K_i was calculated from equation **(9)** as 0.311 ± 0.070 nM (n = 3, error bars represent S.D.).

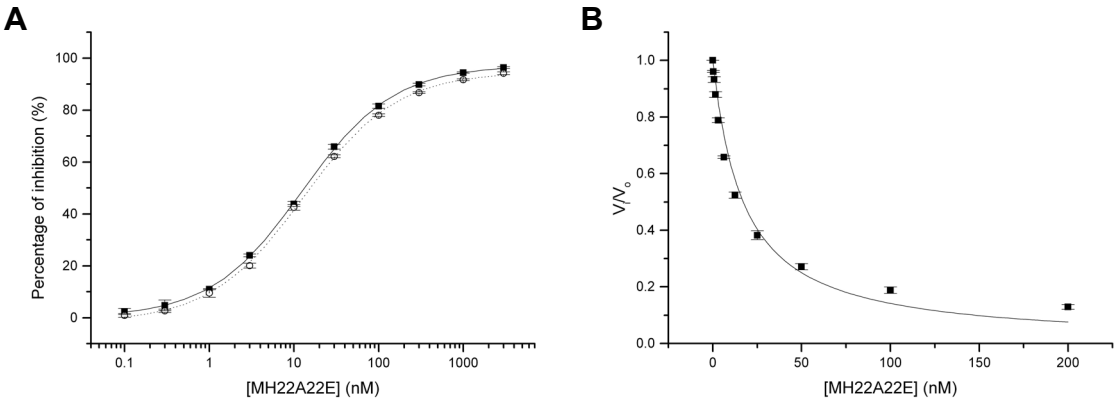

FIGURE 4.17

Variegin variant MH22A22E (fast, tight-binding, non-competitive inhibitor)

(A) MH22A22E (0.1 nM, 0.3 nM, 1 nM, 3 nM, 10 nM, 30 nM, 100 nM, 300 nM, 1000 nM and 3000 nM) inhibition of thrombin (1.65 nM) amidolytic activity were assayed in 100 μM S2238. Dose-response curves are independent of pre-incubation time. IC_{50} are 13.62 ± 0.45 nM without pre-incubation (■ solid line) and 15.63 ± 0.36 nM after 20 min pre-incubation (○ dotted line) (n = 3, error bars represent S.D.).

(B) Since MH22A22E behaved as a fast and tight-binding inhibitor, thrombin (1.65 nM) inhibition was tested with 0.39 nM, 0.78 nM, 1.56 nM, 3.13 nM, 6.25 nM, 12.5 nM, 25 nM, 50 nM, 100 nM and 200 nM of MH22A22E at 100 μM of S2238 (■ solid line). Apparent inhibitory constant K_i' obtained by fitting data to equation **(3)** is 15.1 ± 1.0 nM. The inhibitory constant K_i is calculated to be 15.1 ± 1.0 nM based on equations **(5)** and **(6)** (n = 3, error bars represent S.D.).

4.3.5.11. Optimization of thrombin-s-variegin interactions: C-terminal Tyr27 modifications

Desulfation of Tyr63 in hirudin or hirugen is known to reduce their affinities to thrombin by about 10-fold (Stone and Hofsteenge, 1986; Dodt et al., 1988; Braun et al., 1988a; Maraganore et al., 1989). Interestingly, the analogous residue in native variegin, ^{V}Tyr27, is non-sulfated. C-terminal conformation of s-variegin deviates vastly from that of hirulogs, hirugen or sulfo-hirudin (Figure 4.2). The difference might be due to the four/three residues extension of s-variegin [^{V}(^{29}DDES^{32})] C-terminal (see Section 4.3.3.). Side chain of ^{V}Glu25 occupies a similar position as side chain of sulfotyrosine in sulfo-hirudin or hirugen structures (Figure 4.7). However, ^{V}Glu25 side chain did not make any polar or electrostatic contacts with thrombin. Thus, the binding at this position for thrombin-s-variegin complex appeared to be suboptimal. In view of the truncation of s-variegin C-terminal residues ^{V}(^{29}DDES^{32}), we postulated that the introduction of sulfate moiety at ^{V}Tyr27 can switch s-variegin C-terminal conformation to mimic sulfo-hirudin or hirugen and thereby increasing the binding affinity. Therefore, it would be interesting to investigate whether sulfation in s-variegin improves its activity.

Other than sulfation, another commonly found post-translational modification for tyrosine is phosphorylation. Sulfate and phosphate moieties shared some similarities. Both carry an overall negative charge with almost the same size. Under our assay conditions at pH 7.4, sulfotyrosine side chain has a single negative charge while phosphotyrosine side chain carries two negative charges (Hofsteenge et al., 1990). Consequently, peptides were designed to bear these two modifications – sulfation and phosphorylation – on the ^{V}Tyr27. Based on DV24, DV24K10R and

TABLE 4.14

Optimization of thrombin-s-variegin interactions: C-terminal ^{V}Tyr27 sulfation

Based on sequences of DV24, DV24K10R and MH18, sulfo-Tyr27 was incorporated to produce three variants: DV24Y^{sulf}, DV24K10RY^{sulf} and MH18Y^{sulf} to optimize C-terminal conformation of the variants.

Name	Sequence	Theoretical mass (Da)	Observed mass (Da)	Basis for design
DV24	DVAEPKMHKTAPPFDFEAIPEEYL	2775.1	2775.3	• Template sequence for DV24Y^{sulf} • Fast, tight-binding, competitive inhibitor • Has the same K_i as s-variegin • Lys at P1
DV24Y^{sulf}	DVAEPKMHKTAPPFDFEAIPEEY*L	2855.1	NA	• Sulfation of ^{V}Tyr27 • Tyr-desulfation in hirudin/hirugen results in 10x weaker binding to thrombin • To investigate if sulfation improve affinity for thrombin
DV24K10R	DVAEPRMHKTAPPFDFEAIPEEYL	2803.1	2803.3	• Template sequence for DV23K10RY^{sulf} • Fast, tight-binding, competitive inhibitor • Has the same K_i as s-variegin • Arg at P1
DV24K10RY^{sulf}	DVAEPRMHKTAPPFDFEAIPEEY*L	2883.1	NA	• See DV24Y^{sulf}
MH18	MHKTAPPFDFEAIPEEYL	2135.4	2136.0	• Template sequence for MH18Y^{sulf} • Fast, tight-binding, non-competitive inhibitor • Arg at P1
MH18Y^{sulf}	MHKTAPPFDFEAIPEEY*L	2215.4	NA	• See DV24Y^{sulf}

*represents sulfotyrosine residue; NA: not available (see *Section 4.2.2* for details)

TABLE 4.15

Thrombin inhibitory activity of DV24Y^{sulf}, DV24K10RY^{sulf} and MH18Y^{sulf}

Sulfation of ^{V}Tyr27 drastically improved activities of all new variants compared to their respective template peptides. Affinity of DV24K10RY^{sulf} to thrombin is approximately 70-fold stronger than hirulog-1/bivalirudin.

Name	Sequence	Pre-incubation tine (min)	IC_{50} (nM)	K_i (nM)	Remarks
DV24	DVAEPKMHKTAPPFDFEAIPEEYL	0	7.49 ± 0.28	0.306 ± 0.029	• Fast, tight-binding, competitive inhibitor
		20	10.07 ± 0.60		
DV24Y^{sulf}	DVAEPKMHKTAPPFDFEAIPEEY*L	0	1.66 ± 0.18	0.056 ± 0.018	• Fast, tight-binding, competitive inhibitor
		20	2.02 ± 0.29		
DV24K10R	DVAEPRMHKTAPPFDFEAIPEEYL	0	6.98 ± 0.76	0.259 ± 0.015	• Fast, tight-binding, competitive inhibitor
		20	12.01 ± 0.41		
DV24K10RY^{sulf}	DVAEPRMHKTAPPFDFEAIPEEY*L	0	1.39 ± 0.17	0.0420 ± 0.0061	• Fast, tight-binding, competitive inhibitor
		20	1.66 ± 0.21		
MH18	MHKTAPPFDFEAIPEEYL	0	10.9 ± 1.2	14.94 ± 3.50	• Fast, tight-binding, non-competitive inhibitor
		20	11.7 ± 1.9		
MH18Y^{sulf}	MHKTAPPFDFEAIPEEY*L	0	1.26 ± 0.18	1.25 ± 0.18	• Fast, tight-binding, non-competitive inhibitor
		20	1.17 ± 0.14		

*represents sulfotyrosine residue

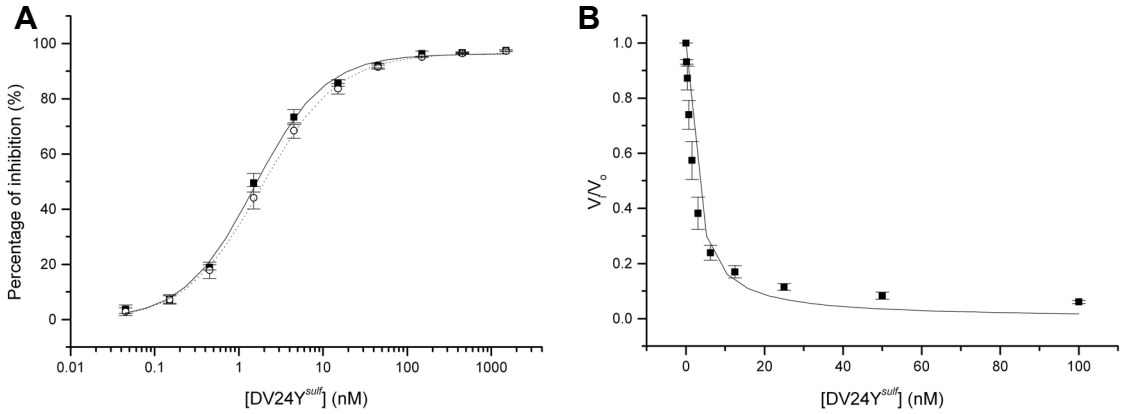

FIGURE 4.18

Variegin variant DV24Y^{sulf} (fast, tight-binding, competitive inhibitor)

(A) DV24Y^{sulf} (0.05 nM, 0.15 nM, 0.45 nM, 1.5 nM, 4.5 nM, 15 nM, 45 nM, 150 nM, 450 nM and 1500 nM) inhibited thrombin (1.65 nM) amidolytic activity in 100 μM S2238. Dose-response curve shifted slightly to the right with increased pre-incubation time due to cleavage. IC_{50} are 1.66 ± 0.18 nM without pre-incubation (■ solid line) and 2.02 ± 0.29 nM after 20 min pre-incubation (○ dotted line) (n = 3, error bars represent S.D.).

(B) Since DV24Y^{sulf} behaved as a fast and tight-binding inhibitor, thrombin (1.65 nM) inhibition was tested with 0.20 nM, 0.39 nM, 0.78 nM, 1.56 nM, 3.13 nM, 6.25 nM, 12.5 nM, 25 nM, 50 nM and 100 nM of DV24Y^{sulf} at 100 μM of S2238 (■ solid line). Apparent inhibitory constant K_i' obtained by fitting data to equation **(3)** is 1.78 ± 0.47 nM. The inhibitory constant K_i is calculated to be 0.056 ± 0.015 nM based on equation **(4)** (n = 3, error bars represent S.D.).

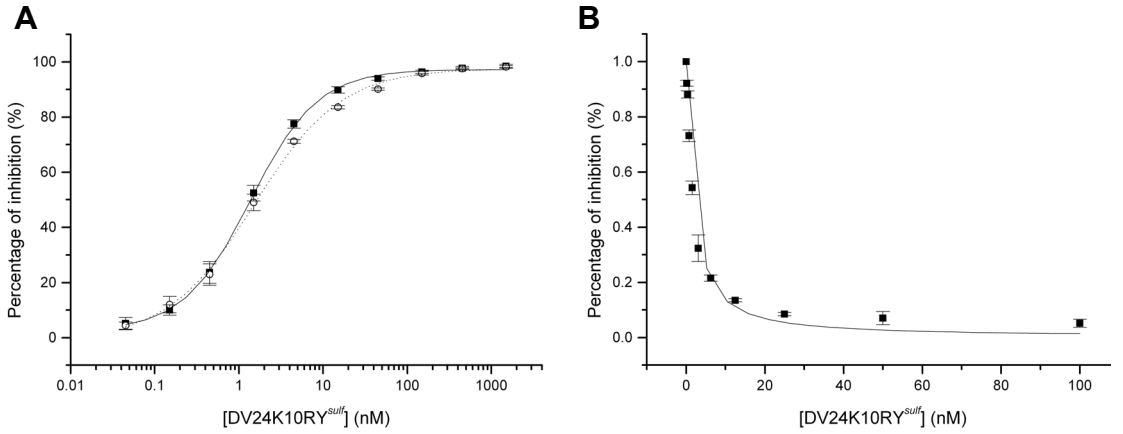

FIGURE 4.19

Variegin variant DV24K10RY^{sulf} (fast, tight-binding, competitive inhibitor)

(A) DV24K10RY^{sulf} (0.05 nM, 0.15 nM, 0.45 nM, 1.5 nM, 4.5 nM, 15 nM, 45 nM, 150 nM, 450 nM and 1500 nM) inhibited thrombin (1.65 nM) amidolytic activity in 100 μM S2238. Dose-response curve shifted slightly to the right with increased pre-incubation time due to cleavage. IC_{50} are 1.39 ± 0.17 nM without pre-incubation (■ solid line) and 1.66 ± 0.21 nM after 20 min pre-incubation (○ dotted line) (n = 3, error bars represent S.D.).

(B) Since DV24K10RY^{sulf} behaved as a fast and tight-binding inhibitor, thrombin (1.65 nM) inhibition was tested with 0.20 nM, 0.39 nM, 0.78 nM, 1.56 nM, 3.13 nM, 6.25 nM, 12.5 nM, 25 nM, 50 nM and 100 nM of DV24Y^{sulf} at 100 μM of S2238 (■ solid line). Apparent inhibitory constant K_i' obtained by fitting data to equation **(3)** is 1.33 ± 0.19 nM. The inhibitory constant K_i is calculated to be 0.0420 ± 0.0061 nM based on equation **(4)** (n = 3, error bars represent S.D.).

MH18 sequences, sulfotyrosine residue was incorporated in three new variants, DV24Y^{sulf}, DV24K10RY^{sulf} and MH18Y^{sulf} (Table 4.14). Similarly, phosphotyrosine residue was included for DV24 and DV24K10R to produce two variants, namely, DV24Y^{phos} and DV24K10RY^{phos} (Table 4.16).

4.3.5.12. Inhibition of thrombin amidolytic activity by tyrosine-modified peptides

IC_{50} for DV24Y^{sulf} are 1.66 ± 0.18 nM (without pre-incubation) and 2.02 ± 0.29 nM (after 20 min pre-incubation). Increase in IC_{50} is due to cleavage by thrombin (Figure 4.18 A). Fitting kinetic data to equations describing fast, tight-binding, competitive inhibitor showed that the K_i (mean ± S.D.) of the peptide is 0.056 ± 0.018 nM (Figure 4.18 B). Thus, for DV24Y^{sulf}, an average of 5-fold in activity and affinity are gained compared to DV24 (Table 4.15). DV24K10RY^{sulf} inhibition of thrombin showed similar extent of improvement compared to DV24K10R (Table 4.15). IC_{50} are 1.39 ± 0.17 nM (without pre-incubation) and 1.66 ± 0.21 nM (after 20 min pre-incubation) (Figure 4.19 A). K_i is 0.0420 ± 0.0061 nM (Figure 4.19 B). Affinity of DV24K10RY^{sulf} to thrombin is approximately 70-fold stronger than hirulog-1/bivalirudin (hirulog-1 K_i = 2.94 ± 0.12 nM). Although cleaved by thrombin, the sulfotyrosine containing cleavage product (MH18Y^{sulf}) also inhibited the enzyme potently. Activity of MH18Y^{sulf} is independent of pre-incubation times, consistent with previous observations of its template peptide MH18. However, compared to the latter, MH18Y^{sulf} IC_{50} values, 1.26 ± 0.18 nM (without pre-incubation) and 1.17 ± 0.14 nM (20 min pre-incubation), are 9-fold lower (Figure 4.20 A). Assuming fast, tight-binding, non-competitive inhibition, K_i of MH18Y^{sulf} is 1.25 ± 0.18 nM, which is 11-fold and 2-fold stronger than MH18 and hirulog-1/bivalirudin respectively (Figure 4.20 B; Table 4.15).

TABLE 4.16

Optimization of thrombin-s-variegin interactions: C-terminal Tyr27 phosphorylation

Based on sequences of DV24 and DV24K10R, phospho-Tyr27 was incorporated to produce two variants: DV24Y^{phos} and DV24K10RY^{phos} to check if phosphorylation increases their affinities for thrombin.

Name	Sequence	Theoretical mass (Da)	Observed mass (Da)	Basis for design
DV24	DVAEPKMHKTAPPFDFEAIPEEYL	2775.1	2775.3	• Template sequence for DV24Y^{phos} • Fast, tight-binding, competitive inhibitor • Has the same K_i as s-variegin • Lys at P1
DV24Y^{phos}	DVAEPKMHKTAPPFDFEAIPEEY^L	2855.1	2855.3	• Phosphorylation of ^{V}Tyr27 • Phosphate group is similar to sulfate in size but has two negative charges (cf. to one in sulfate) • To investigate if phosphorylation improve affinity for thrombin
DV24K10R	DVAEPRMHKTAPPFDFEAIPEEYL	2803.1	2803.3	• Template sequence for DV23K10RY^{phos} • Fast, tight-binding, competitive inhibitor • Has the same K_i as s-variegin • Arg at P1
DV24K10RY^{phos}	DVAEPRMHKTAPPFDFEAIPEEY^L	2883.1	2883.3	• See DV24Y^{phos}

^represents phosphotyrosine residue

TABLE 4.17

Thrombin inhibitory activity of DV24Y^{phos} and DV24K10RY^{phos}

Phosphorylation of ^{V}Tyr27 did not improve peptides affinities as much as sulfation. Affinity of DV24Y^{phos} to thrombin is similar with its template peptide while affinity of DV24K10RY^{phos} to thrombin is slightly higher compared to its template peptide.

Name	Sequence	Pre-incubation tine (min)	IC_{50} (nM)	K_i (nM)	Remarks
DV24	DVAEPKMHKTAPPFDFEAIPEEYL	0	7.49 ± 0.28	0.306 ± 0.029	• Fast, tight-binding, competitive inhibitor
		20	10.07 ± 0.60		
DV24Y^{phos}	DVAEPKMHKTAPPFDFEAIPEEY^L	0	8.67 ± 0.45	0.327 ± 0.032	• Fast, tight-binding, competitive inhibitor
		20	12.4 ± 1.2		
DV24K10R	DVAEPRMHKTAPPFDFEAIPEEYL	0	6.98 ± 0.76	0.259 ± 0.015	• Fast, tight-binding, competitive inhibitor
		20	12.01 ± 0.41		
DV24K10RY^{phos}	DVAEPRMHKTAPPFDFEAIPEEY^L	0	4.64 ± 0.78	0.150 ± 0.018	• Fast, tight-binding, competitive inhibitor
		20	7.8 ± 1.8		

^represents phosphotyrosine residue

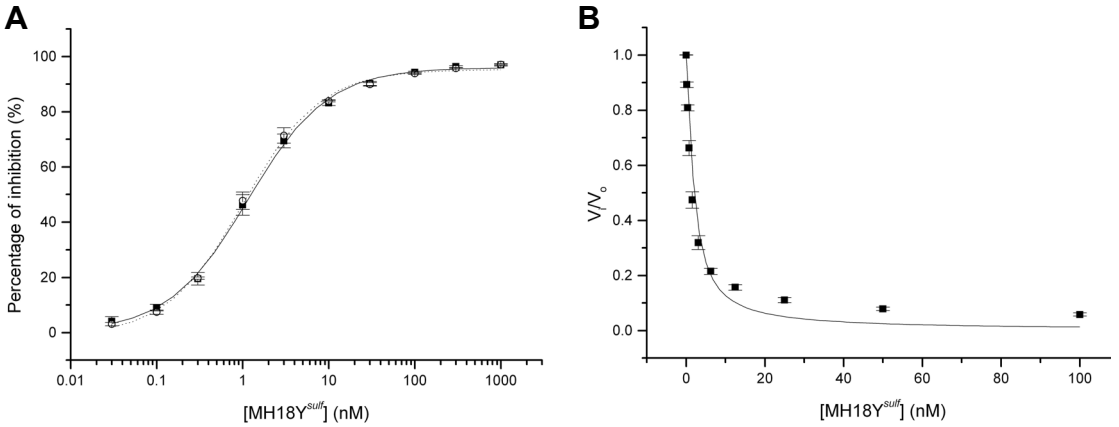

FIGURE 4.20

Variegin variant MH18Y^{sulf} (fast, tight-binding, non-competitive inhibitor)

(A) The abilities of MH18Y^{sulf} (0.03 nM, 0.1 nM, 0.3 nM, 1 nM, 3 nM, 10 nM, 30 nM, 100 nM, 300 nM and 1000 nM) to inhibit amidolytic activity of thrombin (1.65 nM) were assayed in 100 μM S2238. Dose-response curves are independent of pre-incubation time. IC_{50} are 1.26 ± 0.18 nM without pre-incubation (■ solid line) and 1.17 ± 0.14 nM after 20 min pre-incubation (○ dotted line) (n = 3, error bar represents S.D.).

(B) Since MH18Y^{sulf} behaved as a fast and tight-binding inhibitor, thrombin (1.65 nM) inhibition was tested with 0.20 nM, 0.39 nM, 0.78 nM, 1.56 nM, 3.13 nM, 6.25 nM, 12.5 nM, 25 nM, 50 nM and 100 nM of MH18Y^{sulf} at 100 μM of S2238 (■ solid line). Apparent inhibitory constant K_i' obtained by fitting data to equation **(3)** is 1.25 ± 0.18 nM. The inhibitory constant K_i is calculated to be 1.25 ± 0.18 nM based on equation **(5)** and **(6)** (n = 3, error bar represents S.D.).

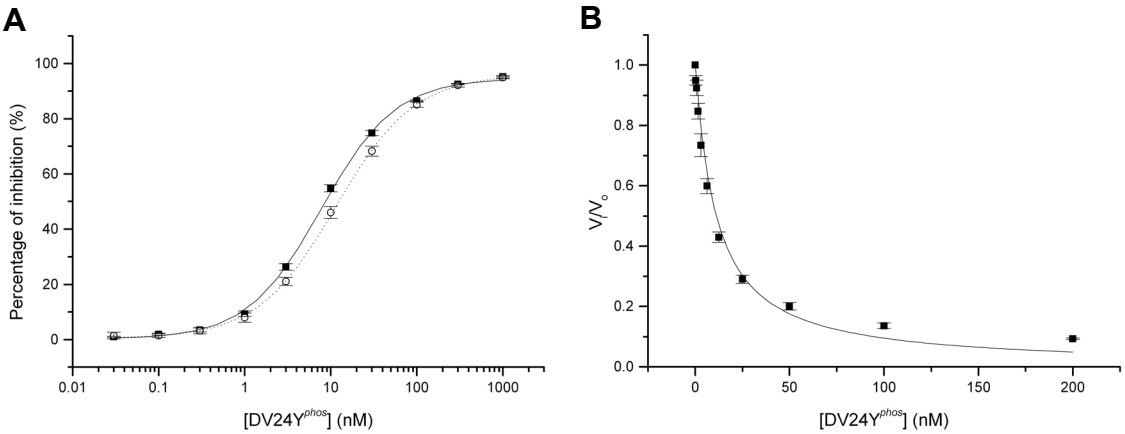

FIGURE 4.21

Variegin variant DV24Y^{phos} (fast, tight-binding, competitive inhibitor)

(A) Dose-response curves of thrombin (1.65 nM) inhibition by DV24Y^{phos} (0.03 nM, 0.1 nM, 0.3 nM, 1 nM, 3 nM, 10 nM, 30 nM, 100 nM, 300 nM and 1000 nM) in 100 μM S2238 showed a right shift with increased pre-incubation time due to cleavage. IC_{50} are 8.67 ± 0.45 nM without pre-incubation (■ solid line) and 12.4 ± 1.2 nM after 20 min pre-incubation (○ dotted line) (n = 3, error bars represent S.D.).

(B) Since DV24Y^{phos} behaved as a fast and tight-binding inhibitor, thrombin (1.65 nM) inhibition was tested with 0.39 nM, 0.78 nM, 1.56 nM, 3.13 nM, 6.25 nM, 12.5 nM, 25 nM, 50 nM, 100 nM and 200 nM of DV24Y^{phos} at 100 μM of S2238 (■ solid line). Apparent inhibitory constant K_i' obtained by fitting data to equation **(3)** is 10.4 ± 1.0 nM. The inhibitory constant K_i is calculated to be 0.327 ± 0.032 nM based on equation **(4)** (n = 3, error bars represent S.D.).

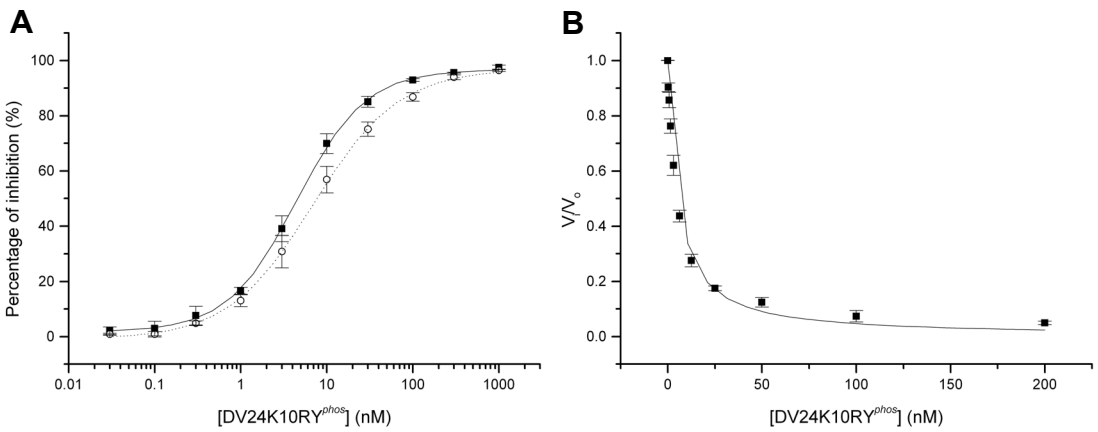

FIGURE 4.22

Variegin variant DV24K10RY^{phos} (fast, tight-binding, competitive inhibitor)

(A) Dose-response curves of thrombin (1.65 nM) inhibition by DV24Y^{phos} (0.03 nM, 0.1 nM, 0.3 nM, 1 nM, 3 nM, 10 nM, 30 nM, 100 nM, 300 nM and 1000 nM) in 100 μM S2238 showed a right shift with increased pre-incubation time due to cleavage. IC_{50} are 4.64 ± 0.78 nM without pre-incubation (■ solid line) and 7.8 ± 1.8 nM after 20 min pre-incubation (○ dotted line) (n = 3, error bars represent S.D.).

(B) Since DV24Ypho behaved as a fast and tight-binding inhibitor, thrombin (1.65 nM) inhibition was tested with 0.39 nM, 0.78 nM, 1.56 nM, 3.13 nM, 6.25 nM, 12.5 nM, 25 nM, 50 nM, 100 nM and 200 nM of DV24K10RY^{phos} at 100 μM of S2238 (■ solid line). Apparent inhibitory constant K_i' obtained by fitting data to equation **(3)** is 4.78 ± 0.57 nM. The inhibitory constant K_i is calculated to be 0.150 ± 0.018 nM based on equation **(4)** (n = 3, error bars represent S.D.).

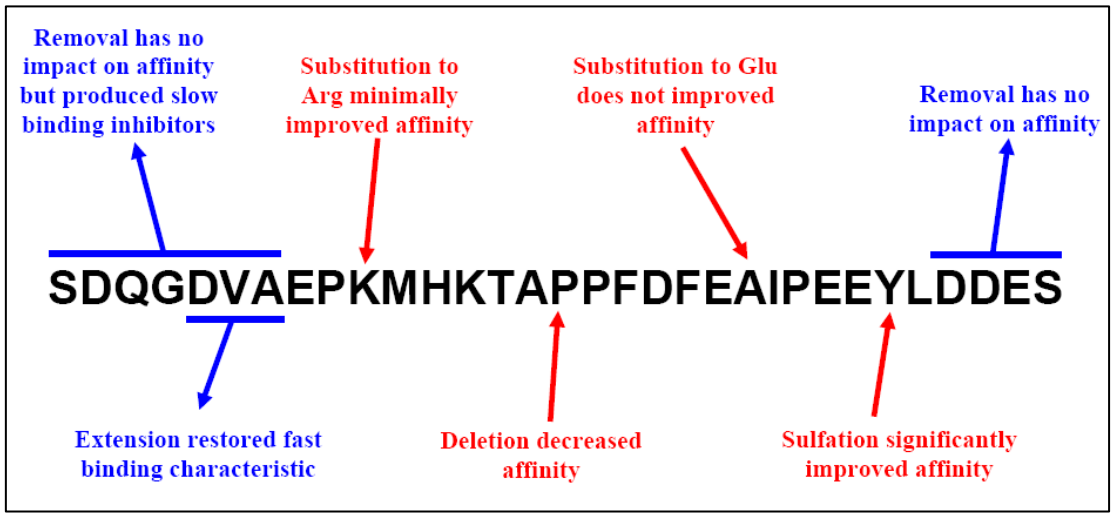

FIGURE 4.23

Effects of various designs

A summary of the effects of various designs employed. See text for details.

Phosphorylation of ^{V}Tyr27 produced results with slightly ambiguous trend. IC_{50} values for DV24Y^{phos} are 8.67 ± 0.45 nM (without pre-incubation) and 12.4 ± 1.2 nM (after 20 min pre-incubation) (Figure 4.21 A). K_i of the peptide is 0.327 ± 0.032 nM (Figure 4.21 B). Thus, when present along with Lys at P1, phosphorylation of ^{V}Tyr27 is marginally less active than DV24 (Table 4.17). However, when present along with Arg at P1, phosphorylation of ^{V}Tyr27 improved activity of peptide by around 1.5-fold. IC_{50} for DV24K10RY^{phos} are 4.64 ± 0.78 nM (without pre-incubation) and 7.8 ± 1.8 nM (after 20 min pre-incubation) (Figure 4.22 A). Inhibitory constant K_i was determined to be 0.150 ± 0.018 nM (Figure 4.22 B; Table 4.17). Therefore, despite similar properties of sulfate and phosphate moiety, sulfation of Tyr27 appeared to be more advantageous in terms of the activity of the peptides. It is very likely that the presence of sulfo-Tyr27 and the truncation of extra residues in variegin variants caused a rearrangement of C-terminal conformation to mimic hirugen/hirudin C-termini. Therefore, strong affinities are obtained in these variants through optimization of C-terminal interactions.

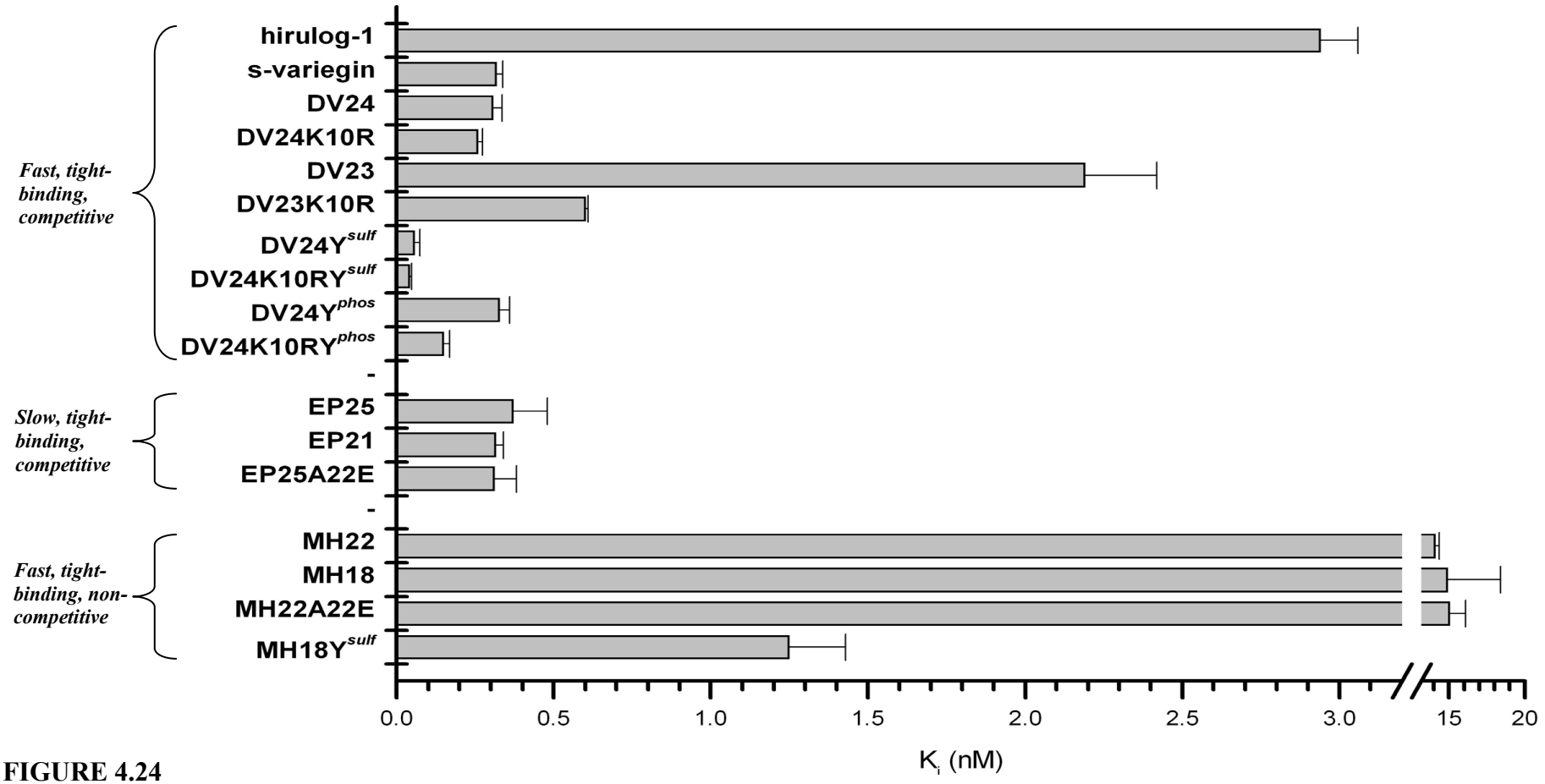

FIGURE 4.24

Inhibitory constant, Ki, of all s-variegin variants compared to hirulog-1

Variegin variants are sorted according to their mechanism of actions. All competitive inhibitors (fast or slow) have higher affinities to thrombin compared to hirulog-1. The most potent variant DV24K10RY^{sulf} is about 70-fold stronger. Even their cleavage products (non-competitive inhibitors) are potent inhibitor, with one of them, MH18Y^{sulf}, binds to thrombin approximately 2-fold tighter than hirulog-1.

4.4. DISCUSSION

Despite the use of full-length s-variegin for co-crystallization with thrombin, only the density of the C-terminal cleavage fragment was observed in our structure. The structure provided the basis to explain the classical non-competitive inhibition observed with variegin cleavage product. In thrombin-hirulog-1 complex, hirulog-1 was cleaved by thrombin and a large portion of C-terminal cleavage fragment was also missing in the structure (Skrzypczak-Jankun et al., 1991). However, unlike s-variegin, hirulog-1 N-terminal cleavage fragment ($_{D}$-FPR) was observed to occupy thrombin active site (at the non-prime subsites). As predicted and discussed in Chapter 3, affinity of s-variegin N-terminal fragment for thrombin is likely to be weaker compared to that of hirulog-1. Thus, it is not surprising that after cleavage, the N-terminal fragment dissociates from thrombin before crystallization. This may in turn explain the long period of time needed for the growth of crystals (six to eight weeks).

Considering the less than ideal interactions provided by s-variegin N-terminus, we substituted P1 Lys with Arg in some of the new variants as this substitution is reported to increase affinity for thrombin by 10-fold through better fit to S1 subsite (Bode et al., 1992; Vindigni et al., 1997). Our results showed that improvement of affinities due to this substitution are variable. The most drastic effect of this change occurred in DV23K10R, with 4-fold decrease in K_i compared to DV23. In other cases such as DV24, DV24Y^{sulf} and DV24Y^{phos}, the effects of substitution is less than 2-fold. It is likely the loose fitting of P1 Lys is compensated by the extensive interactions between s-variegin P′ residues and thrombin S′ subsite. The anchoring effect of P′

residues, along with the narrow cleft of thrombin active site, ensure strong binding of variegin despite loosely fitting P1 Lys. In contrast, DV23/DV23K10R-thrombin interactions around the prime subsites are likely to be disturbed due to deletion of Pro16 (DV23 K_i is 7-fold higher than DV24). In this situation, P1 Arg facilitated stronger binding of $^{V}(^{5}DVAEPR^{10})$ sequence to active site compared to P1 Lys, reflected by the higher gain in affinity. Similarly, less favorable P1 Lys is found in a natural substrate PAR3, which also contains a fragment similar to hirudin C-terminal (Coughlin, 2000).

Instead of directly involved in binding, the segment containing seven s-variegin N-terminal residues was previously shown to dictate s-variegin binding kinetics (Chapter 2). In its absence, EP25 binds thrombin in a less optimized conformation before slowly isomerizing into a stable complex without loss of eventual affinity. An 'electrostatic steering' role for this N-terminal segment was proposed considering the possible complementary charges with thrombin exosite-II (see Figure 2.15 in Chapter 2). Unfortunately, the N-terminal cleavage fragment is not found in the complex structure, and hence the mechanism for fast binding due to the first seven residues remains elusive. However, by extending the slow binding peptide EP21 by three residues on its N-terminus, which includes the negatively charged amino acid Asp, we are able to restore the fast binding characteristics. Thus, the prime subsites anchoring effect (discussed above) mainly drives affinity for thrombin active site, while the N-terminal steering effect is needed for proper pre-orientation of this segment. With a fitting conformation (assisted by N-terminus), s-variegin or DV24 P1 to P3 residues can be inserted rapidly into thrombin active site (assisted by prime

subsites targeting). Once in the acidic S1 pocket, P1 Lys interacts with ^{T}Asp189 with only a minimal overall loss of binding strength compared to P1 Arg.

This mode of binding which results in less stringent requirement for P1 residue in variegin might be exploited for the design of new and specific thrombin inhibitors. Considering the depth of the S1 pocket, residues with long aliphatic side chain such as Leu or Met might replace Lys in variegin variants. Loss of affinity accompanying such substitution might be largely compensated by the prime subsites anchoring and N-terminal steering effects of variegin. Allowance for non-basic P1 residues – Leu in heparin cofactor-II (Baglin et al., 2002), $_{D}$-Tyr (Riester et al., 2005) and Trp (Malikayil et al., 1997) – are possible in cases where interactions at other positions/exosites are optimized. Most of the other blood coagulation serine proteinases (and trypsin) have specificity for basic P1 residue, thus replacement with a neutral side chain could further improve the selectivity of the inhibitor for thrombin. As variegin already has high selectivity for thrombin (more than four orders of magnitude, see Chapter 2), the possibilities of further P1 substitutions were not explored within the scope of this thesis.

Only one ion pair (^{V}Glu27-^{T}Arg75) can be observed in the complex despite the apparent complementary charges between exosite-I and s-variegin C-terminus. In hirudin, electrostatic interactions are important for initial association with thrombin providing both steering (by complementary in electrostatic fields) and tethering (by specific ion pairing) effects (Myles et al., 2001). The ionic tethering is the rate-limiting step (Jackman et al., 1992) and explained the observation that hirudin binds thrombin slowly in solutions with high ionic strength (> 0.2) (Stone and Hofsteenge,

1986). As discussed in Chapter 2, ionic tethering in s-variegin is not the rate-limiting step in its association with thrombin (see Figure 2.15 in Chapter 2). The presence of only one ion pair, thus minimal effect of ionic tethering, in the structure supports this hypothesis. In contrast, extensive non-polar interactions are observed. Similarly, only one ion pair is present in thrombin-hirulogs/hirugen structures (Skrzypczak-Jankun et al., 1991; Qiu et al., 1992). Thus, the role of ion pairings in thrombin exosite-I interactions appeared to be over-emphasized previously (evident from the common use of the name 'anion-binding exosite-I'). This echoes the sentiment of J. A. Huntington that "it is more accurate to call exosite-I the apolar-binding exosite, and exosite-II the anion-binding exosite" (Huntington, 2005).

Compared to the non-prime subsites, understanding of thrombin prime subsites (especially S2′ and beyond) binding preferences is much less complete. Nonetheless, S′ subsites interactions are important for binding (Laskowski, Jr. and Kato, 1980). Pertinent to thrombin, inclusion of P3′ and P4′ residues improved binding affinity of fibrinopeptide A by ~ 10-fold (Marsh, Jr. et al., 1983). Systematic probing of thrombin S′ subsites with 'methyl scan' also produced inhibitors with strong binding affinities demonstrating the potential for targeting thrombin prime subsites in the design of potent inhibitors (Slon-Usakiewicz et al., 1997). In hirulog-1, the glycyl linkers connect the active site and exosite-I binding moieties without displaying specific interactions with thrombin prime subsites. As a result, this segment in is disordered its crystal structure (Skrzypczak-Jankun et al., 1991) and the activity is rapidly lost after cleavage by thrombin [(Witting et al., 1992) and Chapter 3]. When anchored by a non-hydrolyzable active site binding moiety and an exosite-I binding segment, the non-specific linker was forced to fit into the canyon-like cleft in

prime subsites as seen in hirulog-3 (Qiu et al., 1992) and P498 (Fethiere et al., 1996). In these cases, S′ subsite interactions are sub-optimal and lack specific side chain interactions. As a result, extensive and lengthy optimizations through synthetic chemistry using multiple unnatural amino acids were necessary to produce potent prime subsites-binding inhibitors (Matthews et al., 1996; Slon-Usakiewicz et al., 1997; Slon-Usakiewicz et al., 2000). In contrast, tight-fitting to prime subsites in s-variegin is achieved through specific interactions involving side chains of natural amino acids. Information obtained from this structure can help in our understanding of thrombin prime subsites interactions for future drug design. Significantly, Thr14 in native variegin is modified by a hexose. However, the pocket that holds unmodified Thr14 side chain is too small to accommodate the hexose moiety. Thus, binding of glyco-Thr in native variegin might involve rearrangement of thrombin or the inhibitor around this region. Such changes are likely in view of the proximity of the flexible autolysis loop to Thr14. The autolysis loop plays important roles in interactions of FXa (Manithody et al., 2002), FIXa (Yang et al., 2003) and APC (Yang et al., 2005) with their substrates and inhibitors. Extensive interactions of rhodniin and ornithodorin with thrombin autolysis loop were also reported (van de et al., 1995; van de et al., 1996).

This is the first time structural information about thrombin prime subsites was obtained from a natural thrombin inhibitor that is firmly inserted into the thrombin canyon-like cleft extending from active site to exosite-I. None of the naturally occurring thrombin inhibitors that have been crystallized previously binds thrombin in the same way. Among all, hirudin is most similar to s-variegin and the two overlaid well in a short segment where they shared almost identical sequences DFEA(E)I.

However, compared to s-variegin P2′ to P4′ which bind close to the thrombin, corresponding residues (Gln49, Ser50 and His51) in hirudin [PDB entry 1HRT (Vitali et al., 1992) was used for comparison] pointing away from thrombin prime subsites. Distances measured based on Cα atom showed these residues are at an average of 5.79 Å 'above' s-variegin, with respect to thrombin. In the thrombin-sulfo-hirudin complex structure densities for these residues were not traced suggesting minimal contacts with thrombin prime subsites (Liu et al., 2007). Other inhibitors including rhodniin (van de et al., 1995), ornithodorin (van de et al., 1996) and boophilin (Macedo-Ribeiro et al., 2008) do not get inserted into the canyon-like cleft. The presence of relatively bulky Kunitz or Kazal domains in both ends of these molecules precluded close fitting of their linker peptides into the bottom of the cleft. The firm insertion of (variegin) peptides in extended conformation into the cleft is probably the minimum structure needed to achieve maximum and simultaneous binding to thrombin catalytic pocket, prime subsites and exosite-I. This 'minimalist' approach in nature (ticks) confers an advantage of minimum energy expenditure (protein synthesis) for maximum outcome (potent inhibition of coagulation enzymes for blood meals).

4.5. SUMMARY

The 2.4 Å resolution thrombin-s-variegin complex structure was solved. Despite our efforts to crystallize full-length s-variegin, only density for C-terminal segment of s-variegin was traced. Structural basis of non-competitive inhibition of thrombin by s-variegin cleavage product was revealed. Thirteen new variegin variants were designed and synthesized based on the structure as well as other prior knowledge. These variants that have been designed and characterized cover a diverse spectrum of potency, kinetic and mechanism of inhibition, including peptides with affinities ranging from nanomolar to picomolar values, with fast and slow tight-binding, displaying competitive and non-competitive inhibition (Figure 4.24), laying a solid foundation for further development of variegin as a therapeutic agent.

Chapter Five

In vivo antithrombotic effects of variegin variants and their neutralizations *in vitro*

5.1 INTRODUCTION

Variegin potently inhibited thrombin, targeting the catalytic pocket, prime subsites and exosite-I. Depending on the length of N-terminus, variegin variants could either be fast or slow binding. After being hydrolyzed, its cleavage product non-competitively inhibited thrombin active site, resulting in prolonged inhibition of the enzyme. *In vitro* this novel class of inhibitors appeared to be more superior to hirulog-1/bivalirudin, the commercially available peptide-based inhibitor of thrombin. However, as is with all other molecules, reproducing the *in vitro* activities *in vivo* remained one of the biggest hurdles that many fell at. In the development of anticoagulants one has to control the delicate balance between thrombosis and hemostasis and demonstrate the *in vivo* efficacy even at early stages of lead optimization. This is mainly due to the subtle and complex environment where anticoagulant exerts its action: locally high concentrations of coagulation proteinases and cofactors, in the presence of blood cells and vascular wall components, under constant but most of the time abnormal (turbulence and stasis) blood flow, and possibly local hypoxia and acidosis (Levi et al., 2001). Establishment of *in vitro-in vivo* correlations can help in guiding the lead optimization process towards the best drug candidate. Since anticoagulants are useful in the treatment of venous thrombosis (Eikelboom and Hirsh, 2007), we looked to test the variegin peptides in animal models of venous thrombosis.

The use of animal models of venous thrombosis has a history of more than 60 years. These models were used either for investigation of *in vivo* thrombus formation or for evaluation of pharmacological interventions. At least 18 different species are

used, but the most common ones are dogs, rats and rabbits. Techniques used, although highly variable, shared the common principle of inducing either vascular injury, blood stasis or local activation of coagulation and measure the thrombus formation, growth or lysis (Levi et al., 2001). Selection of models depends on the objective of the studies and typically many different models were used for pre-clinical development of anticoagulants to investigate different pharmacodynamics and pharmacokinetics of those molecules (Maraganore, 1993; Markwardt, 1994).

While it is of our interest to evaluate variegin and its variants in venous thrombosis models, our laboratory lacks the experience and technical ability to conduct such studies independently. Therefore, we worked in collaboration with Prof. Pudur Jagadeeswaran from University of North Texas to determine the efficacy of the peptides in zebrafish model. There is a wide collection of information available demonstrating that human and zebrafish have similar hemostatic pathways (Jagadeeswaran et al., 2005; Jagadeeswaran, 2005). Zebrafish plasma was found to be responsive to activators for intrinsic and extrinsic pathways [e.g. ellagic acid, thromboplastin and Russell's viper venom factor X (RVV-X) activator]. The presence of AT-III, HC-II, protein C and vitamin-K-dependent γ-carboxylation proteinases homologues in zebrafish were also demonstrated by the abilities of heparin (antithrombin-dependent thrombin/FXa inhibitor), Protac (protein C activator) and warfarin (vitamin-K antagonist) to inhibit activities of the relevant coagulation factors (Jagadeeswaran and Sheehan, 1999). Full or partial cDNAs of several important coagulation factors were also cloned, further suggested similarities in hemostasis system between zebrafish and mammals. cDNAs or genes of coagulation factors identified include prothrombin (Jagadeeswaran et al., 2000), FVII (Sheehan et al.,

2001), FV, FIX, FX, AT, TFPI, HC-II and plaminogen precursor (Hanumanthaiah et al., 2002). The nucleated equivalents of platelet, thrombocyte, was also found (Jagadeeswaran et al., 1999). Therefore, the large extent of conservation of hemostasis system between zebrafish and mammals makes it a relevant model to study thrombosis and hemostasis *in vivo*.

Dr. Jagadeeswaran and his laboratory have devised a novel method to screen for antithrombotic compounds using venous thrombosis model in zebrafish larvae (Jagadeeswaran, 2008). Zebrafish larva is transparent and has easily visualized, well-defined blood vessels. Established techniques are available for introducing peptides into the blood stream of the larvae as well as accurately inducing uniform vascular wound by laser ablation. Zebrafish thrombocytes (equivalent to platelets in mammals) and other blood cells are large enough for visualization of thrombus formation *in vivo* under the microscope without additional labeling procedures. The time taken for thrombus formation and hence vascular occlusion after laser-induced injuries can be measured to ascertain *in vivo* activities of peptides. Breeding and maintenance of zebrafish is easier than other animals and with possibly up to 17 peptides to be evaluated, zebrafish models will provide faster turnover rate and minimizing unnecessary use of higher animals.

One of the inherent major side effects of anticoagulants is increase risk of bleeding. Therefore, it is desirable for availability of appropriate ways to neutralize bleeding complications in the event such as overdosage (Schulman and Bijsterveld, 2007). We looked into the possibility of identifying an antidote for the variegin

peptides. We tested and demonstrated the ability of protamine sulfate, a clinically available antidote for heparin, to reverse activities of s-variegin and two of its variants.

This chapter deals with two clinically important considerations for the development an anticoagulant: *in vivo* efficacy and availability of antidote. Variegin and its variants compared favorably against hirulog-1/bivalirudin in both aspects, thus demonstrated the viability of developing variegin (and variants) as novel anticoagulants.

5.2. MATERIALS AND METHODS

5.2.1. Materials

Adult zebrafish and zebrafish larvae were maintained in Department of Biological Sciences, University of North Texas, Denton, Texas, USA. All other materials used were as described in Chapter 2. For details please refer to *'Section 2.2.1. Materials'*.

5.2.2. Synthesis, purification and mass spectrometry of peptides

Synthesis, purification and mass spectrometry analysis of all peptide followed the procedures described in Chapter 2 and Chapter 4 (for sulfotyrosine containing peptide). For details please refer to *'Section 2.2.3.1. Peptide synthesis'* in Chapter 2 and *'Section 4.2.2. Synthesis, purification and mass spectrometry of peptides'* in Chapter 4.

5.2.3. Breeding of zebrafish

The zebrafish breeding tank was assembled with two 1 L tanks. The bottom of one tank was cut off and placed onto a sterilized mesh. This tank was subsequently inserted into a second tank with intact bottom. A pair of zebrafish was then placed into the breeding tank at the end of a light cycle. The mesh served to isolate the pair of zebrafish in the top tank. Within the first 2 h of the next light cycle, the fish begin to spawn and eggs collect at the bottom of the breeding tank under the protection of the mesh. After removal of fish, water in the breeding tank was filtered through a brine shrimp net which retains the eggs. The net was immediately inverted over a Petri dish containing E3 media (5 mM NaCl, 0.17 mM KCl, 0.33 mM $CaCl_2$, 0.33

mM $MgSO_4$ and 10^{-5}% methylene blue), releasing the eggs and other contaminating materials such as feces. The eggs were subsequently transferred into fresh E3 media with a plastic Pasteur pipette. This cleaning step was repeated twice before the eggs were transferred into a new tank and maintained at 28.5 °C for hatching.

5.2.4. Microinjection

Larvae at 4 days-post-fertilization (dpf) were used to determine *in vivo* activities of peptides in venous thrombosis model. Intravenous microinjections of peptides were performed using Nanoject II (Drummond, Broomall, Pennsylvania, USA) with glass injection needles (3.5-in. capillaries) pulled on a vertical pipette puller (Knopf, Tujunga, California). The tips of the pulled needles were clipped using small scissors and filled with 500 μM of peptides dissolved in phosphate buffered solution (PBS). Ten nanolitres of peptides or PBS were injected into the larvae circulation through the posterior (caudal) cardinal vein. The site for microinjection of peptides is indicated in Figure 5.1 [adapted from (Isogai et al., 2001)], which showed an angiogram of a zebrafish larva at approximately 4.5 dpf.

5.2.5. Mounting of zebrafish larvae in agarose

Each larvae injected with peptides were placed in 0.5 ml of distilled water added with 6 μl of 10 mM Tricaine solution for anesthetization. To this water containing larvae equal volume of 1% low-melt agarose solution (maintained at 35 °C in a water bath) was added. The mixture (with anesthetized larvae) was poured onto a glass microscopic slide within a rectangular rubber gasket to mount the larvae flat on their side in agarose.

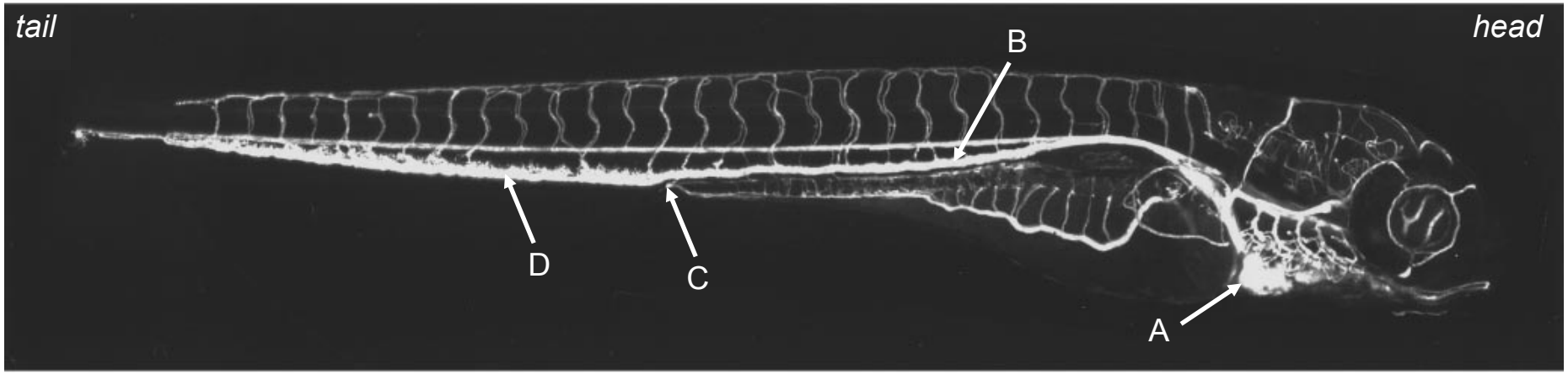

FIGURE 5.1 [adapted from 'The Vascular Anatomy of the Developing Zebrafish: An Atlas of Embryonic and Early Larval Development' (Isogai et al., 2001)]

Angiogram of a zebrafish larva at approximately 4.5 dpf showing its circulation system in lateral view

(A) The heart of the larva

(B) The posterior (caudal) cardinal vein, this is the site where 10 nl of peptide solution were injected

(C) The anal pore

(D) The caudal vein, this is the site for laser ablation which is approximately five somites towards the tail end from anal pore

5.2.6. Laser ablation

Laser ablation of larvae veins were performed with pulsed nitrogen laser light pumped through coumarin 440 dye (445 nm) (MicroPoint Laser system, Photonic Instrument, St Charles, Illinois, USA) at 10 pulses/second with laser intensity setting at 10. Accuracy of the laser was tested before ablations. Laser ablation of each larva was carried out 20 min after microinjection of the peptide. Glass slides were placed under Optipnot phase-contrast fluorescence microscope (Nikon, Melville, New York, USA). The larvae were viewed with 20X lens (10X eyepiece) to locate the site for laser ablations, which was five somites towards the caudal end from the anal pore (Figure 5.1 & 5.2). Laser beam aimed at the caudal vein within the ablation site was triggered for 3 s. The process was recorded using a digital camera attached to a video home system (VHS) recorder and a monitor. Thrombus formation following vein injury due to laser ablation was monitored and the time taken for complete occlusion of injured vein was recorded. Three short video recording the thrombus formation (or lack of) in larvae injected with PBS, MH22 and DV24K10RY^{sulf} were attached in this thesis, see Appendix C for details.

5.2.7. Neutralization of thrombin inhibitory activity of peptides

The ability of protamine sulfate to reverse inhibition of thrombin amidolytic activity by peptides was assayed using the chromogenic substrate S2238. All assays were performed in 96-well microtiter plates in 50 mM Tris buffer (pH 7.4) containing 100 mM NaCl and 1 mg/ml BSA at room temperature. Typically, 100 µl of peptide and 100 µl of protamine sulfate were pre-incubated for 10 min before the addition of 50 µl of human plasma derived thrombin. 50 µl of S2238 were added to initiate the reaction. Details of each experiment are described along with the graphs representing

the results obtained. The rates of formation of colored product *p*NA were followed at 405 nm for 10 min with SPECTRAMax Plus microplate spectrophotometer (Molecular Devices, Sunnyvale, California, USA). Percentages of inhibition in the presence and absence of protamine sulfate were compared for calculation of percentages of reversal.

5.3. RESULTS

5.3.1. *In vivo* antithrombotic effects of the peptides

Five inhibitors were selected as representative peptides to test for their antithrombotic effects *in vivo* using venous thrombosis model of zebrafish larvae. They are: (1) s-Variegin, the full-length sequence of native variegin – a fast, tight-binding competitive inhibitor (K_i = 0.318 ± 0.020 nM); (2) EP25, without seven N-terminal residues, has similar affinity to thrombin (K_i = 0.370 ± 0.11 nM), but it is a slow binding inhibitor; (3) MH22, the cleavage product that is a fast and tight-binding, non-competitive inhibitor (K_i = 14.11 ± 0.29 nM); (4) DV24K10RY^{sulf}, the peptide with the most potent *in vitro* activity (K_i = 0.0420 ± 0.0061 nM); and (5) hirulog-1, fast, tight-binding, competitive inhibitor currently in the market (K_i = 2.94 ± 0.12 nM). Hirulog-1 was used as positive control of the experiments.

All five peptides were injected into the zebrafish larvae circulation through the posterior (caudal) cardinal vein at a single dose (500 μM, 10 nl). Antithrombotic effects of the peptides are measured by the abilities of all peptides to delay time-to-occlusion (TTO) of caudal vein after laser ablation. After laser ablation, control TTO of a wild-type 4 dpf larva is about 21 s (Jagadeeswaran et al., 2006). Typically, if thrombus formation is inhibited (due to either an antithrombotic agent or genetic defect), TTO can be delayed up to 150 s, beyond which complete occlusion will not occur (Seongcheol Kim, personal communication). Therefore, the dose for injection (500 μM, 10 nl) was carefully selected based on a few preliminary experiments such that a definite TTO can be obtained for most, if not all, of the peptides.

Zebrafish larvae injected with the same volume of PBS have a TTO (mean ± S.D.) of 19.0 ± 3.2 s (Figure 5.3 & 5.4; Appendix C). s-Variegin (K_i = 0.318 ± 0.020 nM) is strongly antithrombotic, with TTO of 120.8 ± 7.4 s. In contrast, EP25, despite having similar K_i as s-variegin, does not show any activity. With a TTO of 22.5 ± 6.2 s, EP25 did not show any significant antithrombotic effect compared with same batch of larvae injected with PBS. MH22 (K_i = 14.11 ± 0.29 nM) showed good activity with TTO of 33.3 ± 2.9 s (Figure 5.5; Appendix C). DV24K10RY^{sulf} (K_i = 0.0420 ± 0.0061 nM) is the most potent inhibitor and it completely inhibited of thrombus formation (Appendix C). Hirulog-1/bivalirudin (K_i = 2.94 ± 0.12 nM), as reference drug, prolonged the TTO to 45.0 ± 5.5 s. Overall, other than EP25, the antithrombotic effects of the peptides correlated well with their affinities for thrombin. Thus, slow binding inhibition mode (EP25) is not desirable for *in vivo* efficacy while both fast, competitive (s-variegin, DV24K10RY^{sulf} and hirulog-1) and fast, non-competitive (MH22) inhibition are effective (Figure 5.3). Our results are consistent with similar observations reported earlier about the importance of rapid thrombin inhibition for efficacious antithrombotic agents (Stone and Tapparelli, 1995).

5.3.2. Neutralization of thrombin inhibitory activity of the peptides

The ability of protamine sulfate to reverse inhibition of thrombin amidolytic activity by the peptides was assayed using the chromogenic substrate S2238. Protamine is a mixture of highly cationic peptides originally extracted from fish sperm nuclei. Protamine sulfate is clinically used for the reversal of anticoagulant effect of heparin by binding to the anionic heparin molecules (Schulman and Bijsterveld, 2007). Variegin has several acidic residues at its C-terminus which could

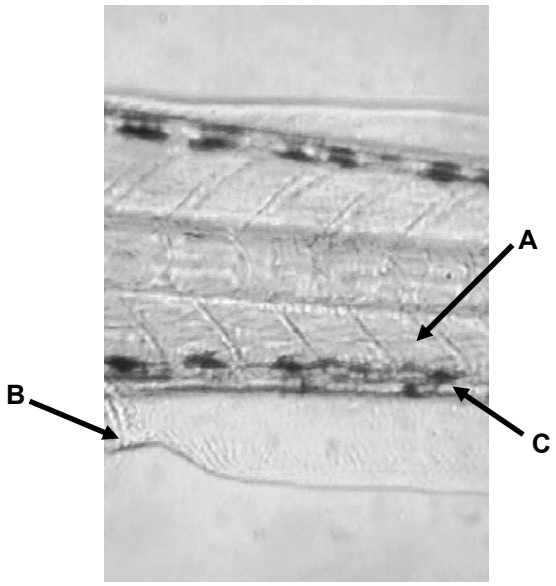

FIGURE 5.2

The site for laser ablation

Zebrafish 4 dpf larva was viewed with 20X lens (10X eyepiece) to locate the site for laser ablation, which was five somites (marked 'A') towards the caudal end from the anal pore (marked 'B'). Laser beam aimed at caudal vein (marked 'C') within the ablation site was triggered for 3 s. Thrombus formation following vein injury due to laser ablation was monitored and the time taken for complete occlusion of injured vein was recorded.

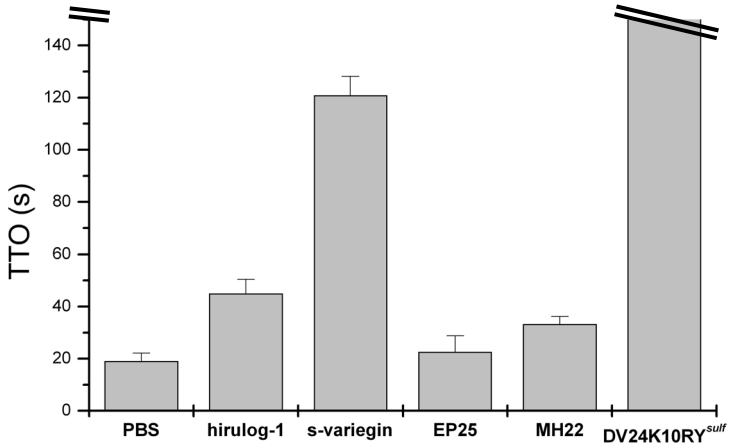

FIGURE 5.3

TTO for zebrafish larvae injected with different peptides

Zebrafish 4 dpf larvae were injected with 10 nl of different peptides at 500 μM or 10 nl of PBS as control. The larvae caudal vein was injured by laser ablation 20 min after injection of the peptides or PBS. TTO after laser ablation were recorded up to 150 s for comparison of antithrombotic effects of different peptides. TTO of PBS, hirulog-1, s-variegin, EP25 and MH22 are 19.0 ± 3.2 s, 45.0 ± 5.5 s, 120.8 ± 7.4 s, 22.5 ± 6.2 s and 33.3 ± 2.9 s, respectively. Within 150 s, no thrombus was formed in larvae injected with DV24K10RY^{sulf}. With the exception of the slow binding inhibitor EP25, the abilities of the peptides to prolong TTO generally correlate with their K_i (n = 4, error bars represent S.D.).

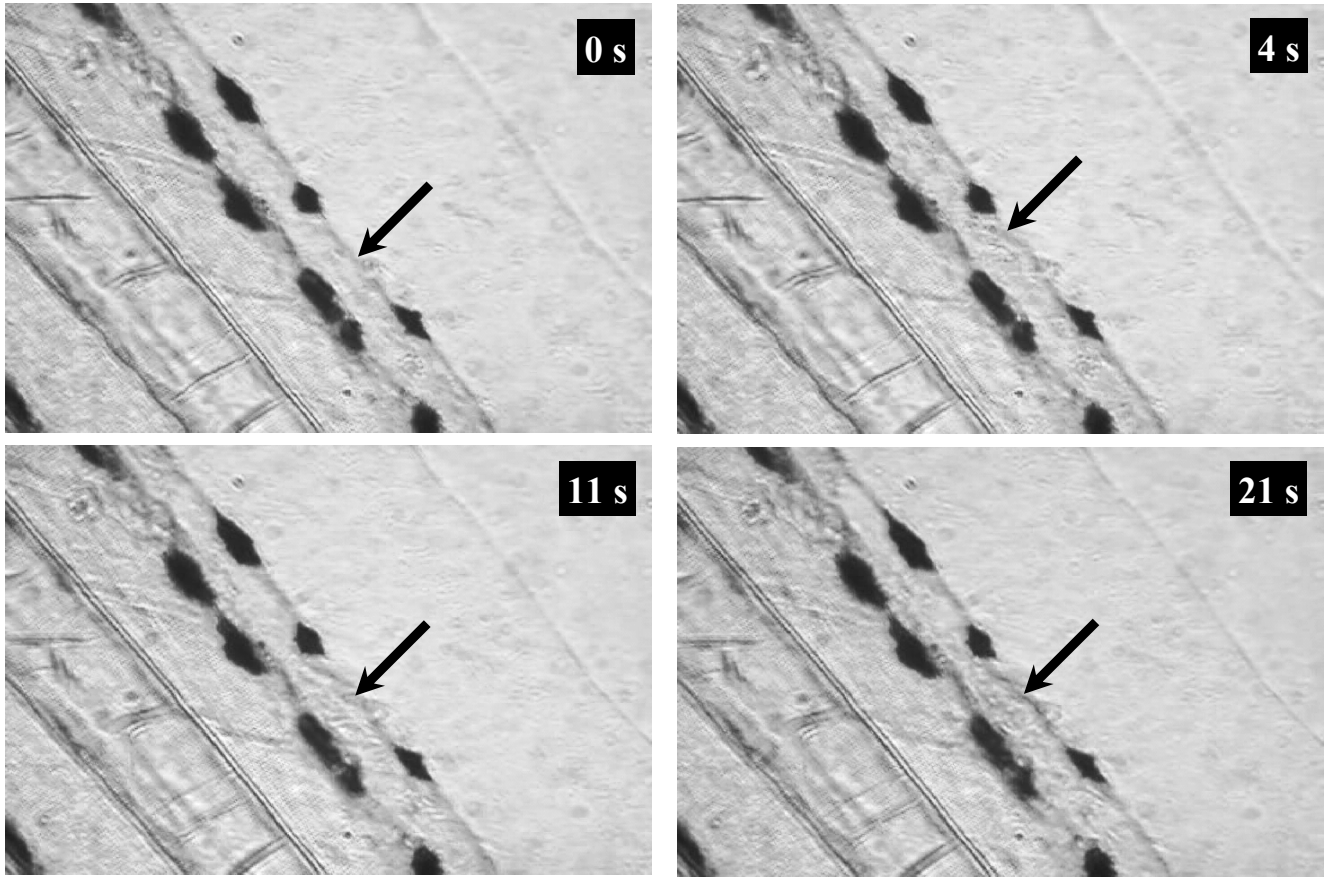

FIGURE 5.4

Thrombus formation in zebrafish larva after laser injury: PBS

Pictures captured from video recording thrombus formation in zebrafish larva after laser injury. The larva was injected with PBS 20 min before laser ablation. At 0 s, laser beam was fired inducing an injury at caudal vein (arrow). After 4 s, blood cells began to adhere at the site of injury. Thrombus grew to a visible size by 11 s. After 21 s, the large thrombus formed totally occluded the flow of blood through the injured vein and this time (TTO) was recorded. See Appendix C for video.

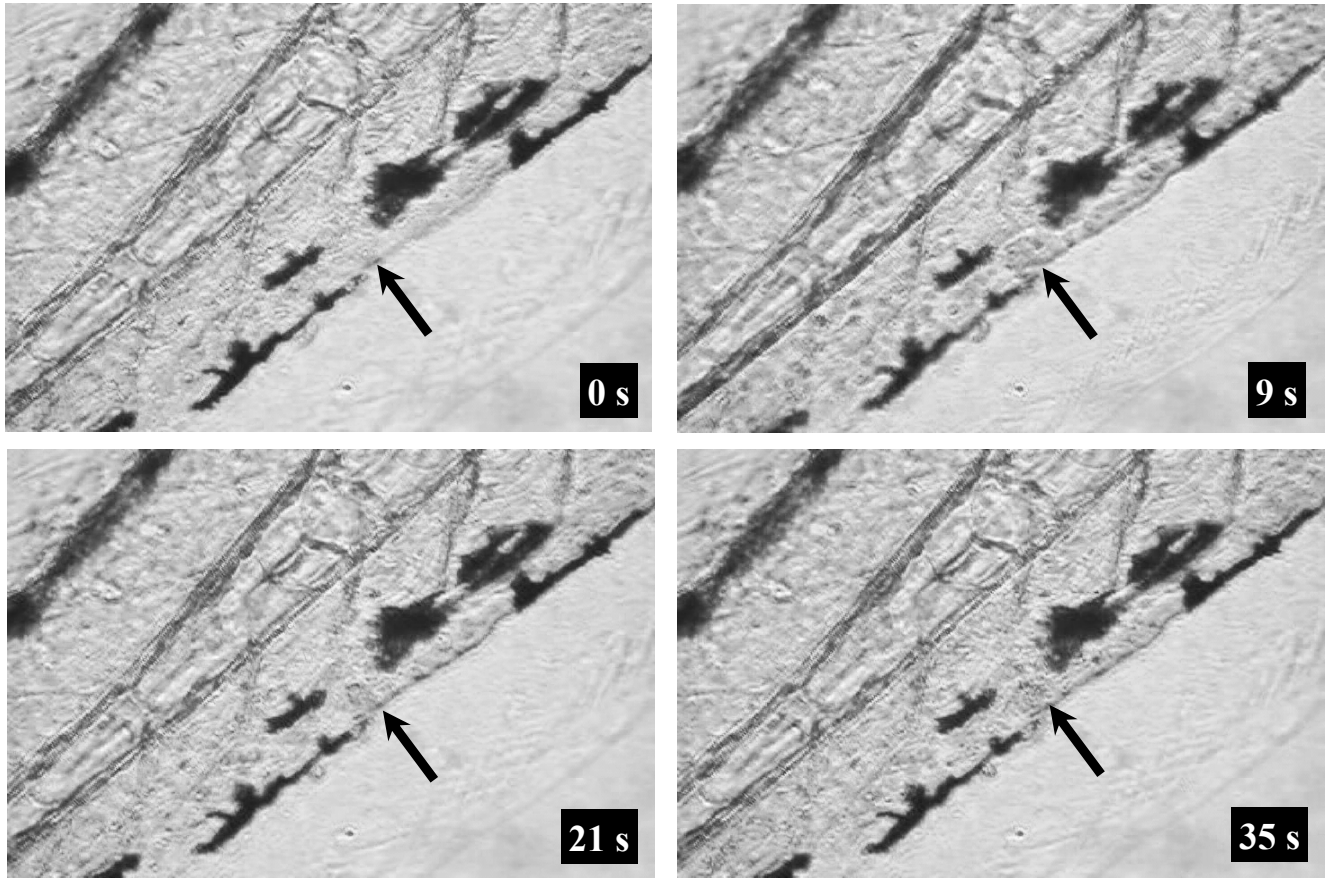

FIGURE 5.5

Thrombus formation in zebrafish larva after laser injury: MH22

Pictures captured from video recording thrombus formation in zebrafish larva after laser injury. The larva was injected with MH22 20 min before laser ablation. At 0 s, laser beam was fired inducing an injury at caudal vein (arrow). Compared to larva injected with PBS, blood cells adherence was delayed to 9 s. Thrombus grew to a visible size by 21 s (cf 11 s in control). TTO was prolonged to 35 s, demonstrating the *in vivo* antithrombotic effect of the peptide. See Appendix C for video.

be the target for protamine sulfate. This option was first explored since there are ample clinical experiences for protamine sulfate administration.

Fixed concentrations of s-variegin, DV24K10RY^{sulf} and MH22 (at their respective IC_{50} and IC_{90}) were incubated with various concentrations of protamine sulfate before assaying their residual thrombin inhibitory activities. Protamine sulfate reversed the effects of all three peptides dose-dependently (Figure 5.6). Activities of s-variegin and MH22 were reversed to similar extent. At IC_{50} of s-variegin (8.25 nM) and MH22 (11.5 nM), approximately 50% of reversal were achieved with 0.1 mg/ml of protamine sulfate. Percentage of reversal saturated at around 75% despite high concentrations of protamine sulfate. In contrast, for DV24K10RY^{sulf} at its IC_{50} concentration (1.4 nM), 1 mg/ml of protamine sulfate was needed for ~ 50% of reversal. As expected, concentrations of protamine sulfate needed to neutralize effects of peptides at their IC_{90}s were higher than at IC_{50}s (Figure 5.6). Therefore, protamine sulfate can neutralize most of the effect of variegin peptides. s-Variegin and MH22 has identical C-termini (represented by MH22 sequence) but DV24K10RY^{sulf} C-terminus (represented by MH18Y^{sulf} sequence) is sulfated and has stronger affinity for thrombin. S-variegin and MH22 were neutralized to the similar extent. Higher concentrations of protamine sulfate are needed for DV24K10RY^{sulf} reversal. Therefore, the binding between protamine sulfate and the peptides are likely to be mediated through the acidic C-termini of variegin peptides.

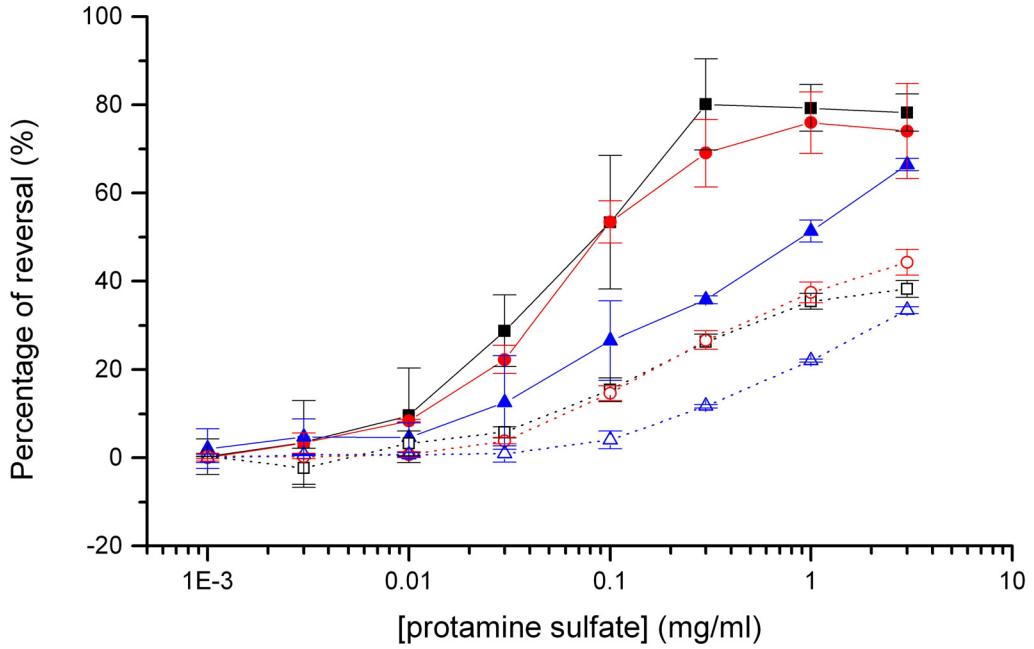

FIGURE 5.6

Thrombin inhibitory effects of the peptides are reversed by protamine sulfate

The ability of protamine sulfate to reverse inhibition of thrombin amidolytic activity by the peptides was assayed using the chromogenic substrate S2238. Protamine sulfate (3 mg/ml, 1 mg/ml, 0.3 mg/ml, 0.1 mg/ml, 0.03 mg/ml, 0.01 mg/ml, 0.003 mg/ml and 0.001 mg/ml) were incubated with peptides at their IC_{50} concentrations (solid lines) – 8.25 nM s-variegin (■), 11.5 nM MH22 (●) and 1.4 nM DV24K10RY^{sulf} (▲) – for 10 min before addition of thrombin (1.65 nM). Amidolytic activity of thrombin was assayed with 100 μM S2238. Percentages of inhibition in the presence and absence of protamine sulfate were compared for calculation of percentages of reversal. s-Variegin and MH22 can be reversed to similar extent but higher concentrations of protamine sulfate are needed for effective reversal of DV24K10RY^{sulf}.

Similar experiments were conducted with the peptides at their IC_{90} concentrations (dotted lines): 167 nM for s-variegin (□), 224 nM for MH22 (○) and 13.6 nM for DV24K10RY^{sulf} (△). Higher concentrations of protamine sulfate are needed for reversal of all three peptides. s-Variegin and MH22 are again neutralized to the same extent, while it is more difficult to neutralize DV24K10RY^{sulf}. Therefore, the peptides acidic C-terminal residues are most likely responsible for protamine sulfate binding.

5.4. DISCUSSION

Clinical experiences showed that prevention of thrombus formation (anticoagulation) are effective for initial and long-term management of both arterial [acute conorary syndrome (ACS) and stroke] and venous [venous thromboembolism (VTE)] thrombosis (Marder et al., 2004; Eikelboom and Hirsh, 2007). Similar to other direct thrombin inhibitors (DTI), variegin will have several advantages over conventional anticoagulants such as heparin and warfarin. For example, variegin efficacy will not be dependent on other endogenous proteins (e.g. AT-III), has no significant binding to other plasma proteins (specific for thrombin), not inhibited by platelet factor 4 (unlike heparin), does not cause HIT (again unlike heparin), able to inhibit both free and clot-bound thrombin (being small enough to diffuse into fibrin clot), has rapid onset of action (especially if parenterally administrated) and with lesser drug-drug and drug-food interactions (unlike warfarin) (Bauer, 2002; Gurm and Bhatt, 2005; White, 2005). Clinically, some of the possible indications for variegin, inferred from other DTIs, include: (1) as heparin replacement in HIT; (2) for venous thrombosis prophylaxis after major orthopedic surgery; (3) for prevention of arterial thrombosis and reocclusions during/after invasive cardiology particularly PCI; and (4) for management of acute coronary syndrome (ACS) and myocardiac infartion (MI) (Bates and Weitz, 2006; Warkentin et al., 2008). In the event where variegin is formulated to become orally available or being used as template to produce peptidomimetics for oral administration, the possible indications would include long-term management of venous thromboembolism (VTE) (Gustafsson et al., 2004).

Clinically, efficacies, indications and side effects of DTIs (hirudin, bivalirudin, argatroban and dabigatran) differ due to inherent differences in their pharmacodynamics and pharmacokinetics. Therefore, it is important that potential clinical benefits of variegin (or its variants) to be considered in the light of its similarities and differences with other DTIs. Variegin and some of its variants inhibited thrombin potently with low K_i (between ~ 0.04 to 0.3 nM). Their affinities for thrombin is stronger than bivalirudin (K_i = 2.3 nM) (Maraganore et al., 1990), argatroban (K_i = 3.2 nM) (Fareed and Jeske, 2004) and dabigatran (K_i = 4.5 nM) (Wienen et al., 2007) but weaker than hirudin (K_i = 0.2 pM) (Stone and Hofsteenge, 1986). Our venous thrombosis experiments in zebrafish larvae showed that *in vivo* antithrombotic effects of peptides are correlated with their *in vitro* affinities for thrombin. Thus, lower K_i of variegin (compared to bivalirudin, argatroban and dabigatran) will translate to low therapeutic dosage needed for the inhibitor, which should help in reducing possible side effects. However, extremely strong affinity for thrombin might not be desirable. The almost irreversible binding of hirudin to thrombin (K_i = 0.2 pM) was suggested to be responsible for the higher risk of major bleeding compared to unfractionated heparin (UFH) (White, 2005). Thus, in terms of affinity to thrombin, it appears that variegin represent a good balance between potency and safety. In addition, immunogenicity is a problem that has been widely reported for hirudin but not for bivalirudin (Alban, 2008). The smaller size of bivalirudin is likely to be the reason for the lower incidences of immunogenicity (Warkentin et al., 2008). Being about the same size as bivalirudin, immunogenicity might also not be a problem for variegin, giving variegin an edge over hirudin.

Other than argatroban, other DTIs are mainly excreted through kidney. Thus, dosage monitoring and adjustment are necessary in patients with renal impairments (Di Nisio et al., 2005). However, bivalirudin excretion is less dependent on renal clearance than hirudin. This is due to enzymatic proteolysis of the peptide in the body (by thrombin and lysosomes in the distal tubule) before excretion (Gladwell, 2002). Thus, bivalirudin is a safer option than hirudin in patients with impaired renal function (Warkentin et al., 2008). Variegin is similar to bivalirudin in size, composition and, to an extent, hydrolysis by thrombin. The metabolism and excretion profile of both might be similar, which confers another advantage to variegin over hirudin. Bivalirudin half-life is extremely short (~ 25 min) (Alban, 2008). Parallel to our work on variegin, our collaborator Dr Patricia Nuttall from Centre for Ecology and Hydrology, NERC, UK, has performed quantitative whole body autoradiography studies in rats injected with [^{3}H]s-Variegin. Preliminary data indicated rapid elimination of the peptide through renal route similar to bivalirudin, with a half-life of ~ 1 h (Patricia A. Nuttall, personal communication).

We showed that C-terminal cleavage fragment of variegin retained strong binding to thrombin resulting in prolonged inhibitory activity (Chapter 3). This fragment (MH22) showed *in vivo* activity in our experiment. Its ability to prolong TTO is about 1.3-fold lower than hirulog-1/bivalirudin, despite having a lower affinity for thrombin and acts non-competitively. Therefore, our data showed that effective prevention of thrombus formation can be achieved by both competitive and non-competitive inhibitors of thrombin active site function. In addition to rendering thrombin catalytic residue Ser195 non-functional (Chapter 4), binding of MH22 to thrombin also makes exosite-I unavailable to fibrinogen. It is therefore not surprising

that MH22 has comparable *in vivo* activity with hirulog-1/bivalirudin. Thus, the longer half-life and prolonged action of variegin (cleavage fragment inhibits thrombin) might allow single dose administration instead of continuous infusion (as in the case of bivalirudin) (Warkentin et al., 2008) especially in short procedures such as PCI.

Considering the prolonged action for variegin, there is a need to explore ways to neutralize its activity. We showed that protamine sulfate can reverse variegin (and variants) activities *in vitro*. From the experience of using protamine sulfate as heparin reversal, the dose needed will depend on dosage and plasma half-life of the anticoagulant (Schulman and Bijsterveld, 2007). Thus, *in vivo* efficacy of variegin reversal by protamine sulfate cannot be verified at this point. The use of protamine sulfate is not risk-free, as it induces histamine release and causing problems such as hypotension and bronchoconstriction. However, clinical experiences in its administration as heparin reversal should ensured a higher benefit to risk ratio when used as variegin reversal. Other options, such as hemodialysis and administration of procoagulant enzyme (eg. FVIIa), are also possible as they are being used for neutralization of other DTIs (Schulman and Bijsterveld, 2007). On the whole, variegin (and variants) represent a fine balance between hirudin and bivalirudin for most of their properties (Ki, sizes, plasma half-life etc.) (Table 5.1). At this point, the strong *in vivo* antithrombotic effects and the availability of an antidote (protamine sulfate) support the continual development of variegin (and variants) as anticoagulant.

TABLE 5.1

Comparison of n-variegin, s-variegin, DV24K10RY^{sulf} and MH18Y^{sulf} with hirudin and hirulog-1

Variegin represent a fine balance between hirudin and hirulog-1 (both available in the market) for most of their properties, underlined the potential of this novel thrombin inhibitor as a good therapeutic agent.

	hirudin	**n-variegin**	**s-variegin**	**DV24K10RY^{sulf}**	**MH18Y^{sulf}**	**hirulog-1**
Size	65 residues	32 residues	32 residues	24 residues	18 residues	20 residues
Modified amino acid	Sulfotyrosine	Glycothreonine	None	Sulfotyrosine	Sulfotyrosine	None
Unnatural amino acid	None	None	None	None	None	$_{D}$-Phe
K_i	0.02 – 0.20 pM	10.40 pM	318 pM	42 pM	1250 pM	2940 pM
Mechanism of inhibition	Fast, tight-binding, competitive	Fast, tight-binding, competitive	Fast, tight-binding, competitive	Fast, tight-binding, competitive	Fast, tight-binding, non-competitive	Fast, tight-binding, competitive
Cleaved by thrombin?	No	Yes (K-M)	Yes (K-M)	Yes (K-M)	No	Yes (R-P)
Cleavage product inhibits thrombin?	Not applicable	Yes	Yes	Yes	Not applicable	No
Plasma half-life	60 – 120 min	?	~ 60 min	?	?	25 min
Clearance	Renal	Renal (proteolysis?)	Renal (proteolysis?)	Renal (proteolysis?)	Renal (proteolysis?)	Renal and proteolysis

5.5. SUMMARY

The *in vivo* antithrombotic effects of four representative variegin variants were tested and compared to that of hirulog-1/bivalirudin in the prevention of thrombus formation in venous thrombosis model of zebrafish larvae. Generally, except for EP25, antithrombotic effects of these peptides correlate well with their affinity for thrombin determined *in vitro*. It is likely slow binding characteristics of EP25 rendered the peptide ineffective *in vivo*. In addition, the thrombin inhibitory action of variegin can be neutralized by protamine sulfate and hence is suitable for development as an antithrombotic therapeutic agent.

Chapter Six

Conclusions and future perspectives

6.1. CONCLUSIONS

Blood-feeding is crucial for the survival of hematophagous animals. Tick saliva contains large number of anticoagulant proteins to help ticks obtain their enormous blood meal during prolonged feeding. The most potent thrombin inhibitor isolated from the SGE of partially fed female *Amblyomma variegatum* – variegin – was studied and described in detail in this thesis. Variegin is a novel, fast and tight-binding competitive inhibitor of thrombin. The peptide, 32 residues, is one of the smallest thrombin inhibitor found in nature. It is dissimilar to any other groups of naturally occurring thrombin inhibitors, thus belongs to a new class of its own. Despite its small size and flexible structure, variegin binds thrombin with strong affinity (K_i = 10.4 pM) and high specificity. The primary structure of variegin is unique among other thrombin substrates/cofactors/inhibitors. We chemically synthesized the full-length sequence of variegin (s-variegin) and managed to understand the kinetic, mechanism and specificity of thrombin inhibition by variegin. Through s-variegin and two truncation variants (EP25 and AP18) we have outlined key structure-function information of variegin: residues 8 to 14 bind to thrombin active site; residues 15 to 32 binds to thrombin exosite-I; and the first seven N-terminal residues of variegin are not in direct contact with thrombin but are needed for its fast binding characteristics.

We showed that variegin binds thrombin with a substrate-like mechanism, and hence is cleaved at the scissile bond between Lys10 and Met11 by the proteinase. The sequence resides in the active site binding segment ($E^{8}PKMHKT^{14}$) is novel and in fact contradicted some of the common knowledge about thrombin substrate

preference. However, this unique sequence, especially those residues located C-terminal to the scissile bond ($M^{11}HKT^{14}$), was found to be in close contact with thrombin prime subsites. This prime subsites binding segment is mainly responsible for the ability of variegin cleavage product to non-competitively inhibit thrombin. This unique property of variegin to bind thrombin strongly before and after cleavage, results in prolonged inhibition of the enzyme.

Although we attempted to obtain the three-dimensional structure of thrombin in complex with full-length s-variegin, only the density of its C-terminal cleavage fragment was traced. The structure provided molecular details of thrombin-s-variegin (cleavage fragment) interactions. Variegin (cleavage fragment) fitted tightly to thrombin in catalytic pocket, prime subsites and exosite-I. The structure provided the basis to explain the classical non-competitive inhibition observed with variegin cleavage product. One of the thrombin catalytic residues, Ser195, was displaced from its normal position. The change is due to the involvement of Ser195 Oγ in a new and extensive hydrogen bonding network involving His12 of s-variegin. The same hydrogen bonding network also perturbed the oxyanion hole by engaging Gly193 backbone N. Overall, the catalytic capability of thrombin is inhibited. The structure also revealed other important information and prompted subsequent design of variegin variants: (1) final four residues of s-variegin are disordered in structure. On this basis we removed these residues and produced shorter inhibitors without loss of activities; (2) Pro16-Pro17 induced a kink in the backbone of s-variegin. We removed one of the Pro but the activities of these variants diminished, probably due to disturbance of prime subsites interactions; and (3) s-variegin C-terminal conformation is vastly different from hirudin/hirugen C-termini. In addition to removing the extra residues,

we incorporated a sulfotyrosine in s-variegin to mimic the structure of hirudin/hirugen C-termini and produced peptides with strong affinities for thrombin (one of them has K_i = 42 pM). The structure also provided explanation for other observations: (1) substitution of P1 Lys with Arg only minimally improved activities of peptides. The less stringent requirement for P1 residue in variegin is probably due to its strong interactions with thrombin prime subsites; and (2) substitution of Ala22 by Glu did not change the potencies of the peptides. The Ala22 side chain is solvent exposed and is not involve in interaction.

We then established the feasibility of developing variegin (and variants) as a clinically available anticoagulant. We have demonstrated that the *in vivo* antithrombotic effects of variegin variants correlate well with their *in vitro* affinities for thrombin with the exception of slow binding variants. In addition, the thrombin inhibitory activities of the peptides can be reversed by protamine sulfate. Through works conducted within the scope of this project, a wide range of peptides with different potencies, kinetics, mechanisms of inhibition are made available. Variegin compares favorably against the other peptide-based direct thrombin inhibitor available in the market (bivalirudin) in every aspect that have been evaluated and discussed. With the conclusion of this work, the stage is now set for further development of variegin into a therapeutic agent.

6.2. FUTURE PERSPECTIVES

6.2.1. On variegin

This study on the structure-function relationships of variegin demonstrated its enormous potential for drug development. However, data presented in this thesis marked the start, but not the end of this long and challenging process. Many interesting questions remained to be answered. Some of which will enhance our basic understanding about the molecule and its interactions with thrombin while others will have direct impact on the drug development process.

6.2.1.1. Three-dimensional structures of MH18Y^{sulf} and other variants

The removal of four C-terminal residues coupled with incorporation of sulfotyrosine drastically improved affinities of the peptides. This is most likely due to a change in their C-terminal conformations to mimic hirudin/hirugen C-termini for optimum interactions with thrombin. The crystal structure of thrombin-MH18Y^{sulf} complex can therefore prove this hypothesis. We are in the process to crystallize this complex. Any new information derived from the structure can also be used to further improve the affinities of the inhibitors. In addition, we are trying to screen for new conditions that will allow crystallization of thrombin with complete full-length s-variegin. Alternatively, a non-hydrolyzable variant can be synthesized (eg. incorporating β-homo-Arg residue similar to hirulog-3) for the study of interactions in the sites N-terminal to the scissile bond (non-prime subsites).

6.2.1.2. Further optimizations of thrombin-variegin interactions

Despite the strong affinity of variegin (and variants) for thrombin, there are still rooms for further optimizations of the interactions. For example, P3 Glu is known to be a poor substrate residue for thrombin. Substitution of this residue with $_{D}$-Phe will definitely enhance the interaction, but the use of unnatural amino acids is best avoidable. Interestingly, there is a report of Asp at P3 along with Arg at P3′ showing strong affinity for thrombin (Su et al., 2004). This mirrored the P3 Glu and Lys P3′ pairing in variegin in the charges of their side chains, although in the same report substitution of P3 Asp by Glu abolished the activity of peptide. We can look into the possibilities of the double substitution of Asp at P3 and Arg at P3′ to improve variegin activity. In addition, the absence of density for Met11 and the classical non-competitive inhibition observed for MH22, suggested that Met11 is not involved in thrombin interaction. Substitution of this P1′ residue with Gly, Ala or Ser (in line with the requirement for an amino acid with small side chain) as well as Pro (for slow rate of cleavage) can also be done.

6.2.1.3. Variegin family of thrombin inhibitors in **Amblyomma** *ticks*

Parallel with this work on structure-function relationships of variegin, our collaborator Dr. Ladislav Roller from Institute of Zoology, Slovakia tried to clone variegin cDNA with degenerate primers. The clone obtained was translated into a polypeptide chain with five repeats of variegin-like sequences. A search in The *Amblyomma variegatum* Gene Index (AvGI) from The Institute of Genomic Research (TIGR) recovered sequences with similar variegin-like repeats. These sequences had around 40% identity with cDNA clone obtained by Dr. Roller. A recently constructed cDNA library of *Amblyomma cajennense* also reported the existence similar clones

(Batista et al., 2008). Therefore, it is likely that variegins are synthesized as precursor proteins before being proteolytically processed into matured peptides. This pool of putative sequences represents multiple isoforms of variegin. We have identified representative sequences from each cDNA clone (from both *A. variegatum* and *A. cajennense*) and will synthesize peptides with these sequences to determine their activities. By comparing the sequences and activities, we will have an idea of the 'best' residues in each position for maximum binding to thrombin. In addition, the studies on gene regulations and the post-translational processing mechanisms of the precursors will probably unveil interesting information about the blood-feeding strategies of the ticks.

6.2.1.4. Other pre-clinical animal studies

In vivo antithrombotic effects of variegin (and variants) need be evaluated in other animal models. Performance of variegin (and variants) can be compared to other direct thrombin inhibitors (eg. hirudin, bivalirudin and dabigatran) and conventional anticoagulants (eg. heparin) in both venous and arterial thrombosis models. Pharmacokinetics and toxicology studies are also needed to demonstrate the benefits of variegin (and variants) in pre-clinical studies.

6.2.2 On the discovery of novel exogenous anticoagulants from hematophagous animals

Much valuable information was gained from the studies of a small number of exogenous anticoagulants from hematophagous animals. These molecules can either be used as a drug [e.g. hirudin (Markwardt, 1994)] or provide a template for drug designs [e.g. bivalirudin (Maraganore et al., 1990)]. Through works conducted within

the scope of this thesis, we have added a promising candidate – variegin – for drug development. In addition, studies on these exogenous anticoagulants often reveal new mechanisms to inhibit coagulation factors. Further, detailed structural analyses of the inhibitor-proteinase complexes often reveal new exosites on coagulation factors that are susceptible for inhibition. For instance, other than thrombin inhibitor (variegin) that has been the theme of this thesis, one can design novel FXa inhibitors with different mechanisms based on competitive (Tuszynski et al., 1987; Dunwiddie et al., 1989; Waxman et al., 1990; Stassens et al., 1996; Lapatto et al., 1997; Wei et al., 1998; Rios-Steiner et al., 2007), noncompetitive (Stark and James, 1995; Stark and James, 1998), partial noncompetitive (Harrison et al., 2002; Mieszczanek et al., 2004a), and uncompetitive (Joubert et al., 1995; Ibrahim et al., 2001b) inhibitors. Since blood coagulation factors are all serine proteinase with highly similar active site, high specificity can often be achieved through molecular interactions with such distinct exosites (Bock et al., 2007). The inhibitors targeting specific exosites will have minimal side effects related to non-specificity. Bivalirudin is a good, specific thrombin inhibitor designed to target thrombin exosite-I and the active site based on information derived from the studies on hirudin C-terminal interactions with thrombin (Maraganore et al., 1990). We believe variegin can emulate and potentially be more successful than bivalirudin.

Currently, only a very small number of hematophagous animals (~ 50, bases on articles listed on Pubmed database) have been studied, that too partially, for their anticoagulants. In nature, hematophagous animals include an estimated 15000 species of arthropods (> 400 genera) (Ribeiro, 1995) *plus* a large number of leeches and hookworms. It is postulated that in hematophagous arthopods alone, blood-feeding

behavior have evolved independently at least six times in history (Ribeiro, 1995). This huge number of species translates into an enormous pool of structurally and functionally diverse exogenous anticoagulants. One of the major limitations in their studies is the availability of only small amounts of salivary gland extracts that leads to difficulties in the identification, isolation and characterization of these interesting proteins. Recent progress in large scale and sensitive genomic, transcriptomic, structural and proteomic analysis has helped to ease the problem. Thus discoveries of new exogenous anticoagulants from distinct lineages will be made in the foreseeable future and the studies of the existing and newly-characterized anticoagulants will provide ideal, fertile and exciting future in the development of anticoagulant therapies.

BIBLIOGRAPHY

Journals, books and patents:

Abebe,M., Cupp,M.S., Champagne,D., and Cupp,E.W. (2008). Simulidin: a black fly (*Simulium vittatum*) salivary gland protein with anti-thrombin activity. J. Insect Physiol *41*, 1001-1006.

Abebe,M., Cupp,M.S., Ramberg,F.B., and Cupp,E.W. (1994). Anticoagulant activity in salivary gland extracts of black flies (Diptera: Simuliidae). J. Med. Entomol. *31*, 908-911.

Abebe,M., Ribeiro,J.M., Cupp,M.S., and Cupp,E.W. (1996). Novel anticoagulant from salivary glands of *Simulium vittatum* (Diptera: Simuliidae) inhibits activity of coagulation factor V. J. Med. Entomol. *33*, 173-176.

Ajjan,R. and Grant,P.J. (2006). Coagulation and atherothrombotic disease. Atherosclerosis *186*, 240-259.

Alban,S. (2008). Pharmacological strategies for inhibition of thrombin activity. Curr. Pharm. Des *14*, 1152-1175.

Andersen,J.F. and Montfort,W.R. (2000). The crystal structure of nitrophorin 2. A trifunctional antihemostatic protein from the saliva of *Rhodnius prolixus*. J. Biol. Chem. *275*, 30496-30503.

Arocha-Pinango,C.L., Marchi,R., and Guerrero,B. (1999). Inventory of exogenous hemostatic factors derived form arthropods. Registry of Exogenous Hemostatic Factors of the Scientific and Standardization Subcommittee of the International Society on Thrombosis and Haemostasis. Thromb. Haemost. *81*, 647-656.

Baglin,T.P., Carrell,R.W., Church,F.C., Esmon,C.T., and Huntington,J.A. (2002). Crystal structures of native and thrombin-complexed heparin cofactor II reveal a multistep allosteric mechanism. Proc. Natl. Acad. Sci. U. S. A *99*, 11079-11084.

Bajusz,S., Barabas,E., Tolnay,P., Szell,E., and Bagdy,D. (1978). Inhibition of thrombin and trypsin by tripeptide aldehydes. Int. J. Pept. Protein Res. *12*, 217-221.

Bates,S.M. and Weitz,J.I. (2006). The status of new anticoagulants. Br. J. Haematol. *134*, 3-19.

Batista,I.F., Chudzinski-Tavassi,A.M., Faria,F., Simons,S.M., Barros-Batestti,D.M., Labruna,M.B., Leao,L.I., Ho,P.L., and Junqueira-de-Azevedo,I.L. (2008). Expressed sequence tags (ESTs) from the salivary glands of the tick *Amblyomma cajennense* (Acari: Ixodidae). Toxicon *51*, 823-834.

Bauer,K.A. (2002). Selective inhibition of coagulation factors: advances in antithrombotic therapy. Semin. Thromb. Hemost. *28 Suppl 2*, 15-24.

Bock,P.E., Panizzi,P., and Verhamme,I.M. (2007). Exosites in the substrate specificity of blood coagulation reactions. J. Thromb. Haemost. *5 Suppl 1*, 81-94.

Bode,W. and Huber,R. (1992). Natural protein proteinase inhibitors and their interaction with proteinases. Eur. J. Biochem. *204*, 433-451.

Bode,W., Mayr,I., Baumann,U., Huber,R., Stone,S.R., and Hofsteenge,J. (1989). The refined 1.9 A crystal structure of human alpha-thrombin: interaction with D-Phe-Pro-Arg chloromethylketone and significance of the Tyr-Pro-Pro-Trp insertion segment. EMBO J. *8*, 3467-3475.

Bode,W., Turk,D., and Karshikov,A. (1992). The refined 1.9-A X-ray crystal structure of D-Phe-Pro-Arg chloromethylketone-inhibited human alpha-thrombin: structure analysis, overall structure, electrostatic properties, detailed active-site geometry, and structure-function relationships. Protein Sci. *1*, 426-471.

Boissel,J.P., Le Bonniec,B., Rabiet,M.J., Labie,D., and Elion,J. (1984). Covalent structures of beta and gamma autolytic derivatives of human alpha-thrombin. J. Biol. Chem. *259*, 5691-5697.

Bowman,A.S. and Sauer,J.R. (2004). Tick salivary glands: function, physiology and future. Parasitology *129 Suppl*, S67-S81.

Bradford,M.M. (1976). A rapid and sensitive method for the quantitation of microgram quantities of protein utilizing the principle of protein-dye binding. Anal. Biochem. *72*, 248-254.

Brankamp,R.G., Blankenship,D.T., Sunkara,P.S., and Cardin,A.D. (1990). Ghilantens: anticoagulant-antimetastatic proteins from the South American leech, *Haementeria ghilianii*. J. Lab Clin. Med. *115*, 89-97.

Braun,P.J., Dennis,S., Hofsteenge,J., and Stone,S.R. (1988a). Use of site-directed mutagenesis to investigate the basis for the specificity of hirudin. Biochemistry *27*, 6517-6522.

Braun,P.J., Hofsteenge,J., Chang,J.Y., and Stone,S.R. (1988b). Preparation and characterization of proteolyzed forms of human alpha-thrombin. Thromb. Res. *50*, 273-283.

Brunger,A.T., Adams,P.D., Clore,G.M., DeLano,W.L., Gros,P., Grosse-Kunstleve,R.W., Jiang,J.S., Kuszewski,J., Nilges,M., Pannu,N.S., Read,R.J., Rice,L.M., Simonson,T., and Warren,G.L. (1998). Crystallography & NMR system: A new software suite for macromolecular structure determination. Acta Crystallogr. D. Biol. Crystallogr. *54*, 905-921.

Buddai,S.K., Toulokhonova,L., Bergum,P.W., Vlasuk,G.P., and Krishnaswamy,S. (2002). Nematode anticoagulant protein c2 reveals a site on factor Xa that is important for macromolecular substrate binding to human prothrombinase. J. Biol. Chem. *277*, 26689-26698.

Campos,I.T., Amino,R., Sampaio,C.A., Auerswald,E.A., Friedrich,T., Lemaire,H.G., Schenkman,S., and Tanaka,A.S. (2002). Infestin, a thrombin inhibitor presents in *Triatoma infestans* midgut, a Chagas' disease vector: gene cloning, expression and characterization of the inhibitor. Insect Biochem. Mol. Biol. *32*, 991-997.

Campos,I.T., Tanaka-Azevedo,A.M., and Tanaka,A.S. (2004). Identification and characterization of a novel factor XIIa inhibitor in the hematophagous insect, *Triatoma infestans* (Hemiptera: Reduviidae). FEBS Lett. *577*, 512-516.

Cappello,M., Bergum,P.W., Vlasuk,G.P., Furmidge,B.A., Pritchard,D.I., and Aksoy,S. (1996). Isolation and characterization of the tsetse thrombin inhibitor: a potent antithrombotic peptide from the saliva of *Glossina morsitans morsitans*. Am. J. Trop. Med. Hyg. *54*, 475-480.

Cappello,M., Li,S., Chen,X., Li,C.B., Harrison,L., Narashimhan,S., Beard,C.B., and Aksoy,S. (1998). Tsetse thrombin inhibitor: bloodmeal-induced expression of an anticoagulant in salivary glands and gut tissue of *Glossina morsitans morsitans*. Proc. Natl. Acad. Sci. U. S. A *95*, 14290-14295.

Cappello,M., Vlasuk,G.P., Bergum,P.W., Huang,S., and Hotez,P.J. (1995). *Ancylostoma caninum* anticoagulant peptide: a hookworm-derived inhibitor of human coagulation factor Xa. Proc. Natl. Acad. Sci. U. S. A *92*, 6152-6156.

Champagne,D.E. (2004). Antihemostatic strategies of blood-feeding arthropods. Curr. Drug Targets. Cardiovasc. Haematol. Disord. *4*, 375-396.

Chang,J.Y. (1986). The structures and proteolytic specificities of autolysed human thrombin. Biochem. J. *240*, 797-802.

Chopin,V., Salzet,M., Baert,J., Vandenbulcke,F., Sautiere,P.E., Kerckaert,J.P., and Malecha,J. (2000). Therostasin, a novel clotting factor Xa inhibitor from the rhynchobdellid leech, *Theromyzon tessulatum*. J. Biol. Chem. *275*, 32701-32707.

Ciprandi,A., de Oliveira,S.K., Masuda,A., Horn,F., and Termignoni,C. (2006). *Boophilus microplus*: its saliva contains microphilin, a small thrombin inhibitor. Exp. Parasitol. *114*, 40-46.

Clore,G.M., Sukumaran,D.K., Nilges,M., Zarbock,J., and Gronenborn,A.M. (1987). The conformations of hirudin in solution: a study using nuclear magnetic resonance, distance geometry and restrained molecular dynamics. EMBO J. *6*, 529-537.

Condra,C., Nutt,E., Petroski,C.J., Simpson,E., Friedman,P.A., and Jacobs,J.W. (1989). Isolation and structural characterization of a potent inhibitor of coagulation factor Xa from the leech Haementeria ghilianii. Thromb. Haemost. *61*, 437-441.

Copeland,R.A. (2000). Enzymes: a practical introduction to structure, mechanism and data analysis. Wiley-VCH, New York.

Coughlin,S.R. (2000). Thrombin signalling and protease-activated receptors. Nature *407*, 258-264.

Crawley,J.T. and Lane,D.A. (2008). The haemostatic role of tissue factor pathway inhibitor. Arterioscler. Thromb. Vasc. Biol. *28*, 233-242.

Davie,E.W. (2003). A brief historical review of the waterfall/cascade of blood coagulation. J. Biol. Chem. *278*, 50819-50832.

Davie,E.W., Fujikawa,K., and Kisiel,W. (1991). The coagulation cascade: initiation, maintenance, and regulation. Biochemistry *30*, 10363-10370.

Davie,E.W. and Ratnoff,O.D. (1964). Waterfall sequence for intrinsic blood clotting. Science *145*, 1310-1312.

Di Cera,E. (2003). Thrombin interactions. Chest *124*, 11S-17S.

Di Nisio,M., Middeldorp,S., and Buller,H.R. (2005). Direct thrombin inhibitors. N. Engl. J. Med. *353*, 1028-1040.

DiMaio,J., Gibbs,B., Munn,D., Lefebvre,J., Ni,F., and Konishi,Y. (1990). Bifunctional thrombin inhibitors based on the sequence of hirudin45-65. J. Biol. Chem. *265*, 21698-21703.

Dodt,J., Kohler,S., and Baici,A. (1988). Interaction of site specific hirudin variants with alpha-thrombin. FEBS Lett. *229*, 87-90.

Duggan,B.M., Dyson,H.J., and Wright,P.E. (1999). Inherent flexibility in a potent inhibitor of blood coagulation, recombinant nematode anticoagulant protein c2. Eur. J. Biochem. *265*, 539-548.

Dunwiddie,C., Thornberry,N.A., Bull,H.G., Sardana,M., Friedman,P.A., Jacobs,J.W., and Simpson,E. (1989). Antistasin, a leech-derived inhibitor of factor Xa. Kinetic analysis of enzyme inhibition and identification of the reactive site. J. Biol. Chem. *264*, 16694-16699.

Eikelboom,J.W. and Hirsh,J. (2007). Combined antiplatelet and anticoagulant therapy: clinical benefits and risks. J. Thromb. Haemost. *5 Suppl 1*, 255-263.

Electricwala,A., Sawyer,R.T., Jones,C.P., and Atkinson,T. (1991). Isolation of thrombin inhibitor from the leech *Hirudinaria manillensis*. Blood Coagul. Fibrinolysis *2*, 83-89.

Eriksson,B.I., Smith,H., Yasothan,U., and Kirkpatrick,P. (2008). Dabigatran etexilate. Nat. Rev. Drug Discov. *7*, 557-558.

Fareed,J. and Jeske,W.P. (2004). Small-molecule direct antithrombins: argatroban. Best. Pract. Res. Clin. Haematol. *17*, 127-138.

Faria,F., Kelen,E.M., Sampaio,C.A., Bon,C., Duval,N., and Chudzinski-Tavassi,A.M. (1999). A new factor Xa inhibitor (lefaxin) from the *Haementeria depressa* leech. Thromb. Haemost. *82*, 1469-1473.

Fernandez,A.Z., Tablante,A., Beguin,S., Hemker,H.C., and Apitz-Castro,R. (1999). Draculin, the anticoagulant factor in vampire bat saliva, is a tight-binding, noncompetitive inhibitor of activated factor X. Biochim. Biophys. Acta *1434*, 135-142.

Fethiere,J., Tsuda,Y., Coulombe,R., Konishi,Y., and Cygler,M. (1996). Crystal structure of two new bifunctional nonsubstrate type thrombin inhibitors complexed with human alpha-thrombin. Protein Sci. *5*, 1174-1183.

Flower,D.R. (1996). The lipocalin protein family: structure and function. Biochem. J. *318 (Pt 1)*, 1-14.

Francischetti,I.M., Mather,T.N., and Ribeiro,J.M. (2004). Penthalaris, a novel recombinant five-Kunitz tissue factor pathway inhibitor (TFPI) from the salivary gland of the tick vector of Lyme disease, Ixodes scapularis. Thromb. Haemost. *91*, 886-898.

Francischetti,I.M., Valenzuela,J.G., Andersen,J.F., Mather,T.N., and Ribeiro,J.M. (2002). Ixolaris, a novel recombinant tissue factor pathway inhibitor (TFPI) from the salivary gland of the tick, *Ixodes scapularis*: identification of factor X and factor Xa as scaffolds for the inhibition of factor VIIa/tissue factor complex. Blood *99*, 3602-3612.

Francischetti,I.M., Valenzuela,J.G., and Ribeiro,J.M. (1999). Anophelin: kinetics and mechanism of thrombin inhibition. Biochemistry *38*, 16678-16685.

Friedrich,T., Kroger,B., Bialojan,S., Lemaire,H.G., Hoffken,H.W., Reuschenbach,P., Otte,M., and Dodt,J. (1993). A Kazal-type inhibitor with thrombin specificity from *Rhodnius prolixus*. J. Biol. Chem. *268*, 16216-16222.

Fuentes-Prior,P., Noeske-Jungblut,C., Donner,P., Schleuning,W.D., Huber,R., and Bode,W. (1997). Structure of the thrombin complex with triabin, a lipocalin-like

exosite-binding inhibitor derived from a triatomine bug. Proc. Natl. Acad. Sci. U. S. A *94*, 11845-11850.

Furie,B., Bing,D.H., Feldmann,R.J., Robison,D.J., Burnier,J.P., and Furie,B.C. (1982). Computer-generated models of blood coagulation factor Xa, factor IXa, and thrombin based upon structural homology with other serine proteases. J. Biol. Chem. *257*, 3875-3882.

Furie,B. and Furie,B.C. (2007). *In vivo* thrombus formation. J. Thromb. Haemost. *5 Suppl 1*, 12-17.

Furie,B. and Furie,B.C. (2008). Mechanisms of thrombus formation. N. Engl. J. Med. *359*, 938-949.

Gailani,D. and Renne,T. (2007). The intrinsic pathway of coagulation: a target for treating thromboembolic disease? J. Thromb. Haemost. *5*, 1106-1112.

Gaspar,A.R., Crause,J.C., and Neitz,A.W. (1995). Identification of anticoagulant activities in the salivary glands of the soft tick, *Ornithodoros savignyi*. Exp. Appl. Acarol. *19*, 117-127.

Gaspar,A.R., Joubert,A.M., Crause,J.C., and Neitz,A.W. (1996). Isolation and characterization of an anticoagulant from the salivary glands of the tick, *Ornithodoros savignyi* (Acari: Argasidae). Exp. Appl. Acarol. *20*, 583-598.

Giugliano,R.P., Wiviott,S.D., Stone,P.H., Simon,D.I., Schweiger,M.J., Bouchard,A., Leesar,M.A., Goulder,M.A., Deitcher,S.R., McCabe,C.H., and Braunwald,E. (2007). Recombinant nematode anticoagulant protein c2 in patients with non-ST-segment elevation acute coronary syndrome: the ANTHEM-TIMI-32 trial. J. Am. Coll. Cardiol. *49*, 2398-2407.

Gladwell,T.D. (2002). Bivalirudin: a direct thrombin inhibitor. Clin. Ther. *24*, 38-58.

Gordon,J.R. and Allen,J.R. (1991). Factors V and VII anticoagulant activities in the salivary glands of feeding *Dermacentor andersoni* ticks. J. Parasitol. *77*, 167-170.

Greinacher,A. and Warkentin,T.E. (2008). The direct thrombin inhibitor hirudin. Thromb. Haemost. *99*, 819-829.

Gross,P.L. and Weitz,J.I. (2008). New anticoagulants for treatment of venous thromboembolism. Arterioscler. Thromb. Vasc. Biol. *28*, 380-386.

Grutter,M.G. (1994). Proteinase inhibitors: another new fold. Structure. *2*, 575-576.

Grutter,M.G., Priestle,J.P., Rahuel,J., Grossenbacher,H., Bode,W., Hofsteenge,J., and Stone,S.R. (1990). Crystal structure of the thrombin-hirudin complex: a novel mode of serine protease inhibition. EMBO J. *9*, 2361-2365.

Guex,N. and Peitsch,M.C. (1997). SWISS-MODEL and the Swiss-PdbViewer: an environment for comparative protein modeling. Electrophoresis *18*, 2714-2723.

Gurm,H.S. and Bhatt,D.L. (2005). Thrombin, an ideal target for pharmacological inhibition: a review of direct thrombin inhibitors. Am. Heart J. *149*, S43-S53.

Gustafsson,D., Bylund,R., Antonsson,T., Nilsson,I., Nystrom,J.E., Eriksson,U., Bredberg,U., and Teger-Nilsson,A.C. (2004). A new oral anticoagulant: the 50-year challenge. Nat. Rev. Drug Discov. *3*, 649-659.

Hanumanthaiah,R., Day,K., and Jagadeeswaran,P. (2002). Comprehensive analysis of blood coagulation pathways in teleostei: evolution of coagulation factor genes and identification of zebrafish factor VIIi. Blood Cells Mol. Dis. *29*, 57-68.

Harrison,L.M., Nerlinger,A., Bungiro,R.D., Cordova,J.L., Kuzmic,P., and Cappello,M. (2002). Molecular characterization of *Ancylostoma* inhibitors of coagulation factor Xa. Hookworm anticoagulant activity *in vitro* predicts parasite bloodfeeding in vivo. J. Biol. Chem. *277*, 6223-6229.

Haruyama,H. and Wuthrich,K. (1989). Conformation of recombinant desulfatohirudin in aqueous solution determined by nuclear magnetic resonance. Biochemistry *28*, 4301-4312.

Hermanson,G.T. (2008). Bioconjugate techniques. Academic Press.

Hofsteenge,J., Stone,S.R., Donella-Deana,A., and Pinna,L.A. (1990). The effect of substituting phosphotyrosine for sulphotyrosine on the activity of hirudin. Eur. J. Biochem. *188*, 55-59.

Hong,S.J. and Kang,K.W. (1999). Purification of granulin-like polypeptide from the blood-sucking leech, *Hirudo nipponia*. Protein Expr. Purif. *16*, 340-346.

Horn,F., dos Santos,P.C., and Termignoni,C. (2000). *Boophilus microplus* anticoagulant protein: an antithrombin inhibitor isolated from the cattle tick saliva. Arch. Biochem. Biophys. *384*, 68-73.

Hovius,J.W., Levi,M., and Fikrig,E. (2008). Salivating for knowledge: potential pharmacological agents in tick saliva. PLoS. Med. *5*, e43.

Huntington,J.A. (2005). Molecular recognition mechanisms of thrombin. J. Thromb. Haemost. *3*, 1861-1872.

Huntington,J.A. (2008). How Na^+ activates thrombin--a review of the functional and structural data. Biol. Chem. *389*, 1025-1035.

Ibrahim,M.A., Ghazy,A.H., Maharem,T., and Khalil,M. (2001a). Isolation and properties of two forms of thrombin inhibitor from the nymphs of the camel tick *Hyalomma dromedarii* (Acari: Ixodidae). Exp. Appl. Acarol. *25*, 675-698.

Ibrahim,M.A., Ghazy,A.H., Maharem,T.M., and Khalil,M.I. (2001b). Factor Xa (FXa) inhibitor from the nymphs of the camel tick *Hyalomma dromedarii*. Comp Biochem. Physiol B Biochem. Mol. Biol. *130*, 501-512.

Isawa,H., Yuda,M., Orito,Y., and Chinzei,Y. (2002). A mosquito salivary protein inhibits activation of the plasma contact system by binding to factor XII and high molecular weight kininogen. J. Biol. Chem. *277*, 27651-27658.

Isawa,H., Yuda,M., Yoneda,K., and Chinzei,Y. (2000). The insect salivary protein, prolixin-S, inhibits factor IXa generation and Xase complex formation in the blood coagulation pathway. J. Biol. Chem. *275*, 6636-6641.

Isogai,S., Horiguchi,M., and Weinstein,B.M. (2001). The vascular anatomy of the developing zebrafish: an atlas of embryonic and early larval development. Dev. Biol. *230*, 278-301.

Iwanaga,S., Okada,M., Isawa,H., Morita,A., Yuda,M., and Chinzei,Y. (2003). Identification and characterization of novel salivary thrombin inhibitors from the ixodidae tick, *Haemaphysalis longicornis*. Eur. J. Biochem. *270*, 1926-1934.

Jackman,M.P., Parry,M.A., Hofsteenge,J., and Stone,S.R. (1992). Intrinsic fluorescence changes and rapid kinetics of the reaction of thrombin with hirudin. J. Biol. Chem. *267*, 15375-15383.

Jackson,C.M. and Nemerson,Y. (1980). Blood coagulation. Annu. Rev. Biochem. *49*, 765-811.

Jacobs,J.W., Cupp,E.W., Sardana,M., and Friedman,P.A. (1990). Isolation and characterization of a coagulation factor Xa inhibitor from black fly salivary glands. Thromb. Haemost. *64*, 235-238.

Jagadeeswaran,P. (2005). Zebrafish: a tool to study hemostasis and thrombosis. Curr. Opin. Hematol. *12*, 149-152.

Jagadeeswaran, P. (4-15-2008). Method for creating a uniform vascular wound in zebrafish or zebrafish larva. US Patent No: [US 7357916 B2]

Jagadeeswaran,P., Gregory,M., Day,K., Cykowski,M., and Thattaliyath,B. (2005). Zebrafish: a genetic model for hemostasis and thrombosis. J. Thromb. Haemost. *3*, 46-53.

Jagadeeswaran,P., Gregory,M., Zhou,Y., Zon,L., Padmanabhan,K., and Hanumanthaiah,R. (2000). Characterization of zebrafish full-length prothrombin cDNA and linkage group mapping. Blood Cells Mol. Dis. *26*, 479-489.

Jagadeeswaran,P., Paris,R., and Rao,P. (2006). Laser-induced thrombosis in zebrafish larvae: a novel genetic screening method for thrombosis. Methods Mol. Med. *129*, 187-195.

Jagadeeswaran,P. and Sheehan,J.P. (1999). Analysis of blood coagulation in the zebrafish. Blood Cells Mol. Dis. *25*, 239-249.

Jagadeeswaran,P., Sheehan,J.P., Craig,F.E., and Troyer,D. (1999). Identification and characterization of zebrafish thrombocytes. Br. J. Haematol. *107*, 731-738.

Jaworski,D.C. (2003). Tick "talk": protein release by tick salivary cells. Trends Parasitol. *19*, 427-429.

Johnson,D.J., Adams,T.E., Li,W., and Huntington,J.A. (2005). Crystal structure of wild-type human thrombin in the Na^+-free state. Biochem. J. *392*, 21-28.

Jones,T.A., Zou,J.Y., Cowan,S.W., and Kjeldgaard,M. (1991). Improved methods for building protein models in electron density maps and the location of errors in these models. Acta Crystallogr. A *47 (Pt 2)*, 110-119.

Joubert,A.M., Crause,J.C., Gaspar,A.R., Clarke,F.C., Spickett,A.M., and Neitz,A.W. (1995). Isolation and characterization of an anticoagulant present in the salivary glands of the bont-legged tick, *Hyalomma truncatum*. Exp. Appl. Acarol. *19*, 79-92.

Kato,N., Iwanaga,S., Okayama,T., Isawa,H., Yuda,M., and Chinzei,Y. (2005). Identification and characterization of the plasma kallikrein-kinin system inhibitor, haemaphysalin, from hard tick, *Haemaphysalis longicornis*. Thromb. Haemost. *93*, 359-367.

Kazimirova,M., Jancinova,V., Petrikova,M., Takac,P., Labuda,M., and Nosal',R. (2002). An inhibitor of thrombin-stimulated blood platelet aggregation from the salivary glands of the hard tick *Amblyomma variegatum* (Acari: Ixodidae). Exp. Appl. Acarol. *28*, 97-105.

Kazimirova,M., Sulanova,M., Trimnellt,A.R., Kozanek,M., Vidlicka,L., Labuda,M., and Nuttall,P.A. (2002). Anticoagulant activities in salivary glands of tabanid flies. Med. Vet. Entomol. *16*, 301-309.

Kitagawa,K., Aida,C., Fujiwara,H., Yagami,T., Futaki,S., Kogire,M., Ida,J., and Inoue,K. (2001). Facile solid-phase synthesis of sulfated tyrosine-containing peptides: total synthesis of human big gastrin-II and cholecystokinin (CCK)-39. J. Org. Chem. *66*, 1-10.

Kim,D.R. and Kang,K.W. (1998). Amino acid sequence of piguamerin, an antistasin-type protease inhibitor from the blood sucking leech *Hirudo nipponia*. Eur. J. Biochem. *254*, 692-697.

Koh,C.Y., Kazimirova,M., Trimnell,A., Takac,P., Labuda,M., Nuttall,P.A., and Kini,R.M. (2007). Variegin, a novel fast and tight binding thrombin inhibitor from the tropical bont tick. J. Biol. Chem. *282*, 29101-29113.

Krissinel,E. and Henrick,K. (2007). Inference of macromolecular assemblies from crystalline state. J. Mol. Biol. *372*, 774-797.

Krowarsch,D., Cierpicki,T., Jelen,F., and Otlewski,J. (2003). Canonical protein inhibitors of serine proteases. Cell Mol. Life Sci. *60*, 2427-2444.

Krstenansky,J.L. and Mao,S.J. (1987). Antithrombin properties of C-terminus of hirudin using synthetic unsulfated N alpha-acetyl-hirudin45-65. FEBS Lett. *211*, 10-16.

Labuda,M. and Nuttall,P.A. (2004). Tick-borne viruses. Parasitology *129 Suppl*, S221-S245.

Lai,R., Takeuchi,H., Jonczy,J., Rees,H.H., and Turner,P.C. (2004). A thrombin inhibitor from the ixodid tick, *Amblyomma hebraeum*. Gene *342*, 243-249.

Lane,D.A., Philippou,H., and Huntington,J.A. (2005). Directing thrombin. Blood *106*, 2605-2612.

Lapatto,R., Krengel,U., Schreuder,H.A., Arkema,A., de Boer,B., Kalk,K.H., Hol,W.G., Grootenhuis,P.D., Mulders,J.W., Dijkema,R., Theunissen,H.J., and Dijkstra,B.W. (1997). X-ray structure of antistasin at 1.9 A resolution and its modelled complex with blood coagulation factor Xa. EMBO J. *16*, 5151-5161.

Laskowsi,R.A., MacArthur,M.W., Moss,D.S., and Thornton,J.M. (1993). PROCHECK: a program to check the stereochemical quality of protein structures. J. Appl. Crystallogr. *26*, 283-291.

Laskowski,M., Jr. and Kato,I. (1980). Protein inhibitors of proteinases. Annu. Rev. Biochem. *49*, 593-626.

Le Bonniec,B.F. and Esmon,C.T. (1991). Glu-192----Gln substitution in thrombin mimics the catalytic switch induced by thrombomodulin. Proc. Natl. Acad. Sci. U. S. A *88*, 7371-7375.

Ledizet,M., Harrison,L.M., Koskia,R.A., and Cappello,M. (2005). Discovery and pre-clinical development of antithrombotics from hematophagous invertebrates. Curr. Med. Chem. Cardiovasc. Hematol. Agents *3*, 1-10.

Levi,M., Dorffle-Melly,J., Johnson,G.J., Drouet,L., and Badimon,L. (2001). Usefulness and limitations of animal models of venous thrombosis. Thromb. Haemost. *86*, 1331-1333.

Liao,M., Zhou,J., Gong,H., Boldbaatar,D., Shirafuji,R., Battur,B., Nishikawa,Y., and Fujisaki,K. (2008). Hemalin, a thrombin inhibitor isolated from a midgut cDNA library from the hard tick *Haemaphysalis longicornis*. J. Insect Physiol.

Limo,M.K., Voigt,W.P., Tumbo-Oeri,A.G., Njogu,R.M., and ole-MoiYoi,O.K. (1991). Purification and characterization of an anticoagulant from the salivary glands of the ixodid tick *Rhipicephalus appendiculatus*. Exp. Parasitol. *72*, 418-429.

Liu,C.C., Brustad,E., Liu,W., and Schultz,P.G. (2007). Crystal structure of a biosynthetic sulfo-hirudin complexed to thrombin. J. Am. Chem. Soc. *129*, 10648-10649.

Lovato,D.V., Nicolau,d.C., I, Amino,R., and Tanaka,A.S. (2006). The full-length cDNA of anticoagulant protein infestin revealed a novel releasable Kazal domain, a neutrophil elastase inhibitor lacking anticoagulant activity. Biochimie *88*, 673-681.

Macedo-Ribeiro,S., Almeida,C., Calisto,B.M., Friedrich,T., Mentele,R., Sturzebecher,J., Fuentes-Prior,P., and Pereira,P.J. (2008). Isolation, cloning and structural characterisation of boophilin, a multifunctional Kunitz-type proteinase inhibitor from the cattle tick. PLoS. ONE. *3*, e1624.

Macfarlane,R.G. (1964). An enzyme cascade in the blood clotting mechanism, and its function as a biochemical amplifier. Nature *202*, 498-499.

Malikayil,J.A., Burkhart,J.P., Schreuder,H.A., Broersma,R.J., Jr., Tardif,C., Kutcher,L.W., III, Mehdi,S., Schatzman,G.L., Neises,B., and Peet,N.P. (1997). Molecular design and characterization of an alpha-thrombin inhibitor containing a novel P1 moiety. Biochemistry *36*, 1034-1040.

Manithody,C., Yang,L., and Rezaie,A.R. (2002). Role of basic residues of the autolysis loop in the catalytic function of factor Xa. Biochemistry *41*, 6780-6788.

Mans,B.J., Andersen,J.F., Schwan,T.G., and Ribeiro,J.M. (2008). Characterization of anti-hemostatic factors in the argasid, *Argas monolakensis*: Implications for the

evolution of blood-feeding in the soft tick family. Insect Biochem. Mol. Biol. *38*, 22-41.

Mans,B.J., Louw,A.I., and Neitz,A.W. (2002a). Amino acid sequence and structure modeling of savignin, a thrombin inhibitor from the tick, *Ornithodoros savignyi*. Insect Biochem. Mol. Biol. *32*, 821-828.

Mans,B.J., Louw,A.I., and Neitz,A.W. (2002b). Evolution of hematophagy in ticks: common origins for blood coagulation and platelet aggregation inhibitors from soft ticks of the genus *Ornithodoros*. Mol. Biol. Evol. *19*, 1695-1705.

Maraganore,J.M. (1993). Pre-clinical and clinical studies on Hirulog: a potent and specific direct thrombin inhibitor. Adv. Exp. Med. Biol. *340*, 227-236.

Maraganore,J.M., Bourdon,P., Jablonski,J., Ramachandran,K.L., and Fenton,J.W. (1990). Design and characterization of hirulogs: a novel class of bivalent peptide inhibitors of thrombin. Biochemistry *29*, 7095-7101.

Maraganore,J.M., Chao,B., Joseph,M.L., Jablonski,J., and Ramachandran,K.L. (1989). Anticoagulant activity of synthetic hirudin peptides. J. Biol. Chem. *264*, 8692-8698.

Marder,V.J., Rosove,M.H., and Minning,D.M. (2004). Foundation and sites of action of antithrombotic agents. Best. Pract. Res. Clin. Haematol. *17*, 3-22.

Markwardt,F. (1994). The development of hirudin as an antithrombotic drug. Thromb. Res. *74*, 1-23.

Marsh,H.C., Jr., Meinwald,Y.C., Thannhauser,T.W., and Scheraga,H.A. (1983). Mechanism of action of thrombin on fibrinogen. Kinetic evidence for involvement of aspartic acid at position P10. Biochemistry *22*, 4170-4174.

Matthews,J.H., Krishnan,R., Costanzo,M.J., Maryanoff,B.E., and Tulinsky,A. (1996). Crystal structures of thrombin with thiazole-containing inhibitors: probes of the S1' binding site. Biophys. J. *71*, 2830-2839.

Mende,K., Petoukhova,O., Koulitchkova,V., Schaub,G.A., Lange,U., Kaufmann,R., and Nowak,G. (1999). Dipetalogastin, a potent thrombin inhibitor from the blood-sucking insect. *Dipetalogaster maximus* cDNA cloning, expression and characterization. Eur. J. Biochem. *266*, 583-590.

Mieszczanek,J., Harrison,L.M., and Cappello,M. (2004a). *Ancylostoma ceylanicum* anticoagulant peptide-1: role of the predicted reactive site amino acid in mediating inhibition of coagulation factors Xa and VIIa. Mol. Biochem. Parasitol. *137*, 151-159.

Mieszczanek,J., Harrison,L.M., Vlasuk,G.P., and Cappello,M. (2004b). Anticoagulant peptides from *Ancylostoma caninum* are immunologically distinct and localize to

separate structures within the adult hookworm. Mol. Biochem. Parasitol. *133*, 319-323.

Monteiro,R.Q., Rezaie,A.R., Bae,J.S., Calvo,E., Andersen,J.F., and Francischetti,I.M. (2008). Ixolaris binding to factor X reveals a precursor state of factor Xa heparin-binding exosite. Protein Sci. *17*, 146-153.

Monteiro,R.Q., Rezaie,A.R., Ribeiro,J.M., and Francischetti,I.M. (2005). Ixolaris: a factor Xa heparin-binding exosite inhibitor. Biochem. J. *387*, 871-877.

Morrison,J.F. and Walsh,C.T. (1988). The behavior and significance of slow-binding enzyme inhibitors. Adv. Enzymol. Relat Areas Mol. Biol. *61*, 201-301.

Motoyashiki,T., Tu,A.T., Azimov,D.A., and Ibragim,K. (2003). Isolation of anticoagulant from the venom of tick, *Boophilus calcaratus*, from Uzbekistan. Thromb. Res. *110*, 235-241.

Muller,F. and Renne,T. (2008). Novel roles for factor XII-driven plasma contact activation system. Curr. Opin. Hematol. *15*, 516-521.

Murakami,M.T., Rios-Steiner,J., Weaver,S.E., Tulinsky,A., Geiger,J.H., and Arni,R.K. (2007). Intermolecular interactions and characterization of the novel factor Xa exosite involved in macromolecular recognition and inhibition: crystal structure of human Gla-domainless factor Xa complexed with the anticoagulant protein NAPc2 from the hematophagous nematode *Ancylostoma caninum*. J. Mol. Biol. *366*, 602-610.

Myles,T., Le Bonniec,B.F., Betz,A., and Stone,S.R. (2001). Electrostatic steering and ionic tethering in the formation of thrombin-hirudin complexes: the role of the thrombin anion-binding exosite-I. Biochemistry *40*, 4972-4979.

Nakajima,C., Imamura,S., Konnai,S., Yamada,S., Nishikado,H., Ohashi,K., and Onuma,M. (2006). A novel gene encoding a thrombin inhibitory protein in a cDNA library from *Haemaphysalis longicornis* salivary gland. J. Vet. Med. Sci. *68*, 447-452.

Narasimhan,S., Koski,R.A., Beaulieu,B., Anderson,J.F., Ramamoorthi,N., Kantor,F., Cappello,M., and Fikrig,E. (2002). A novel family of anticoagulants from the saliva of *Ixodes scapularis*. Insect Mol. Biol. *11*, 641-650.

Naski,M.C., Fenton,J.W., Maraganore,J.M., Olson,S.T., and Shafer,J.A. (1990). The COOH-terminal domain of hirudin. An exosite-directed competitive inhibitor of the action of alpha-thrombin on fibrinogen. J. Biol. Chem. *265*, 13484-13489.

Neeper,M.P., Waxman,L., Smith,D.E., Schulman,C.A., Sardana,M., Ellis,R.W., Schaffer,L.W., Siegl,P.K., and Vlasuk,G.P. (1990). Characterization of recombinant tick anticoagulant peptide. A highly selective inhibitor of blood coagulation factor Xa. J. Biol. Chem. *265*, 17746-17752.

Nienaber,J., Gaspar,A.R., and Neitz,A.W. (1999). Savignin, a potent thrombin inhibitor isolated from the salivary glands of the tick *Ornithodoros savignyi* (Acari: Argasidae). Exp. Parasitol. *93*, 82-91.

Noeske-Jungblut,C., Haendler,B., Donner,P., Alagon,A., Possani,L., and Schleuning,W.D. (1995). Triabin, a highly potent exosite inhibitor of thrombin. J. Biol. Chem. *270*, 28629-28634.

Nutt,E., Gasic,T., Rodkey,J., Gasic,G.J., Jacobs,J.W., Friedman,P.A., and Simpson,E. (1988). The amino acid sequence of antistasin. A potent inhibitor of factor Xa reveals a repeated internal structure. J. Biol. Chem. *263*, 10162-10167.

Otlewski,J., Jelen,F., Zakrzewska,M., and Oleksy,A. (2005). The many faces of protease-protein inhibitor interaction. EMBO J. *24*, 1303-1310.

Otwinowski,Z. and Minor,W. (1997). Processing of X-ray diffraction data collected in oscillation mode. Methods in Enzymology *276*, 307-326.

Page,M.J., Macgillivray,R.T., and Di Cera,E. (2005). Determinants of specificity in coagulation proteases. J. Thromb. Haemost. *3*, 2401-2408.

Pereira,M.H., Souza,M.E., Vargas,A.P., Martins,M.S., Penido,C.M., and Diotaiuti,L. (1996). Anticoagulant activity of *Triatoma infestans* and *Panstrongylus megistus* saliva (Hemiptera/Triatominae). Acta Trop. *61*, 255-261.

Perez de Leon,A.A., Valenzuela,J.G., and Tabachnick,W.J. (1998). Anticoagulant activity in salivary glands of the insect vector *Culicoides variipennis sonorensis* by an inhibitor of factor Xa. Exp. Parasitol. *88*, 121-130.

Perona,J.J. and Craik,C.S. (1995). Structural basis of substrate specificity in the serine proteases. Protein Sci. *4*, 337-360.

Qiu,X., Padmanabhan,K.P., Carperos,V.E., Tulinsky,A., Kline,T., Maraganore,J.M., and Fenton,J.W. (1992). Structure of the hirulog 3-thrombin complex and nature of the S' subsites of substrates and inhibitors. Biochemistry *31*, 11689-11697.

Rezaie,A.R. (2000). Identification of basic residues in the heparin-binding exosite of factor Xa critical for heparin and factor Va binding. J. Biol. Chem. *275*, 3320-3327.

Rezaie,A.R. (2004). Kinetics of factor Xa inhibition by recombinant tick anticoagulant peptide: both active site and exosite interactions are required for a slow- and tight-binding inhibition mechanism. Biochemistry *43*, 3368-3375.

Ribeiro,J.M. (1995). Blood-feeding arthropods: live syringes or invertebrate pharmacologists? Infect. Agents Dis. *4*, 143-152.

Ribeiro,J.M. and Francischetti,I.M. (2003). Role of arthropod saliva in blood feeding: sialome and post-sialome perspectives. Annu. Rev. Entomol. *48*, 73-88.

Ribeiro,J.M., Schneider,M., and Guimaraes,J.A. (1995). Purification and characterization of prolixin S (nitrophorin 2), the salivary anticoagulant of the blood-sucking bug *Rhodnius prolixus*. Biochem. J. *308 (Pt 1)*, 243-249.

Ricci,C.G., Pinto,A.F., Berger,M., and Termignoni,C. (2007). A thrombin inhibitor from the gut of *Boophilus microplus* ticks. Exp. Appl. Acarol. *42*, 291-300.

Richardson,J.L., Kroger,B., Hoeffken,W., Sadler,J.E., Pereira,P., Huber,R., Bode,W., and Fuentes-Prior,P. (2000). Crystal structure of the human alpha-thrombin-haemadin complex: an exosite II-binding inhibitor. EMBO J. *19*, 5650-5660.

Riester,D., Wirsching,F., Salinas,G., Keller,M., Gebinoga,M., Kamphausen,S., Merkwirth,C., Goetz,R., Wiesenfeldt,M., Sturzebecher,J., Bode,W., Friedrich,R., Thurk,M., and Schwienhorst,A. (2005). Thrombin inhibitors identified by computer-assisted multiparameter design. Proc. Natl. Acad. Sci. U. S. A *102*, 8597-8602.

Rios-Steiner,J.L., Murakami,M.T., Tulinsky,A., and Arni,R.K. (2007). Active and exo-site inhibition of human factor Xa: structure of des-Gla factor Xa inhibited by NAP5, a potent nematode anticoagulant protein from *Ancylostoma caninum*. J. Mol. Biol. *371*, 774-786.

Rydel,T.J., Ravichandran,K.G., Tulinsky,A., Bode,W., Huber,R., Roitsch,C., and Fenton,J.W. (1990). The structure of a complex of recombinant hirudin and human alpha-thrombin. Science *249*, 277-280.

Rydel,T.J., Tulinsky,A., Bode,W., and Huber,R. (1991). Refined structure of the hirudin-thrombin complex. J. Mol. Biol. *221*, 583-601.

Rydel,T.J., Yin,M., Padmanabhan,K.P., Blankenship,D.T., Cardin,A.D., Correa,P.E., Fenton,J.W., and Tulinsky,A. (1994). Crystallographic structure of human gamma-thrombin. J. Biol. Chem. *269*, 22000-22006.

Salzet,M. (2001). Anticoagulants and inhibitors of platelet aggregation derived from leeches. FEBS Lett. *492*, 187-192.

Salzet,M., Chopin,V., Baert,J., Matias,I., and Malecha,J. (2000). Theromin, a novel leech thrombin inhibitor. J. Biol. Chem. *275*, 30774-30780.

Sant'Anna,A.S., Sasaki,S.D., Torquato,R.J., Andreotti,R., Andreotti,E., and Tanaka,A.S. (2003). *Rhipicephalus sanguineus* trypsin inhibitors present in the tick larvae: isolation, characterization, and partial primary structure determination. Arch. Biochem. Biophys. *417*, 176-182.

Sasaki,S.D., Azzolini,S.S., Hirata,I.Y., Andreotti,R., and Tanaka,A.S. (2004). *Boophilus microplus* tick larvae, a rich source of Kunitz type serine proteinase inhibitors. Biochimie *86*, 643-649.

Scacheri,E., Nitti,G., Valsasina,B., Orsini,G., Visco,C., Ferrera,M., Sawyer,R.T., and Sarmientos,P. (1993). Novel hirudin variants from the leech *Hirudinaria manillensis*. Amino acid sequence, cDNA cloning and genomic organization. Eur. J. Biochem. *214*, 295-304.

Scharf,M., Engels,J., and Tripier,D. (1989). Primary structures of new 'iso-hirudins'. FEBS Lett. *255*, 105-110.

Schechter,I. and Berger,A. (1967). On the size of the active site in proteases. I. Papain. Biochem. Biophys. Res. Commun. *27*, 157-162.

Schmitz,T., Rothe,M., and Dodt,J. (1991). Mechanism of the inhibition of alpha-thrombin by hirudin-derived fragments hirudin(1-47) and hirudin(45-65). Eur. J. Biochem. *195*, 251-256.

Schulman,S. and Bijsterveld,N.R. (2007). Anticoagulants and their reversal. Transfus. Med. Rev. *21*, 37-48.

Schwienhorst,A. (2006). Direct thrombin inhibitors - a survey of recent developments. Cell Mol. Life Sci. *63*, 2773-2791.

Sheehan,J., Templer,M., Gregory,M., Hanumanthaiah,R., Troyer,D., Phan,T., Thankavel,B., and Jagadeeswaran,P. (2001). Demonstration of the extrinsic coagulation pathway in teleostei: identification of zebrafish coagulation factor VII. Proc. Natl. Acad. Sci. U. S. A *98*, 8768-8773.

Skrzypczak-Jankun,E., Carperos,V.E., Ravichandran,K.G., Tulinsky,A., Westbrook,M., and Maraganore,J.M. (1991). Structure of the hirugen and hirulog 1 complexes of alpha-thrombin. J. Mol. Biol. *221*, 1379-1393.

Slon-Usakiewicz,J.J., Purisima,E., Tsuda,Y., Sulea,T., Pedyczak,A., Fethiere,J., Cygler,M., and Konishi,Y. (1997). Nonpolar interactions of thrombin S' subsites with its bivalent inhibitor: methyl scan of the inhibitor linker. Biochemistry *36*, 13494-13502.

Slon-Usakiewicz,J.J., Sivaraman,J., Li,Y., Cygler,M., and Konishi,Y. (2000). Design of P1' and P3' residues of trivalent thrombin inhibitors and their crystal structures. Biochemistry *39*, 2384-2391.

Soejima,K., Mimura,N., Yonemura,H., Nakatake,H., Imamura,T., and Nozaki,C. (2001). An efficient refolding method for the preparation of recombinant human prethrombin-2 and characterization of the recombinant-derived alpha-thrombin. J. Biochem. (Tokyo) *130*, 269-277.

Sonder,S.A. and Fenton,J.W. (1984). Proflavin binding within the fibrinopeptide groove adjacent to the catalytic site of human alpha-thrombin. Biochemistry *23*, 1818-1823.

Stark,K.R. and James,A.A. (1995). A factor Xa-directed anticoagulant from the salivary glands of the yellow fever mosquito *Aedes aegypti*. Exp. Parasitol. *81*, 321-331.

Stark,K.R. and James,A.A. (1998). Isolation and characterization of the gene encoding a novel factor Xa-directed anticoagulant from the yellow fever mosquito, *Aedes aegypti*. J. Biol. Chem. *273*, 20802-20809.

Stassens,P., Bergum,P.W., Gansemans,Y., Jespers,L., Laroche,Y., Huang,S., Maki,S., Messens,J., Lauwereys,M., Cappello,M., Hotez,P.J., Lasters,I., and Vlasuk,G.P. (1996). Anticoagulant repertoire of the hookworm *Ancylostoma caninum*. Proc. Natl. Acad. Sci. U. S. A *93*, 2149-2154.

Steen,N.A., Barker,S.C., and Alewood,P.F. (2006). Proteins in the saliva of the Ixodida (ticks): pharmacological features and biological significance. Toxicon *47*, 1-20.

Steiner,V., Knecht,R., Bornsen,K.O., Gassmann,E., Stone,S.R., Raschdorf,F., Schlaeppi,J.M., and Maschler,R. (1992). Primary structure and function of novel O-glycosylated hirudins from the leech *Hirudinaria manillensis*. Biochemistry *31*, 2294-2298.

Stone,S.R. and Hofsteenge,J. (1986). Kinetics of the inhibition of thrombin by hirudin. Biochemistry *25*, 4622-4628.

Stone,S.R. and Tapparelli,C. (1995). Thrombin inhibitors as antithrombotic agents: the importance of rapid inhibition. J. Enzyme Inhib. *9*, 3-15.

Strube,K.H., Kroger,B., Bialojan,S., Otte,M., and Dodt,J. (1993). Isolation, sequence analysis, and cloning of haemadin. An anticoagulant peptide from the Indian leech. J. Biol. Chem. *268*, 8590-8595.

Su,Z., Vinogradova,A., Koutychenko,A., Tolkatchev,D., and Ni,F. (2004). Rational design and selection of bivalent peptide ligands of thrombin incorporating P4-P1 tetrapeptide sequences: from good substrates to potent inhibitors. Protein Eng Des Sel *17*, 647-657.

Tanaka,A.S., Andreotti,R., Gomes,A., Torquato,R.J., Sampaio,M.U., and Sampaio,C.A. (1999). A double headed serine proteinase inhibitor--human plasma kallikrein and elastase inhibitor--from *Boophilus microplus* larvae. Immunopharmacology *45*, 171-177.

Tuszynski,G.P., Gasic,T.B., and Gasic,G.J. (1987). Isolation and characterization of antistasin. An inhibitor of metastasis and coagulation. J. Biol. Chem. *262*, 9718-9723.

Vagin,A. and Teplyakov,A. (2000). An approach to multi-copy search in molecular replacement. Acta Crystallogr. D. Biol. Crystallogr. *56*, 1622-1624.

Valenzuela,J.G. (2004). Exploring tick saliva: from biochemistry to 'sialomes' and functional genomics. Parasitology *129 Suppl*, S83-S94.

Valenzuela,J.G., Francischetti,I.M., and Ribeiro,J.M. (1999). Purification, cloning, and synthesis of a novel salivary anti-thrombin from the mosquito *Anopheles albimanus*. Biochemistry *38*, 11209-11215.

van de,L.A., Lamba,D., Bauer,M., Huber,R., Friedrich,T., Kroger,B., Hoffken,W., and Bode,W. (1995). Two heads are better than one: crystal structure of the insect derived double domain Kazal inhibitor rhodniin in complex with thrombin. EMBO J. *14*, 5149-5157.

van de,L.A., Stubbs,M.T., Bode,W., Friedrich,T., Bollschweiler,C., Hoffken,W., and Huber,R. (1996). The ornithodorin-thrombin crystal structure, a key to the TAP enigma? EMBO J. *15*, 6011-6017.

Vindigni,A., Dang,Q.D., and Di Cera,E. (1997). Site-specific dissection of substrate recognition by thrombin. Nat. Biotechnol. *15*, 891-895.

Vitali,J., Martin,P.D., Malkowski,M.G., Robertson,W.D., Lazar,J.B., Winant,R.C., Johnson,P.H., and Edwards,B.F. (1992). The structure of a complex of bovine alpha-thrombin and recombinant hirudin at 2.8-A resolution. J. Biol. Chem. *267*, 17670-17678.

Waidhet-Kouadio,P., Yuda,M., Ando,K., and Chinzei,Y. (1998). Purification and characterization of a thrombin inhibitor from the salivary glands of a malarial vector mosquito, *Anopheles stephensi*. Biochim. Biophys. Acta *1381*, 227-233.

Warkentin,T.E., Greinacher,A., and Koster,A. (2008). Bivalirudin. Thromb. Haemost. *99*, 830-839.

Waxman,L., Smith,D.E., Arcuri,K.E., and Vlasuk,G.P. (1990). Tick anticoagulant peptide (TAP) is a novel inhibitor of blood coagulation factor Xa. Science *248*, 593-596.

Wei,A., Alexander,R.S., Duke,J., Ross,H., Rosenfeld,S.A., and Chang,C.H. (1998). Unexpected binding mode of tick anticoagulant peptide complexed to bovine factor Xa. J. Mol. Biol. *283*, 147-154.

White,C.M. (2005). Thrombin-directed inhibitors: pharmacology and clinical use. Am. Heart J. *149*, S54-S60.

Wienen,W., Stassen,J.M., Priepke,H., Ries,U.J., and Hauel,N. (2007). *In-vitro* profile and *ex-vivo* anticoagulant activity of the direct thrombin inhibitor dabigatran and its orally active prodrug, dabigatran etexilate. Thromb. Haemost. *98*, 155-162.

Witting,J.I., Bourdon,P., Brezniak,D.V., Maraganore,J.M., and Fenton,J.W. (1992). Thrombin-specific inhibition by and slow cleavage of hirulog-1. Biochem. J. *283 (Pt 3)*, 737-743.

Wu,K.K. and Matijevic-Aleksic,N. (2005). Molecular aspects of thrombosis and antithrombotic drugs. Crit Rev. Clin. Lab Sci. *42*, 249-277.

Yang,L., Manithody,C., Olson,S.T., and Rezaie,A.R. (2003). Contribution of basic residues of the autolysis loop to the substrate and inhibitor specificity of factor IXa. J. Biol. Chem. *278*, 25032-25038.

Yang,L., Manithody,C., and Rezaie,A.R. (2005). The functional significance of the autolysis loop in protein C and activated protein C. Thromb. Haemost. *94*, 60-68.

Yeh,R.W. and Jang,I.K. (2006). Argatroban: update. Am. Heart J. *151*, 1131-1138.

Yonemura,H., Imamura,T., Soejima,K., Nakahara,Y., Morikawa,W., Ushio,Y., Kamachi,Y., Nakatake,H., Sugawara,K., Nakagaki,T., and Nozaki,C. (2004). Preparation of recombinant alpha-thrombin: high-level expression of recombinant human prethrombin-2 and its activation by recombinant ecarin. J. Biochem. (Tokyo) *135*, 577-582.

Zhang,D., Cupp,M.S., and Cupp,E.W. (2002). Thrombostasin: purification, molecular cloning and expression of a novel anti-thrombin protein from horn fly saliva. Insect Biochem. Mol. Biol. *32*, 321-330.

Zhang,Y., Ribeiro,J.M., Guimaraes,J.A., and Walsh,P.N. (1998). Nitrophorin-2: a novel mixed-type reversible specific inhibitor of the intrinsic factor-X activating complex. Biochemistry *37*, 10681-10690.

Zhu,K., Bowman,A.S., Brigham,D.L., Essenberg,R.C., Dillwith,J.W., and Sauer,J.R. (1997a). Isolation and characterization of americanin, a specific inhibitor of thrombin, from the salivary glands of the lone star tick *Amblyomma americanum* (L.). Exp. Parasitol. *87*, 30-38.

Zhu,K., Sauer,J.R., Bowman,A.S., and Dillwith,J.W. (1997b). Identification and characterization of anticoagulant activities in the saliva of the lone star tick, *Amblyomma americanum* (L.). J. Parasitol. *83*, 38-43.

Zingali,R.B., Jandrot-Perrus,M., Guillin,M.C., and Bon,C. (1993). Bothrojaracin, a new thrombin inhibitor isolated from *Bothrops jararaca* venom: characterization and mechanism of thrombin inhibition. Biochemistry *32*, 10794-10802.

Zorio,E., Gilabert-Estelles,J., Espana,F., Ramon,L.A., Cosin,R., and Estelles,A. (2008). Fibrinolysis: the key to new pathogenetic mechanisms. Curr. Med. Chem. *15*, 923-929.

Internet websites:

http://www.nuvelo.com/products/rNAPc2/index.html
The announcement for suspension of recombinant NAPc2 development on the website of Nuvelo, Inc.

http://www.cfsph.iastate.edu/FactSheets/pdfs/amblyomma_variegatum.pdf
Some nformation about *Amblyomma variegatum* on the website of The Center for Food Security & Public Health, Iowa State University, USA.

http://www.themedicinescompany.com/products_angiomax.shtml
The product information of bivalirudin on the website of The Medicines Company

LIST OF PUBLICATIONS

Articles:

1. **Koh,C.Y.**, Kazimirova,M., Trimnell,A., Takac,P., Labuda,M., Nuttall,P.A., and Kini,R.M. (2007). Variegin, a novel fast and tight binding thrombin inhibitor from the tropical bont tick. J. Biol. Chem. *282*, 29101-29113. (cover page)

2. **Koh,C.Y.**, and Kini,R.M. (2008). Anticoagulants from hematophagous animals. Expert Rev. Hematol. 1, 135-139.

Patent:

Koh,C.Y., Kazimirova,M., Nuttall,P.A., and Kini,R.M. Thrombin inhibitors. *Patent filed.*

International Conference Presentations:

1. **Koh,C.Y.**, Kazimirova,M., Trimnell,A., Takac,P., Labuda,M., Nuttall,P.A., and Kini,R.M. Variegin, a novel class of thrombin inhibitor from the salivary gland extract of the hard tick Amblyomma variegatum. XXIst CONGRESS OF THE INTERNATIONAL SOCIETY ON THROMBOSIS AND HAEMOSTASIS, Geneva, Switzerland, 6-12 July 2007.
   Poster presentation

2. **Koh,C.Y.**, Kazimirova,M., Trimnell,A., Takac,P., Labuda,M., Nuttall,P.A., and Kini,R.M.. Nature's design of hirulog: Isolation, characterization and structure-function relationship study of variegin, a thrombin inhibitor from the salivary gland extract of tropical bont tick. THE 30th CONGRESS OF JAPANESE SOCIETY ON THROMBOSIS AND HEMOSTASIS, Shima City, Japan, 15-17 November 2007.
   Young Investigator's Award, Oral presentation

3. **Koh,C.Y.**, Kazimirova,M., Trimnell,A., Takac,P., Labuda,M., Nuttall,P.A., and Kini,R.M.. Structure-function relationships studies of variegin, a novel thrombin inhibitor from the salivary gland extract of tropical bont tick. 5th

CONFERENCE OF THE ASIAN-PACIFIC SOCIETY ON THROMBOSIS & HEMOSTASIS, Singapore, 18-20 September 2008.

Oral presentation

4. **Koh,C.Y.**, Kazimirova,M., Trimnell,A., Takac,P., Labuda,M., Nuttall,P.A., and Kini,R.M.. Lessons from nature on drug design: variegin, a novel thrombin inhibitor from tropical bont tick. JOINT 5th STRUCTURAL BIOLOGY & FUNCTIONAL GENOMICS AND 1st BIOLOGICAL PHYSICS INTERNATIONAL CONFERENCE, Singapore 9-11 December 2008.

   Poster presentation

Media coverage:

Clogged artery? Ticks might do the trick. The Straits Times (Singapore newspaper article). 31st December 2007. Page H3.
(http://newshub.nus.edu.sg/news/0712/pdf/ARTERY-st-31Dec-pH3.pdf)

APPENDIX A. Purification of peptides

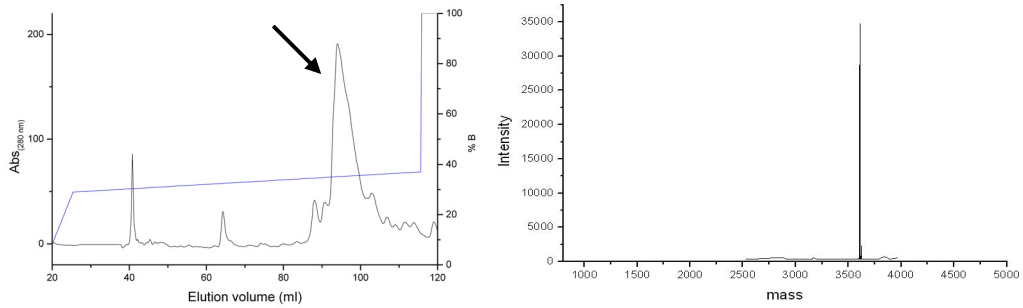

s-variegin: elution gradient was 29 – 37% B in 90 ml. Reconstructed ESI-MS spectrum showed mass of 3609.0 Da.

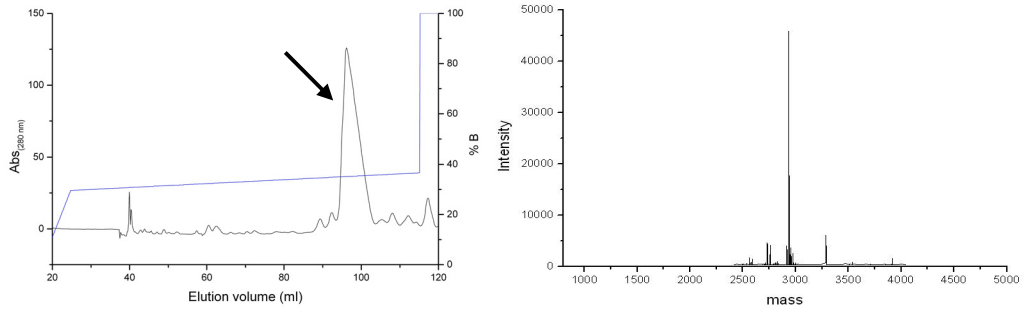

EP25: elution gradient was 29.6 – 36.6% B in 90 ml. Reconstructed ESI-MS spectrum showed mass of 2936.4 Da.

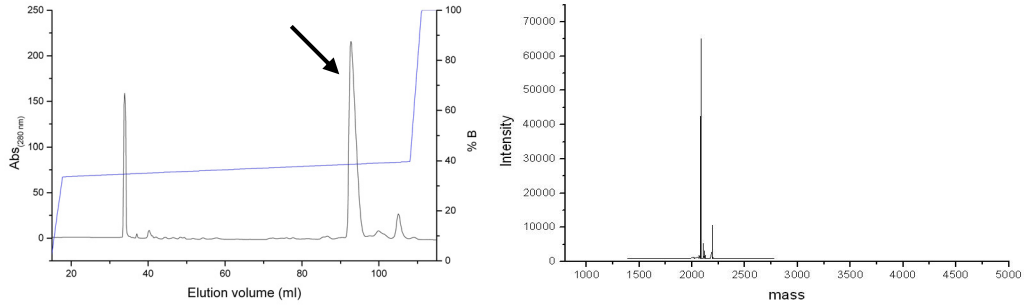

AP18: elution gradient was 33.6 – 39.6% B in 90 ml. Reconstructed ESI-MS spectrum showed mass of 2084.4 Da.

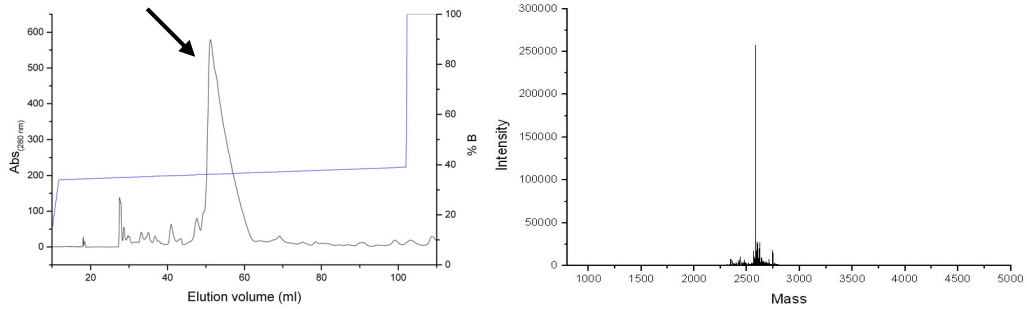

MH22: elution gradient was 34 – 39% B in 90 ml. Reconstructed ESI-MS spectrum showed mass of 2581.8 Da.

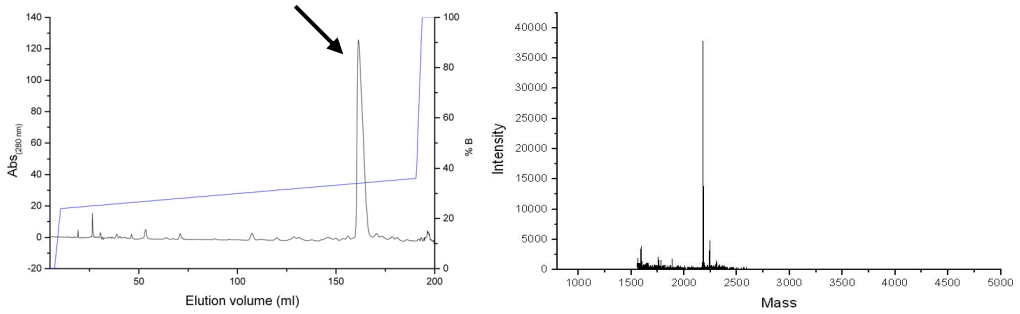

Hirulog-1: elution gradient was 24 – 36% B in 180 ml. Reconstructed ESI-MS spectrum showed mass of 2179.6 Da.

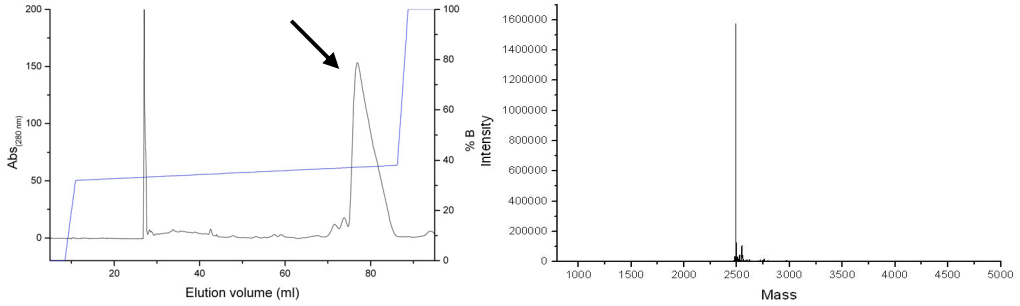

EP21: elution gradient was 32 – 38% B in 75 ml. Reconstructed ESI-MS spectrum showed mass of 2490.2 Da.

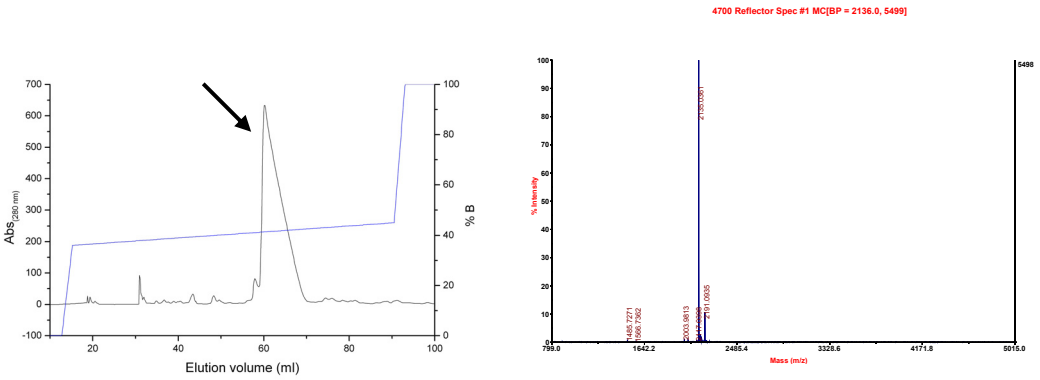

MH18: elution gradient was 36 – 45% B in 75 ml. MALDI-TOF spectrum showed mass of 2136.0 Da.

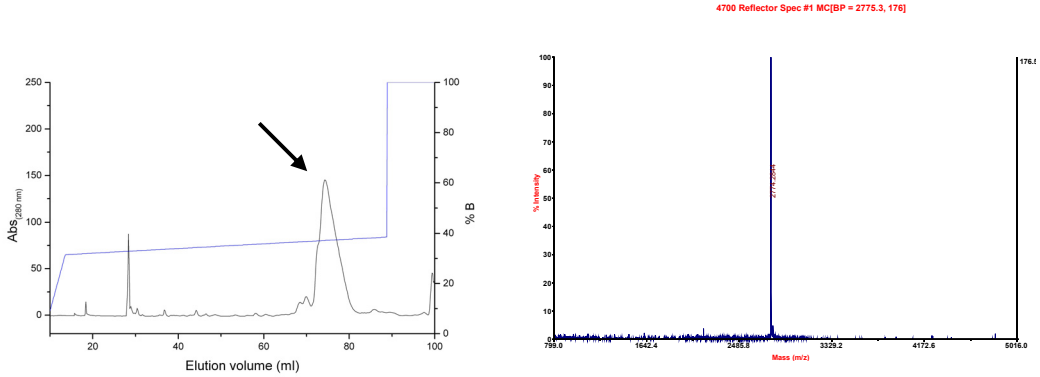

DV24: elution gradient was 31.5 – 38.5% B in 75 ml. MALDI-TOF spectrum showed mass of 2775.3 Da

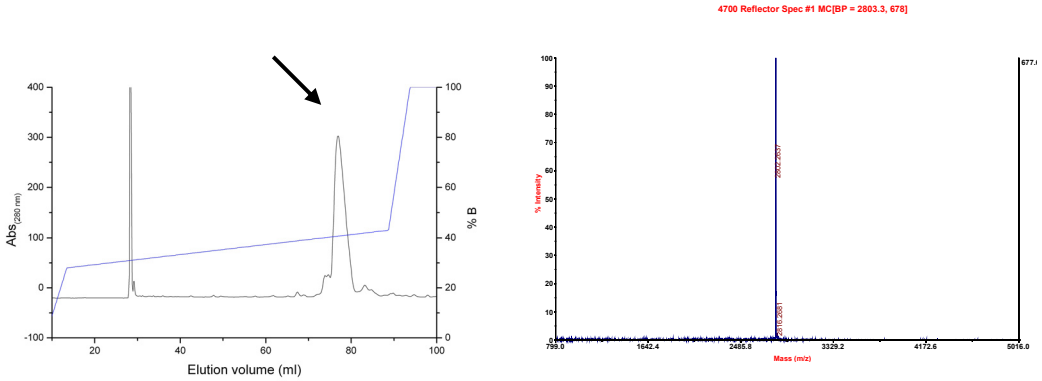

DV24K10R: elution gradient was 28 – 43% B in 75 ml. MALDI-TOF spectrum showed mass of 2803.3 Da

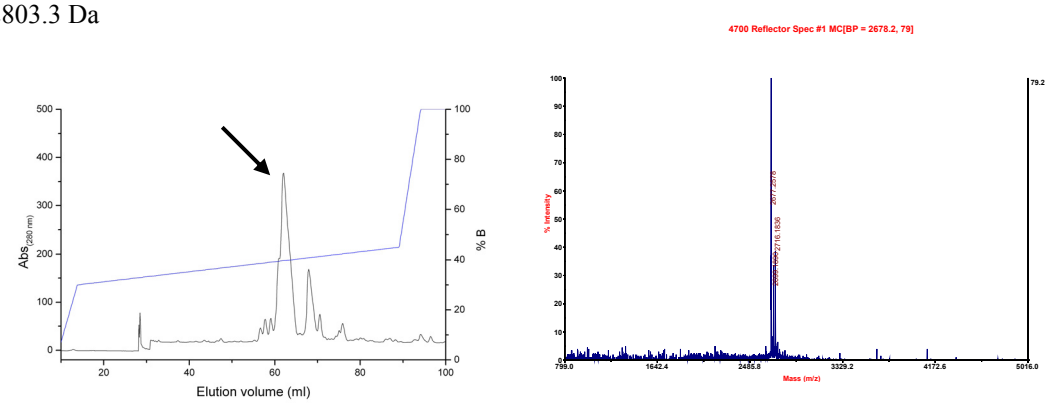

DV23: elution gradient was 30 – 45% B in 75 ml. MALDI-TOF spectrum showed mass of 2678.2 Da

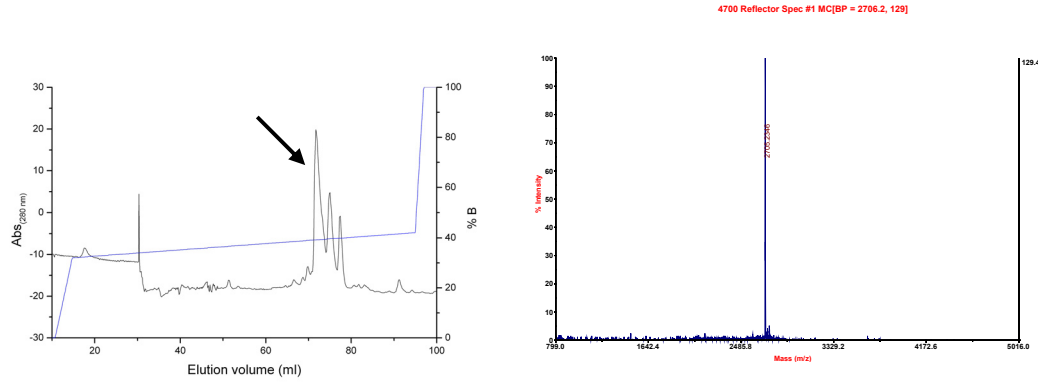

DV23K10R: elution gradient was 32 – 42% B in 80 ml. MALDI-TOF spectrum showed mass of 2706.2 Da

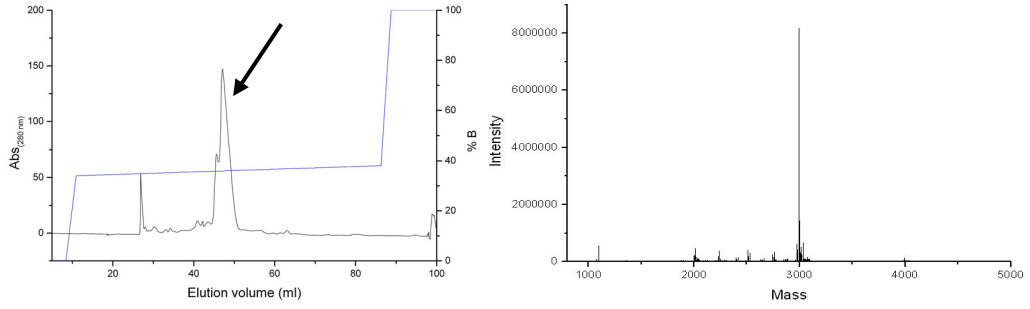

EP25A22E: elution gradient was 34 – 38% B in 75 ml. Reconstructed ESI-MS spectrum showed mass of 2994.4 Da.

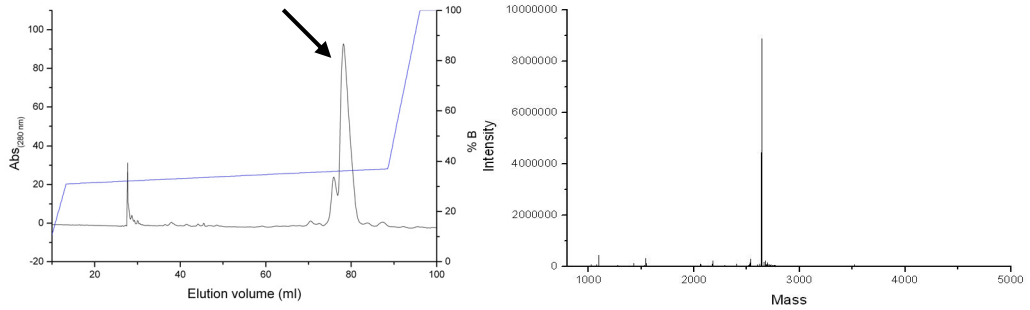

MH22A22E: elution gradient was 31 – 37% B in 75 ml. Reconstructed ESI-MS spectrum showed mass of 2640.1 Da.

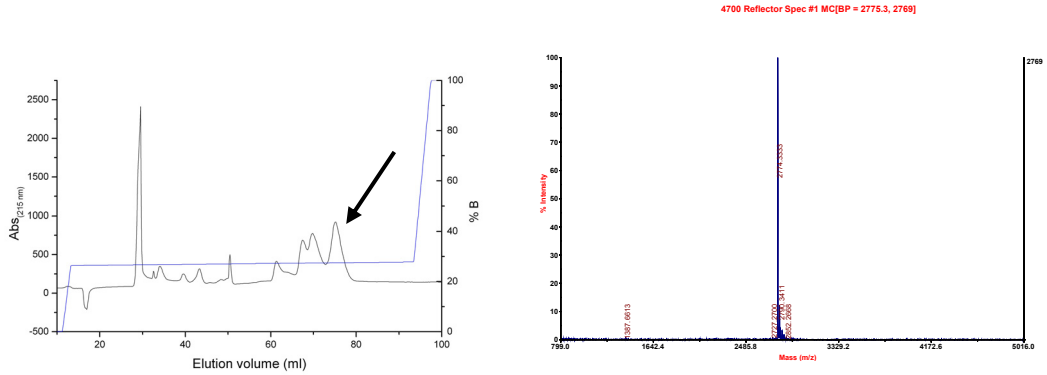

DV24Y^{sulf}: elution gradient was 26.4 – 27.8% B in 80 ml. MALDI-TOF spectrum showed desulfated mass of 2775.3 Da

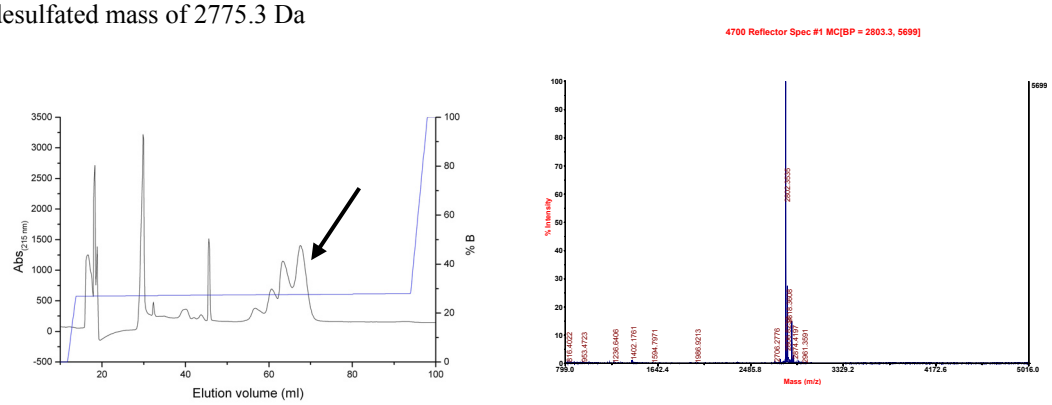

DV24K10RY^{sulf}: elution gradient was 26.9 – 27.9% B in 80 ml. MALDI-TOF spectrum showed desulfated mass of 2803.3 Da

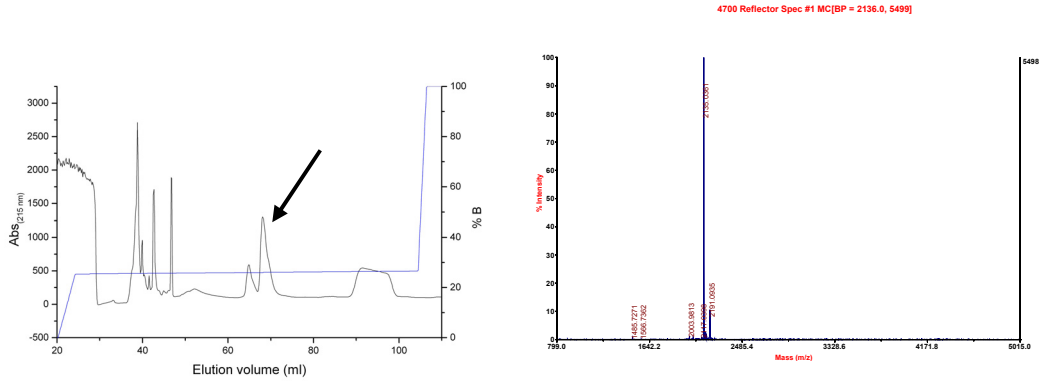

MH18Y^{sulf}: elution gradient was 25.4 – 26.6% B in 80 ml. MALDI-TOF spectrum showed desulfated mass of 2136.0 Da.

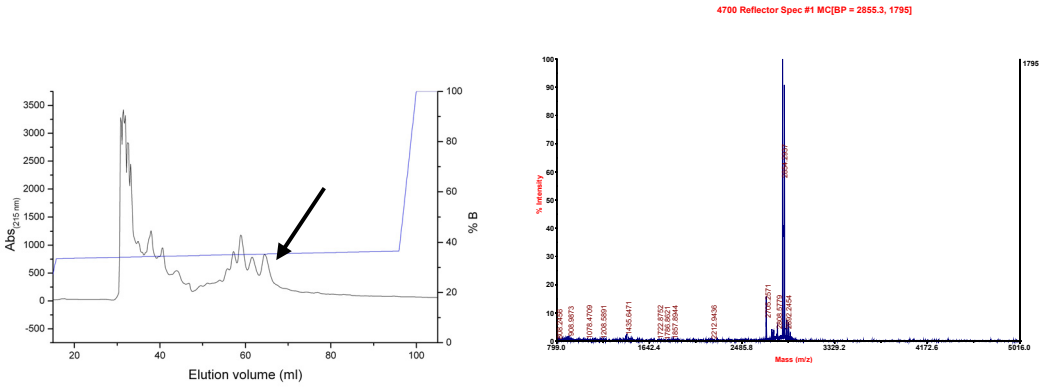

DV24Y^{phos}: elution gradient was 33.5 – 36.5% B in 80 ml. MALDI-TOF spectrum showed mass of 2855.3 Da.

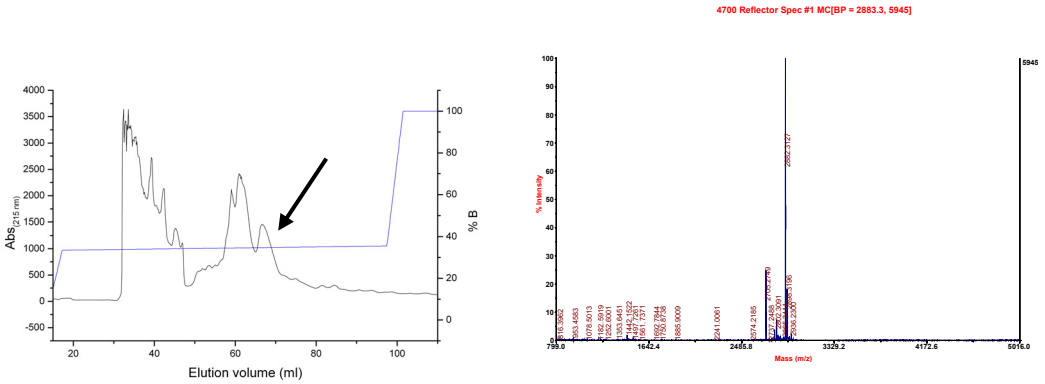

DV24K10RY^{phos}: elution gradient was 33.5 – 35.5% B in 80 ml. MALDI-TOF spectrum showed mass of 2883.3 Da.

APPENDIX B. Coordinates file for the thrombin-s-variegin structure

Submission of the structure to PBD is put on hold for publication. The coordinates file for the structure is recorded in the CD attached at the end of this thesis. The file can be found in CD at this location: /appendix B/thrombin-variegin.pdb

---

APPENDIX C. Videos recording thrombus formation in zebrafish larvae

Three short video recording the thrombus formation (or lack of) in larvae injected with PBS, MH22 and DV24K10RY^{sulf} were copied into the CD attached. Although thrombus formation can be directly followed on the monitor attached to the microscope throughout the whole experiment, the digital camera attached can only record short videos with a maximum duration of 39 s.

The file for the larva injected with PBS (TTO ~ 21 s) can be found at this location: /appendix C/PBS_1.avi

The file for the larva injected with MH22 (TTO ~ 35 s) can be found at this location: /appendix C/MH22_1.avi

The file for the larva injected with DV24K10RY^{sulf} (no thrombus formed) can be found at this location: /appendix C/DV24K10RYsulf_1.avi

---

APPENDIX D. Publications

Soft copies of the two publications related to this thesis were recorded in the CD attached at this location: /appendix D/JBC.pdf; and /appendix D/Expert Rev Hematol.pdf